

AMERICAN UNIVERSITY OF BEIRUT

ENERGY EFFICIENT STRATEGIES FOR REDUCED CROSS-
CONTAMINATION BETWEEN OCCUPANTS IN OFFICE
SPACES

by
CARINE HANNA HABCHI

A dissertation
submitted in partial fulfillment of the requirements
for the degree of Doctor of Philosophy
to the Department of Mechanical Engineering
of the Faculty of Engineering and Architecture
at the American University of Beirut

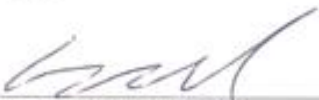
Beirut, Lebanon
April 2016

AMERICAN UNIVERSITY OF BEIRUT


ENERGY EFFICIENT STRATEGIES FOR REDUCED CROSS-
CONTAMINATION BETWEEN OCCUPANTS IN OFFICE
SPACES

by
CARINE HANNA HABCHI

Approved by:




Dr. Kamel Ghali, Professor
Department of Mechanical Engineering, AUB
Advisor




Dr. Nesreen Ghaddar, Professor
Department of Mechanical Engineering, AUB
Member of Committee



Dr. Fadl Moukalled, Professor
Department of Mechanical Engineering, AUB
Member of Committee



Dr. Michel Hayek, Professor
Department of Mechanical Engineering, NDU
Member of Committee



Dr. Khalil Khoury, Professor
Department of Mechanical Engineering, Lebanese University
Member of Committee

Date of dissertation defense: April 20, 2016

ACKNOWLEDGMENTS

I would like to thank my advisor Prof. Kamel Ghali and co-adviser Prof. Nesreen Ghaddar for their guidance and support throughout my research work. I had the chance to benefit from their research experience and critical thinking. I would like also to thank the members of my dissertation committee Prof. Michel Hayek, Prof. Khalil Khoury, and Prof. Fadl Moukalled for their valuable comments and recommendations and the faculty members and staff of the Mechanical Engineering Department at the American University of Beirut for their help in the achievement of this work.

I would also like to express cordial gratitude to my colleagues and friends at the American University of Beirut who motivated me to strive towards my goal: Nagham Ismail, Hanin Hamdan, Alain Makhoul, Mohammad Allouche, Mohammad Baassiri, Mohammad Kanaan, Amer Keblawi, Abed AlKader Al Saidi, Maryam Itani, Manar, Younes, Hussein Daoud, Raghid Farhat, Hajar Fawaz, Hussein Maanieh, Khaled Abou Hweij, Mohammad Rida, Bachir El Fil, Sylvie Antoun, Walid Abou Hweij, Albert Touma, and Mohammad Bassel Kazzaz.

Special thanks to my family. Your presence has always been a source of joy and motivation, and your compassion is highly appreciated. Words cannot express how grateful I am for your encouragement and support.

At the end, I would like to express my appreciation and love to my husband Mansour Habchi who was always my support in the hard times. Great thanks for your understanding, patience and for being beside me to achieve my goals successfully.

AN ABSTRACT OF THE DISSERTATION OF

Carine Hanna Habchi for Doctor of Philosophy
Major: Mechanical Engineering

Title: Energy Efficient Strategies for Reduced Cross-Contamination between Occupants in Office Spaces

IAQ in indoor environments is one of the major concerns of public health organizations. People constitute one of the main sources of particles carrying contaminants in indoor environments by exhalation resulting from the different respiratory activities. The HVAC system should be effectively designed to reduce disease transmission between occupants at a minimal energy cost. This work aims towards investigating by modeling and experimentation the effectiveness of two localized air conditioning systems in decreasing the risk of cross-infection: displacement ventilation (*DV*) system assisted by chair fans (*CF*); and ceiling personalized ventilation (*CPV*) system equipped by desk fans (*DF*)/ chair fans (*CF*).

Computational fluid dynamics (CFD) and simplified numerical models are developed and validated experimentally and by literature data to simulate disease transmission in office spaces under different ventilation configurations. Simplified multi-zonal models incorporating the main physics affecting particle transport including particle deposition and gravitational effect were developed to assess the effectiveness of the standalone *DV* system in terms of providing good IAQ and to come-up with recommendations to enhance its performance. CFD models were used to simulate more complex situations when fans were equipped to the *DV* and the *CPV* systems. Optimization of the fans flow rate was conducted to increase the energy savings for both configurations and use the space more efficiently for the *CPV* system. Implementing fans with *DV* and *CPV* systems was shown to be very efficient in decreasing cross-contamination between occupants in office spaces with an acceptable comfort level and reduced energy cost.

CONTENTS

ACKNOWLEDGEMENTS.....	v
ABSTRACT.....	vi
LIST OF ILLUSTRATIONS.....	xi
LIST OF TABLES.....	xvi
LIST OF ABBREVIATIONS.....	xviii

Chapter

1. INTRODUCTION.....	1
1.1. Thesis Objectives	7
2. LOCALIZED VENTILATION FOR REDUCED CROSS- CONTAMINATION AND ENERGY SAVINGS	9
2.1. Mixed Ventilation Limitations	9
2.2. Displacement Ventilation.....	10
2.2.1. <i>DV</i> assisted by <i>CF</i>	12
2.3. Ceiling Personalized Ventilation	12
2.3.1. <i>CPV</i> assisted by <i>DF</i> versus <i>CF</i>	14
2.4. Exhaled Contaminants Contributing to Cross-Infection	16

3. ANALYTICAL AND NUMERICAL METHODS.....	18
3.1. Simplified <i>DV</i> Model	18
3.1.1. Description of the Problem.....	18
3.1.2. Mathematical Formulation.....	22
3.1.2.1. Plumes Flow Rates	22
3.1.2.2. Modeling of Particle Distribution.....	24
3.1.2.3. Modeling of Particle Deposition.....	25
3.1.2.4. Transport Model of Exhaled Particles.....	27
3.1.2.5. Transient Propagation of the Exhaled Jet.....	31
3.1.2.6. Transient Zonal Model for Particle Distribution	34
3.1.2.7. Particle Distribution within the Thermal Plumes	35
3.1.2.8. Mass balances for the Different Zones.....	36
3.1.2.8.1. Infected Plume Zone.....	36
3.1.2.8.2. Exposed Plume Zone	37
3.1.2.8.3. First Microclimate Zone.....	38
3.1.2.8.4. Second Microclimate Zone.....	40
3.1.2.8.5. Macroclimate Zone.....	42
3.1.3. Boundary Conditions and Numerical Methods.....	43
3.2. CFD Model.....	45
3.2.1. Airflow and Energy Modeling	45
3.2.2. Discrete Phase Modeling.....	46
3.2.3. Boundary Conditions.....	51
3.3. Thermal Comfort Assessment.....	52
3.3.1. Coupling of CFD and PMV/PPD Models.....	52
3.3.2. Coupling of CFD and Bio-Heat Models	53
3.4. Ventilation Effectiveness Assessment.....	55
3.5. Cross-Contamination Assessment.....	55
3.6. Interpersonal Exposure Assessment.....	56

4. EXPERIMENTAL METHODS.....	58
4.1. Experimental validation of the <i>DV</i> Models.....	58
4.1.1. Validation of the Simplified <i>DV</i> Model.....	60
4.1.2 Validation of the <i>DV+CF</i> CFD Model.....	62
4.2. Experimental Validation of the <i>CPV</i> CFD Models.....	62
5. RESULTS AND DISCUSSIONS.....	68
5.1. <i>DV</i> System Performance	68
5.1.1. Simplified <i>DV</i> Model Results	68
5.1.1.1. Validation with Literature Data	68
5.1.1.2. Validation with Experimental Data	77
5.1.1.3. Case Study of Non-Equal Heat Strength Sources	82
5.1.1.4. Case Study of Different Respiratory Activities...	93
5.1.1.5. Transient Interpersonal Exposure for HMRA...	98
5.1.1.5.1. <i>DV</i> Flow Rate Effect	99
5.1.1.5.2. Cough Velocity Effect	103
5.1.1.5.3. Particle Diameter Effect.....	104
5.1.1.5.4. Separating Distance Effect.....	106
5.1.1.5.5. Steady versus Transient Modeling...	108
5.1.2. Effect of Assisting <i>DV</i> with <i>CF</i>	110
5.1.2.1. <i>DV+CF</i> CFD Model Experimental Validation...	109
5.1.2.2. <i>DV+CF</i> Case Study	112
5.1.2.3. Energy Savings of the Optimal <i>DV+CF</i> Design.	121
5.2. <i>CPV</i> System Performance	124
5.2.1. <i>CPV+DF/CF</i> CFD Model Experimental Validation.....	124
5.2.2. Effect of Assisting <i>CPV</i> with <i>DF</i>	127
5.2.2.1. <i>CPV+DF</i> Case Study	127
5.2.2.2. Energy Savings of the Optimal <i>CPV+DF</i> Design	138
5.2.3. <i>CPV</i> System Assisted by <i>CF</i> versus <i>DF</i>	141
5.2.3.1. <i>CPV+DF/CF</i> Case Study.....	141
5.2.3.1.1. IAQ Assessment	142
5.2.3.1.2. Thermal Comfort Assessment.....	149
5.2.3.2. Energy Savings of the Optimal <i>CPV+CF</i> Design	154

6. CONCLUSION AND RECOMMENDATIONS	156
6.1. Development of a Simplified <i>DV</i> Model	156
6.2. Cross-Contamination from HMRA in <i>DV</i> Spaces	157
6.3. <i>DV+CF</i> Performance	159
6.4. <i>CPV+DF</i> Performance	160
6.5. Effect of Assisting <i>CPV</i> with <i>CF</i> versus <i>DF</i>	162
REFERENCES	164

..

ILLUSTRATIONS

Figure	Page
3.1. Spatial discretization of the space ventilated by the <i>DV</i> system.....	19
3.2. Penetration of the horizontal jet through the thermal boundary layer.....	21
3.3. Convective flows through sub-microclimate 2 number <i>j</i> within the generation layer.....	33
3.4. Representation of the physical phenomena affecting the contaminant concentration within a layer <i>i</i>	34
3.5. Flowchart illustrating the sequence of operations for solving for the different variables.....	44
3.6. Mesh of the CFD model for a space ventilated by: a) <i>DV</i> system; b) <i>CPV</i> system.....	49
3.7. Flowchart summarizing the coupling between CFD and bio-heat models.....	54
4.1. Schematic of the <i>DV</i> experimental set-up.....	59
4.2. Equipment of CO ₂ and particles: a) generation; and b) concentration measurement.....	61
4.3. Representation of the <i>CPV</i> system experimental set-up: (a) Frontal view (b) Top view.....	64
4.4. a) Illustration of the constructed <i>CPV</i> experimental set-up in the controlled climatic chamber; b) Top view of the experimental layout illustrating the location of the contaminant generation sources.....	65
5.1. Schematic of the set-up studied by Li et al. [28] at the mid-plane	69
5.2. Plot of the predicted variation of the average normalized concentration with height compared to published model results of Li et al. [28] at particle diameters of a) 1 μm; b) 5 μm; c) 10 μm.....	70
5.3. Comparison of the intake fractions predicted for different diameters	71
5.4. Plot of the total rate of deposited mass of particles obtained from both our current model and that of Li et al. [28] for different particle diameters.....	72

5.5.	Comparison of a) the vertical walls deposited mass rate (kg/s) predicted for different diameters; b) the floor deposited mass rate (kg/s) predicted for different diameters.....	74
5.6.	Comparison of a) the mean deposited rate (1/h) predicted for different diameters; b) the mean deposition velocity (m/h) predicted for different diameters.....	75
5.7.	Comparison of current model prediction of personal exposure in % as a function of time with values published by Gao and Niu [71].....	76
5.8.	Variation of the normalized concentration of CO ₂ in microclimate 2 with height within a 90% confidence interval at different jet velocities: a) 1 m/s; b) 3 m/s; c) 10 m/s.....	78
5.9.	Variation of the normalized concentration of CO ₂ and 5 μm particles with height within a 90% confidence interval at a jet velocity of 3 m/s within different zones: a) microclimate 1; b) microclimate 2; c) macroclimate.....	79
5.10.	Plot of variation in time of the predicted and experimentally determined values of normalized particle concentration of the exhaled jet at distances of 0.5 m, 1 m, and 1,5 m from particle generation location.....	81
5.11.	Representation of the discretized domain with non-equal heat sources strength.....	82
5.12.	Variation of the normalized particle concentration with height for different particle diameters in the surrounding air zone for a flow rate of 60 L/s.....	84
5.13.	Variation of the normalized particle concentration with height within the different zones for a flow rate of 60 L/s and a particle diameter of 1 micrometer.....	88
5.14.	Increase of the flow rate to meet the IAQ criteria to a value of: a) 80 L/s; b) 100 L/s.....	91
5.15.	Variation with height of the normalized concentration of 1 μm particles in microclimate 2 for different DV supply flow rates.....	95
5.16.	Variation with height of the normalized concentration in microclimate 2 for different particle diameters for a DV flow rate of 100 L/s.....	96

5.17.	Variation with height of the normalized concentration of 1 μm particles in microclimate 2 for different distances between the occupants for a DV flow rate of 100 L/s.....	97
5.18.	Variation with distance between the occupants of the concentration peak of 1 μm particles in microclimate 2 for a DV flow rate of 100 L/s.....	98
5.19.	Effect of the DV supply flow rate on the variation with time of: a) the normalized concentration at the breathing level of the exposed person; b) the infection index.....	100
5.20.	Effect of the cough velocity on the tranient of: a) the normalized concentration at the breathing level of the exposed person; b) the infection index.....	104
5.21.	Effect of the particle diameter on the variation with time of: a) the normalized concentration at the breathing level of the exposed person; b) the infection index.....	105
5.22.	Effect of the distance between occupants on the variation with time of: a) the normalized concentration at the breathing level of the exposed person; b) the infection index.....	106
5.23.	Variation with distance between the occupants of the total inhaled dose.....	107
5.24.	Comparison of the inhaled dose predicted by transient and steady modeling for the parameters: a) DV flow rate; b) cough velocity; c) distance between the occupants.....	109
5.25.	Variation of the normalized concentration with respect to the concentration of generation with height for the fans-off configuration within a 90% confidence interval at a) the centerline of the infected plume; b) the centerline of the exposed plume; c) the centerline between the occupants within the surrounding air.....	111
5.26.	Variation of the normalized concentration with respect to the concentration of generation with height for the fans-on configuration within a 90% confidence interval at a) the centerline of the infected plume; b) the centerline of the exposed plume; c) the centerline between the occupants within the surrounding air.....	112
5.27.	Effect of the chair fans on the vertical component of the velocity field within the <i>CF</i> symmetry plane for a supply flow rate of 80 L/s of a fan flow rate of: (a) zero L/s; (b) 5.0 L/s; (c) 7.5 L/s; (d) 10.0 L/s.....	114

5.28.	Normalized concentration of 1 μm particles at the occupants' plane for a supply flow rate of 80 L/s for a flow rate per chair fan for (a) zero L/s; (b) 5.0 L/s; (c) 7.5 L/s; (d) 10.0 L/s.....	115
5.29.	. Effect of the chair fans flow rate on the variation with height (z direction) of the average normalized concentration of 1 μm particles within the surrounding air for a supply flow rate of 80 L/s.....	116
5.30.	Effect of the chair fans flow rate on the intake fraction of particles of 1 μm in diameter of the exposed occupant for different supply flow rates.....	118
5.31.	Normalized concentration of 10 μm particles at the occupants' plane for a supply flow rate of 80 L/s for a fan flow rate per chair of (a) zero L/s; (b) 5.0 L/s; (c) 7.5 L/s; (d) 10.0 L/s.....	119
5.32.	Effect of the chair fans flow rate on the intake fraction of particles of 10 μm in diameter of the exposed occupant for different supply flow rates.....	120
5.33.	Fan effect on the thermal field within the CF symmetry plane showing (a) standalone DV , $Q_s = 70$ L/s; (b) $DV+CF$, $Q_s = 70$ L/s and $q_f = 7.5$ L/s; (c) standalone DV , $Q_s = 100$ L/s.....	122
5.34.	Validation of the ability of the CFD model in predicting the effect of the desk fan flow rate on particle behavior	125
5.35.	Validation of the ability of the CFD model in assessing the effect of desk and chair fans on particle behavior.....	126
5.36.	Representation of the: a) velocity, b) temperature, and concentration fields of 1 μm particles in the two-station office space at the symmetry plane for mixing ventilation at $d2$	128
5.37.	Effect of the distance between the occupants on: a) the deposited fraction (DFr); and b) the intake fraction (IF) for different particle diameters in case of mixing ventilation.....	129
5.38.	Representation of the: a) velocity, b) temperature, and concentration fields of 1 μm particles in the two-station office space at the symmetry plane for CPV ventilation at $d2$	131
5.39.	Effect of the ventilation configuration on the variation with distance of: a) DFr ; b) IF for 1 μm particles	133
5.40.	Effect of the ventilation configuration on the variation with distance of: a) DFr ; b) IF for 10 μm particles	134

5.41.	Variation of a) the deposited fraction; and b) the intake fraction with the fan flow rate for different distances between the occupants in the case of <i>CPV+DF</i> configuration for 1 μm particle.....	135
5.42.	Representation of the: a) velocity, b) temperature, and concentration fields of 1 μm particles in the two-station office space at the symmetry plane for the optimal <i>CPV+DF</i> (10L/s) at <i>d2</i>	136
5.43.	Effect of the desk fan flow rate: a) 5L/s, b) 10L/s, and c) 15 L/s on the intake fraction of 10 μm particles for the <i>CPV+DF</i> ventilation at <i>d2</i>	138
5.44.	Concentration field of 1 μm particle in the exposed person station at the symmetry plane for: a) <i>MV</i> at <i>d1</i> ; b) <i>CPV</i> at <i>d2</i> ; c) <i>CPV+DF</i> (10 L/s) at <i>d2</i> ; d) <i>CPV+DF</i> (10 L/s) at <i>d3</i>	139
5.45.	Illustration of the velocity field at the symmetry plane of the two-station office space for shift distances <i>sd1=0 cm</i> (occupant at the left) and <i>sd3=20 cm</i> (occupant at the right) for: a) Standalone <i>CPV</i> ; b) <i>CPV+DF</i> ; c) <i>CPV+CF</i>	143
5.46.	Illustration of the velocity field at the symmetry plane of the two-station office space for <i>CPV+DF</i> for the healthy occupant shift of: a) <i>sd1=0 cm</i> ; b) <i>sd2=10 cm</i> ; c) <i>sd3=20 cm</i>	145
5.47.	Illustration of the CO ₂ field at the symmetry plane of the two-station office space for shift distances <i>sd1=0 cm</i> (occupant at the left) and <i>sd3=20 cm</i> (occupant at the right) for: a) <i>CPV+DF</i> ; b) <i>CPV+CF</i>	146
5.48.	Illustration of 1 μm particle concentration field at the symmetry plane of the two-station office space for shift distances <i>sd1=0 cm</i> (occupant at the left) and <i>sd3=20 cm</i> (occupant at the right) for: a) <i>CPV+DF</i> ; b) <i>CPV+CF</i>	148
5.49.	Segmental and overall comfort for the different configurations studied.....	150
5.50.	Segmental and overall sensation for the different configurations studied	151
5.51.	Illustration of the temperature field at the symmetry plane of the two-station office space for shift distances <i>sd1=0 cm</i> (occupant at the left) and <i>sd3=20 cm</i> (occupant at the right) for: a) <i>CPV+DF</i> ; b) <i>CPV+CF</i>	153

TABLES

Table	Page
5.1. Influence of flow rate and particle diameter on normalized concentrations.....	85
5.2. Influence of flow rate and particle diameter on particle deposition.....	86
5.3. Performance of the <i>DV</i> system in terms of Thermal comfort for different supply conditions.....	93
5.4. Effect of the <i>DV</i> supply flow rate on different model geometric and physical parameters.....	99
5.5. Periods of the three stages of the variation of inhaled concentration with time for different <i>DV</i> supply flow rates.....	101
5.6. Inhaled dose during the different stages for different <i>DV</i> supply flow rates.....	102
5.7. Effect of particle diameter and fan flow rate on particle deposition.....	113
5.8. Comparison of the performance of different HVAC configurations in terms of IAQ.....	121
5.9. Comparison of the performance of different HVAC configurations in terms of thermal comfort.....	124
5.10. Effect of particle diameter on particle deposition.....	130
5.11. Effect of the HVAC configuration on a) particle deposition at the proximity of the exposed person (<i>DRF</i>) and b) intake fraction (<i>IF</i>) for different diameters.....	132
5.12. Effect of the HVAC configuration on a) the increments in <i>DFr</i> (ΔDFr) and b) the increments in <i>IF</i> (ΔIF) for different diameters when the distance between the occupants is reduced from 4.0 to 2.0 m.....	133
5.13. % of reductions of the <i>DFr</i> and <i>IF</i> when changing the configuration from <i>MV</i> at <i>d1</i> to <i>CPV+DF</i> (10 L/s) at <i>d3</i> for different particle diameters.....	140
5.14. Effect of the shift distance and the ventilation system on the ventilation effectiveness, intake fraction (<i>IF</i>) and the particle deposition at the proximity of the exposed person (<i>DRF</i>) for different particle diameters.....	142

5.15.	Effect of assisting ceiling personalized ventilation (CPV) with desk fans (DF) and chair fans (CF) on a) the increase in DFr (ΔDFr) and b) the increase in IF (ΔIF) for different diameters when the shift distance is increased from 0 to 20 cm.....	149
5.16.	Comparison of the performance of DF and CF when the occupant is beneath the CPV jet.....	155

ABBREVIATIONS

Symbols

A	: area (m^2)
C	: particle concentration (kg/m^3)
CF	: chair fan
CFD	: computational fluid dynamics
CPV	: ceiling personalized ventilation
d_{inj}	: hydraulic diameter of the mouth (m)
d_p	: particle diameter (m)
dt	: particle residence time (s)
D	: diameter of the cylinder simulating the occupant (m)
D_p	: particle Brownian diffusion (m^2/s)
D_t	: turbulent diffusion coefficient (m^2/s)
DF	: desk fan
DFr	: deposited fraction of particles at the vicinity of the exposed occupant
DRW	: discrete random walk model
DV	: displacement ventilation
\vec{F}_a	: forces acting on a particle (m/s^2)
F_D	: inverse of relaxation time (s^{-1})
\vec{g}	: gravitational settling vector
Gr	: Grashof number
h	: height above the heat source (m)
HVAC	: heating, ventilation, and air conditioning
HMRA	: High momentum respiratory activities
I	: infection index (kg)
I_{cl}	: clothing insulation (clo)
ID	: inhaled dose (kg)
IF	: intake fraction
IAQ	: indoor air quality
IPE	: inter-personal exposure
J_d	: deposition flux of particles towards a wall ($kg/m^2.s$)
K	: local turbulence intensity
L	: length of the cylinder simulating the occupant (m)
LMRA	: low momentum respiratory activities
\dot{m}	: mass flow rate associated with particles trajectory (kg/s)
M	: mass flow rate (kg/s)
MV	: mixing ventilation
Pr	: Prandtl number
PSI-C	: particle source in-cell scheme
PV	: personalized ventilation
q_f	: flow rate per fan (L/s)
Q_H	: heat source load (W)
Q_g	: generated flux (m^3/s)
Q_p	: penetrating flux (m^3/s)
Q_s	: supply flow rate of the DV system (L/s)

R	: radius of the plume at a certain horizontal level (m)
Re	: Reynold number
sd	: shift distance from the <i>CPV</i> center
$S_{p,i}$: contaminant generation in layer <i>i</i> inside the plume (Kg/m ³ .s)
S_{ai}	: contaminant generation in layer <i>i</i> outside the plume (Kg/m ³ .s)
Sc	: Schmidt number
t	: time (s)
t_{rl}	: cough release time (s)
t_{tr}	: traveling time (s)
T	: temperature (K)
TP	: thermal plumes
TRA	: transient respiratory activities
u	: vertical velocity component within the boundary layer (m/s)
\vec{u}	: airflow velocity vector (m/s)
\vec{u}_p	: particle velocity vector (m/s)
u_i'	: turbulent fluctuating component of the velocity
u^*	: friction velocity (m/s)
v	: horizontal velocity component within the boundary layer (m/s)
v_d	: deposition velocity (m/s)
v_s	: absolute component of the particle settling velocity (m/s)
V	: velocity (m/s)
X	: wall width (m)
z_c	: critical height (m)
z_{mi}	: mid-height of layer <i>i</i> (m)
z_s	: point source height (m)

Greek symbols

α	: thermal diffusivity (m ² /s)
β	: thermal expansion coefficient (1/K)
ρ	: air density (kg/m ³)
ρ_p	: particle density (kg/m ³)
ν	: kinematic viscosity of air (m ² /s)
ϵ_v	: ventilation effectiveness
ζ	: normally distributed number randomly generated
λ	: proportion of particles penetrating the thermal boundary layer
δ_w	: wall boundary layer thickness (m)
ξ	: transformation coordinate
η	: transformation coordinate
θ	: non-dimensional temperature
ψ	: stream function
ϕ	: index of the wall orientation
χ	: uni-directional horizontal jet decay
ΔT	: excess temperature which is the difference between the temperature inside the plume and its surrounding (K)
ΔT_o	: excess temperature at the plume centerline (K)

ΔT_{wa} : difference in temperature between the wall and the surrounding air

Subscripts

a : air
c : ceiling
sur : surrounding
d : deposition
ent : entrainment
ex : exposed
g : generation
f : floor
h : horizontal
i : layer number
in : inhaled
inf : infected
inj : injection
int : interaction
j : sub-microclimate 2 number
max : maximum
mac : macroclimate
mic : microclimate
p : particle
pl : plume
s : settling
v : vertical
w : wall

CHAPTER 1

INTRODUCTION

Indoor air quality (IAQ) is one of the major concerns of public health organizations [1, 2, 3] given that people nowadays spend the majority of their time inside residential and office buildings [4,5,6]. Epidemiological studies revealed significant relation between the particle pollution and people's mortality and morbidity where high particle concentration increases the risk of cardiovascular accidents, lung cancer, asthma and a variety of respiratory diseases [7,8,9]. Therefore, the breathable air quality in indoor spaces should be maintained high to avoid occupants' infection. The indoor particle dynamics depends largely on the air flow field associated with space air conditioning configuration [10]. The heating, ventilation, and air conditioning (HVAC) system should be designed to effectively remove particle contaminants in order to minimize infectious disease, while also providing thermal comfort at minimal energy consumption.

Recently, localized air conditioning has gained popularity as it locally provides the occupants needs minimizing energy costs [11,12,13]. Two main types of localized ventilation are present in the HVAC industry: vertical and horizontal localized ventilation where the space is divided into zones in the vertical and horizontal directions respectively. The most popular vertical localized system is displacement ventilation (*DV*) known for its effectiveness in providing high IAQ at a lower energy cost and widely used in office buildings [14,15,16]. Unlike conventional air conditioning systems, *DV* systems turn the air distribution upside down by supplying fresh air near the floor level at a low velocity of less than 0.2 m/s and temperature greater than 18 °C

to avoid thermal draft to occupants in the lower zone [15,17]. The relatively high *DV* supply temperature compared to conventional mixing ventilation (*MV*) limits its applicability to cooling loads lower than 40 W/m^2 [18,19]. Therefore, for higher loads other localized systems should be used.

Horizontal localized systems dividing the space horizontally into microclimates around the occupants surrounded by a macroclimate have captured the attention of many researchers [20,21]. In fact, localized airflows lead to temperature and particle concentration segregations with low air mixing between the microclimates and macroclimate which allow controlling the transmission of contaminated particles [13]. A recent type of horizontal localized flows consist on ceiling personalized ventilation (*CPV*) systems which are practical to use since they don't require additional installation cost and can be retrofitted to spaces ventilated by mixed ventilation (*MV*) systems of ceiling supply type [20,22].

In this work, the ability of vertical and horizontal localized systems in reducing cross-contamination between occupants in office spaces were investigated and new engineering strategies were proposed to enhance their performance. The effectiveness of *DV* system in removing contaminants from the occupied zone has been extensively studied in the literature especially when it comes to tracer gas contaminants that can be easily picked up by the rising thermal plumes [23,24]. Nevertheless, IAQ is not restricted to tracer gases such as CO_2 particles emanating from the occupants. If a clean occupied zone is desired, the particle concentration in the occupied zone should be determined for a wide range of particle diameters covering the inhalable range [25]. As the diameter of a particle increases, the gravitational effect increases acting against the upward air motion and thus challenging the performance of the *DV* system and

complicating the modeling of the particle transport inside the space. To our knowledge, previous simplified plume models simulating *DV* and thermal plumes have not separated emitting and non-emitting contaminant heat sources or non-equal strength heat sources. Non-equal heat sources induce different critical plume heights which influence the presence of particles in the zone between stratification height and plumes critical heights [24]. This is why most of the literature studies on active particle transport are conducted using computational fluid dynamics (CFD) models despite of their costly computational time [26-28]. Accurate prediction of particle deposition and transport using CFD for a flow field driven by buoyancy requires a fine mesh resulting in a significant simulation time [29]. Theoretical analysis relies on the understanding of the fundamental physics of the problem and on the proper choice of reasonable assumptions to simplify the complex problem. In addition, simplified models that capture physics have a small computational overhead and still form a crucial part of the design process [30]. Therefore, it is very important to extend the simplified *DV* models that were developed for the passive contaminants to include different heat sources as well as active particles that are largely present in indoor environments. Modeling transport of active particles is more challenging due to the drift flux term resulting from the gravitational settling effect representing the relative velocity between the particle and the airflow [31]. Furthermore, deposition on surfaces is a physical process that affects particle concentration and should be included in the modeling process [32].

DV was shown to be efficient in the removal of particles resulting from normal breathing since the thermal plumes rising from the infected occupants transport upward the majority of the exhaled particles due to their small horizontal momentum [33]. On the other hand, high momentum respiratory activities (HMRA) might reduce the

effectiveness of *DV* system in particle removal since they would spread particles horizontally at the breathing level [34,35]. This raises the need to understand the physics affecting horizontal spread of contaminants resulting from HMRA. Due to low momentum of exhaled jet during breathing, the vertical upward motion dominated particles distribution and horizontal interaction was limited to the entrainment process between the plumes and the surrounding [24]. Nevertheless, in order to model particle distribution resulting from other respiratory activities as coughing and sneezing gradients of concentration in the horizontal direction outside the thermal plumes [34,35] could not be neglected. The development of a transient simplified model of particle transport and distribution in *DV* spaces would be important to assess the risk of cross-contamination between occupants and arrive at proper recommendations for reduced internal exposure due to HMRA.

DV system is energy intensive since 100% fresh air is supplied. To improve the IAQ, source control of contaminants is the most effective method in mitigating pollutants levels and its effects on occupants. In order to compromise between IAQ criteria and energy consumption, innovative engineering solutions are needed. These solutions include the use of personalized ventilation (*PV*) devices to aid *DV* [15]. Watanabi et al. [36] investigated the thermal performance of a chair containing two fans at different locations: under the seat and behind the backrest. The fans were designed to supply isothermal forced airflow to the seated person. It was shown that the use of chair fans by the occupants allowed reaching acceptable thermal comfort even for room temperature as high as 30 °C. Nevertheless, to our knowledge the effectiveness of chair fans in terms of reducing cross-contamination between occupants was not investigated in literature. Assisting *DV* by chair fans (*CF*) is expected to enhance its performance in

terms of air quality and energy consumption by strengthening the rising thermal plumes and creating a micro-climate around the occupant.

Cross-infection between occupants can take place via different paths: direct inhalation and contact of contaminated surfaces. Infected persons release droplets that probably contain viruses or bacteria that may lead to infection of healthy persons by either direct inhalation [32] or indirectly via a contaminated surface-to-hand-to-mouth contact [37]. The majority of the previous studies on cross-contamination investigated the probability of infection due to the direct inhalation without regarding the indirect path via the contact of contaminated surfaces. Reducing locally the level of infectious agents in the inhaled air of occupants does not necessarily indicate a clean non-infectious environment for the office occupants. Pathogens such as bacteria and viruses can survive on surfaces for hours to days resulting in a higher probability of being transmitted to susceptible occupants [38-40].

Nowadays offices are becoming more crowded with occupants [41,42] with short distances separating the stations increasing the probability of respiratory cross-infection. Hence, cross-contamination is becoming a serious issue with increased occupational density and load per unit area challenging the use of *DV* for loads larger than 40 W/m^2 . In multi-station office space design, the distance between the workstations constitutes one of the main factors affecting direct and indirect cross-contamination. In conventional mixed ventilation systems (*MV*), the possibility of cross infection is controlled by increasing the distance between stations which would result in inefficient use of the space. Hence, when considering the layout of office spacing, a designer should take into consideration the need to minimize cross-infection with efficient use of the space by reducing dead space areas for both economic and energy

efficiency reasons. Therefore, there is a need to come up with new cooling and ventilation strategies for the proper design of a practical energy efficient air distribution system to reduce direct and indirect cross-contamination between work stations when placed close to each other compared to the conventional *MV* system. Ceiling personalized ventilation (*CPV*) systems assisted by desk or chair fans were found able to control the convective plumes emanating from the human body allowing the personalized air to reach the breathing level more effectively [22,43], but their ability to reduce cross-contamination between occupants was not investigated. The performance of *CPV* needs to be investigated and compared to conventional *MV* technique to identify the design parameters that will decrease direct and indirect cross-contamination of airborne particles at minimal distance between the workstations and optimize the design of the innovative *CPV* system. Furthermore, the shift in occupant design position might significantly degrade the *CPV* system performance. A seated occupant is most likely to move the chair position relative to the desk and will not always sit directly beneath the *CPV* jet. It is not clear how critical these shifts are on the *CPV* performance especially in crowded office spaces. A slight movement away from the desk would position the occupant breathing zone away from the *CPV* jet central clean air region. Therefore, the occupant shift effect on the performance of the *CPV* system assisted by *DF* or *CF* in terms of reduction of cross-contamination between occupants in addition to thermal comfort and ventilation effectiveness should be investigated.

The aim of this thesis is to investigate the ability of vertical localized *DV* and horizontal localized *CPV* in decreasing disease transmission between occupants in office spaces while insuring thermal comfort and inducing energy savings. Simplified models that can be used as design tools were developed to investigate the performance

of the standalone *DV* system, while CFD models were developed to study the performance of more complex configurations as *DV* and *CPV* equipped with fans. Experimental and literature data was used to validate the developed models. Parametric studies were conducted to optimize the design of the studied ventilation configurations for minimal cross-infection between the occupants.

1.1. Thesis Objectives

This thesis work aims towards investigating cross-contamination in indoor spaces in both vertical localizing *DV* and horizontal localizing *CPV* systems. Implementing new engineering strategies to the studied ventilation systems is expected to enhance their performance allowing to obtain acceptable IAQ with lower energy consumption. This thesis mainly focuses on the following objectives:

- Simulate by simplified modeling the behavior of particles generated by different respiratory activities in indoor environments ventilated by *DV* systems in order to come-up with recommendations to reduce the inter-personal exposure.
- Investigate the performance of *CF* equipped with *DV* system and optimize the fan flow rate for same level of IAQ with reduced energy consumption.
- Study the performance of *CPV* systems in minimizing particle dispersion and reducing both direct and indirect cross-contamination compared to conventional *MV*.
- Enhance the performance of the *CPV* system in terms of IAQ by assisting it with fans and optimize the design for safe increased occupational density.

- Investigate the occupant shift effect on the performance of the *CPV* system assisted by *DF* or *CF* in terms of reduction of cross-contamination between occupants in addition to thermal comfort and ventilation effectiveness.

The originality of this work consists on developing simplified models that can be used as a design tool to reduce cross-infection in *DV* spaces and simulate by CFD the effect of implementing fans to *DV* and *CPV* systems as innovative engineering strategies to reduce cross-infection between occupants with reduced energy consumption and more efficient use of the space.

CHAPTER 2

LOCALIZED VENTILATION FOR REDUCED CROSS-CONTAMINATION AND ENERGY SAVINGS

When designing an HVAC system, efficient energy use and good IAQ are one of the main concerns. However, enhancing the IAQ challenges the possibility of reducing the energy consumption. Engineers face a lot of constraints in compromising between decreased energy costs and increased quality of breathable air. Among the existing HVAC systems, localized ventilation systems have shown enhanced performance compared to traditional systems presenting a potential for reduced cross-contamination and energy savings in office spaces. In this chapter, a literature review on localized systems versus traditional HVAC systems is presented.

2.1. Mixed Ventilation Limitations

Mixed ventilation (*MV*) is the conventional HVAC configuration. *MV* consists on maintaining constant temperature and homogenous IAQ within the space [44-45] through mixing fresh and return air before their delivery by ceiling mounted inlets. Irrespective of the occupants' location, the space air temperature is nearly the same within the ventilated place since a single thermostat control it. *MV* had been widely used in residential and commercial buildings for its facility of installation and simplicity. Nevertheless, this ventilation technique presents many shortcomings. For instance, it suffers from inefficient fresh air delivery to the occupants because of its mixture with re-circulated air. Furthermore, as the temperature is uniform within the space, *MV* leads to unnecessary increment in the energy cost because it conditions both occupied and

non-occupied zones. To overcome these constraints, the concept of localized ventilation arises relying on the control of the environmental conditions in occupied zones.

2.2. Displacement Ventilation

Displacement ventilation (*DV*) system is one of the ventilation systems that is known for its effectiveness in providing high indoor air quality at a lower energy cost and is widely used in office buildings [46]. It creates a relatively clean occupied zone versus an upper mixed zone mitigating contaminated particles within the breathing level [19,47]. Unlike conventional air conditioning systems, *DV* turn the air distribution system upside down by supplying fresh air near the floor level at a low velocity of less than 0.2 m/s and temperature greater than 18 °C to avoid thermal draft to occupants in the lower zone. The air motion of a *DV* system is mainly triggered by buoyancy forces creating the rising thermal plumes capable of carrying the contaminant away from the occupant's zone [15]. This ventilation technique results in a stratification in the temperature which increases from the floor to the ceiling level due to the rising plumes leading to lower energy consumption compared to the conventional mixing ventilation system characterized by a homogeneous space temperature [16,48]. The temperature stratification in *DV* system always results in a positive temperature gradient and in having two zones: a lower air temperature occupied zone and a higher air temperature zone [15]. On the other hand, the contaminant floor-ceiling concentration profile depends largely on the relation between heat and contamination sources [49]. When heat sources are also the contamination sources, the rising convective thermal plumes (TP) emanating from the heat sources increase the ventilation effectiveness when using a *DV* system [16]. In such a system, the air entrained by the convective TP will be

warmed transporting the contaminants upwards towards ceiling where it is exhausted from the space [46].

The effectiveness of the *DV* in mitigating contaminants' concentration in the occupied zone has been thoroughly investigated particularly when considering tracer gas contaminants easily removed by the rising thermal plumes. For example, Mundt [23] studied the effect of the *DV* system supply air flow rate, the heat source load and the room gradient temperature on the tracer gases spread within the space. Kanaan et al. [24] developed a simplified model based on Mundt [23] model by combining all sources into single source with the purpose of determining the clean zone bounded by the stratification height at which the plume upward flow is equal to supply air flow. Kanaan et al. [24] determined carbon dioxide spread in spaces ventilated by chilled-ceiling *DV* and decided on the optimized fraction of the return air in the *DV* supplied air that insures good IAQ in the occupied zone.

Nevertheless, the *DV* system supplies cool and fresh air at the floor level to be spread over the whole occupied zone which is an energy intensive strategy. In order to decrease the energy consumption of the *DV* system, the supply flow rate is lowered such that the stratification height (defined as the level at which *DV* supply flow rate is equal to upward plumes flow rate) takes place just above the breathing level. Such a strategy worked well in keeping low CO₂ concentration at the breathing level [50] but might not be effective for active particles and contaminates. In fact, for dense particles as the size increases, the gravitational force on the particle increases, and the particle may not be effectively convected out of the occupied region by a rising plume, resulting in particle accumulation in the breathing zone. To improve the IAQ at the breathing level, source control of contaminants is the most effective method in mitigating pollutants levels and

their effects on occupants. Nielson et al. [51] has found that contaminants might stagnate between occupants near the stratification height increasing the risk of cross-contamination. Therefore, a solution to facilitate the upward motion of particles without the need to shift-up the stratification height should be found. For this reason, looking for a complementary system to be incorporated with *DV* to satisfy the thermal comfort and IAQ requirements while inducing energy savings is important.

2.2.1. *DV* Assisted by *CF*

Coupling fans with *DV* system has a potential in enhancing its performance in terms of improving breathable air quality. As occupants constitute one of the main sources of particles in indoor environments, the transport of particle by the infected TP should be enhanced. This can be achieved by increasing the strength of the infected plume and minimizing its interaction with the surrounding by blowing air flow from low level in the upward direction using *CFs* placed at the fronts of the seated person. On the other hand, the use of *CFs* in the same way might increase the protective effectiveness of the exposed plume by blowing relatively clean air upward.

However, Yuan et al. [19] found that the load removal of *DV* system was limited to $40\text{W}/\text{m}^2$ of floor area due to the constraint of thermal draft since cool air is supplied at low level. From here raise the need to look for other localized systems when relatively higher cooling loads are involved.

2.3. Ceiling Personalized Ventilation

Interest in *PV* has increased since it locally provides the occupants cooling and fresh air needs while minimizing energy costs [11]. Different types of *PV* systems were

studied in literature [11,52] and were found to enhance the IAQ when used in conjunction with various HVAC configurations such as mixing, displacement and under floor ventilations [53-56]. The majority of original *PV* systems are desk-mounted systems [11,52]. However, this type of task ventilators is costly since it requires extending ducting system of the task ventilators into the occupied zone (for example, the raised floor system) [57]. A recent type of localized systems consisting of *CPV* systems were considered as practical to use since they do not require additional installation cost and can be retrofitted to spaces ventilated by *MV* systems of ceiling supply type [20,57]. Furthermore, *CPV* presents the advantages of higher furniture layout flexibility and improvement in indoor aesthetics [57]. Yang [57] proposed to integrate ceiling single core jets to conventional *MV* systems in which the *CPV* delivers fresh air while the conventional diffuser supplies re-circulated air. However, this system presented a limited efficiency because of the short propagation length of the *CPV* fresh air jet [20,57]. The *CPV* proposed by Yang [20,57] has better practicality than original personalized ventilation systems but limited effectiveness; nonetheless it is better than conventional *MV*.

Placing the personalized ventilator at the ceiling level is more challenging than placing it near the occupant (desk-mounted *PV* system) as the jet may entrain contamination before reaching the breathing zone and should overcome the opposing rising human TP to effectively reach the occupant. For the *CPV* nozzle to be effective the fresh air of the *PV* jet should reach the occupant's breathing zone with minimal entrainment of contaminated room air and it should have sufficient terminal velocity to penetrate the occupant's free convective plumes. Melikov [58] investigated the benefit of airflow interaction control in the human body micro-environment for enhancement of

thermal comfort and inhaled air quality. In ceiling mounted jets, the convective plumes emanating from the occupant's body reduces the effective delivery of fresh air to the occupant's breathing zone. Desk personalized coaxial jets tested by Khalifa et al. [59,60] showed an improved performance by lengthening the potential core region and delivering fresh air more effectively. Besides, Bolashikov [61,62] showed that desk mounted fans were able to control the convective plumes emanating from the human body when using *PV* nozzles mounted on the desktop leading to more efficient fresh air delivery.

Makhoul et al. [21] proposed an innovative *CPV* design to enhance the performance of standalone *CPV* systems [21,63,64]. The system consisted of ceiling coaxial *PV* jets delivering clean air effectively by lengthening the potential core region at the center of a peripheral angled diffuser creating a canopy localizing the flow around the occupant. However, coaxial nozzles presented the disadvantage of requiring additional ducting system and difficulty of control of two jets of equal velocities.

2.3.1. CPV Assisted by DF versus CF

To overcome the constraints of the coaxial system, a practical design to control the convective plumes consisted of assisting the *CPV* nozzle by fans that could be mounted in the desk or the chair position for suction of the TP emanating from the human body [22,43]. Makhoul et al. [22] proposed to aid the single *CPV* jet of Yang et al. [57] with *DF* which were able to control the convective plumes emanating from the human body allowing the personalized air to reach the breathing level more effectively. The reduction of the convective plumes around the occupant allowed the free jet to penetrate the TP and reach the occupant with less mixing with the surrounding air [22].

The *CPV* system assisted by *DF* proposed by Makhoul et al. [22] provides the occupant with control of its own microclimate environmental conditions by changing the *PV* jet conditions (temperature and flow rate) and re-circulated canopy temperature.

Furthermore, the occupant can tune his personalized comfort by adjusting the flow rate of the *DF* [22].

Makhoul et al. [22] studied extensively their proposed system in terms of thermal comfort, ventilation effectiveness and energy savings. They examined the segmental comfort of the different body parts since local draft might present a risk on thermal comfort depending on operating conditions of the *CPV* jet assisted by *DF* [22]. Furthermore, Makhoul et al. [22] performed an energy analysis to reveal the energy savings provided by his proposed system compared to *MV* under equal thermal comfort and ventilation effectiveness. He found relatively high energy savings up to 13.25% when the *DF* was operated despite of the additional power consumption induced by the operation of the fan. Therefore, the *CPV* system assisted by *DF* overcame the complexities of the original system while insuring effective *CPV* jet delivery and energy savings. Similarly El-Fil et al. [43] showed that the operation of *CF* at its optimal configuration led to considerable energy savings of 17%.

Nevertheless the work of Makhoul et al. [22] and El-Fil et al [43] was constrained with the assumption of fixed occupant position which would not be the case based on human behavioral and desk activity. Furthermore, their work was restricted to one station office where the occupant was directly seated beneath the *CPV* jet and did not consider the effectiveness of these systems in reducing cross-infection by particle transport towards the exposed occupant breathing zone. The shift in occupant design position might significantly degrade the *CPV* system performance. A seated occupant is

most likely to move the chair position relative to the desk and will not always sit directly beneath the *CPV* jet. It is not clear how critical these shifts are on the *CPV* performance especially in crowded office spaces. A slight movement away from the desk would position the occupant breathing zone away from the *CPV* jet central clean air region. In this situation, the performance of the *CPV* system assisted by *DF* or *CF* should be evaluated for reduction of cross-contamination between occupants in addition to thermal comfort and ventilation effectiveness.

2.4. Exhaled Contaminants Contributing to Cross-Infection

With the increased time spent by people in indoor environments and the outbreaks of the Severe Acute Respiratory Syndrome (SARS) [5] a lot of concerns have been raised on people health in indoor environments, particularly on the control and possible prevention of airborne disease transmission [2]. Humans generate particles by the different respiratory activities (talking, breathing, sneezing, and coughing) [65] and through emissions from the skin, hair, and clothes etc. [66]. Exhaled droplets produced by the different human respiratory activities constitute one of the main sources of infectious particles in indoor environments [33,67,68]. Respiratory patterns can be categorized into LMRA (breathing) [69,70] and HMRA (coughing, and sneezing) [27,71]. Since breathing is the most frequent respiratory activity, it significantly contributes to the possibility of disease transmission between occupants. On the other hand, despite their limited period, HMRA also present a high risk of cross-contamination [72] due to higher penetration length of the exhalation jet and larger number of particles it carries [34,73].

Human exhaled droplets are subject to fast evaporation before reaching their equilibrium diameter of droplets nuclei [65,67,74]. In many cases, these emitted particles (droplets after evaporation) become airborne and can spread within the space before being escaped, deposited or inhaled by other healthy occupants [26,74,75].

In order to insure good IAQ both gas-phase (e.g. CO₂) and particle contaminants should be considered [76]. Suspended particles carry and transport bacteria and viruses leading to cross-infection between the occupants. Particle sizes can be categorized into three modes depending on their size [10]: ultrafine (diameter lower than 0.1 μm); accumulation (diameter between 0.1 and 2 μm); and coarse (diameter higher than 2 μm). Gas-phase contaminants and fine particles can be treated as passive since they are easily carried by the airflow while coarse particles are active since the gravitational settling affect particle motion. The indoor particle dynamics depends largely on their diameter (size) and the air flow field associated with space air conditioning system. Therefore the HVAC design plays a major role in removing exhaled contaminants and reducing cross-contamination between occupants.

CHAPTER 3

ANALYTICAL AND NUMERICAL METHODS

Analytical and numerical methods used in this work are detailed in this chapter. Simplified models were developed to study the performance of standalone *DV* system using empirical correlations developed in literature, thermodynamics laws and conservation of mass and energy as described in section 3.1. CFD modeling was adopted for complex flow configurations as *DV* assisted by *CF* and *CPV* systems as detailed in section 3.2.

3.1. Simplified *DV* Model

3.1.1. *Description of the Problem*

The developed physical model predicts the temperature, velocity and concentration fields within a space ventilated by a *DV* system focusing on cross-contamination between occupants and including particle deposition. Chen et al. [74] found that when the normalized evaporation time is lower than 0.051 which is the case for initial particle diameter below 100 μm , the evaporation time can be neglected in the modeling. Hence, the evaporation process is neglected and exhaled droplets (after complete evaporation) are referred to as particles with equilibrium diameters. In order to capture the vertical motion of the air surrounding the TP and the convective buoyant flows effect, the domain is discretized into horizontal layers with several lumped regions within each layer (Fig 3.1). Vertically three main zones are identified:

- Zone I which is characterized by upward flow in the air surrounding the thermal plumes extending from the floor to the stratification height defined

as the height at which the total upward convective flow equals the supply flow rate [47,77];

- Zone II is bounded by the stratification and critical height where rising plumes expand [78]
- Zone III is a recirculation zone where TP and air circulating between them merge together [78].

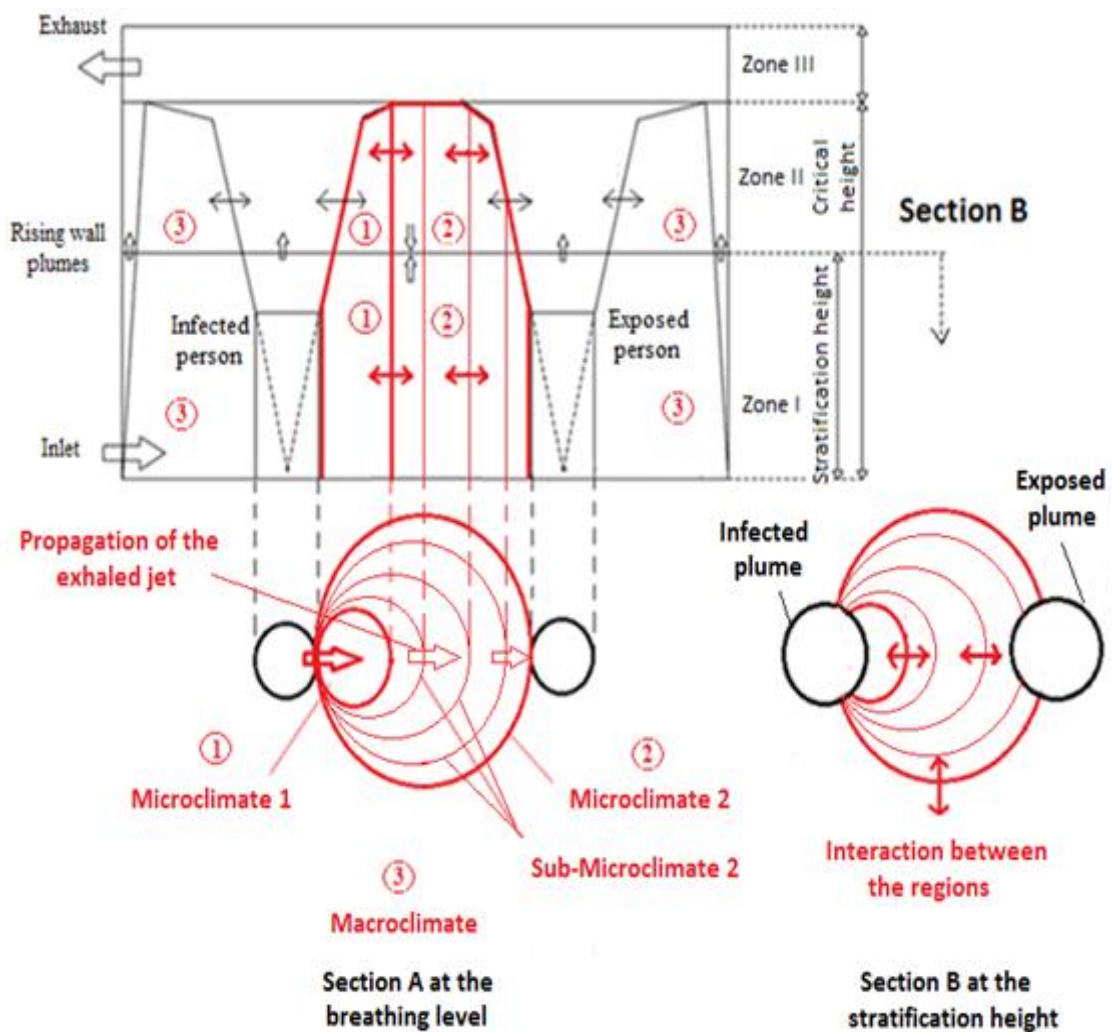


Fig.3.1: Spatial discretization of the space ventilated by the *DV* system.

The air surrounding the plumes was divided into three regions (two microclimates and one macroclimate) to capture the horizontal gradients in concentration created by the horizontal exhaled flow [51,79]:

- Infected plume zone associated with the contaminated person
- Exposed plume zone associated with the healthy person
- Microclimate 1: a cylindrical region tangent to the infected person from the side of particle penetration limited by the plume expansion at the critical height extending along zone I and zone II. The cross-sectional area of this region is reduced as the infected plume expands. This region represents the contaminated zone resulting from particles penetrating the thermal plumes.
- Microclimate 2: a cylindrical region tangent to the occupants limited by their rising plumes until their expansion extending along zone I and zone II. The diameter of this region is equal to the distance between the occupants. The cross-sectional area of this zone is reduced as the infected and exposed plumes spread. This zone is of interest to determine the exposure-risk due to cross- contamination between the occupants.
- Macroclimate region: this zone surrounds the microclimate regions and the thermal plumes extending along zone I and zone II.

When particles are exhaled by an occupant a portion is transported by the rising human thermal plume while the remaining portion penetrates it (Fig. 3.2). These portions depend on the momentum of the exhaled jets. When LMRA are considered the penetrating portion is negligible therefore no significant concentration gradients are observed between microclimate 1,2 and the macroclimate which can be lumped in one

region. On the other hand, when HMRA are investigated, the exhaled jet is highly unidirectional propagating and decaying with time from the infected to the exposed occupants leading to considerable horizontal gradients within the microclimates. In order to capture the transient propagation of the exhaled jet and to assess accurately the exposure risk, microclimate 2 is discretized into several tangent cylindrical sub-microclimates zones (Fig. 3.1).

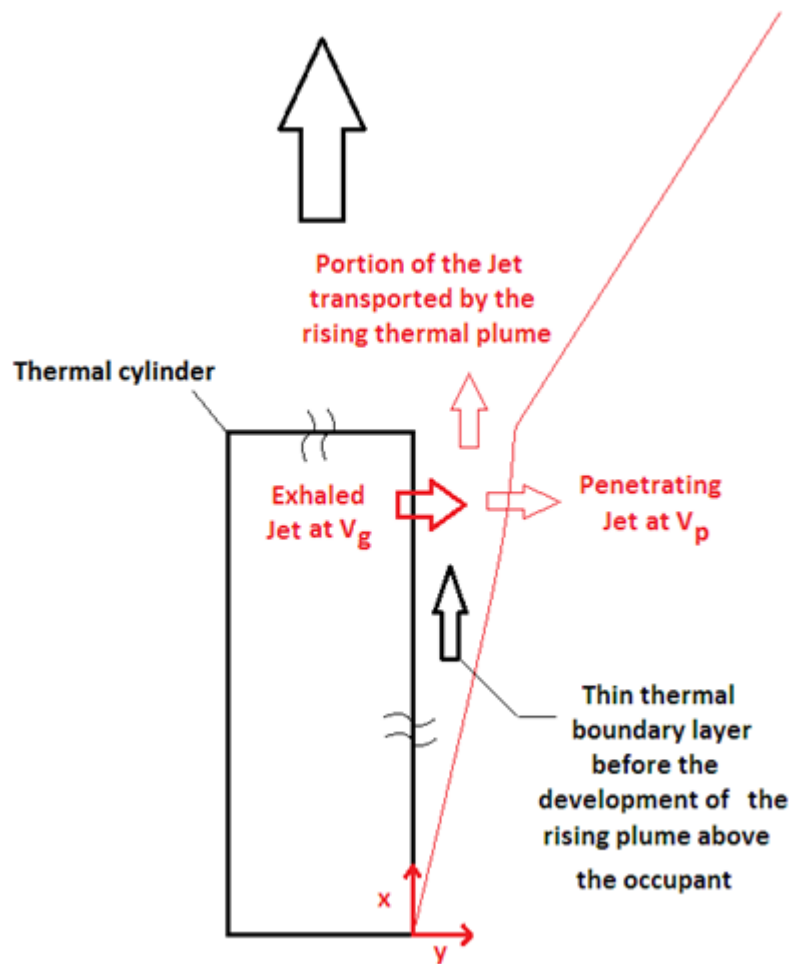


Fig.3.2: Penetration of the horizontal jet through the thermal boundary layer

In order to compute particle distribution within the DV space, two sub-models should be coupled. A transport model of exhaled particles computes the percentage of generated particles penetrating the infected thermal plume, and tracks the exhaled jet propagation with distance and time when transient respiratory activities (as sneezing and coughing) are considered. This model is coupled with another transport model for particles' behavior and exchange between the different affected zones.

3.1.2. Mathematical Formulation

3.1.2.1. Plumes Flow Rates

In order to determine the particle distribution within the ventilated space, it is important to establish the flow field in the room. In DV systems, lateral air motion is neglected compared to vertical flow in the region below the recirculation zone. The resulting stratification and critical heights are determined by the strength of the internal thermal plumes and the DV system air flow rate. The rising plumes air flow rates are found from the plume model of Mundt [47] as follows:

$$M_{pl} = 2.38 * 10^{-3} \rho Q_H^{3/4} \left(\frac{dT_\infty}{dz} \right)^{-5/8} m_n \quad (3.1.a)$$

$$m_n = 0.004 + 0.039z_n + 0.38z_n^2 - 0.062z_n^3 \quad (3.1.b)$$

$$z_n = 2.86 * z_s \left(\frac{dT_\infty}{dz} \right)^{3/8} Q_H^{-1/4} \quad (3.1.c)$$

where ρ is the air density, T_∞ the room temperature, z_s the point source height, Q_H the heat source strength, and m_n , and z_n non-dimensional parameters. The mass flow rate entrained by a thermal plume within a horizontal layer i , $M_{ent,i}$, is given by:

$$M_{ent,i} = M_{pl,i} - M_{pl,i-1} \quad (3.1.d)$$

where $M_{pl,i-1}$ is the plume mass flow rate entering layer i and $M_{pl,i}$ is the plume mass flow rate exiting layer i .

Cylindrical heat sources are replaced by a virtual point source such that the border of the plume above the point source passes through the upper edge of the real cylindrical source [80] with half-angle of lateral spread of 12.5° [81-83]. Hence, the plumes expansion geometry can be easily computed allowing the determination of the required minimum distance between any two internal heat sources to be considered non-interactive. The wall plume flow rate, M_w , at level z above the floor is determined by Jaluria [84] expression:

$$M_w = 2.87 * 10^{-3} \rho (\Delta T_{wa})^{1/4} z^{3/4} X \quad (3.1.e)$$

where X is the wall width and ΔT_{wa} is the difference in temperature between the wall and the surrounding air.

A mass balance for each horizontal layer gives the expression of the mass flow rate of the surrounding air $M_{a,i}$ as:

$$M_{a,i} = M_s - \sum_{j=1}^n M_{w,(i,j)} - \sum_{k=1}^m M_{pl,(i,k)} \quad (3.1.f)$$

where n refers to the vertical walls number within a layer i , and m to the number of remaining rising plumes, M_s is the mass supply flow rate, $M_{a,i}$, $M_{w,(i,j)}$, $M_{pl,(i,k)}$, are respectively the mass flow rates of the surrounding air, the wall plumes and the internal thermal plumes at the interface between layers i and $i+1$.

The rising plume mathematical expressions of Mundt [47] and Jaluria [84] depend on the temperature field within the room which was determined using the thermal space model developed by Makhoul et al. [85]. The required input parameters for this model are the outdoor conditions, wall layering, properties and strengths of the

internal heat sources. Makhoul et al. [85] took into consideration the different physical processes (as convection, conduction...) affecting the thermal field in order to determine the external and internal wall temperatures and the convective coefficients. The temperature variation within the space was determined by solving the energy balances for the different layers taking into consideration the different lumped regions within each layer. Hence, the vertical temperature gradient within the space was determined and then used in the calculation of the air, wall and plume flow rates within the different regions.

3.1.2.2. Modeling of Particle Distribution

The model should be able to capture the principal physics affecting particle behavior which, in addition to convection and deposition, include drag, gravitational settling, and turbulent and Brownian diffusion. Brownian and turbulent diffusion affect significantly particle behavior within the concentration boundary layer affecting particle deposition, and hence they are accounted for in the current model in addition to drag and gravitational settling effect. Other mechanism that affect particle dispersion exist such as Basset history, virtual mass, pressure gradient forces, thermophoresis, turbophoresis, electrophoresis, and virtual mass forces [31,86,87]. These mechanisms are reported to be one to several order of magnitudes smaller than the drag and gravitational forces hence they are neglected in the current model [31,32,87-89]. Since temperature gradients in *DV* conditioned spaces are relatively small (less than 10 °C), thermophoresis can be neglected [89].

3.1.2.3. Modeling of Particle Deposition

Deposition on surfaces is a determinant factor in the behavior of active particles and should be appropriately modeled. Boundary deposition fluxes J_d of particles towards the walls is determined from the expression of deposition velocities established by Lai & Nazaroff [32] as:

$$J_d(y=0) = v_d C_\infty \quad (3.2.a)$$

where v_d is the deposition velocity on the corresponding wall, C_∞ is the core concentration outside the concentration boundary layer which in the current case is equal to the surrounding air concentration $C_{a,i}$ which vary with each horizontal layer i , and y is the distance from the wall. Lai & Nazaroff [32] determined the expression of deposition velocities including the Brownian and turbulent diffusion in addition to the gravitational settling effect on particle behavior for walls of different orientations ($\phi=0$ for vertical wall, $\phi=1$ for floor, $\phi=-1$ for ceiling):

$$J_d = -(\varepsilon_p + D) \frac{\partial C}{\partial y} - \phi v_s C \quad (3.2.b)$$

where ε_p is the turbulent diffusivity, D is the Brownian diffusivity C is the concentration within the momentum boundary layer and v_s the settling velocity defined by:

$$v_s = \frac{\rho_p d_p^2 g}{18\mu} \quad (3.2.c)$$

The turbulent diffusion is assumed to equal the turbulent kinematic viscosity of the air as indoor flow conditions and particle diameter range insure that the particle relaxation time does not exceed the value for which this assumption is valid.

The expression of the air turbulent kinematic viscosity as a function of y is determined by direct numerical simulation within the three momentum boundary sub-layers allowing to determine the deposition velocities as a function of the settling velocity v_s , the friction velocity u^* , and the integral number IN obtained by integrating equation (3.2.b) within the three momentum boundary sub-layers [32]:

$$IN = 3.64Sc^{2/3}(a - b) + 39 \quad (3.2.d)$$

$$a = \frac{1}{2} \ln \left[\frac{(10.92Sc^{-1/3} + 4.3)^3}{Sc^{-1} + 0.0609} \right] + \sqrt{3} \arctan \left[\frac{8.6 - 10.92Sc^{-1/3}}{10.92\sqrt{3}Sc^{-1/3}} \right] \quad (3.2.e)$$

$$b = \frac{1}{2} \ln \left[\frac{10.92Sc^{-1/3} + r^+)^3}{Sc^{-1} + 7.669e^{-4}(r^+)^3} \right] + \sqrt{3} \arctan \left[\frac{2r^+ - 10.92Sc^{-1/3}}{10.92\sqrt{3}Sc^{-1/3}} \right] \quad (3.2.f)$$

Hence, the expressions of the deposition velocities on a vertical wall v_{dv} , on the floor v_{df} , and on the ceiling v_{dc} are respectively obtained for $\phi = 0$, $\phi = 1$ and $\phi = -1$:

$$v_{dv} = \frac{u^*}{IN} \quad (3.2.g)$$

$$v_{df} = \frac{v_s}{1 - \exp\left(\frac{-v_s IN}{u^*}\right)} \quad (3.2.h)$$

$$v_{dc} = \frac{v_s}{\exp\left(\frac{v_s IN}{u^*}\right) - 1} \quad (3.2.i)$$

Lai & Nazaroff [32] formulation has been adopted in the current model and an average friction velocity of 1.5 cm/s was used which is within indoor environments reported values between 0.3 and 3 cm/s. The sensitivity of the predicted particle concentration to friction velocity within the indoor range was assessed by performing many simulations and the validity of this selected average value was verified when validating the model with published data from the literature.

3.1.2.4. Transport Model of Exhaled Particles

When considering the case of generation of particles within the plume at high momentum in the horizontal direction (as coughing or sneezing), a portion of the exhaled particles penetrates the plume constituting a source of particles within the first microclimate zone.

It is necessary to determine the proportion of particles penetrating the infected plume and the interaction terms between the different designated regions so that particle dispersion at the horizontal level i is accurately modeled. In the generation layer, particles spread horizontally from the thermal plume to the microclimate 1 by convection resulting from the proportion of the horizontal exhaled jet flux that penetrates the plume. Then particles diffuse from microclimate 1 to microclimate 2 by convection and Brownian diffusion.

As the rising plume constitutes a barrier to the propagation of the generated jet, only a portion of the exhaled flow penetrates to the surrounding (Fig. 3.2). This portion can be determined from the definition of the coefficient λ relating the generated flux (Q_g) to the penetrating flux (Q_{pen}) given by:

$$Q_{pen} = \lambda Q_g \quad (3.3.a)$$

This portion λ can be determined by the ratio of the penetrating velocity V_{pen} to the generation velocity V_g . In fact, as the exhaled jet gets away from the mouth it expands [90]. However, the thickness of the developing thermal plume at the mouth level is very thin (of the order of millimeters) [91] thus the penetrating area is nearly equal to the generating area. Therefore λ is given by:

$$\lambda = \frac{Q_{pen}}{Q_g} = \frac{A_{pen} V_{pen}}{A_g V_g} = \frac{V_{pen}}{V_g} \quad (3.3.b)$$

To determine the penetration velocity, we should solve for the velocity field for the developing boundary layer at the thermal cylinder surface inducing the rising thermal plume above the heated cylinder. The thermal cylinder boundary layer can be treated as a vertical heated flat plate since the cylinder diameter (D) to length (L) ratio satisfies the following condition [92]:

$$\frac{D}{L} \geq \frac{35}{Gr_L^{1/4}} \quad (3.4)$$

where Gr_L is the Grashof number at the cylinder height L . The thermal boundary layer is then derived from the coupled two-dimensional equations of continuum, momentum, and energy [93] given respectively by:

$$\frac{\partial u}{\partial x} + \frac{\partial v}{\partial y} = 0 \quad (3.5.a)$$

$$u \frac{\partial u}{\partial x} + v \frac{\partial u}{\partial y} = \nu \frac{\partial^2 u}{\partial y^2} + g\beta(T - T_\infty) \quad (3.5.b)$$

$$u \frac{\partial T}{\partial x} + v \frac{\partial T}{\partial y} = \alpha \frac{\partial^2 T}{\partial y^2} \quad (3.5.c)$$

where x and y are the vertical (upward) and horizontal coordinates respectively (Fig. 3.2) and u and v are the velocity components corresponding to these directions, T is the temperature, ν is the kinematic viscosity of air, g is the gravitational constant, β is the thermal expansion coefficient used for the Boussinesq approximation, and α is the thermal diffusivity. The associated velocity and thermal boundary conditions are given by:

$$u(x,0) = u(x,\infty) = 0 \quad (3.6.a)$$

$$v(x,0) = V_g \text{ for } x_{gb} \leq x \leq x_{ge} \quad (3.6.b.1)$$

$$v(x,0) = 0 \text{ elsewhere} \quad (3.6.b.2)$$

$$T(x,0) = T_0 \quad (3.6.c.1)$$

$$T(x,\infty) = T_\infty \quad (3.6.c.2)$$

where $u(x,\infty)$ is the upward velocity in the surrounding air but it is considered negligible due to the low momentum of the DV system flow compared to rising flows by natural convection ($Gr/Re^2 \gg \gg 1$) [94]. The exhaled velocity of particle generation is V_g , x_{gb} and x_{ge} represent the coordinates of beginning and end of the generation, the average skin temperature is T_0 , and the average air temperature around the heated cylinder T_∞ is obtained from the thermal model. These parameters are used as inputs for the exhaled particles' transport model.

A two dimensional stream function $\psi(x, y)$ can be used to transform the problem into integral form since it satisfies the continuity equation and allows solving the momentum equation for one variable (ψ) instead of two variables (u and v). Once the differential equations are solved the velocity of penetration V_{pen} can be determined as:

$$V_{pen} = -\frac{\partial \psi}{\partial x}(x_g, \infty) \quad (3.7.a)$$

The stream function is defined by [95]:

$$\psi = -\int_0^x v(x,0)dx + F(x, y) \quad (3.7.b)$$

with:

$$F = v(4\xi)^{3/4} f(\xi, \eta) \beta^{-1/2} \Delta T^{-1/2} \quad (3.7.c)$$

The non-dimensional temperature is given by:

$$\theta(\xi, \eta) = \frac{T - T_\infty}{T_w - T_\infty} \quad (3.7.d)$$

where ξ and η are transformation coordinates and are given by [95]:

$$\xi = \beta \left(\frac{g}{\nu^2} \right)^{1/3} \Delta T L \quad (3.7.e)$$

$$\eta = \beta^{1/2} \left(\frac{g}{4^{3/4} \nu^2} \right)^{1/3} \Delta T^{1/2} y \xi^{-1/4} \quad (3.7.f)$$

Then, the mass, momentum and energy equations are transformed using equations (3.7.b to 3.7.f) to a set of two coupled ordinary differential equations (ODE) [95] (3.8.a for the velocity field, and 3.8.b for the temperature field) that can be solved by the finite volume technique.

$$f''' + 3ff'' - \gamma f'' - 2f'^2 + \theta = 4\xi \left[f' \frac{\partial f'}{\partial \xi} - f'' \frac{\partial f}{\partial \xi} \right] \quad (3.8.a)$$

$$\frac{\theta''}{Pr} + 3f\theta' - \gamma\theta' = 4\xi \left[f' \frac{\partial \theta}{\partial \xi} - \theta' \frac{\partial f}{\partial \xi} \right] \quad (3.8.b)$$

where Pr is the Prandtl number and

$$\gamma(\xi) = \nu(x,0) \left[\frac{4\xi \left(\frac{\nu^2}{g} \right)^{1/3}}{g\beta^2 \nu^2 \Delta T^2} \right]^{1/4} \quad (3.8.c)$$

The associated boundary conditions are:

$$f'(\xi,0) = f(\xi,0) = f'(\xi,\infty) = \theta(\xi,0) = 0 \quad (3.8.d)$$

$$\theta(\xi,0) = 1 \quad (3.8.e)$$

3.1.2.5. Transient Propagation of the Exhaled Jet

In order to model particle spread resulting from coughing or sneezing, the transient propagation of the exhaled jet should be accurately modeled.

A top-hat profile was used for the generation velocity [71,96]:

$$\begin{aligned} V_{gen}(t) &= V_g && \text{if } t \leq t_{rl} \\ V_{gen}(t) &= 0 && \text{if } t > t_{rl} \end{aligned} \quad (3.9.a)$$

where $V_{gen}(t)$ is the generation velocity function of time, V_g is the generation velocity during the cough and t_{rl} is the cough release time. Chen et al. [97] modeled transient propagation of high momentum jets and validated their model for different ventilations configurations. Chen formulation [97] is used in the current study and is summarized below.

The horizontal jet peak V_{max} decreases with the horizontal coordinate y from the source and is a function of the injection velocity V_{inj} and the hydraulic diameter of the mouth d_{inj} . V_{max} is given by the following expression [97]:

$$\begin{aligned} V_{max}(y) &= V_{inj} && \text{if } y < 6.8d_{inj} \\ V_{max}(y) &= \frac{6.8d_{inj}V_{inj}}{y} && \text{if } y \geq 6.8d_{inj} \end{aligned} \quad (3.9.b)$$

The propagation jet is stopped by an obstruction (e.g. wall, exposed occupant) or damped when the jet peak becomes lower than a reference velocity of 0.25 m/s [97]. Thus, the maximal propagation distance y_{max} is given by:

$$y_{max} = \min\left(y_{ob}; \frac{6.8d_{inj}V_{inj}}{V_r}\right) \quad (3.9.c)$$

where V_r is the reference velocity and y_{ob} is the obstruction distance.

The time needed by the jet to reach a position y is given by [97]:

$$t_{tr}(y) = \int_0^y \frac{1}{V_{\max}(y)} dy = \frac{6.8d_{inj}}{V_{inj}} + \frac{y^2 - (6.8d_{inj})^2}{13.6V_{inj}d_{inj}} \quad (3.9.d)$$

The decay of the velocity with time after the jet had reached a certain distance y along the unidirectional propagation line [97] (for y between 0 and y_{max}) is given by:

$$V(y,t) = V_{\max}(y)e^{-t/\tau} \quad (3.9.e)$$

where τ is the time constant given by the following expression [97]:

$$\tau = \int_0^{y_{\max}} \frac{1}{V_{\max}(y)} dy = \frac{6.8d_{inj}}{V_{inj}} + \frac{y_{\max}^2 - (6.8d_{inj})^2}{13.6V_{inj}d_{inj}} \quad (3.9.f)$$

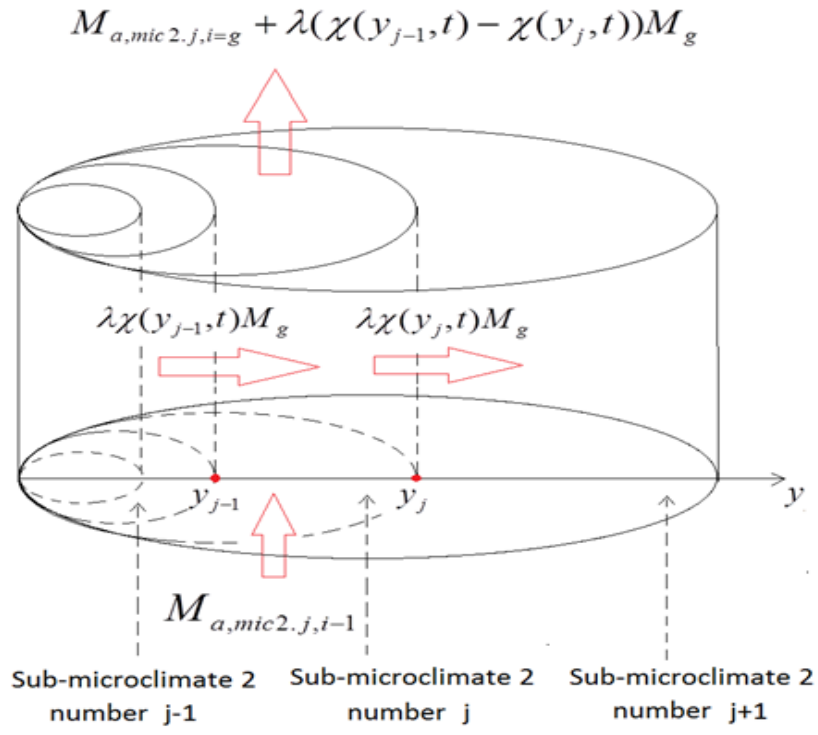
The unidirectional horizontal jet decay $\chi(y,t)$ along the propagation line (illustrated in Fig. 3.3) can be computed from:

$$\chi(y,t) = \frac{V(y,t)}{V_{inj}} = \frac{V(y,t)}{V_{pen}} = \frac{V(y,t)}{\lambda V_g} \quad (3.9.g)$$

where V_{inj} is the penetrating velocity computed from the exhaled particles model. In fact, the upward plume of the infected person obstructs the propagation of the generated jet, thus the exhaled flow does not penetrate completely to the surrounding. The penetrating portion λ can be determined by resolving for the Navier-Stokes equations within the thermal boundary to compute the penetrating velocity V_{pen} .

The propagation of the exhaled jet with time and distance affects the upward DV flow within each zone such that mass balances are conserved. The variation with time of the horizontal flow entering a sub-microclimate 2 number j ($\lambda\chi(y_{j-1},t)M_g$) is different from the horizontal exiting flow ($\lambda\chi(y_j,t)M_g$) due to the time delay and flow decay resulting from the jet propagation. The difference between the horizontal entering and exiting flows is compensated by the vertical air motion within the surrounding air.

Convective flows through a sub-microclimate 2 number j within the generation layer are illustrated in Fig. 3.3.



**Propagation of the exhaled jet
with distance and time**

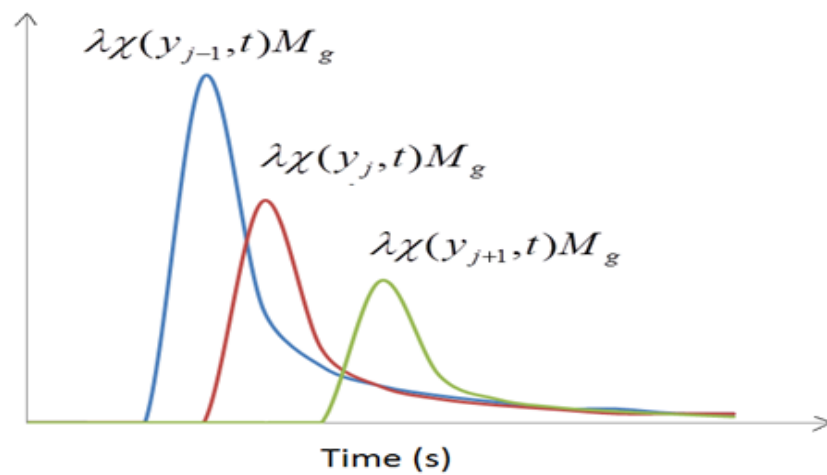


Fig. 3.3: Convective flows through sub-microclimate 2 number j within the generation layer

3.1.2.6. Transient Zonal Model for Particle Distribution

The transient formulation of the jet propagation is used as boundary conditions for the transient multi-zonal model for spaces ventilated by *DV* system to predict particle spread resulting from human generation by different respiratory activities. In order to predict the concentration field in the different vertical zones and lumped horizontal regions, the variable physical phenomena affecting particle distribution within the space were included in the model. Fig. 3.4 illustrates the different physics determining particles' behavior and the interaction between a rising thermal plume and the surrounding air due to lateral diffusion flux and room air entrainment by the thermal plume. Convection and diffusion within each region are presented by the vertical convective and diffusive fluxes. In addition, since active particles are considered, gravitational effect and particle deposition on walls are included in the model (see Fig. 3.4).

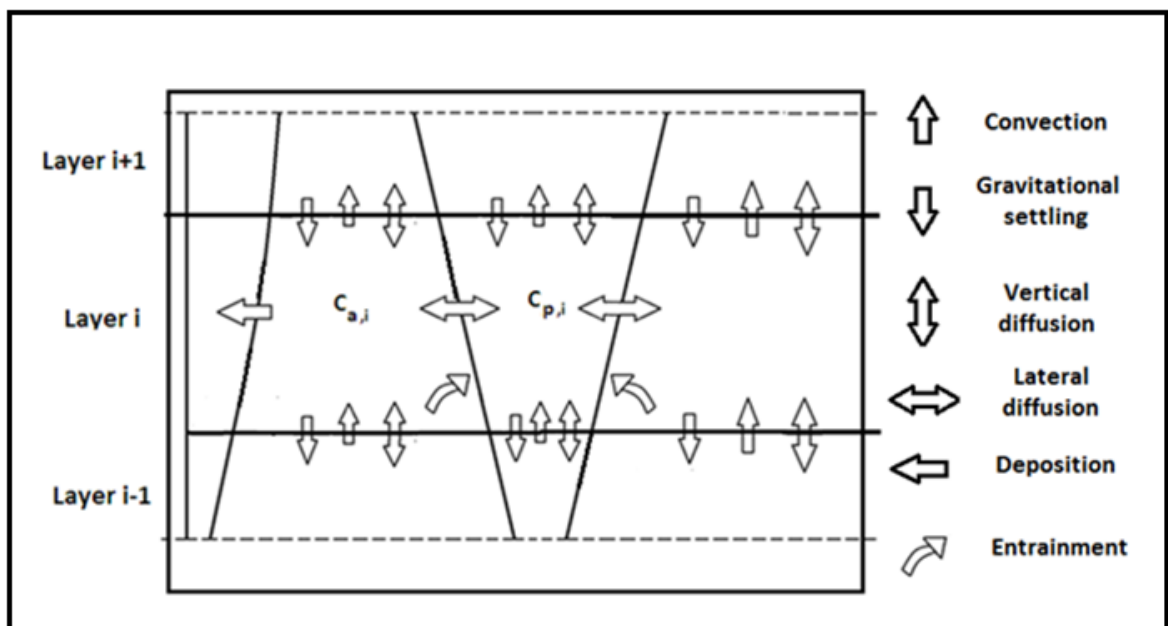


Fig. 3.4: Representation of the physical phenomena affecting the contaminant concentration within a layer i

3.1.2.7. Particle Distribution within the Thermal Plumes

The spread of particles within the space is largely dependent on the buoyant flows, gravitational effect and interaction between the surrounding air and the different internal plumes. To develop the particles' mass conservation equation, the interactive diffusion between the thermal plume and its surrounding should be known. To this end, the parabolic particle profile developed by Kanaan et al. [24] was used in the current model:

$$c_{pl,i} = a_i + b_i \left(\frac{r}{R} \right)_i + c_i \left(\frac{r}{R} \right)_i^2 \quad (3.10.a)$$

The constants a_i , b_i and c_i are determined for each layer i from the contaminant mass balances and concentration profile boundary conditions. At the thermal plume centerline the concentration gradient within each layer i is equal to zero ($b_i = 0$) and at the boundary between the thermal plume and the surrounding air there is continuity of the contaminant concentration.

The mean value of the concentration $C_{pl,i}$ at the mid-level of a layer i can be related to the coefficients a_i and c_i [24] through the following expression:

$$C_{pl,i} = \frac{\int_0^{R_i} c_{pl,i} V_{pl,i} r dr}{\int_0^{R_i} V_{pl,i} r dr} \quad (3.10.b)$$

Morton et al [82] observed that heat sources of different shapes give a Gaussian shaped plume above them. The airflow velocity V_{pl} profile inside the plume is also of Gaussian type and is governed by the following equations [98]:

$$V_{pl}(r, h) = V_0(h) \exp \left[- \left(\frac{r}{R} \right)^2 \right] \quad (3.10.c)$$

where R is the radius of the plume at a certain level, and r the radial coordinate from the centerline of the plume, h the height above the heat source, and V_0 the velocity of the airflow at the plume centerline.

Once the concentration profile in the rising plumes is determined, the variation of particle concentration within each of the non-interactive internal thermal plumes should be determined as they interact with the surrounding air and affect the particle distribution within the space.

3.1.2.8. Mass Balances for the Different Zones

3.1.2.8.1. Infected Plume Zone

The infected plume zone interacts with the microclimate zones 1 and 2 and the macroclimate as shown in Fig. 3.1. The particle concentration in this zone is governed by equation (3.11.a) where C is the particle concentration, v_s is the settling velocity, D_p is the molecular diffusion coefficient, D_t is the turbulent diffusion coefficient, M is the mass flow rate. The subscripts: i refers to the layer number, a refers to the air outside the thermal plumes (surrounding air), pl refers to the air inside the thermal plume, ent refers to entrainment, and g refers to generation. $(1-\lambda)$ is the fraction of the exhaled jet transported upward by the infected plume. The parameter $A_{pl,inf,i}$ is the cross sectional area at the interface between the layers i and $i+1$ inside the infected thermal plume, $A_{int,inflmic1,i}$, $A_{int,inflmic2,i}$ and $A_{int,inflmac,i}$ are the interaction areas between the infected plume and the microclimate zones 1 and 2 and macroclimate zone respectively within layer i . These areas are found mathematically as the intersection between two surfaces of defined geometry (conical shape for the plumes and circular shape for the microclimates and macroclimate zones).

$$Y1 + Y2 + Y3 + Y4 + Y5 + Y6 = Y7 \quad (3.11.a)$$

where

$$Y1 = M_{pl,inf,i-1} C_{pl,inf,i-1}(t) - M_{pl,inf,i} C_{pl,inf,i}(t)$$

= vertical convective flux in the infected plume

$$Y2 = \rho v_s A_{pl,inf,i} C_{pl,inf,i+1}(t) - \rho v_s A_{pl,inf,i-1} C_{pl,inf,i}(t) = \text{gravitational flux}$$

$$Y3 = -A_{pl,inf,i-1} D_p \rho \left(\frac{\partial C_{pl,inf}(t)}{\partial z} \right)_{i-1} + A_{pl,inf,i} D_p \rho \left(\frac{\partial C_{pl,inf}(t)}{\partial z} \right)_i = \text{vertical diffusion flux}$$

$$Y4 = A_{int,inf,lmic1,i} (D_p + D_t) \rho \left(\frac{\partial c_{pl,inf/mic1}(t)}{\partial r} \right)_{R_i, z_{mi}} + A_{int,inf,lmic2,i} (D_p + D_t) \rho \left(\frac{\partial c_{pl,inf/mic2}(t)}{\partial r} \right)_{R_i, z_{mi}}$$

$$+ A_{int,inf,lmac,i} (D_p + D_t) \rho \left(\frac{\partial c_{pl,inf/mac}(t)}{\partial r} \right)_{R_i, z_{mi}} = \text{lateral diffusion interaction}$$

$$Y5 = M_{ent,inf/mic1,i} C_{a,mic1,i}(t) + M_{ent,inf/mic2,i} C_{a,mic2,i}(t) + M_{ent,inf/mac,i} C_{a,mac,i}(t)$$

= entrainment flux by the infected plume from its surrounding

$$Y6 = (1 - \lambda) M_g C_g(t) = \text{portion of the generated particles transported by the plume}$$

$$Y7 = \rho V_{pl,inf,i} \frac{\partial C_{pl,inf,i}(t)}{\partial t} = \text{transient storage term}$$

3.1.2.8.2. Exposed Plume Zone

The exposed plume zone interacts with the microclimate 2 and the macroclimate as shown in Fig. 3.1. The concentration in this zone is governed by equation (3.11.b) where $A_{pl,exp,i}$ is the cross sectional area at the interface between the layers i and $i+1$ inside the exposed thermal plume, $A_{int,explmic2,i}$ and $A_{int,explmac}$ are the

interaction areas between the exposed plume and the microclimate 2 and macroclimate zones respectively within layer i .

$$Y1 + Y2 + Y3 + Y4 + Y5 = Y6 \quad (3.11.b)$$

where

$$Y1 = M_{pl,expj-1} C_{pl,expj-1}(t) - M_{pl,expj} C_{pl,expj}(t) = \text{vertical convective flux in the exposed plume}$$

$$Y2 = \rho v_s A_{pl,expj} C_{pl,expj+1}(t) - \rho v_s A_{pl,expj-1} C_{pl,expj}(t) = \text{gravitational flux}$$

$$Y3 = -A_{pl,expj-1} D_p \rho \left(\frac{\partial C_{pl,exp}(t)}{\partial z} \right)_{i-1} + A_{pl,expj} D_p \rho \left(\frac{\partial C_{pl,exp}(t)}{\partial z} \right)_i = \text{vertical diffusion flux}$$

$$Y4 = A_{int,exp/mic2,i} (D_p + D_t) \rho \left(\frac{\partial c_{pl,exp/mic2}(t)}{\partial r} \right)_{R_i, z_{mi}} + A_{int,exp/mac,i} (D_p + D_t) \rho \left(\frac{\partial c_{pl,exp/mac}(t)}{\partial r} \right)_{R_i, z_{mi}}$$

= lateral diffusion interaction between the plume and its surrounding

$$Y5 = M_{ent,exp/mic2,i} C_{a,mic2,i}(t) + M_{ent,exp/mac,i} C_{a,mac,i}(t)$$

= entrainment flux by the exposed plume from its surrounding

$$Y6 = \rho V_{pl,expj} \frac{\partial C_{pl,expj}(t)}{\partial t} = \text{transient storage term}$$

3.1.2.8.3. First Microclimate Zone

The first microclimate zone interacts with microclimate 2 and the infected thermal plume as shown in Fig. 3.1. The concentration in this zone is governed by equation (3.11.c):

$$Y1 + Y2 + Y3 + Y4 + Y5 + Y6 + Y7 = Y8 \quad (3.11.c)$$

where

$$\begin{aligned} Y1 &= (\max(M_{a,mic1,i-1} + \lambda(1 - \chi(y_1, t))M_g)_{i>g}; 0)C_{a,mic1,i-1}(t) \\ &+ \max(-M_{a,mic1,i} - \lambda(1 - \chi(y_1, t))M_g)_{i>g}; 0)C_{a,mic1,i+1}(t) \\ &- (\max(M_{a,mic1,i} + \lambda(1 - \chi(y_1, t))M_g)_{i \geq g}; 0) \\ &+ \max(-M_{a,mic1,i-1} - \lambda(1 - \chi(y_1, t))M_g)_{i \geq g}; 0)C_{a,mic1,i}(t) \\ &= \text{vertical convective flux in microclimate 1} \end{aligned}$$

$$Y2 = \rho v_s A_{a,mic1,i} C_{a,mic1,i+1}(t) - \rho v_s A_{a,mic1,i-1} C_{a,mic1,i}(t) = \text{gravitational flux}$$

$$Y3 = A_{a,mic1,i} D_p \rho \left(\frac{\partial C_{a,mic1}(t)}{\partial z} \right)_i - A_{a,mic1,i-1} D_p \rho \left(\frac{\partial C_{a,mic1}(t)}{\partial z} \right)_{i-1} = \text{vertical diffusion flux}$$

$$Y4 = -A_{int,inf/mic1,i} (D_p + D_t) \rho \left(\frac{\partial c_{pl,inf}(t)}{\partial r} \right)_{R_i, z_{mi}} = \text{lateral diffusion interaction}$$

$$Y5 = -M_{ent,inf/mic1,i} C_{a,mic1,i}(t) = \text{entrainment flux by the infected plume from mic1}$$

$$Y6 = -A_{int,mic1/mic2,i} D_p \rho \frac{C_{a,mic1,i}(t) - C_{a,mic2,i}(t)}{r_{mic1}} = \text{horizontal diffusion by Brownian motion}$$

$$Y7 = \lambda M_g [(C_g(t) - \chi(y_1, t)C_{a,mic1,i}(t))]_{i=g} = \text{horizontal convection due to the exhaled jet penetration within the generation layer}$$

$$Y8 = \rho V_{mic1,i} \frac{\partial C_{mic1,i}(t)}{\partial t} = \text{transient storage term}$$

where $A_{int,mic1/mic2,i}$ is the interaction area between microclimates 1 and 2 within layer i .

r_{mic1} is the radius of the microclimate zone 1. The maximum function is introduced to account for the variation in the surrounding airflow direction allowing the equation to

be applicable within the different zones defined in the vertical direction. For instance,

the flow is upward below the stratification height while it is downward above the stratification height. $A_{int,mic1mic2,i}$ is the interaction area between microclimates 1 and 2 within layer i . r_{mic1} is the radius of the microclimate zone 1.

3.1.2.8.4. Second Microclimate Zone

The second microclimate is divided into several sub-microclimates regions as described in section 3.1.1. A sub-microclimate 2 region number j interacts with the adjacent regions and the infected or/and exposed TP and the concentration in this zone is governed by equation (3.11.d) where $A_{int,mic2mac,i}$ is the interaction area between microclimate 2 and the macroclimate within layer i . m is the number of rising plumes, r_{mic2} is the radius of the microclimate zone 2.

$$Y1 + Y2 + Y3 + Y4 + Y5 + Y6 + Y7 = Y8 \quad (3.11.d)$$

where

$$\begin{aligned} Y1 &= \max(M_{a,mic2,j,i-1} + \lambda(\chi(y_{j-1},t) - \chi(y_j,t))M_g)_{i>g}; 0) C_{a,mic2,j,i-1}(t) \\ &+ \max(-M_{a,mic2,j,i} - \lambda(\chi(y_{j-1},t) - \chi(y_j,t))M_g)_{i>g}; 0) C_{a,mic2,j,i+1}(t) \\ &- (\max(M_{a,mic2,j,i} + \lambda(\chi(y_{j-1},t) - \chi(y_j,t))M_g)_{i \geq g}; 0) \\ &+ \max(-M_{a,mic2,j,i-1} - \lambda(\chi(y_{j-1},t) - \chi(y_j,t))M_g)_{i \geq g}; 0)) C_{a,mic2,j,i}(t) \\ &= \text{vertical convective flux in microclimate 2} \end{aligned}$$

$$Y2 = \rho v_s A_{a,mic2,j,i} C_{a,mic2,j,i+1}(t) - \rho v_s A_{a,mic2,j,i-1} C_{a,mic2,j,i}(t) = \text{gravitational flux}$$

$$Y3 = A_{a,mic2,j,i} D_p \rho \left(\frac{\partial C_{a,mic2,j}(t)}{\partial z} \right)_i - A_{a,mic2,j,i-1} D_p \rho \left(\frac{\partial C_{a,mic2,j}(t)}{\partial z} \right)_{i-1} = \text{vertical diffusion flux}$$

$$Y4 = \sum_{k=1}^m A_{int,mic2,j/pl(i,k)} (D_p + D_t) \rho \left(\frac{\partial c_{pl(i,k)}(t)}{\partial r} \right)_{R_i, z_{mi}} = \text{lateral diffusion interaction}$$

$$Y5 = \sum_{k=1}^m M_{ent,mic2,j/pl(i,k)} C_{a,mic2,j,i}(t) = \text{entrainment flux by the plumes from mic 2}$$

$$\begin{aligned} Y6 &= D_p A_{int,mic2,j/mic2,j-1,i} \rho \frac{C_{a,mic2,j-1,i}(t) - C_{a,mic2,j,i}(t)}{r_{mic2,j} - r_{mic2,j-1}} \\ &- D_p A_{int,mic2,j/mic2,j+1,i} \rho \frac{C_{a,mic2,j,i}(t) - C_{a,mic2,j+1,i}(t)}{r_{mic2,j+1} - r_{mic2,j}} \\ &= \text{horizontal diffusion by Brownian motion [35]} \end{aligned}$$

$$Y7 = \left[\lambda \chi(y_{j-1},t) M_g C_g - \lambda \chi(y_j,t) M_g C_g \right]_{i=g} = \text{horizontal convection due to the exhaled jet penetration}$$

$$Y8 = \rho V_{a,mic2,j,i} \frac{\partial C_{a,mic2,j,i}(t)}{\partial t} = \text{transient storage term}$$

3.1.2.8.5. Macroclimate Zone

The macroclimate zone interacts with microclimate 2 and the TP and the concentration in this zone is governed by equation (3.11.e):

$$Y1 + Y2 + Y3 + Y4 + Y5 + Y6 + Y7 = Y8 \quad (3.11.e)$$

where

$$\begin{aligned} Y1 &= \max(M_{a,mac,i-1};0) C_{a,mac,i-1}(t) + \max(-M_{a,mac,i};0) C_{a,mac,i+1}(t) \\ &\quad - (\max(M_{a,mac,i};0) + \max(-M_{a,mac,i-1};0)) C_{a,mac,i}(t) \\ &= \textit{vertical convective flux in the macroclimate} \end{aligned}$$

$$Y2 = \rho v_s A_{a,mac,i} C_{a,mac,i+1}(t) - \rho v_s A_{a,mac,i-1} C_{a,mac,i}(t) = \textit{gravitational flux}$$

$$\begin{aligned} Y3 &= A_{a,mac,i} D_p \rho \left(\frac{\partial C_{a,mac}(t)}{\partial z} \right)_i - A_{a,mac,i-1} D_p \rho \left(\frac{\partial C_{a,mac}(t)}{\partial z} \right)_{i-1} \\ &= \textit{vertical diffusion flux} \end{aligned}$$

$$\begin{aligned} Y4 &= - \sum_{k=1}^m A_{int,mac/pl(i,k)} (D_p + D_t) \rho \left(\frac{\partial c_{pl,k}(t)}{\partial r} \right)_{R(i,k),z_{mi}} \\ &= \textit{lateral diffusion interaction} \end{aligned}$$

$$\begin{aligned} Y5 &= - \sum_{k=1}^m M_{ent,mac/pl(i,k)} C_{a,mac,i}(t) \\ &= \textit{entrainment flux by the plumes from the macroclimate} \end{aligned}$$

$$\begin{aligned} Y6 &= - \sum_{j=1}^n \rho v_{d(i,j)} A_{w,(i,j)} C_{a,mac,i}(t) \\ &= \textit{deposition flux on the walls from the macroclimate} \end{aligned}$$

$$\begin{aligned} Y7 &= A_{int,mac/mic2} D_p \rho \frac{C_{a,mic2,i}(t) - C_{a,mac,i}(t)}{r_{mic2}} \\ &= \textit{horizontal diffusion by Brownian motion} \end{aligned}$$

$$Y8 = \rho V_{a,mac,i} \frac{\partial C_{a,mac,i}(t)}{\partial t} = \textit{transient storage term}$$

The deposition fluxes are determined as boundary conditions modeled by Lai and Nazaroff [32]. The subscript j refers to the wall number within a layer surrounded by n walls, and k refers to the thermal plumes number. The parameter $A_{a,mac,i}$ represents the cross sectional area of the macroclimate zone at the interface between the layers i and $i+1$ while $A_{w,(i,j)}$ represents the surface area of wall j within layer i . $A_{int,mac/pl(i,k)}$ is the interaction area between the macroclimate zone and plume k within the layer i .

3.1.3. Boundary Conditions and Numerical Methods

The domain was discretized within the space into N horizontal layers in the vertical direction and a number of lumped regions in the horizontal direction. In order to run the algorithm solving for velocity, temperature and concentration fields in the studied room, the required inputs are the supply flow rate and temperature at the inlet, the indoor heat and contamination sources, and the outdoor conditions determining the imposed heat flux from the exterior. The space thermal model adopted from Makhoul et al. [85] allowed the determination of wall temperatures but required the knowledge of indoor temperatures. On the other hand, the wall temperatures were required to solve for the energy balances of the different layers. For this reason, the solution for wall temperatures and indoor temperatures was conducted by iteration connecting between the thermal space model and energy balances and at each step the mass flow rates which depend largely on the temperature gradients were updated until convergence was reached as shown in the flowchart of Fig. 3.5. Once, the flow rates were determined they were used in solving for the mass balances determining the concentration distribution within the space.

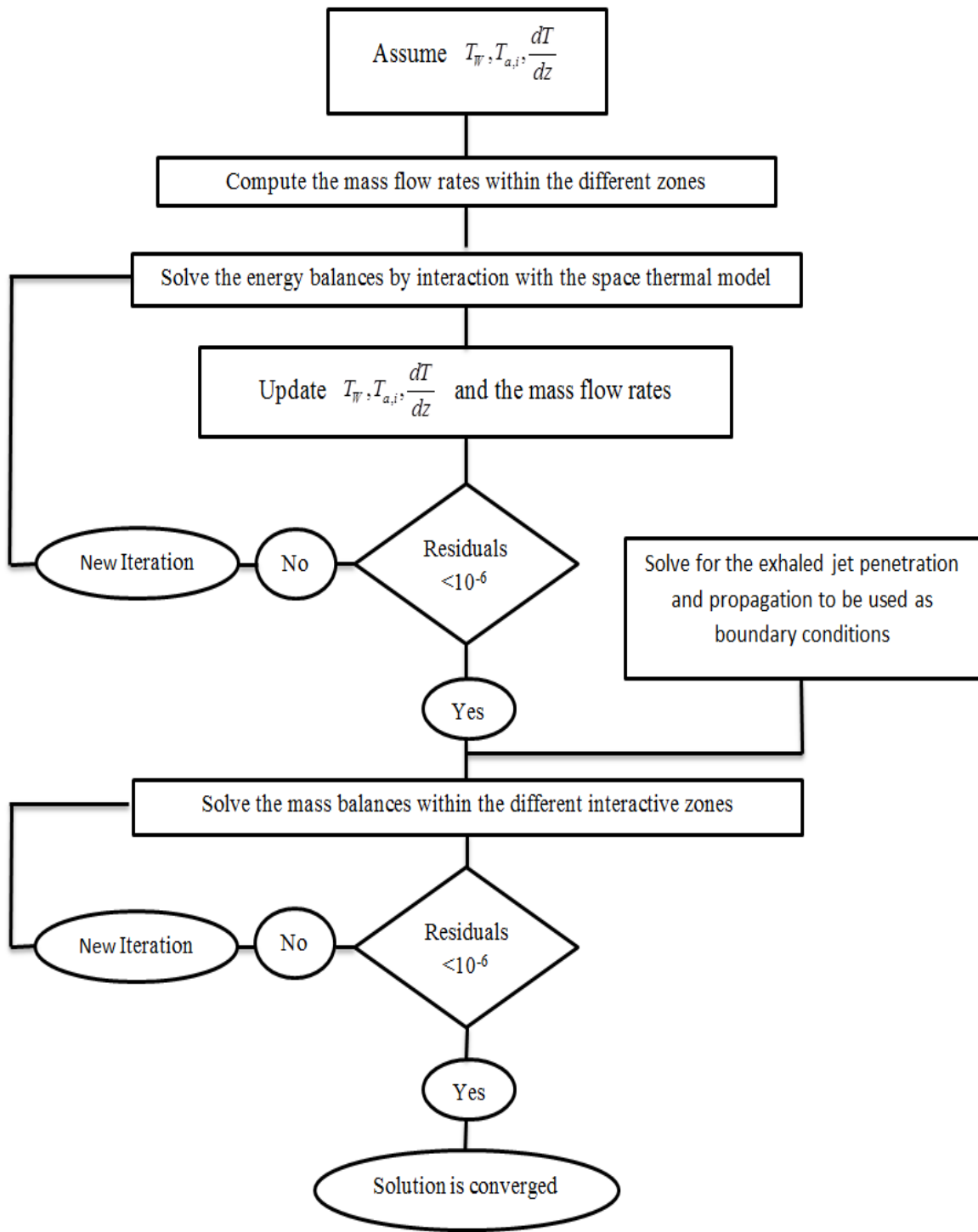


Fig. 3.5: Flowchart illustrating the sequence of operations for solving for the different variables.

The coupled mass and energy equations are discretized into algebraic equations using the finite volume method developed by Patankar [99]. The convergence criterion for the residuals of the different equations was set to 10^{-6} . The predicted variables were the concentrations within the internal plumes and surrounding air and temperature distribution in the room. In addition, the variation of friction velocity was found not to affect significantly the concentration of particles. For small particles less than $1\ \mu\text{m}$, the variation in concentration due to change in friction velocity from 0.3 to 3 cm/s was in the order of 1% and for larger diameter particles concentration change was much less than 1%.

3.2. CFD Model

Coupling *DV* and *CPV* with fans induced complex flow interaction between the fan jets and the rising TP affecting the behavior of the upward convective plumes and the particle distribution within the space. CFD modeling has been shown to be effective in predicting airflow pattern and distribution of particles of different densities and diameters within enclosed spaces for different HVAC configurations [15,64,100]. Hence, it constitutes a viable tool to study the performance of ventilation systems in indoor environments and their generated flow and thermal fields. For this reason, CFD modeling is used in the current work to investigate the performance of assisting *DV* and *CPV* with fans.

3.2.1. Airflow and Energy Modeling

A detailed CFD model that can accurately predict the entrainment of air by the rising plumes and their interaction with the fans' jets was developed. For robust CFD

results, accurate modeling of flow physics is essential including turbulence, buoyancy effects, and development of boundary layers near the surfaces. In addition, the control of the grid resolution near the surfaces is important to capture properly the shear-layer entrainment process and the different TP as well as the fluid/thermal boundary layers around the occupants.

The commercial software ANSYS Fluent was selected to solve for the velocity, thermal, and particle concentration fields within the space by numerical modeling. The air within the room can be considered as a continuous fluid; hence it might be simulated by the Eulerian approach [101]. ANSYS Fluent which solves the Navier-Stokes equations gives different choices for modeling turbulence. One of the widely used turbulence models is the realizable k - ε model which was selected in addition to the enhanced wall treatment option. The ideal gas law was used for the density variation modeling in order to account for the buoyancy effects. The interaction between fluid and particle phases was selected as one way coupling hence the effect of particles on the airflow field was neglected. This assumption is valid because the discrete phase volume is negligible compared to the room volume [102]. The CFD software solves for the Navier-Stokes equations by transforming them to algebraic equations offering different schemes for their discretization. A second-order upwind discretization scheme was selected to solve for the momentum, k , ε , and energy equations. The “PRESTO!” staggered scheme was used for the pressure [64,103]. The SIMPLE algorithm was selected to couple the pressure and velocity fields [64].

3.2.2. Discrete Phase Modeling

While the Eulerian approach was used for solving for the continuous fluid fields,

the Lagrangian approach which is a discrete trajectory method was selected to predict the particle trajectories. It consists of tracking numerous particles within the airflow domain.

Active particles are not only influenced by the flow pattern but also by different forces related to particle properties (shape, size, density) such as drag force and gravity. The Lagrangian particle tracking method was used to calculate individual trajectories by solving the Newton's second law equation. The momentum equation, relating the particle inertia to the external forces, can be expressed as [64,96,103]:

$$\frac{d\vec{u}_p}{dt} = F_D (\vec{u} - \vec{u}_p) + \frac{\vec{g}(\rho_p - \rho)}{\rho_p} + \vec{F}_a \quad (3.12)$$

where \vec{u}_p is the particle velocity vector, F_D is the inverse of relaxation time (s^{-1}) [64,96,102]; ρ and ρ_p are respectively the density of air and the particles. All the forces of equation (3.12) are per unit mass of particle (m/s^2). The left-hand side illustrates the inertial force (m/s^2). The first term on the right hand side represents the drag force which follows the Stokes-Cunningham drag law; the second term represents the gravitational and buoyancy forces, and \vec{F}_a includes other forces (Brownian motion, thermophoretic and shear-induced lift forces) [64, 96, 102].

Brownian motion, thermophoretic and shear-induced lift forces are in general two magnitudes smaller than the drag force in ventilated rooms [103]. The Brownian and Saffman's lift forces may become comparable to the drag force when fine particles are considered in a flow field. Furthermore, the Brownian and lift forces might become stronger and affect the deposition process and particles motion especially near the walls

in the turbulent boundary layer as reported by Li and Ahmadi [104]. Hence, Brownian and Saffman's lift forces were considered.

The discrete random walk model (DRW) was used to model the influence of local turbulence intensities on the path of particles. It uses a stochastic approach in modeling particle trajectories [105] as expressed in equation (3.13) as:

$$u_i' = \zeta \sqrt{\frac{2K}{3}} \quad (3.13)$$

where u_i' is the turbulent fluctuating component of the velocity, ζ a normally distributed number randomly generated by the DRW model, and K the local turbulence intensity.

In the Lagrangian approach, the concentration field of particles is not directly obtained. The particle source in-cell (PSI-C) scheme correlating the concentration with the particle trajectories within each computational cell was used [103] as follows:

$$C = \frac{\dot{m} \sum_{i=1}^n dt(i, j)}{V_j} \quad (3.14)$$

where i and j represent the trajectory index and cell index respectively, C is the concentration in cell j , \dot{m} is the mass flow rate associated with each trajectory, dt is the residence time, V_j is the volume of cell j , and n is the number of trajectories tracked.

Particles within the viscous sub layer might be subjected to abnormal high fluctuating velocity normal to the wall which would lead to over-prediction of particle-wall collision frequency and thus of particle deposition. Hence, a special treatment of the mesh is required to avoid over-estimation of particle deposition. A tetrahedral unstructured grid was generated for the different studied configurations. Figure 3.6 shows the grid that was used in modeling the *DV* and *CPV* conditioned spaces.

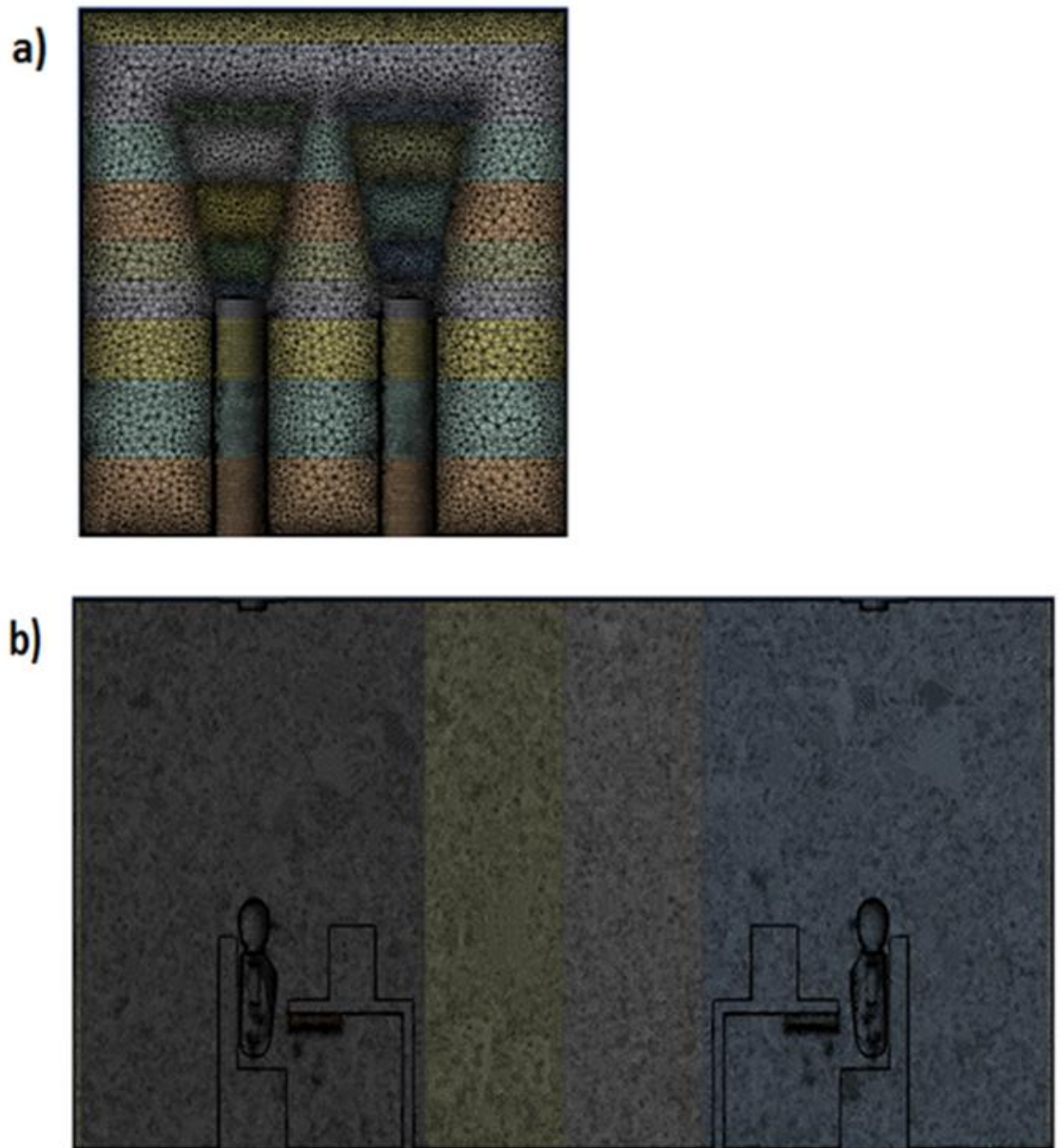


Fig. 3.6: Mesh of the CFD model for a space ventilated by: a) *DV* system; b) *CPV* system.

In order to resolve the boundary layer, a combination of face sizing and surface inflation was adopted to refine the mesh. Accordingly, different combinations of face sizing and first layer inflation thickness were tested. The selected combination should account for the boundary viscous sub-layer. For each face size tested, the first layer

inflation size was varied such that the corresponding y^+ values fall in the range of 0.8 and 4 to capture the boundary layer development [21].

Furthermore, in order to model the near wall flow and boundary layer development the enhanced wall treatment option was selected [21,22,102]. This method permit to switch between the two-layer model and the enhanced wall functions according to the grid size. In regions where y^+ is of the order of unity, the two-layer model is used and the laminar sub-layer is resolved. However, in regions where the boundary layer is not fully resolved ($3 < y^+ < 10$), an enhanced wall function is used [21,22,102]. In order to reduce the computational time without affecting results accuracy, a grid independence test was conducted to refine the mesh and decide on the number of elements.

Numerical convergence was judged using several criteria: scaled residuals reported by Fluent should reach a minimum value of 10^{-5} , but convergence was not reached until the net heat flux of the computational domain was below 1% of the total heat gain and the particle concentration in the breathing zone was stabilized [64].

The concentration field was resolved using the Lagrangian approach which treats the particles as a discrete phase by distributing particles in a certain number of trajectories and tracking their path. By evaluating the statistical distribution of the particle trajectories, the Lagrangian method allows the calculation of the concentration in each control volume. Hence, it was essential to determine the number of tracked particle trajectories that is statistically sufficient for obtaining a stable solution. Once the energy and velocity field reached convergence, particle tracking simulation was repeated many times resulting in variations in the evaluated particle concentrations because of the used statistical approach. To reduce the fluctuations of the calculated

concentration field, the number of trajectories was increased resulting in a more stable solution [64, 100]. The criterion adopted to estimate the required number of trajectories to accurately resolve the concentration field is that the fluctuations in the computed particle concentration and deposition do not exceed $\pm 5\%$ of the mean concentration resulting from 10 particle tracking simulations. It was found that 200,000 particle trajectories were enough to achieve statistically stable results.

3.2.3. Boundary Conditions

Boundary conditions for airflow, energy and particle concentration should be specified for proper CFD modeling and are summarized in this section.

For airflow modeling, the supply velocity and direction, hydraulic diameter of the supply grill and turbulent intensity at the inlet were specified. The exhaust was modeled as a pressure outlet with a zero gage pressure. For the fans, the “fan” boundary condition was imposed at the inlet with a determined pressure drop [22]. Thermally, heat fluxes were imposed on the different surfaces.

Literature studies indicated that alternative respiration does not considerably affect particle behavior [106, 107] and therefore, continuous generation can be assumed [108]. To model particle behavior, particle injection characteristics due to normal breathing were specified: i) horizontal generation rate from the mouth of the infected person is $5e^{-5}$ kg/s; ii) exhaled jet spreads in the form of conical geometry with a mean flow rate of 8.4 L/min for sedentary respiration [28]. At the outlet the “escape” boundary condition was selected and when particle trajectory reached a surface the “trap” condition was used; the latter condition is appropriate for micro- and nano-particles because vander Waals forces are dominant at this size scale [109]. The escaped

and trapped trajectories terminate while the remaining trajectories are tracked within the space.

3.3. Thermal Comfort Assessment

3.3.1. Coupling of CFD and PMV/PPD Models

The predicted mean vote (PMV) (which scales between -3 for very cold and +3 for very warm) and predicted Percentage of People Dissatisfied (PPD) are well-known models for assessment of thermal comfort. PMV and PPD can be computed using an online calculator [110]. The online calculator requires as inputs the metabolic energy production (which can be between 58 and 232 W/m²), the rate of mechanical work (which is normally set to 0), the ambient air temperature (which can be between 10-30), the mean radiant temperature (which is often close to ambient air temperature), the relative air velocity (which can be between 0.1 to 1 m/s), the relative humidity of the air, and the basic clothing insulation (where 1 clo = 0.155 W/m²K) .

It was assumed that the indoor relative humidity is equal to 50 % and the sedentary occupants (metabolic energy production of 58.15 W/m²) are wearing medium clothing ($I_{cl} = 1$ clo) and that the mean radiant temperature equals the ambient air temperature. When cylinders were used to simulate occupants, from the CFD simulations, the air velocity and temperature around the occupants were obtained by averaging air velocity and temperature of different points of the microclimate air around the occupants which is taken as 2 cm from the cylinder surface since for larger distances the temperature becomes nearly equal to the surrounding temperature. The averaging technique is valid if air flow velocities around the occupants are lower than 0.3 m/s and temperature gradients in the occupied zone are not very large which in general is the

case in *DV* spaces. Once all the required inputs were specified, the online calculator [110] was used to obtain the PMV and PPD as outputs in order to assess the occupant thermal comfort.

3.3.2. Coupling of CFD and Bio-Heat Models

When thermal asymmetry is involved segmental comfort not only overall comfort should be assessed. For this reason multi-segments thermal manikins were used in CFD simulations of the *CPV* system, and a validated bio-heat model [111,112] was coupled with the developed CFD model to assess the occupants' comfort. The bio-heat model was based on Zhang's models [113-115] mainly predicting human thermal comfort and sensation states. Eleven body segments were considered in the developed bio-heat model with the following divisions: head, upper arm, lower arm, hands, chest, abdomen, back, buttocks, thighs, calves and feet. The interaction between the CFD and bio-heat models allowed capturing the human thermal response and flow characteristics at his/her vicinity [111]. At each segment, the simulation of the physiological/thermal response allowed using Zhang's models [113-115] to predict the segmental and overall comfort/sensation. The thermal comfort scaled from -4 (very uncomfortable) to +4 (very comfortable) where 0 referred to just comfortable. The thermal sensation also scaled from -4 (very cold) to +4 (very hot) where -3 referred to cold, -2 to cool, -1 to slightly cool, 1 to slightly warm, 2 to warm, and 3 to hot [113-115].

A flowchart summarizing the coupling methodology between CFD and bio-heat models is represented in Fig. 3.7.

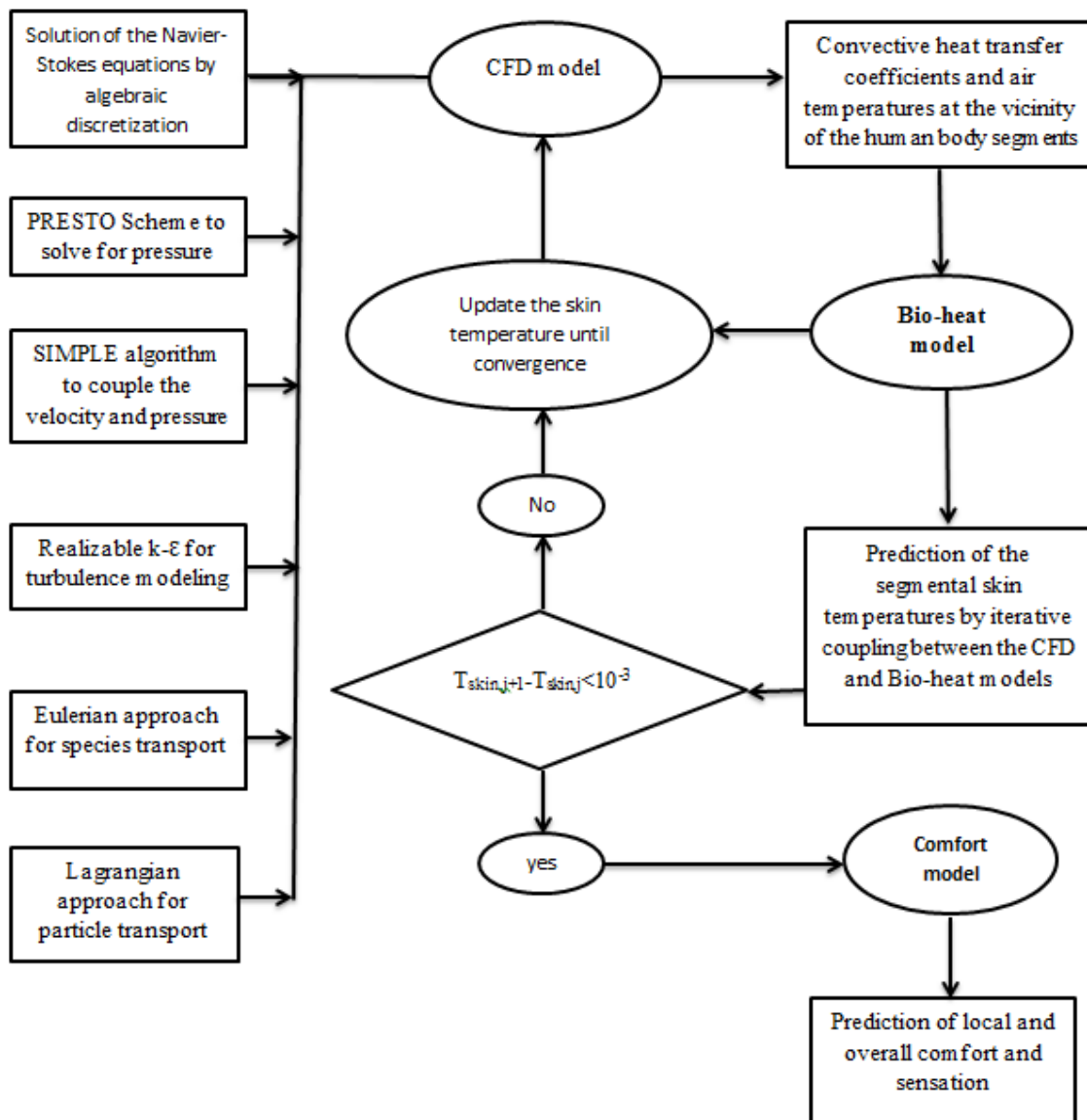


Fig. 3.7: Flowchart summarizing the coupling between CFD and bio-heat models.

To begin with, conventional skin temperatures were used as initial guess to run the CFD simulations. The air temperature and heat transfer coefficient at the vicinity of each of the body segment were computed from the converged simulation and constituted inputs for the bio-heat model giving as output updated skin temperatures of the different body parts [116]. Final segmental skin temperatures were obtained after

successive iterations when the absolute difference between the two last segmental temperatures became lower than 10^{-3} .

3.4. Ventilation Effectiveness Assessment

The ventilation effectiveness index was adopted to assess the mixing level of re-circulated air and delivered fresh air using the CO₂ tracer gas. Fresh air was characterized by 400 ppm of CO₂ concentration which was the CO₂ concentration of relatively clean outdoor air. The ventilation effectiveness is given by the following expression:

$$\varepsilon_v = \frac{C_r - C_b}{C_r - C_f} \quad (3.15)$$

where C_r and C_f are the CO₂ concentrations of the re-circulated air and fresh air respectively, and C_b its concentration at the breathing zone defined as a small sphere [60,98,117] of 1 cm radius, at 2.5 cm from the occupant nose [21].

3.5. Cross-Contamination Assessment

Two parameters are examined as criteria of comparison between the ventilation systems studied with respect to direct and indirect cross-contamination. The first parameter, representing the criterion of comparison for direct cross-contamination, is the intake fraction (IF) defined by:

$$IF = \frac{\textit{Particle concentration at breathing level of healthy person}}{\textit{Particle generation concentration}} \quad (3.16)$$

The intake fraction index is widely used to investigate cross-infection between occupants since it represents the proportion of contaminants generated by the infected occupant that is inhaled by the exposed occupant [71,108,118].

The second parameter, representing the criterion of comparison for indirect cross-contamination, is the deposited fraction (*DFr*) of particles at the vicinity of the exposed occupant expressed by:

$$DFr = \frac{\text{Number of particles deposited at the vicinity of the exposed person}}{\text{Number of particles generated by the infected person}} \quad (3.17)$$

Where the number of particles deposited at the vicinity of the exposed person was obtained by summing particles deposited at its proximity (human body, computer, desk's front, and chair).

3.6. Interpersonal Exposure Assessment

When transient HMRA were involved, in order to assess the inter-personal exposure (IPE), two parameters were defined and their variation with time was observed. The first parameter is the normalized concentration given by equation (3.18.a):

$$\text{Normalized Concentration} = \frac{\text{Concentration at the breathing level of the exposed person}}{\text{Concentration at generation}} \quad (3.18.a)$$

where the breathing level of the exposed person is simulated by the last sub-microclimate 2 which is adjacent to the exposed person at the nose level (centered at 1.05 m in height). The second parameter introduced is the infection index *I* in kg defined by the following equation [71]:

$$I(t) = \int_0^t \frac{C_{in}}{C_g} M_{in} dt \quad (3.18.b)$$

where C_{in} (kg/m³) is the inhaled concentration by the exposed person equal to the concentration within the last sub-microclimate 2 zone, M_{in} (kg/s) is the inhalation rate of

the exposed person, C_g (kg/m^3) the concentration of generation, t (s) the time. The inhaled dose (ID) during a certain period of time (T) can be determined according to the following equation:

$$ID_T = I(t_{e,T}) - I(t_{b,T}) \quad (3.19)$$

where $t_{b,T}$ and $t_{e,T}$ are respectively the beginning and end time of the considered period.

CHAPTER 4

EXPERIMENTAL METHODS

A numerical model performance is assessed by its prediction accuracy of actual results. Therefore, experimentation constitutes a validation tool for developed models by comparison of measured and numerically predicted results. In this work, different HVAC configurations were considered involving different experimental set-ups. This chapter describes the experimental spaces and protocols for the variable configurations studied.

4.1. Experimental Validation of the *DV* Models

In order to validate *DV* models, an experimental set-up was constructed in a controlled climatic chamber ventilated by a *DV* system. The chamber is of inner dimensions 2.5 m × 2.75 m × 2.8 m with supply and return grills cross-sectional area of respectively 0.582 m (width) × 0.24 m (height) and 0.44 m (width) × 0.19 m (height) (Fig. 4.1). Two heated cylinders of 0.3m in diameter and 1.2 m in height were used to simulate the thermal effects of two individual occupants. The load was distributed between the lighting and thermal cylinders such that the load per unit floor area is approximately 40 W/m² resulting in 100 W lighting load and 100 W for each thermal cylinder. Each cylinder was equipped with two front chair fans with controllable flow rate. The *DV* flow rate used was equal to 100 L/s with a supply temperature of 22 °C. Thermo anemometer ABK precision 731A was installed downstream of the fans. It is characterized by an accuracy of ± 0.6°C for temperature measurements and an accuracy of ± 2% of full scale for velocity measurements.

Air was introduced to the experimental chamber using a variable speed blower to allow control of the supply flow rate. High efficiency particulate filters (KS-NG-K1/2 HEPA filters) were used to remove particles from the supply air prior to its introduction into the chamber. Prior to each set of measurements, the light and the heated cylinders were turned on and the *DV* system was run for 3 to 4 hours to reach steady-state conditions before generating particles.

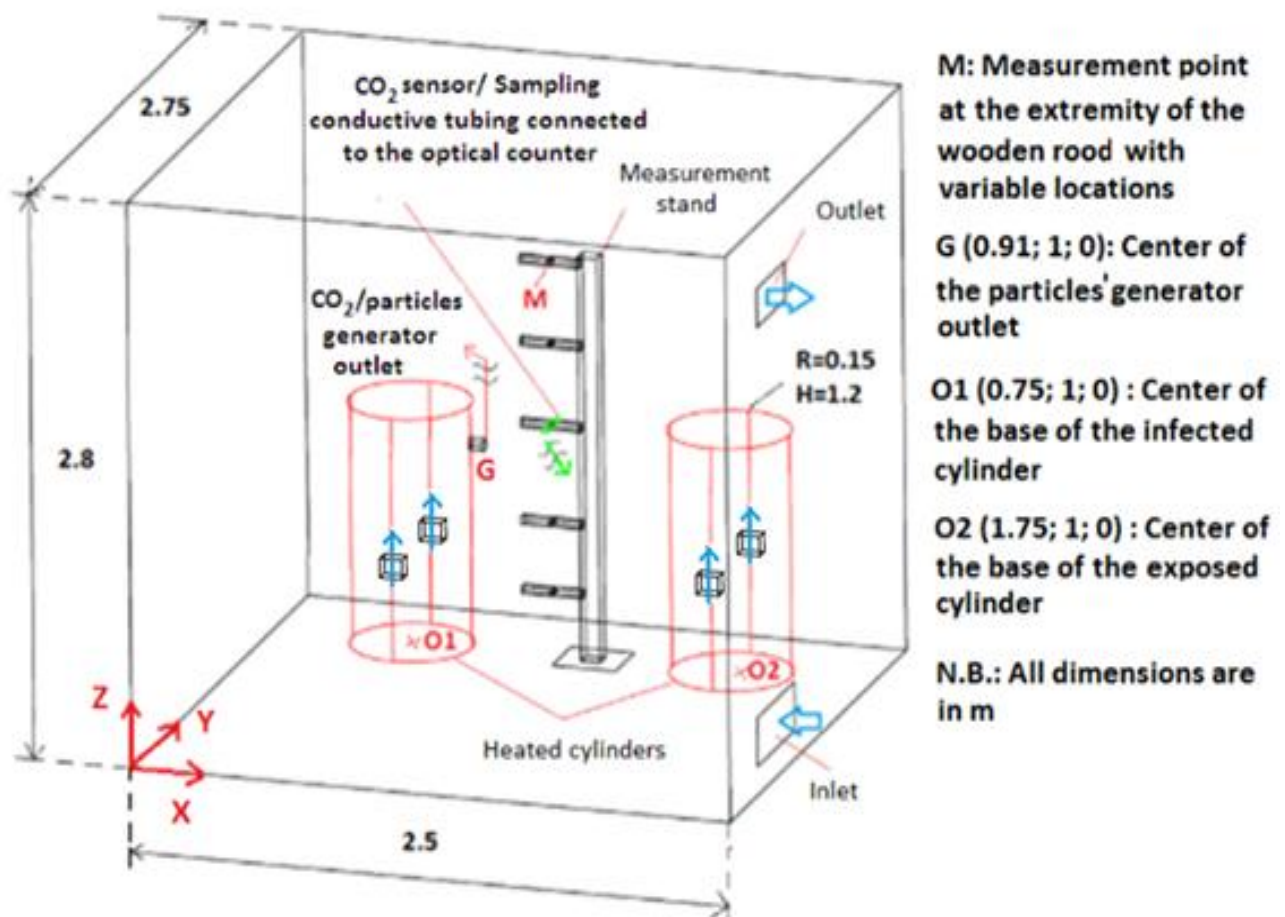


Fig. 4.1: Schematic of the *DV* experimental set-up.

4.1.1. Validation of the Simplified DV Model

In a first set of experiments, different momentum respiratory activities were simulated for validation of the simplified *DV* model. In order to look at the effect of the exhaled velocity on the particle penetration experiments were conducted on CO₂ for three different generation velocities (1, 3 and 10 m/s) representing respectively low, medium and high velocities and corresponding to generated flow rates of (1.33, 4 and 13.33 L/min). The CO₂ gas was generated from a pure CO₂ source under controlled conditions, using a flow meter (Fig. 4.2.a). The validation consisted of comparing separately measured and predicted CO₂ concentrations for different generation velocities (1, 3 and 10 m/s) within the macroclimate and microclimates zones. Furthermore, in order to validate the ability of the model in capturing the gravitational effect, experiments was conducted using heavy (density of 912 Kg/m³) 5 µm particles generated from a condensation aerosol generator (TSI Model 3475) (Fig. 4.2.a).

CO₂ sensors of type CDM4161-Figaro (Fig. 4.2.b) were used for measurement of the CO₂ concentration in ppm (parts per million) with an accuracy of ±20 ppm. On the other hand, for active particles, an optical particle sizer (TSI model 3330) (Fig. 4.2.b) giving measurements with a relative error lower than 5% was used. The measured concentrations were normalized by the generation concentration for comparison with the predictions of the simplified model.



Fig. 4.2: Equipment of CO₂ and particles: a) generation; and b) concentration measurement.

4.1.2. Validation of the DV+CF CFD Model

In a second set of experiments, low momentum breathing activities were simulated for *CF* off and on. Particles were introduced into the chamber continuously from an atomizer simulating particle exhaled from an infected occupant. The particles were introduced via a six-jet atomizer (TSI9306) (Fig. 4.2.a) operating at a flow rate of 8.4 L/min. The resulting generated jet flow was horizontal and the injection velocity was equal to 0.9 m/s.

The atomizer was cleaned well before being used and then filled with deionized water. Polystyrene latex spheres (PSLs) of 0.5 μ m diameter (NanosphereTM Size Standards) and 1050 kg/m³ in density were then added to the water. The droplets generated by the atomizer rapidly evaporate upon entry into the chamber [65,67,74], resulting in a mono-disperse aerosol of PSLs.

Samples were drawn at different locations via electrically conductive tubing by a suction pump at a flow rate of 0.3 l/min into a Scanning Electrical Mobility SpectrometerTM (Brechtel, Inc.) (see Fig. 4.2.b) operating with a sheath flow rate of 5 l/min with a scan time of 60 sec, providing 60 discrete particle size bins spanning the range of 10 to 1000 nm. Results were recorded automatically by a computer for post-processing. The measured particle number concentrations in the 500 nm size bin were normalized by the concentrations measured at the atomizer outlet for comparison with the predictions of the *DV+CF* CFD model.

4.2. Experimental Validation of the CPV CFD Models

Makhoul et al. [22] and El-Fil et al. [43] performed experiments to validate the ability of the CFD model used in this work in computing the fields of velocity,

temperature and CO₂ concentration for the *DF* and *CF* assisting the *CPV* system. The CFD model was found to accurately predict the jet profiles delivered by the *CPV* nozzle, and the effect of the *DF* and *CF* on the ventilation effectiveness and human body skin temperatures [22,43]. Nevertheless, the performance of the CFD model in computing the effect of the fans operation on particle transport towards the breathing zone of the exposed occupant was not investigated experimentally. For this reason, an experimental set-up was constructed as shown in Fig. 4.3 with a main purpose of validating the CFD model predictions of particle concentration in the occupant breathing zone when the fans' mounted on the chair or desk were operated.

The experimental set-up was built in a climatic chamber of inner dimensions (3.4 m × 3.4 m × 2.8 m) ventilated by a *CPV* system (see Fig. 4.3-a-b) with the option of operating *DF* or *CF*. Desk fans were installed under desks at a height of 0.7 m from the floor sucking air horizontally while four chair fans were mounted symmetrically on each chair with an optimal configuration as found by Fil et al at a height of 0.47 cm [43] blowing air downward.

Measurement technology north western thermal manikin" was used in the experiments simulating an adult human being, having an average surface area of 1.8 m² and divided into 20 segments. The breathing process was not considered since different studies indicated that it does not considerably affect the exposure level [107,119]. The experimental room was of a total load of 60 W/m² and a lighting load of 10 W/m². The thermal manikin (39 W/m²) was seated in the middle of the experimental room and a computer mock-up (100W) was placed on the desk in front of it (Fig. 4.3.a and 4.4.a).

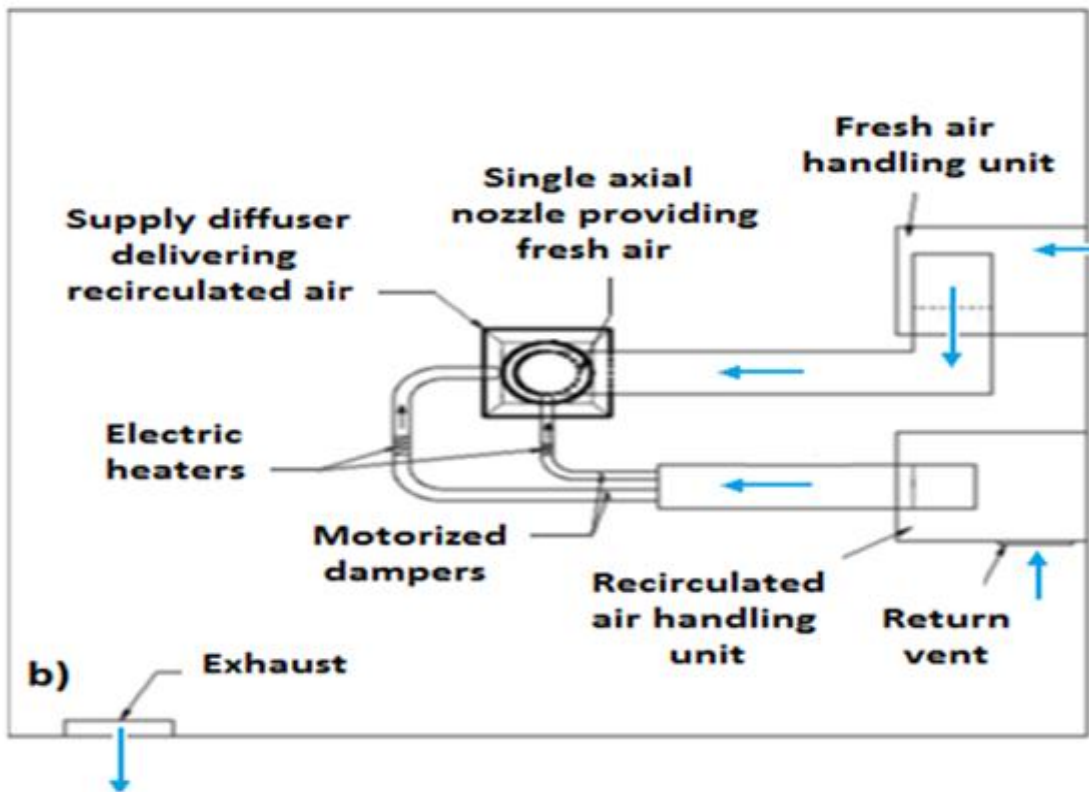
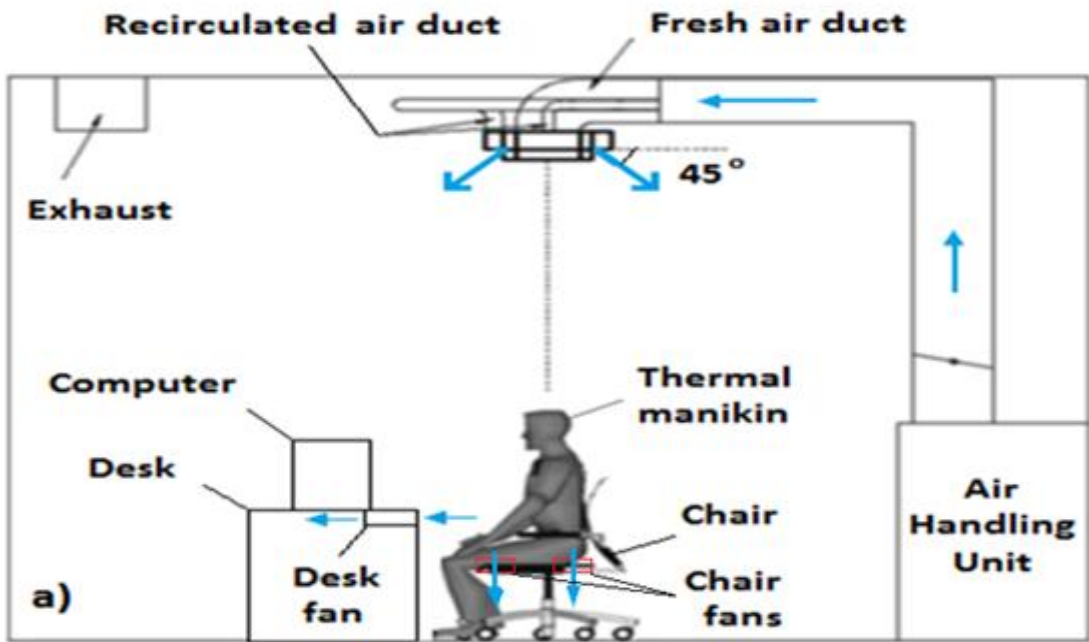


Fig. 4.3: Representation of the CPV system experimental set-up: (a) Frontal view (b) Top view

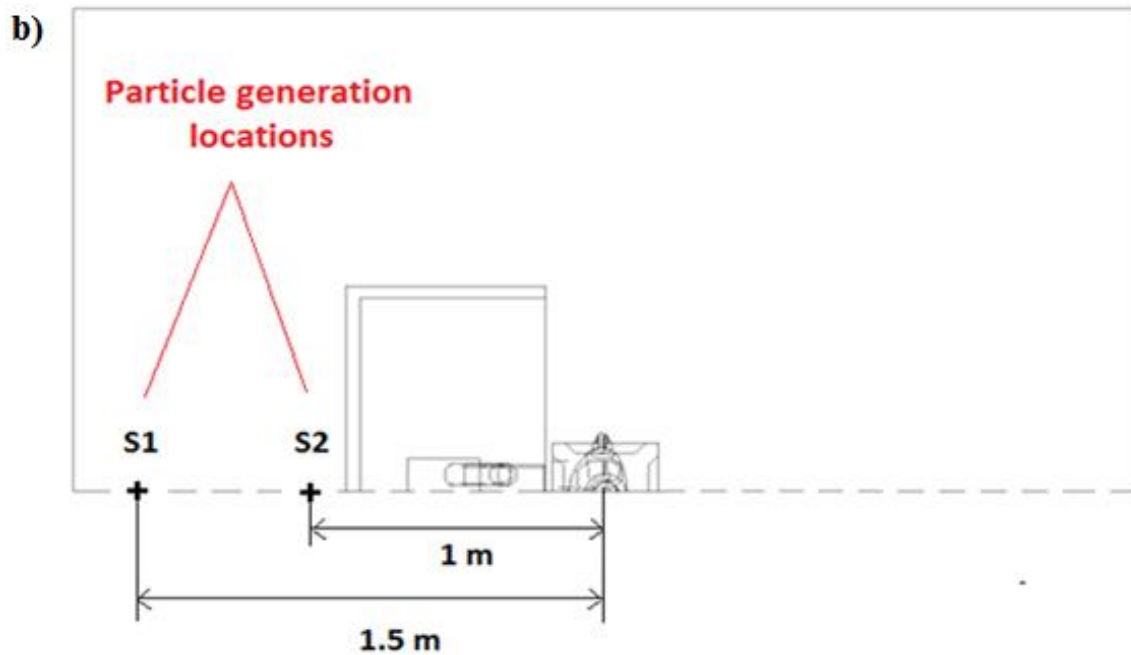


Fig. 4.4: a) Illustration of the constructed *CPV* experimental set-up in the controlled climatic chamber; b) Top view of the experimental layout illustrating the location of the contaminant generation sources.

The single axial ceiling nozzle integrated with a slot diffuser was centered over the manikin's head (Fig. 4.3.a and 4.4.a). The space is conditioned by two air-handling units (AHU) of 2637.7 W cooling capacity (see Fig. 4.3.b). The first AHU cooled the re-circulated air to 16 °C while the second AHU delivered 10 L/s of conditioned fresh air at 16°C (Fig. 4.3.b). The recirculation AHU supplied to the peripheral ceiling diffuser 35 L/s of cooled re-circulated air filtered by pleated filters. This delivery was controlled by motorized dampers (see Fig. 4.3.b). Thermo anemometer ABK precision 731A was used for measuring temperatures with an accuracy of $\pm 0.6^{\circ}\text{C}$, and velocities with an accuracy of $\pm 2\%$ of full scale.

The validation consisted of comparing measured and predicted intake fractions for variable *DF* and *CF* flow rates (0; 2.5; 5; 7.5; 10; 12.5 and 15 L/s) and different particle source locations (generation at the breathing level directed towards the thermal manikin with two separating distances of 1 and 1.5 m as shown in Fig. 4.4.b). Preceding each experimental run, the experimental chamber was thoroughly cleaned then the light, thermal manikin and ventilation system were operated for nearly four hours to reach steady-state conditions. Then 5 μm particles of 912 kg/m^3 density were generated continuously from a condensation aerosol generator (TSI Model 3475) (Fig. 4.2.a) with a flow rate of 4 L/min. The aerosol generator used generates mono-disperse particles with an aerosol geometric standard deviation < 1.10 . After one hour of generation, particle concentration within the breathing zone of the thermal manikin at 2.5 cm from the nose was stabilized. This concentration was measured by sampling air at a rate of 1 L/min at 2.5 cm from the nose using conductive tubing (to minimize particle loss by deposition) connected to an optical particle sizer (TSI model 3330) (Fig. 4.2.b) giving measurements with a relative error lower than 5%. Results were recorded automatically

by a computer for post-processing. The measured concentrations at the breathing level of the occupant were normalized by the generation concentration for comparison with the predictions of the *CPV* CFD model. Each experiment was repeated 5 times to ensure repeatability of the findings and the error obtained was within the experimental error of the equipment.

CHAPTER 5

RESULTS AND DISCUSSIONS

5.1. DV System Performance

5.1.1. *Simplified DV Model Results*

5.1.1.1. Validation with Literature Data

Extensive validation was performed in comparison with published data to insure that the current simplified model is capable of predicting cross-contamination within a space ventilated by a *DV* system. For the simplified plumes' model to be robust, it should predict deposition of particles on different surfaces accurately as well as the particle distribution within the different horizontal zones, particularly the air layer from which air is extracted to the breathing zone of the exposed person.

The validation of the model was conducted in two steps. First, in order to validate the simplified model, the well-tested computational fluid dynamics (CFD) model developed by Li et al. [28] was used. Their CFD model was validated by the experimental work of Lai et al. [121] when studying steady-state particle distribution in a two-zone chamber. Their obtained results showed good agreement with experimental data insuring the accuracy of their CFD model in predicting the concentration and flow fields. Li et al. [28] used their model to perform detailed CFD simulations to study particle behavior and cross-contamination between two occupants (60 W each) one representing the infected person and the other the exposed one in a typical office of dimensions 4 m × 3 m × 2.7 m. The space is ventilated by a *DV* system with air supply temperature of 20 °C and flow rate of 57 L/s (see Fig. 5.1). A 200 W flux from the window constitutes the external heat source. The concentration of generation was

imposed as 0.05 g/m^3 for the different particle sizes of 1, 2.5, 5, and $10 \text{ }\mu\text{m}$ at a breathing rate of 8.4 L/min .

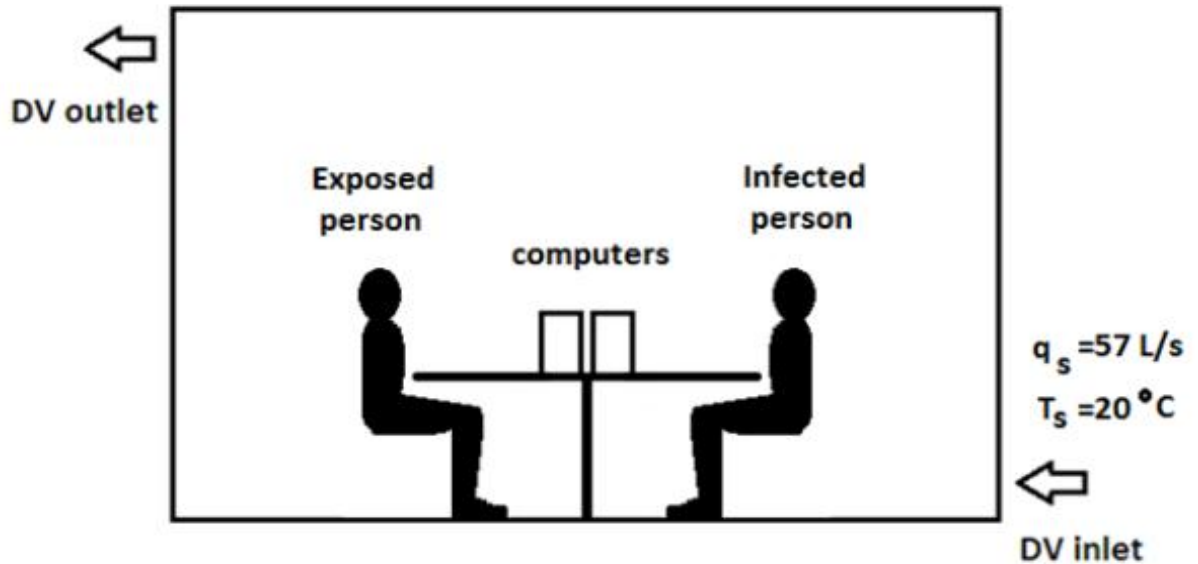


Fig. 5.1: Schematic of the set-up studied by Li et al. [28] at the mid-plane.

The CFD case of Li et al. [28] was simulated by the current model with the appropriate boundary conditions. The simplified model considered the case of three rising plumes and their expansion at different critical heights. Two rising plume emanated from the infected and exposed persons while the two computers resulted in one rising plume. In the work of Li et al. [28], the two computers (120 W each) were very close and their rising plumes can be lumped by an equivalent plume of double strength [80]. The averaged horizontal concentration (including the surrounding air and all the rising plumes) normalized by the concentration of generation was determined as function of height for different particle diameters. Furthermore, the intake fraction defined as the ratio of the concentration of particle at the breathing level of the exposed person to the concentration of generation was predicted for the variable diameters

investigated. Total deposition rates (including deposition on surfaces other than walls) were also reported [28].

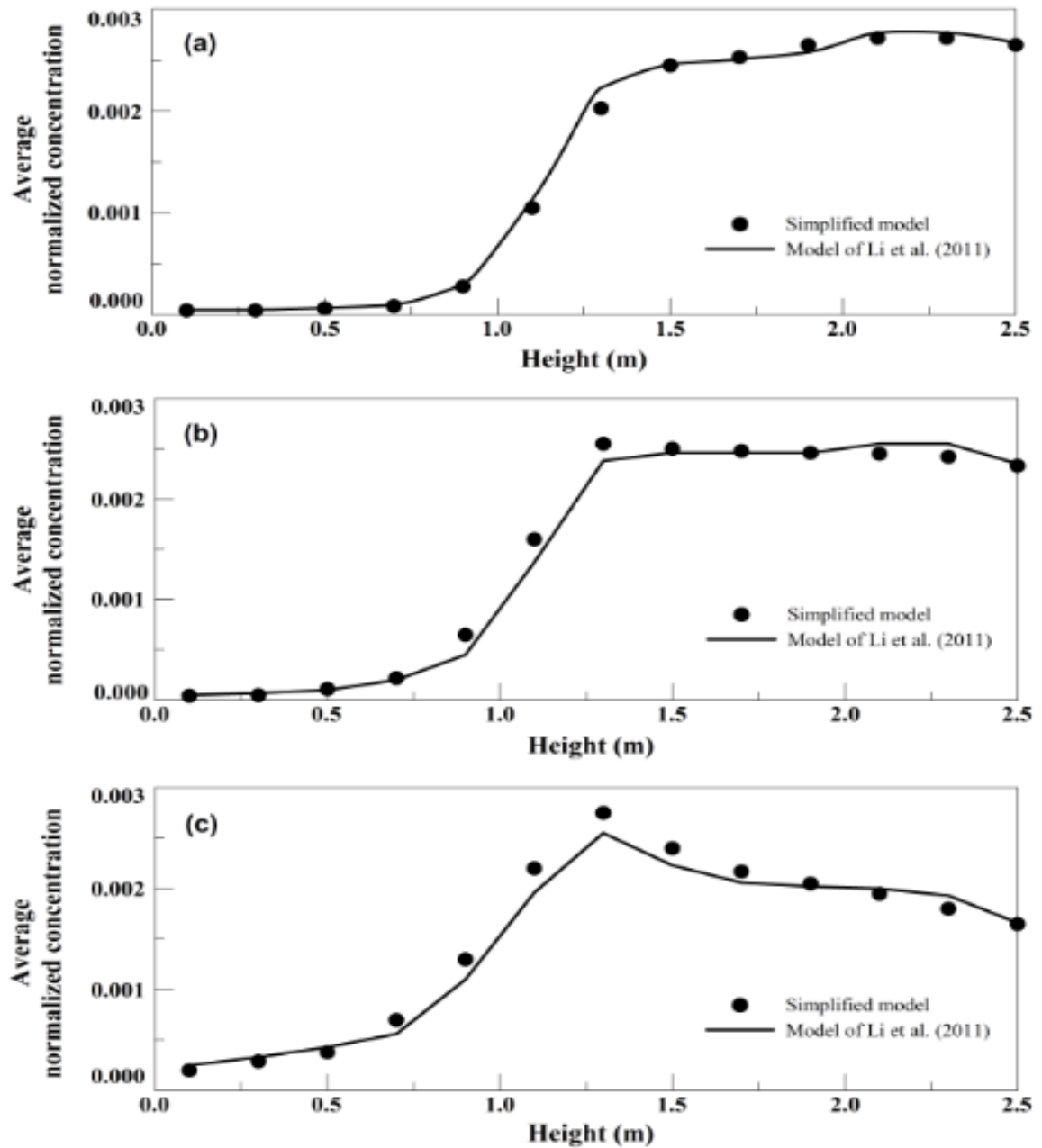


Fig. 5.2: Plot of the predicted variation of the average normalized concentration with height compared to published model results of Li et al. [28] at particle diameters of a) 1 μm ; b) 5 μm ; c) 10 μm .

Figure 5.2 shows the predicted variation of the average normalized concentration with height compared to published model results of Li et al. [28] for different diameters of a) 1 μm ; b) 5 μm ; c) 10 μm . Although, the simplified model predicted the concentrations within the different horizontal lumped regions, the variation of the average normalized concentration was found to be comparable with Li et al. [28] results. Good agreement was obtained between our model results and published values of normalized concentrations with a maximum relative error of 5%, 8%, and 10% respectively for particles of 1, 5 and 10 μm .

Since the breathing level of the target person is within the first layer of the non-infected plume, the concentration of particle within this zone was used to predict the intake fraction at the breathing level of the receiver. Figure 5.3 presents the intake fractions predicted by the current simplified model as well as the reported values by Li et al. [28] for different particle sizes.

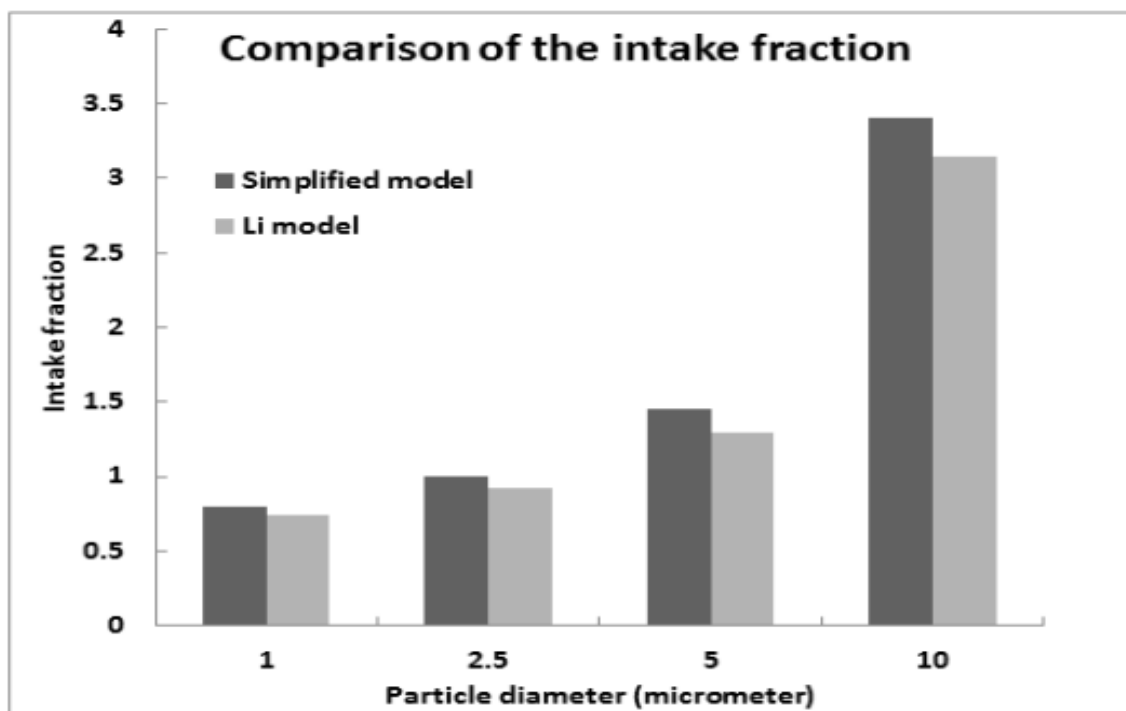


Fig. 5.3: Comparison of the intake fractions predicted for different diameters.

The simplified model showed that the removal effectiveness is higher for fine particles providing a relatively clean occupied zone and contaminated upper zone (Fig. 5.2). As the diameter increases, the gravitational effect becomes more pronounced increasing particle concentration in the occupied region (Fig. 5.2) and hence increasing the intake fraction. As shown in Figs. 5.2 and 5.3, the obtained results from our model and that of Li et al. [28] match well with a relative error increasing from the fine to the coarse mode where it reaches 10%.

In the model of Li et al. [28], deposition of particles was considered on different surfaces including occupants and desks. However, the simplified model accounts only for deposition on walls neglecting deposition on other surfaces. This assumption is validated by the comparison with the published model of Li et al. [28]. Figure 5.4 illustrates the total rate of deposited mass of particles obtained from both our current model and that of Li et al. [28] for different particle diameters (2.5, 5 and 10 μm).

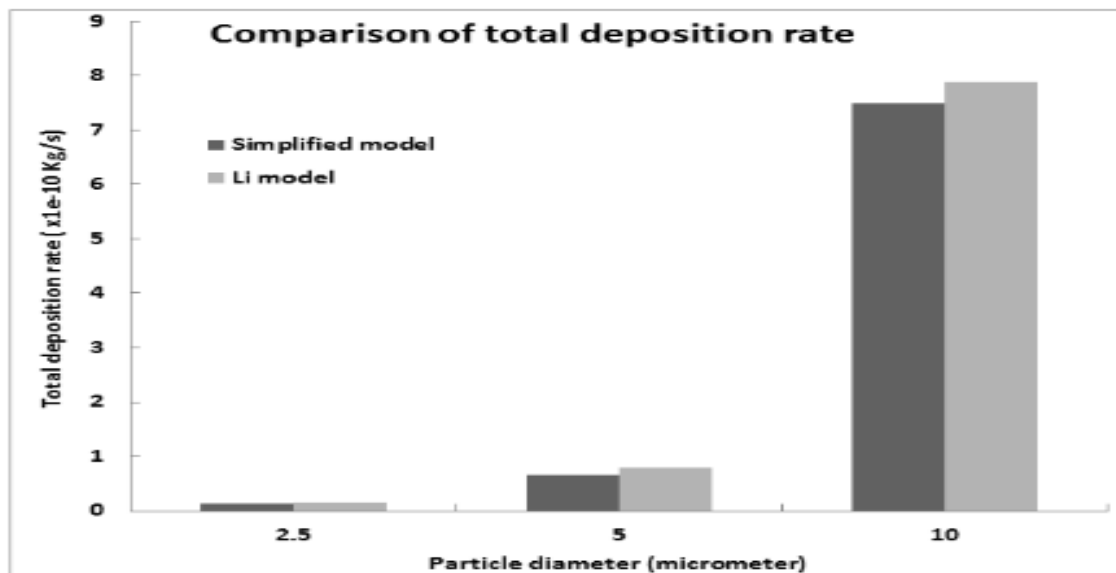


Fig. 5.4: Plot of the total rate of deposited mass of particles obtained from both our current model and that of Li et al. [28] for different particle diameters.

It is expected that as the diameter increases, deposition on the desk, computers and humans increases due to the gravitational effect. This explains the increasing relative error in predicting total deposition with the increase in diameter. However, the relative errors observed are below 10% hence the predicted results are within the engineering acceptable accuracy. In conclusion, the multi-plume simplified model in *DV* ventilated space is shown to accurately predict the average concentration, intake fraction and total deposition for the different particle sizes.

Second, in order to validate the model prediction of the deposition velocities and deposition rates on different walls orientation the numerical model of Zhao et al. [122] was used. This model was validated by experimental results [86,123] and was successfully used to predict temperature, velocity and concentration fields within a space ventilated by *DV* system.

The simplified model was used to simulate a set-up similar to the one studied by Zhao et al. [122]. The boundary conditions stated by Zhao et al. [122] were implemented as inputs to the simplified model so that the results can be comparable. The set-up consisted of a room of dimensions 5.16mx2.43mx3.65 m occupied by two persons with their personal computers ventilated by a *DV* system characterized by inlet flow temperature of 13 °C and rate of 64.1 L/s. The lighting load from the ceiling was 136 W and an external load of 135 W was imposed. Four heat plumes with different critical heights were considered to simulate the two occupants (75W each) and computers (108 and 173W). In the simulated case the two occupants were generating particles assumed to be of spherical shape characterized by a density of 1050 Kg/m³ with a rate of 0.0916µg/s for each of the particle sizes studied.

Deposition mass rates on vertical walls and floor in addition to mean deposition and velocity rates obtained from the simulated model were compared with the results presented by Zhao et al. [122]. The comparison was conducted for the different particles sizes investigated by Zhao et al [122] (1, 2.5, 5, 7.5 and 10 μm) and is illustrated in Figs 5.5 and 5.6. Good agreement was obtained between the simplified and CFD model results with a relative error lower than 5% validating the developed simplified model prediction of deposition.

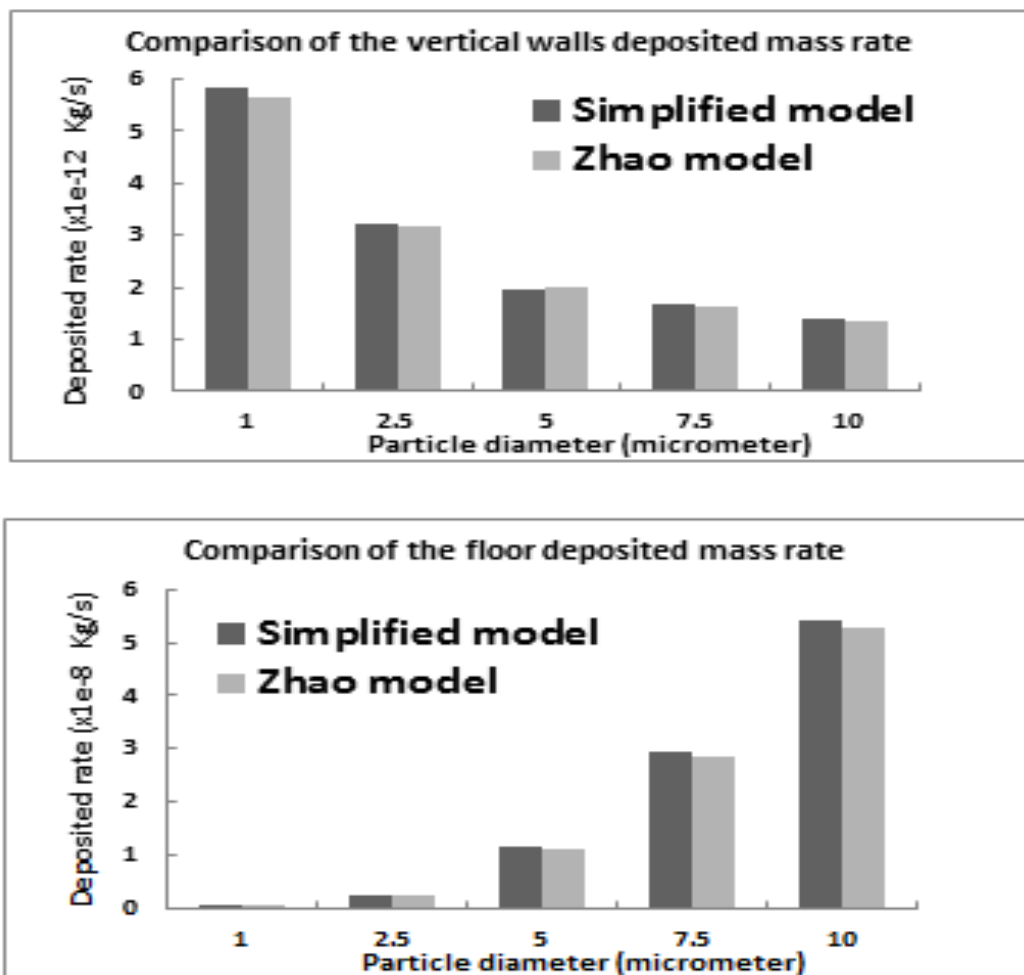


Fig. 5.5: Comparison of a) the vertical walls deposited mass rate (kg/s) predicted for different diameters; b) the floor deposited mass rate (kg/s) predicted for different diameters.

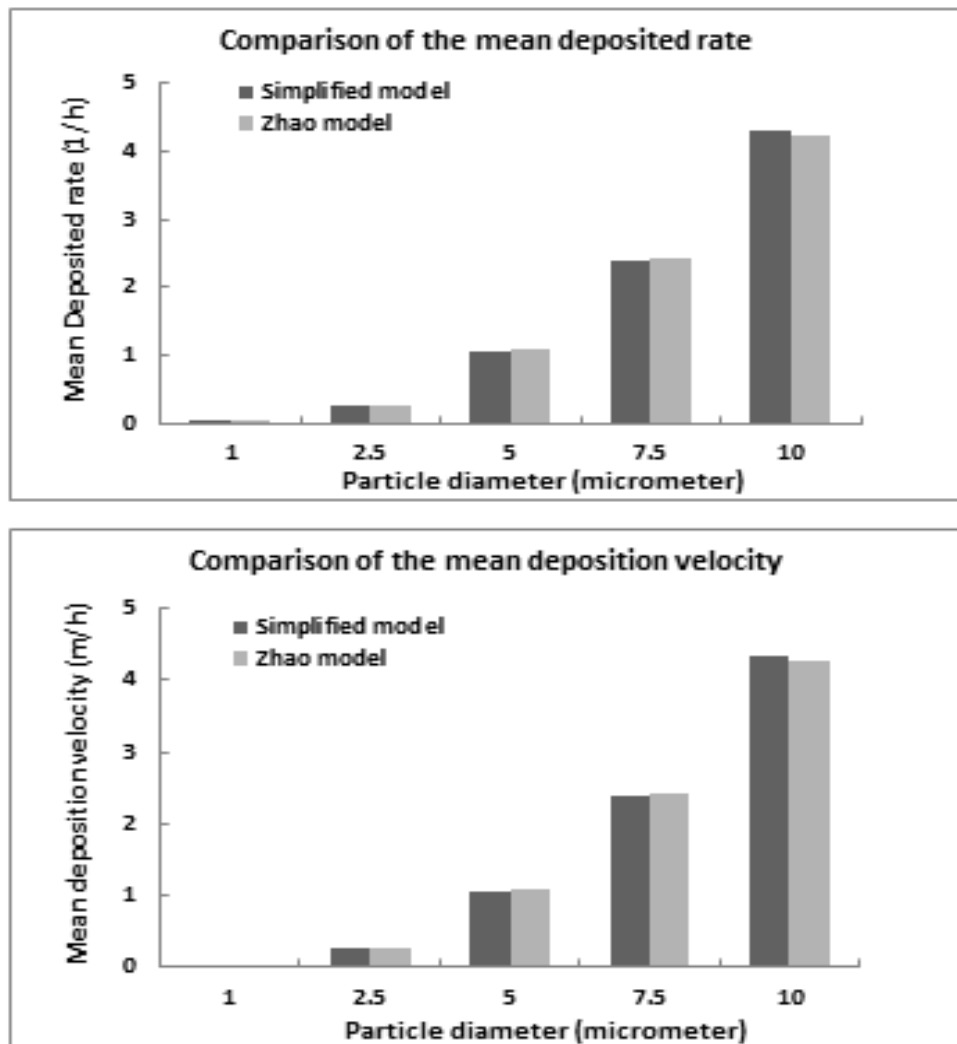


Figure 5.6: Comparison of a) the mean deposited rate (1/h) predicted for different diameters; b) the mean deposition velocity (m/h) predicted for different diameters.

Furthermore, the research study of Gao and Niu [71] was used to validate the ability of the model in predicting the variation of the inter-personal exposure (IPE) with time when transient respiratory activities were involved. In their work, two persons (contaminated and exposed occupants) in the seated position facing each other and separated by a distance of 1.2 m occupy a chamber of dimensions (2.7 m × 2.6 m × 2.2 m). The chamber was ventilated by the *DV* system with a supply flow rate of 0.024 m³/s and a temperature of 22 °C. One sneeze exhaled from the mouth of the infected

occupant lasting for 1 s with a volume flow rate of 250 l/min was simulated [71]. The variation of the inhaled fraction by the exposed occupant was computed during and after the sneeze. The case study of Gao and Niu [71] was simulated by our developed model.

Fig. 5.7 represents the comparison between Gao and Niu [71] and model results of the variation of the IPE with time. The results are in agreement with a relative error of the order of 10% with a maximum error of 15%. The obtained agreement validated the ability of the model in predicting the variation of the IPE with time by simulating it as the concentration within the last sub-microclimate 2 which is at the breathing level of the exposed person.

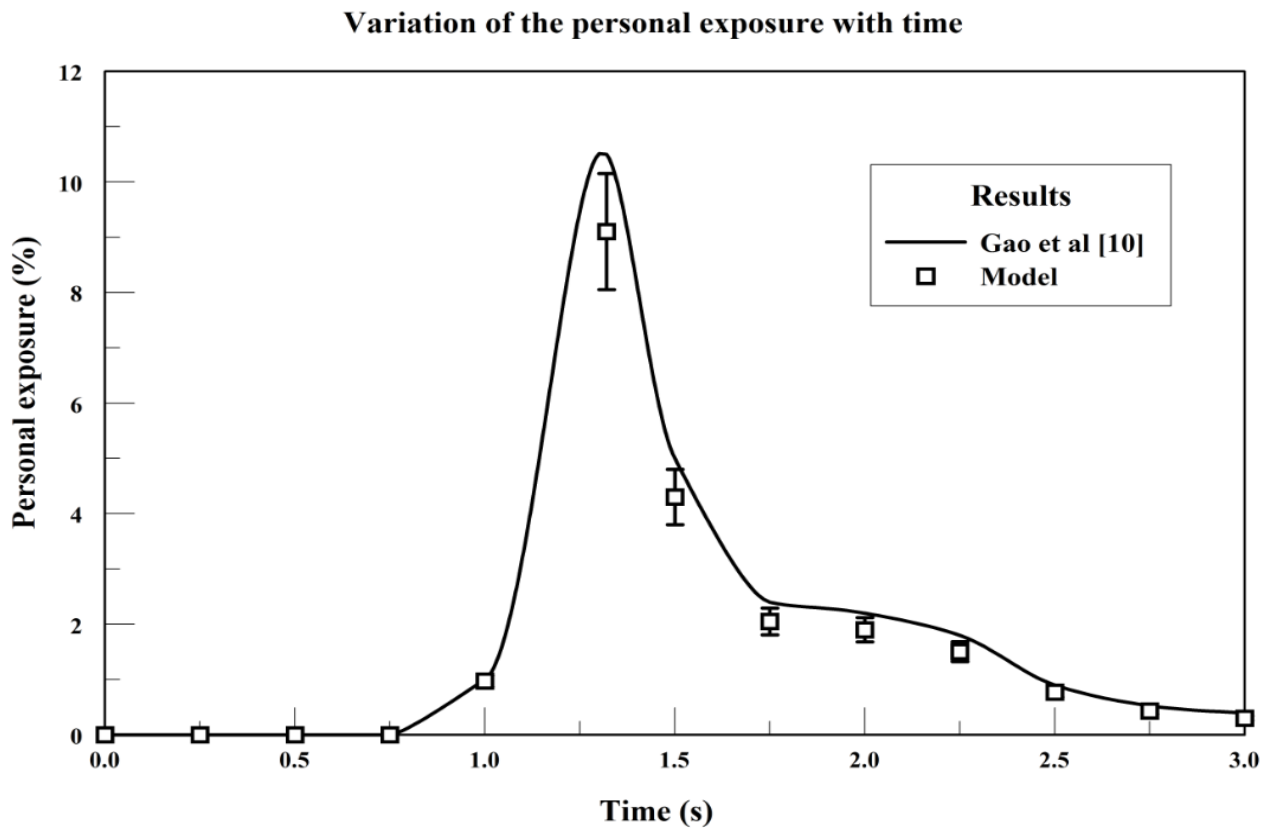


Fig.5.7: Comparison of current model prediction of personal exposure in % as a function of time with values published by Gao and Niu [71].

5.1.1.2. Validation with Experimental Data

Experiments were performed using the experimental set-up of the *DV* space described in section 4.2. Figure 5.8 represents a comparison of experimental and modeling results for the variation with height of averaged normalized CO₂ concentrations within microclimate 2 (the exposed zone) for different injection velocities (1, 3, and 10 m/s).

Good agreement was obtained between theoretical and experimental results with a relative error of the order of 10%. From this first set of experiments, it is observed that as the velocity of the exhaled jet increases, the proportion of particles penetrating the rising thermal plumes increases creating a concentration peak at the breathing level of the exposed person (Fig. 5.8). For mean exhalation velocities lower than 1 m/s corresponding to normal breathing activities the proportion of particles escaping the rising plumes is very small as no concentration peak is observed at the breathing level (Fig. 5.8.a). This justifies the assumption that for normal respiration activity particles are entirely transported by the upward plumes. Therefore, the variation of normalized concentrations in microclimates 1 and 2 and the macroclimate are nearly the same as no horizontal concentration gradients are present within the surrounding air. As the exhalation velocity increases more particles escaped towards the microclimates creating horizontal gradients in concentration within the surrounding.

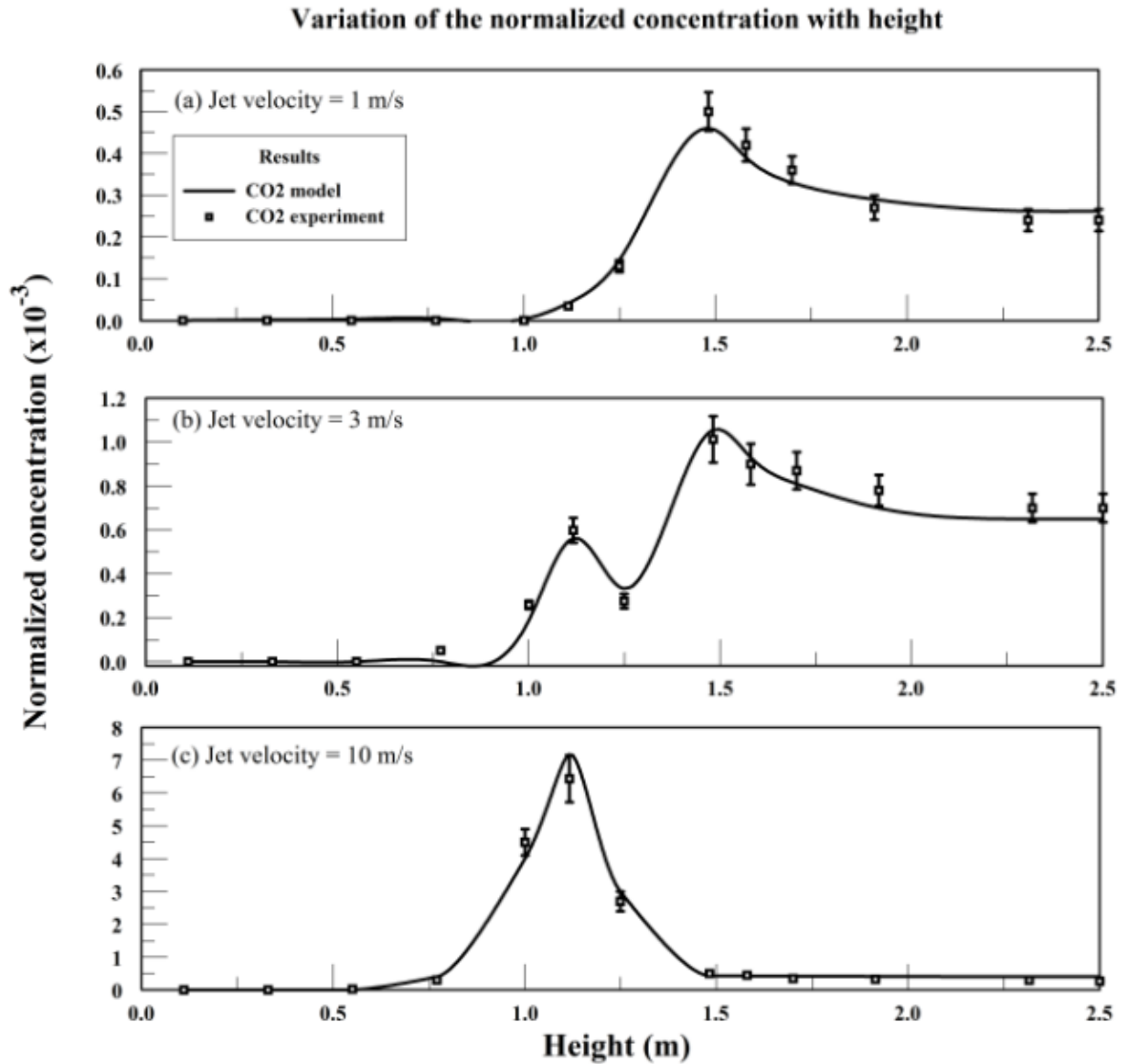


Fig. 5.8: Variation of the normalized concentration of CO₂ in microclimate 2 with height within a 90% confidence interval at different jet velocities: a) 1 m/s; b) 3 m/s; c) 10 m/s.

Fig. 5.9 illustrates the variation of the normalized concentration of CO₂ and 5 μ m particles with height within a 90% confidence interval at a jet velocity of 3 m/s within microclimates 1 and 2 and the macroclimate. The agreement between the model and experimental results for 5 μ m particles validate the ability of the model in capturing the gravitational effect. The gravitational effect opposed the upward transport of

particles by the *DV* system increasing the peaks at the breathing level and decreasing the peaks at the stratification height (Fig. 5.9). From the experimental results, it was clear that for CO₂ and 5 μm particles the concentration within microclimate 1 adjacent to the generation is higher than microclimate 2 since particle penetration creates horizontal gradients in concentration within the surrounding.

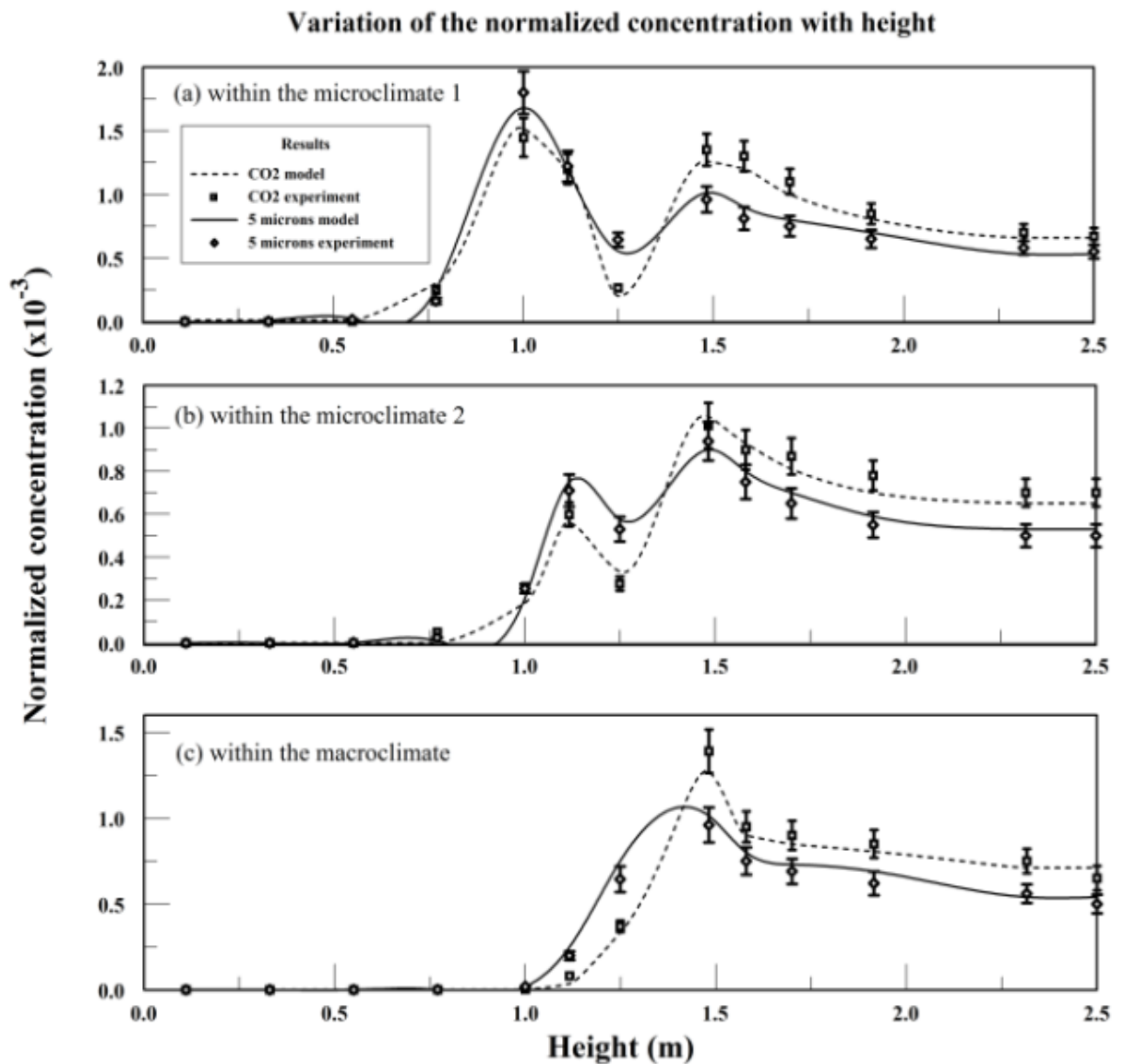


Fig. 5.9: Variation of the normalized concentration of CO₂ and 5 μm particles with height within a 90% confidence interval at a jet velocity of 3 m/s within different zones: a) microclimate 1; b) microclimate 2; c) macroclimate.

Two concentration peaks were recorded in the two microclimates as shown in Fig. 5.9.(a-b). The first peak at the level of particles generation is due to penetration of particles from the ascending infected plume to the microclimate zones because of the high exhalation momentum.

As the exhaled flow is unidirectional it affects largely the two microclimates (representing the microenvironment between the two occupants facing each other) which explain the observation of the penetration peak only for the microclimate zones (fig. 5.9.(a-b)) and not for the macroclimate zone (fig. 5.9.c). On the other hand, the second peak at the stratification level is created by the airflow motion in the air surrounding the plumes within the space ventilated by the *DV* system (fig. 5.9). In fact, the stratification height is physically the height at which the total upward convective flow equals the supply flow rate [47,77]. Thus, above this height the flow in the air surrounding the plumes (the microclimates and the macroclimate) is upward while below it, it is downward. Therefore, particles accumulate at this level within the microclimates and the macroclimate zones resulting in the apparition of the stratification peak (fig. 5.9.(a-b-c)). For large velocities as 10 m/s, the penetrating proportion became significantly high accumulating particles at the breathing level leading to an exhalation peak dominating the stratification one which nearly disappear (fig. 5.8.c) increasing the risk of cross-contamination (fig. 5.8). Therefore, HMRA reduce the effectiveness of the *DV* system since particles are not completely transported by the rising convective plumes to be effectively evacuated from the space.

Fig. 5.10 represents the comparison between the model and experiments of the variation with time and distance of the particle concentration normalized by the generation concentration. Three cases were investigated at distances from generation of

0.5, 1 and 1.5 m while keeping occupants' separating distance fixed at 1.5 m. After generation, the normalized concentration increases with time reaching a peak and then decays. As the distance from generation increases, the concentration peak decreases due to the exhalation jet decay and the time needed to reach this peak increases because of the time delay resulting from the jet propagation. Good agreement of the order of 10% with a maximum error of 16% was obtained between the model and experimental results validating the ability of the model in capturing the exhaled jet propagation and decay with time and distance.

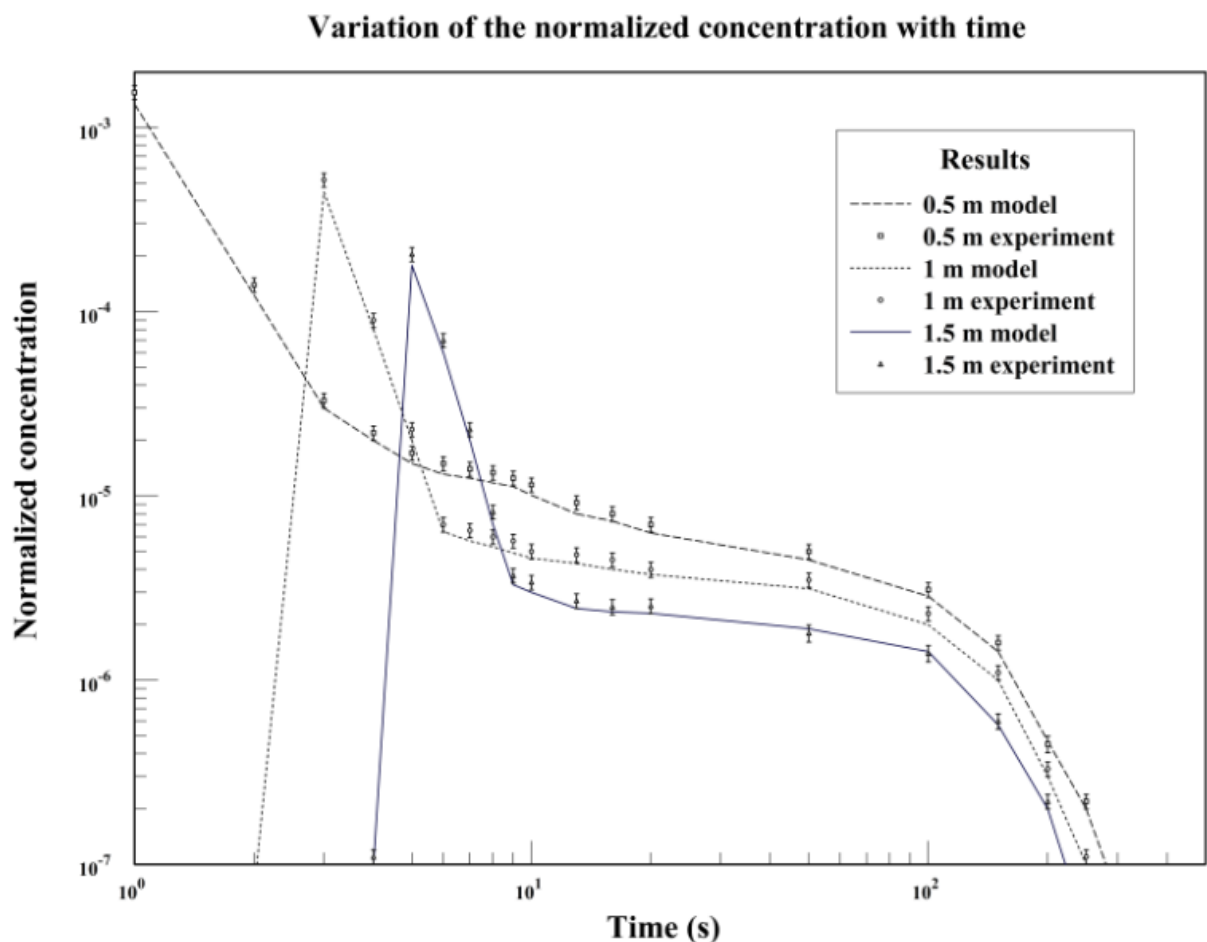


Fig. 5.10: Plot of variation in time of the predicted and experimentally determined values of normalized particle concentration of the exhaled jet at distances of 0.5 m, 1 m, and 1,5 m from particle generation location.

5.1.1.3. Case Study of Non-Equal Heat Strength Sources

The developed model was applied to study the cross-contamination between occupants in typical offices ventilated by *DV* systems with non-equal heat strength sources (see Fig. 5.11). For this goal, the simplified model was applied to a typical internal office layout occupied by an infected and exposed persons. The investigation of different supply conditions was performed to come up with recommendations on the required design of the *DV* system to satisfy both thermal comfort and IAQ criteria.

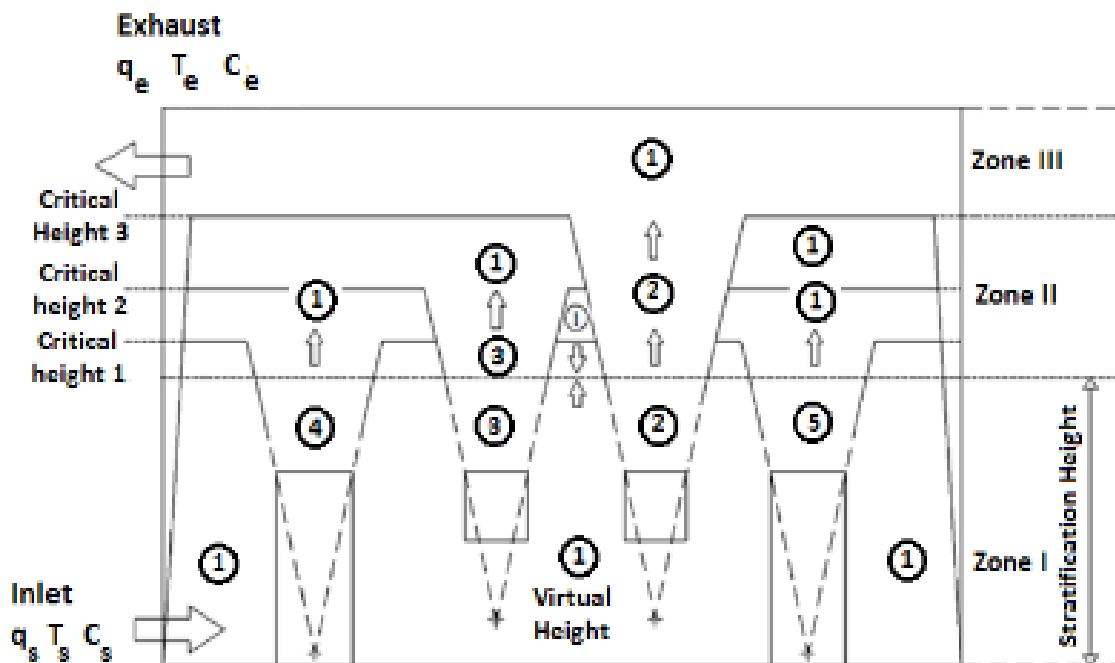


Fig. 5.11: Representation of the discretized domain with non-equal heat sources strength.

The domain consists of a room occupied by two sitting persons; one is generating particles representing the infected person and the other is the exposed person. The load distribution was selected to represent a typical internal office configuration: two sitting humans simulating two persons at rest (75 W each) equipped

by their personal computer (100 W each), and lighting (50 W) constitute the internal heat sources, and a load of 150 W from the external wall is considered. For the studied case, four non-interactive thermal plumes (as in fig. 5.11) are considered where the infected and exposed plumes of equal strength expand at the first critical height, and the two identical computer plumes expand at the second critical height because of their higher heat strength (in this case there is no additional distinct critical height).

The inlet conditions of the supply airflow were varied to satisfy the thermal and indoor air quality criteria. For instance, a low intake fraction is recommended at the breathing level of the exposed person for the inhalable range of particles particularly for particle diameter lower than 10 μm constituting the critical range since they present the highest potential to penetrate the airways and reach the alveoli increasing the possibility of contaminating the exposed person [124,125]. In addition, the temperature in the occupied zone should be between 23 and 26 $^{\circ}\text{C}$ [126] and the temperature difference between the feet and the head should not exceed 2 $^{\circ}\text{C}$ to 3 $^{\circ}\text{C}$ [126]. The supply temperature was fixed at 22 $^{\circ}\text{C}$ which is 3 $^{\circ}\text{C}$ below the set-point room temperature to avoid thermal draught [127]. For this temperature, the flow rate was changed until meeting all the load removal and IAQ requirements.

The flow rate largely affects the particles dispersion within the space and the level of the stratification height. For tracer gases, it is recommended to have the stratification height just above the breathing level to insure good IAQ [16,50]. For this reason, the first flow rate investigated was 60 L/s insuring a level of 1.2 m for the stratification height that is slightly higher than the occupied zone which guarantees a high IAQ for tracer gases. The particle distribution was studied for different diameters within the inhalable range (0.1, 1, 2.5, 5, 7.5, 10, 12.5 and 15 μm). It was shown that for

a flow rate of 60 L/s, the performance of the DV system in terms of IAQ for particle diameters between 5 and 12.5 μm is weakened due to the gravitational effect opposing the upward flow motion.

The particle diameter plays a major role in the determination of particle distribution within the space and deposition on different surfaces. Figure 5.12 shows the variation of the normalized particle concentration with height for different diameters (1, 5, 10, 12.5, 15 μm) from the fine to the coarse mode in the surrounding air zone for a flow rate of 60 L/s.

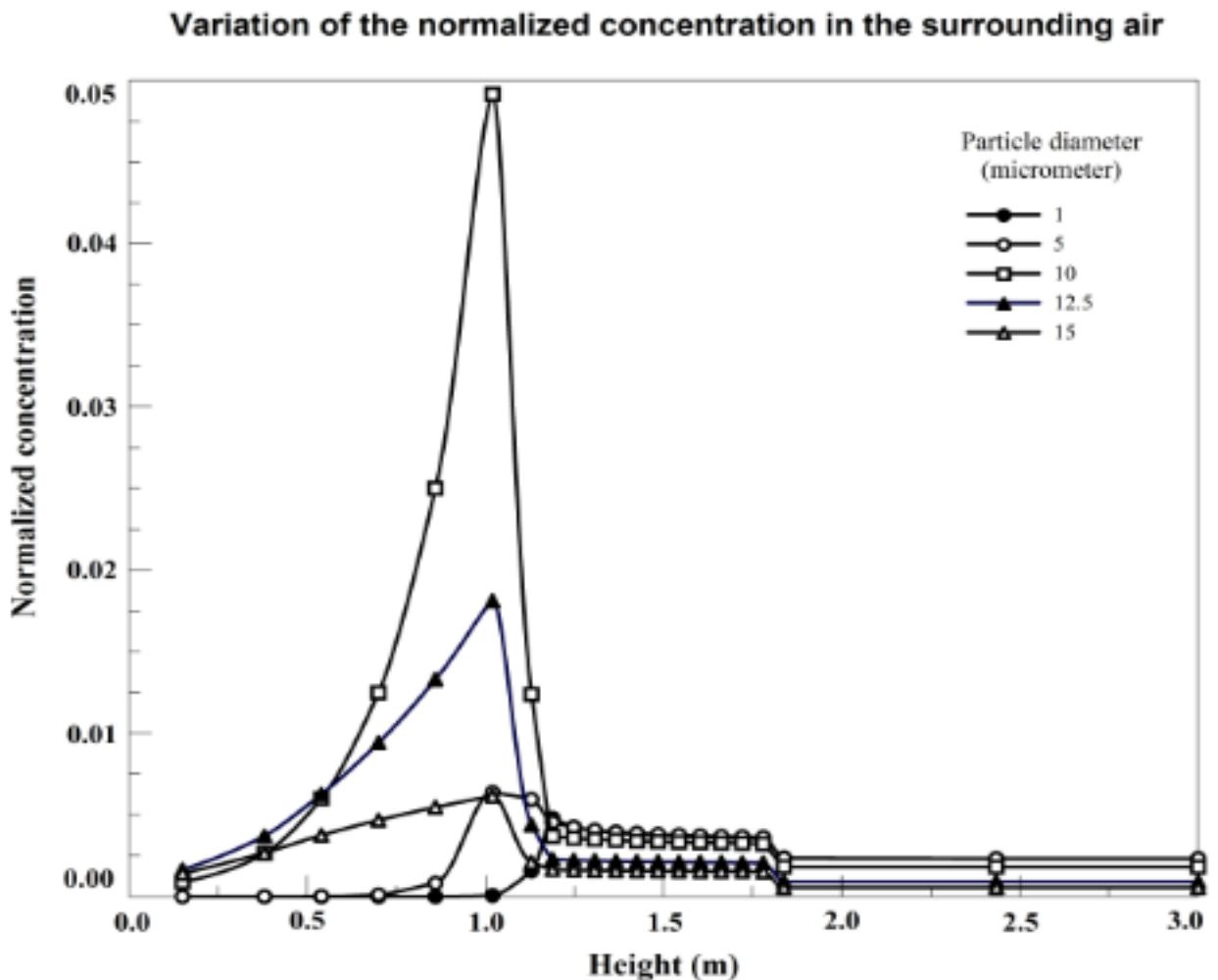


Fig. 5.12: Variation of the normalized particle concentration with height for different particle diameters in the surrounding air zone for a flow rate of 60 L/s.

Table 5.1 summarizes the predicted maximum normalized concentration and the normalized concentrations at the breathing level and at the exhaust for particles from 0.1 μm to 15 μm .

Table 5.1: Influence of flow rate and particle diameter on normalized concentrations.

Stratification/ Critical 1 / Critical 2 heights	Simulated case [q_s , d_p]	Normalized concentration (%) at the breathing level	Exhaust Normalized concentration	Maximum normalized concentration in the surrounding air
1.2/1.75/1.85	[60,0.1]	1.4541e-4	2.333e-3	4.709e-3
	[60,1]	1.6542e-4	2.332e-3	4.788e-3
	[60,2.5]	2.6972e-4	2.329e-3	4.805e-3
	[60,5]	6.2965e-4	2.322e-3	6.379e-3
	[60,7.5]	1.202e-3	2.291e-3	2.728e-2
	[60,10]	1.31e-3	1.804e-3	4.915e-2
	[60,12.5]	4.687e-4	9.039e-4	1.811e-2
	[60,15]	2.2743e-4	5.456e-4	6.148e-3
1.3/1.9/2	[80,0.1]	5.213e-6	1.7497e-3	3.3354e-3
	[80,1]	5.461e-6	1.7496e-3	3.3365 e-3
	[80,2.5]	8.433e-6	1.7484e-3	3.366e-3
	[80,5]	6.1402e-5	1.7436e-3	3.379e-3
	[80,7.5]	2.5702e-4	1.7342e-3	3.383e-3
	[80,10]	6.556e-4	1.7047e-3	5.668e-3
	[80, 12.5]	9.477e-4	1.4396e-3	1.2116e-2
	[80,15]	5.398e-4	8.348e-4	8.253e-3
1.4/2.1/2.2	[100,0.1]	4.0062e-6	1.3998e-3	2.6854e-3
	[100,1]	4.0719e-6	1.3997e-3	2.6942e-3
	[100,2.5]	4.5157e-6	1.3987e-3	2.7072e-3
	[100, 5]	1.0488e-5	1.3951e-3	2.7098e-3
	[100,7.5]	5.3548e-5	1.388e-3	2.7115e-3
	[100,10]	2.0382e-4	1.378e-3	2.7178e-3
	[100,12.5]	5.0561e-4	1.339e-3	3.2907e-3
	[100,15]	6.9509e-4	1.097e-3	6.074e-3

As the particle diameter increases, the effect of the gravitational settling increases resulting in: 1) a decrease in the exhaust concentration for all diameters, and

2) an increase in the maximum normalized concentration within the air for particle diameter below 10 μm (see Fig. 5.12).

Table 5.2 illustrates the effect of flow rate and particle diameter on the percentage of deposition of particles and their distribution on different walls' orientation.

Table 5.2: Influence of flow rate and particle diameter on particle deposition.

Simulated case [q_s, d_p] q_s (L/s): flow rate d_p (μm): particle diameter	% of particle deposition	Fraction of particles deposited on the vertical walls (%)	Fraction of particles deposited on the ceiling (%)	Fraction of particles deposited on the floor (%)
[60,0.1]	0.9	81.98	18.02	0
[60,1]	0.32	55.45	0	44.55
[60,2.5]	0.56	45.37	0	54.63
[60,5]	3.36	8.72	0	91.28
[60,7.5]	12.46	0.63	0	99.37
[60,10]	20.17	0.0225	0	99.9775
[60,12.5]	57.96	0.0038	0	99.9962
[60,15]	72.62	0.0015	0	99.9985
[80,0.1]	0.61	73.31	26.69	0
[80,1]	0.21	91.34	0	8.66
[80,2.5]	0.15	75.23	0	24.77
[80,5]	1.67	38.89	0	61.11
[80,7.5]	6.33	15.78	0	84.22
[80,10]	13.15	1.76	0	98.24
[80,12.5]	19.97	0.05	0	99.95
[80,15]	51.45	0.004	0	99.996
[100,0.1]	0.21	73.25	26.75	0
[100,1]	0.16	100	0	0
[100,2.5]	0.13	81.82	0	18.18
[100,5]	0.1	49.89	0	50.11
[100,7.5]	1.29	22.04	0	77.96
[100,10]	4.03	2.52	0	97.48
[100,12.5]	10.05	0.07	0	99.93
[100,15]	17.03	0.0075	0	99.9925

For small diameters, turbulent diffusion and Brownian motion are the dominant physical mechanisms affecting deposition while gravitation plays a minor effect. This explains the high percentage of deposition on vertical walls and ceiling for sub-micrometer particles although the percentage of total deposition from those generated is relatively small. For large particle diameters, the effect of turbulent diffusion and Brownian motion on particle deposition is lower leading to the decrease in percentage of particle deposition. On the other hand, the settling effect of larger particles is more pronounced. When the gravitational effect is significant, the percentage of deposition reaches relatively high values. For example, for a flow rate of 60L/s, total deposition is lower than 1% for particle diameters lower than 2.5 μm but increases significantly for larger/heavier particles reaching a value of 72.62% for particles of 15 μm with 99.99% depositing on the floor (see Table 5.2). Floor deposition plays a significant role in reducing particle exposure only for particle diameters larger than 10 μm . The deposition of particles on the floor acts against the principle of *DV* system featured with reduction of contaminants in the occupied zone by entraining them into the upward buoyant flows. Deposition on the floor would not then play a positive role in particle removal unless it overcomes the upward flow in the surrounding air created by the *DV* system below the stratification height.

Figure 5.13 shows the predicted normalized particle concentration vertical distribution within the plumes of the computers and within the infected and exposed persons plume zones and the surrounding air zone at supply flow rate of 60 L/s, and particle diameter of 1 μm . As particles are generated within the thermal plume of the infected occupant, this plume favors their transport toward the ceiling level to be removed from the exhaust. This is why the highest concentrations of particles are within

the plume zone of the infected person. As the plume of the non-infected person and the computer one rise, they entrain relatively contaminated air from the surrounding.

Therefore within the exposed person plume, the concentration increases gradually from the breathing level of the exposed person until the critical height of the plume providing protection to a certain extent (see Fig. 5.13). As the surrounding zone constitutes the connection between the contaminated and exposed plumes, the concentration in this zone lies between the two. The merging of plumes within the surrounding at different critical heights is also illustrated in Fig. 5.13.

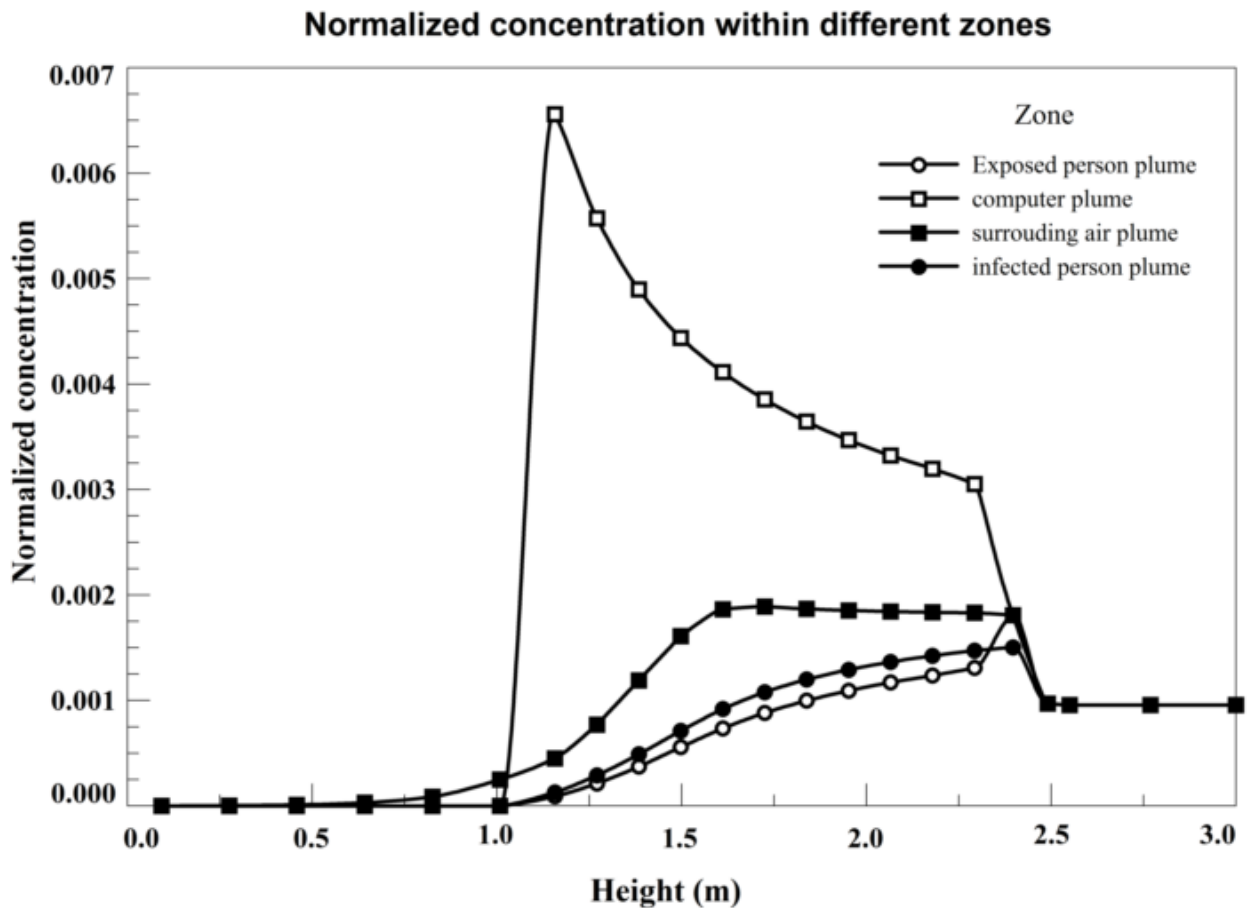


Fig. 5.13: Variation of the normalized particle concentration with height within the different zones for a flow rate of 60 L/s and a particle diameter of 1 micrometer.

At the level of the first critical height (approximately at 1.75 m), the plumes of the infected and exposed person merge with the surrounding. For the computer plumes, the plume expansion takes place at a higher level at the second critical height (approximately at 1.85 m).

The variation of the normalized concentration at the breathing level of the exposed person (Table 5.1) is determined by a balance between the upward flow motion of the *DV* system and the downward settling due to the gravitational effect on the particle. In the first stage, as the particle diameter increases the settling effect becomes stronger which increases the concentration of particles in the occupied zone and thus augments the concentration at the breathing level of the exposed person resulting in a decrease in the protection effectiveness provided by the ascending thermal plume of the exposed person. When the settling effect opposing the upward flow becomes dominant, the floor deposition increases significantly acting as a particle removal factor decreasing the intake fraction as the particle diameter increases (Tables 5.1-5.2). At low flow rate of 60 L/s, it is observed that as the particle diameter increases from 0.1 μm to 10 μm , the particle normalized concentration at the breathing level of the exposed person is augmented reaching a maximum value of 1.31×10^{-3} for 10 μm particles, which is relatively high. As particle diameter exceeds 10 μm , the maximum normalized concentration decreases (see Fig. 5.13) due to settling and floor deposition leading to a decrease in the particle normalized concentration at the breathing level of the exposed person (Table 5.1). The occurrence of the maximum intake fraction for a diameter of 10 μm within the critical range increases the risk of cross-infection between the occupants which should be avoided. In other words, the gravitational effect associated with large particle sizes opposes the upward flow motion and results in accumulating particles

below the stratification height leading to higher risk of cross-contamination unlike tracer gases (airborne particles). A higher level for the stratification height is the required for large size particles to satisfy IAQ criteria for the inhalable range. This is achieved by increasing the flow rate to elevate the stratification height well above the breathing level of exposed occupants.

It is of interest to maintain the stratification effect for a wide range of particle diameters which can be achieved by increasing supply air flow rate to overcome the considerable downward settling motion for large diameter particles. This is demonstrated in Fig. 5.14 where the vertical variation of normalized concentrations within the surrounding air of the different particle sizes are shown for higher DV supply flow rates of (a) 80 L/s and (b) 100 L/s.

By increasing the supply flow rate from 60 to 80 L/s, the stratification and the first critical height are shifted upward respectively from 1.2 to 1.3 and from 1.75 to 1.9 m increasing the removal of contamination effectiveness leading to a considerable decrease of particles concentration in the space especially at the breathing level of the exposed person for the wide range of particle diameters. The effect of the settling velocity is reduced as the upward flow velocities increase at higher flow rates. For example, the maximum intake fraction within the critical range decreased from

1.31×10^{-3} to 6.655×10^{-4} when the supply flow rate increased from 60 to 80 L/s (see Table 5.1). Additionally, the particle diameter at which the maximum intake fraction takes place is shifted from 10 to 12.5 μm respectively (Table 5.1 and Fig. 5.12 and Fig. 5.14.a) while the particle diameter above which the maximum normalized concentration takes place is shifted from 5 to 7.5 μm respectively. At fixed particle diameter, the total deposition rate decreases as the flow rate increases due to the higher

removal efficiency of the *DV* system. The particle diameter at which minimum deposition occurs is shifted from 1 to 2.5 μm due to the weakening of the gravitational settling effect. The IAQ performance at *DV* flow rate of 80 L/s is much better than at 60 L/s.

L/s.

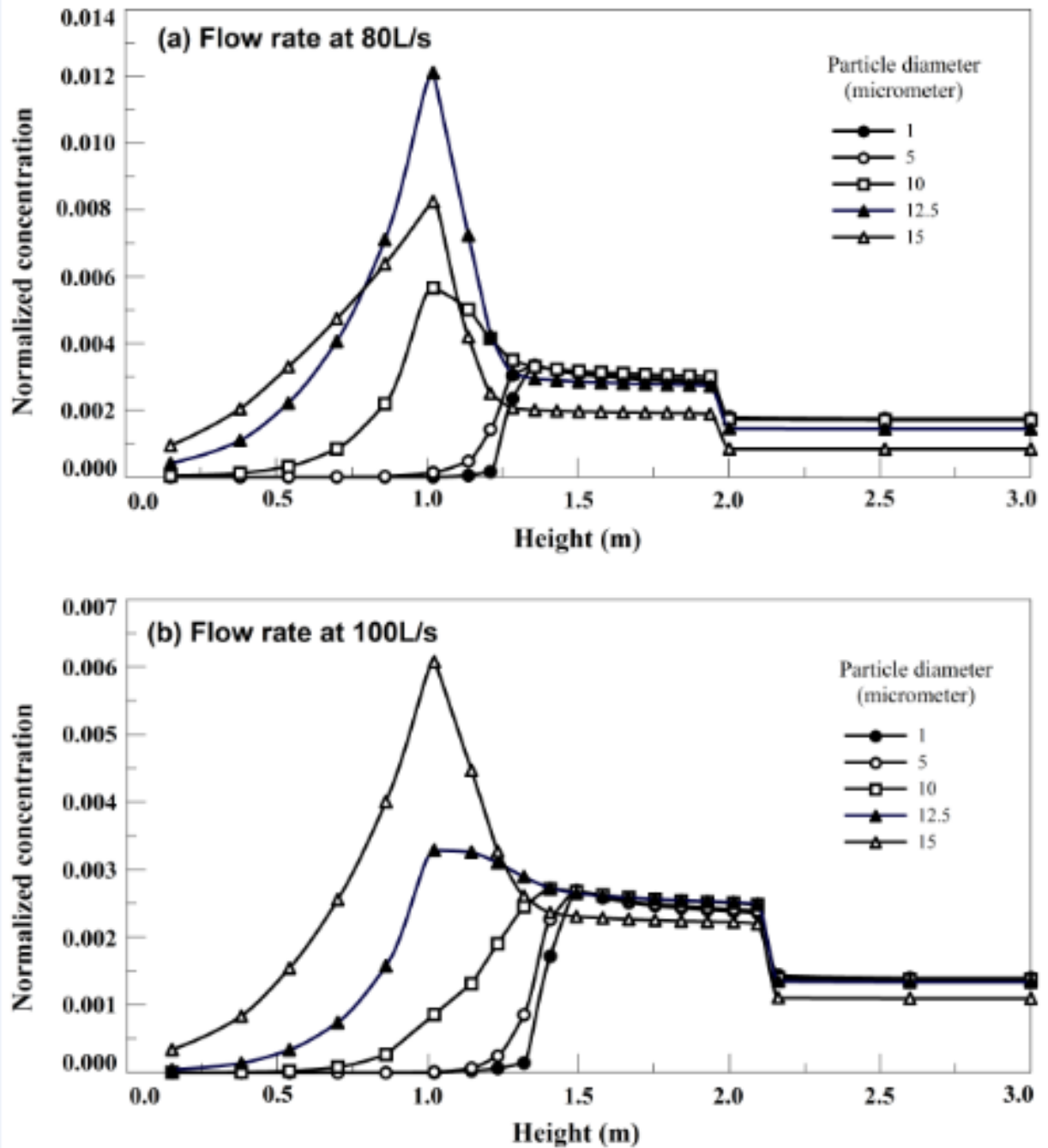


Fig. 5.14: Increase of the flow rate to meet the IAQ criteria to a value of: a) 80 L/s; b) 100 L/s.

However, particles for diameters in the critical range between 7.5 and 10 μm still accumulate at the breathing level increasing the possibility of contamination. For this reason, when the flow rate was further increased to a value of 100 L/s, the maximum normalized concentration for particles less than 10 μm within the surrounding air takes place at the stratification level of 1.4 m approximately as seen in Fig. 5.14.b. The maximum intake fraction within the critical range is decreased to 2.0832×10^{-4} (Table 5.1) for a flow rate of 100 L/s. Therefore, this flow rate is required to insure good IAQ criteria not only for tracer gases but also for particle diameters within the critical range. It can then be concluded that having a stratification height just above the breathing level [16,50] is not enough for insuring good IAQ for the critical inhalable range which is satisfied in our case study at a stratification height higher than 1.4 m.

As mentioned earlier, the supply air conditions should not only meet the IAQ criteria but also the thermal comfort and load removal requirements in the space. Therefore, the performance of the *DV* system in terms of thermal comfort for the different supply conditions studied was investigated and the results obtained are summarized in Table 5.3.

As the flow rate vary from 60 to 100 L/s, the temperature difference between the feet and the head for a seated person decreases from 4.45 to 2.65 $^{\circ}\text{C}$ and the temperature range within the occupied zone is reduced from [23.33 $^{\circ}\text{C}$; 27.78 $^{\circ}\text{C}$] to [23.2 $^{\circ}\text{C}$; 25.85 $^{\circ}\text{C}$]. Thus as the flow rate increases from 60 to 80 L/s to 100 L/s, the performance of the *DV* system in terms of thermal comfort is enhanced. The two criteria for thermal comfort are both satisfied for the supply conditions of 22 $^{\circ}\text{C}$ and 100

L/s for which the temperature in the occupied is between 23 and 26 °C [125] and the temperature difference between the feet and the head is lower than 3 °C [125].

Table 5.3: Performance of the *DV* system in terms of Thermal comfort for different supply conditions.

Supply conditions [q_s , T_s] q_s (L/s): supply flow rate T_s (°C): supply temperature	Difference in temperature (°C) between the feet and the head	Temperature range in the occupied zone
[60,22]	4.45	[23.33; 27.78]
[80,22]	3.33	[23.24;26.57]
[100,22]	2.65	[23.2; 25.85]

5.1.1.4. Case Study of Different Respiratory Activities

The studied case investigate cross-contamination between two occupants (75 W each) within a space of dimensions 3.4 m × 3.4 m × 2.6 m ventilated by a *DV* system. The frequently encountered heat sources (occupants, lighting, external heat from walls) were considered. The lighting load was set to 100 W and wall heat fluxes to 200W. The case studied was selected to represent typical office load and the design case was conducted at 40 W/m² based on upper limit of load removal by *DV* system [18,19]. The generality of the obtained result stems from the fact that office spaces are usually configured in modular workstation units where each unit would have identical number of occupants as well as electrical load. One occupant generated particles constituting the infected person while the second occupant was healthy simulating the exposed person. The *DV* supply flow rate was varied in the range of [50 L/s-200 L/s]. In fact, as described in section it was found that a flow rate of 100 L/s is required to insure both

thermal comfort and IAQ for typical office spaces loaded by 40 W/m^2 ventilated by *DV* system. However, they just considered normal respiratory activities. Coughing velocities vary between 6 and 22 m/s [128] challenging the performance of the *DV* system. In the case study the critical velocity of 22 m/s and exhalation area of 4 cm^2 [128] were used. In order to assess the risk of HMRA, the effect of different variables (*DV* supply flow rate, particle diameter, distance between the occupants) on cross-contamination was studied.

Fig. 5.15 represents the effect of the *DV* supply flow rate on the variation with height of $1 \mu\text{m}$ particle concentration in the microclimate 2 which represents the exposed zone. As the flow rate increases, the concentration within this zone decreases reducing the risk of disease transmission between the occupants. Furthermore, the penetration peak is shifted upward. However this shift stills not sufficient even for a supply flow rate of 200 L/s which is much larger than conventional flow rates of the *DV* system for similar conditioned space. In fact, by increasing the *DV* flow rate from 50 to 200 L/s the penetration peak is just shifted from 1 to 1.2 m remaining in the breathing zone which is limited by the head level extending from 1 to 1.2 m in height for a seated person. Therefore the standalone *DV* system is not able of preventing particle accumulation at the breathing level and its performance can be enhanced by implementing engineering strategies to it. For instance, assisting *DV* by chair fans blowing air upward, increases the strenght of the rising human thermal plumes and thus reduces particle penetration towards the exposed zone. In addition, using *DV* system with personalised ventilation delivering fresh air at the proximity of the breathing level of the exposed person can also be a solution.

Variation of the normalized concentration with height

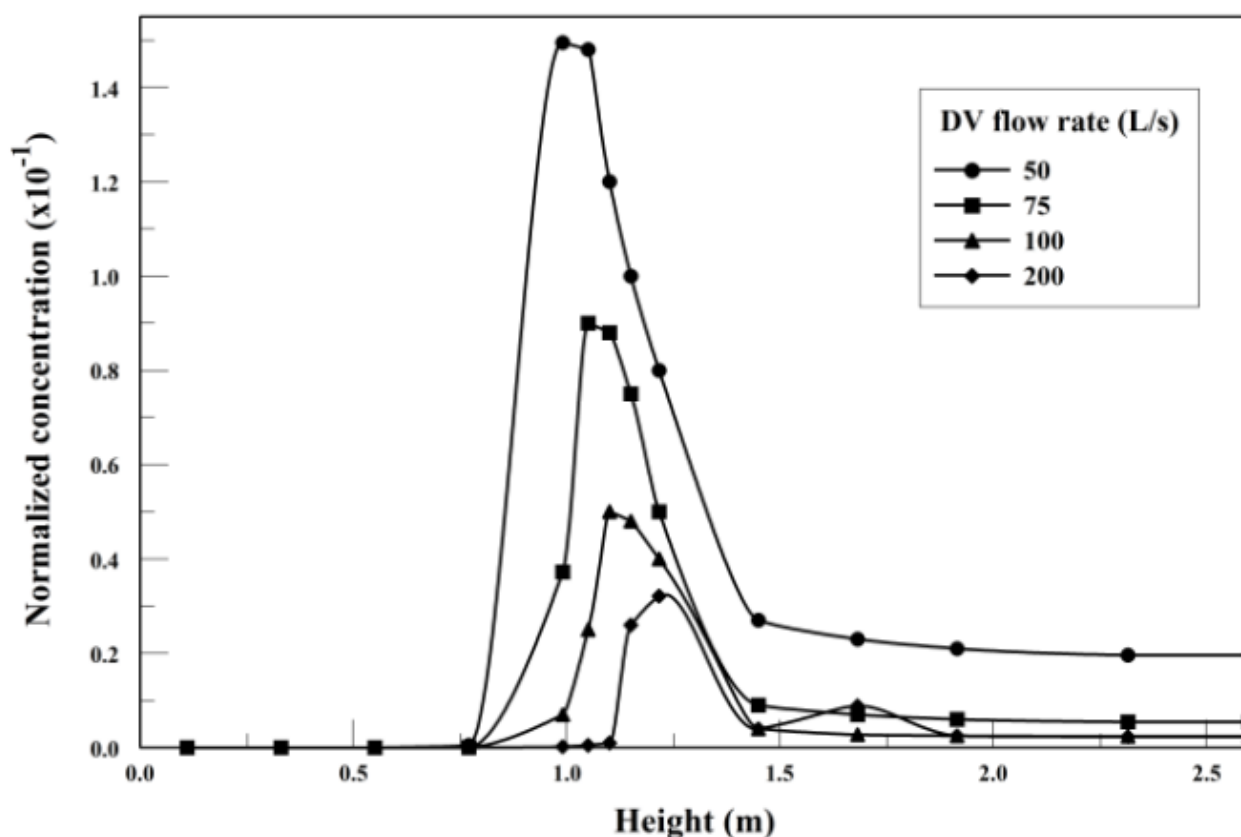


Fig.5.15: Variation with height of the normalized concentration of 1 μm particles in microclimate 2 for different DV supply flow rates.

Figure 5.16 illustrates the effect of the particle diameter on the variation of particle concentration with height within microclimate 2 for a DV flow rate of 100 L/s. As the particle diameter increases, the gravitational effect opposes the upward transport of particles within the macroclimate and microclimate zones accumulating particles within the occupied zone but at the same time deposition by the gravitational settling effect increases acting as a sink of particles.

For particles of diameter lower than 20 μm , as the diameter increases the exhalation peak becomes higher due to the opposition to the upward DV airflow. For particles of diameter higher than 30 μm , the deposition effect becomes dominant

playing a positive effect in reducing the risk of cross-infection between the occupants. For a particle diameter larger than 50 μm cross-contamination is significantly reduced. Altering the size of exhaled particles using a proper medical treatment can be beneficial to reduce disease transmission by enhancing particle deposition.

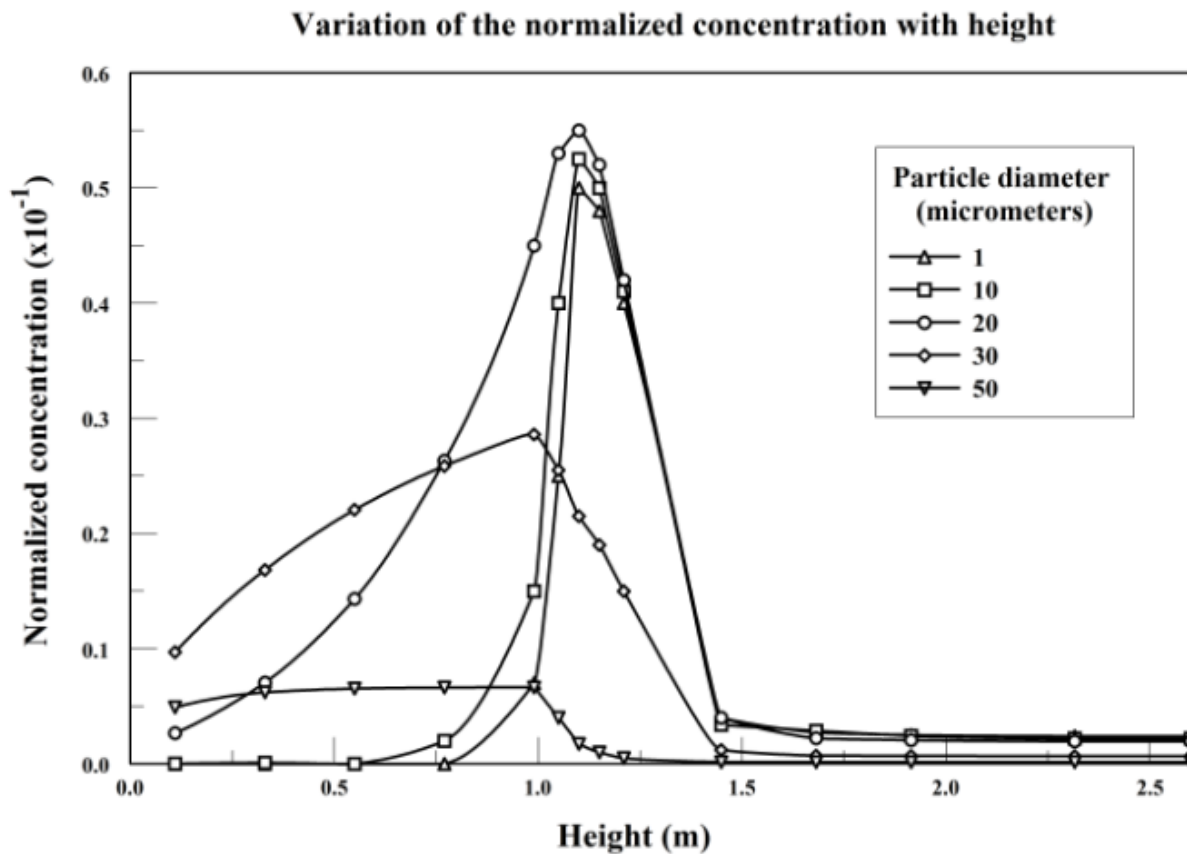


Fig. 5.16: Variation with height of the normalized concentration in microclimate 2 for different particle diameters for a DV flow rate of 100 L/s.

Figure 5.17 shows the effect of the distance between occupants on the variation with height of 1 μm particle concentration in the microclimate 2 for a DV flow rate of 100 L/s. It is evident that as the distance between occupants increases the concentration of particles at the breathing level of the exposed person decreases therefore the risk of cross-infection between occupants is reduced.

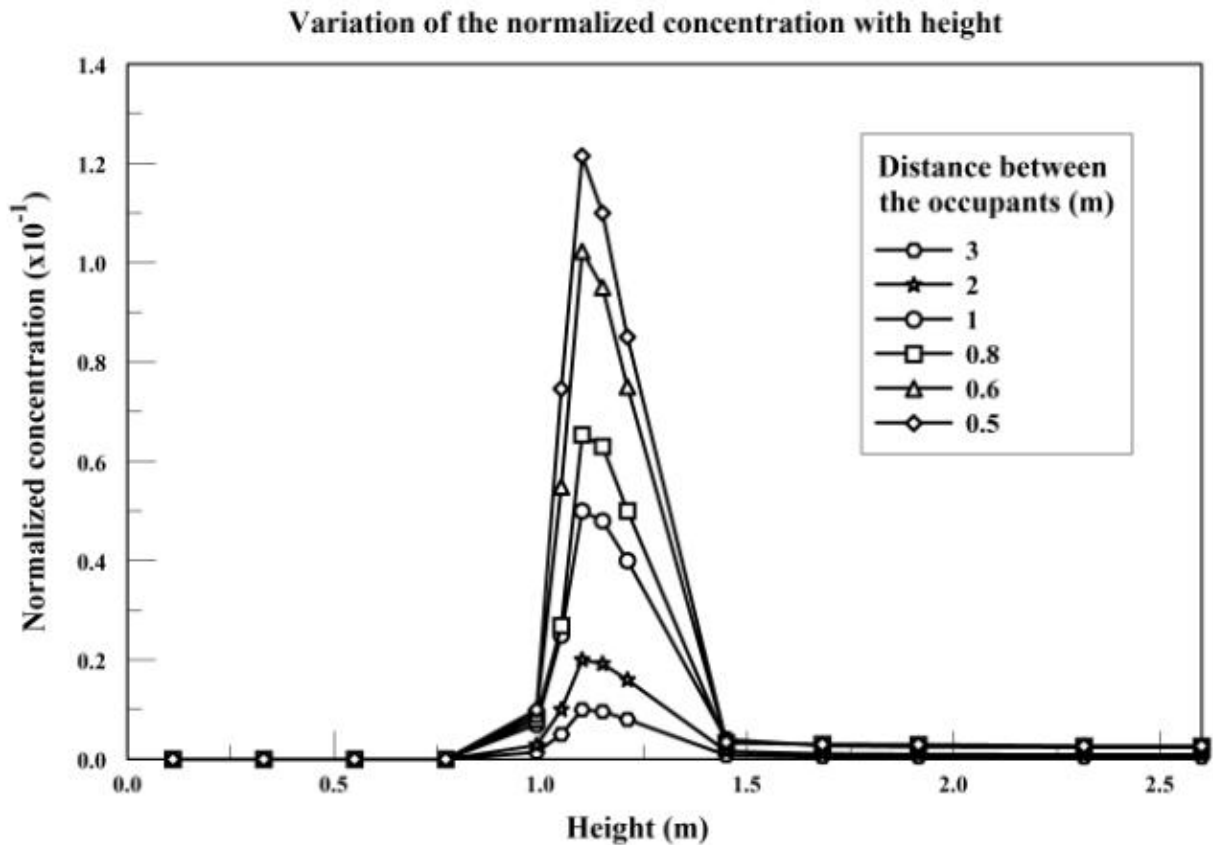


Fig. 5.17: Variation with height of the normalized concentration of 1 μm particles in microclimate 2 for different distances between the occupants for a *DV* flow rate of 100 L/s.

Figure 5.18 illustrates the variation with distance between the occupants of the concentration peak of 1 μm particles in microclimate 2 for a *DV* flow rate of 100 L/s. It is observed that for distances lower than 1 m the rate of increase of the penetration peak with decreased distance is largely incremented constituting a very dangerous zone.

Variation of the normalized peak concentration in microclimate 2

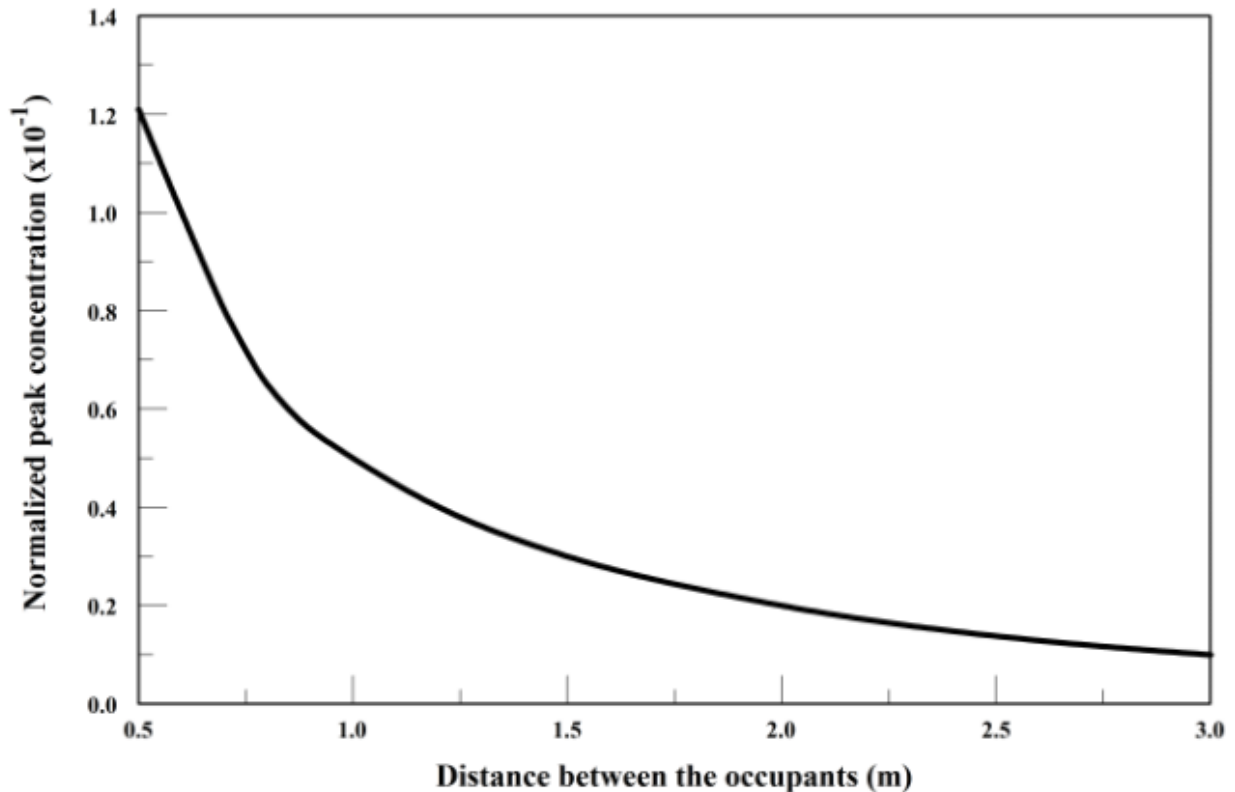


Fig. 5.18: Variation with distance between the occupants of the concentration peak of 1 μm particles in microclimate 2 for a DV flow rate of 100 L/s.

5.1.1.5. Transient Interpersonal Exposure for HMRA

One occupant generated particles transiently during one second simulating a cough released by an infected person while the second occupant was healthy simulating the exposed person. In order to assess the risk of HMRA, the effect of different variables such *DV* flow rate, coughing velocity, particle diameter, and distance between the occupants on cross-infection is studied. The *DV* supply flow rate is varied in the range of [50 L/s - 200 L/s] and the supply temperature is fixed to 22 °C. A typical cough velocity in the interval of 6 m/s to 22 m/s and an exhalation area of 4 cm² [128,129] are used. Particle diameter is varied in the range of 1 μm to 50 μm and the distance between the occupants is varied between 0.5 m and 3 m.

Interpersonal exposure was studied for different *DV* supply flow rates (50, 75, 100 L/s), cough velocities (6, 11, and 22 m/s), particles diameters (1, 20, 30, and 50 μm), and distances between the occupants (0.5, 1, 2, and 3 m). Each of these factors was varied while the other variables were fixed to capture the studied parameter effect on IPE.

5.1.1.5.1. DV Flow Rate Effect

Table 5.4 summarizes the effect of the *DV* flow rate on different parameters.

Table 5.4: Effect of the *DV* supply flow rate on different model geometric and physical parameters.

Model Parameters	<i>DV</i> supply flow rate (L/s)		
	50 L/s	75 L/s	100 L/s
Height of Zone I (m)	1.25	1.35	1.55
Height of Zone II (m)	0.41	0.47	0.55
Height of Zone III (m)	0.94	0.78	0.5
Strength of the occupant plume before expansion at the critical height (kg/s)	0.044	0.053	0.067
Maximum air velocity in Zone I (m/s)	0.00432	0.00648	0.00865
Air temperature at the floor level ($^{\circ}\text{C}$)	23.49	23.38	23.27
Air temperature at the ceiling level ($^{\circ}\text{C}$)	31.12	29.10	27.08

As the *DV* flow rate increases, the stratification and critical heights are shifted upward resulting in an increase in Zones I and II heights and a decrease in Zone III height. It is clear that the increment of the *DV* supply rate strengthened the occupants' thermal plume and the upward velocity in Zone I. This velocity decreases from a maximum value at the floor level to zero at the stratification height due to air entrainment by the convective rising plumes. The vertical air motion by buoyancy

effects leads to temperature stratification within the space resulting in a temperature increase from the floor to the ceiling levels (see Table 5.4). As *DV* flow rate increases, room air temperature gradient decreases.

IPE was studied for different *DV* supply flow rates (50, 75, 100 L/s) for a cough velocity of 22 m/s, 1 μm particles in diameter, and 1 m separating distance between occupants.

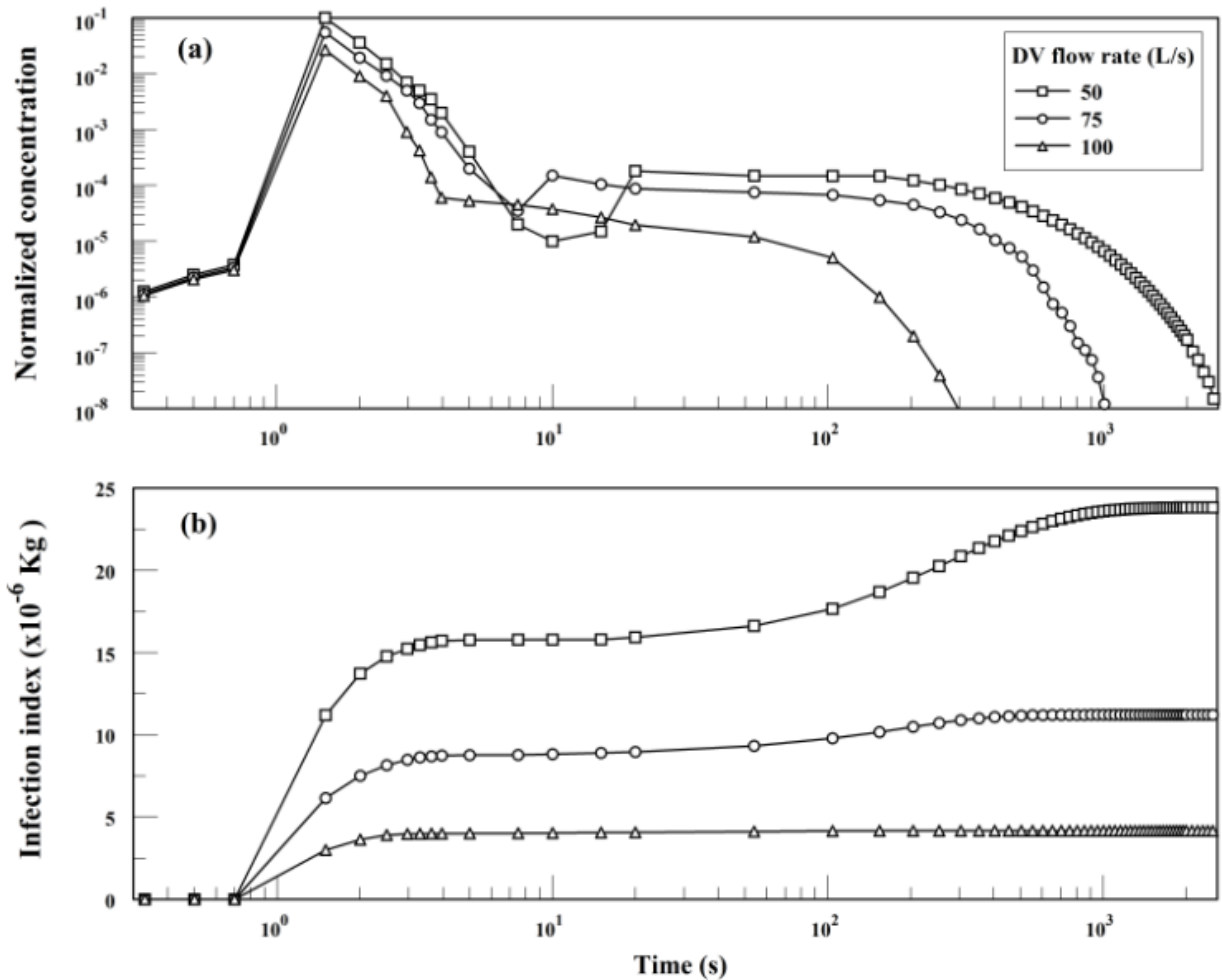


Fig. 5.19: Effect of the *DV* supply flow rate on the variation with time of: a) the normalized concentration at the breathing level of the exposed person; b) the infection index.

Figure 5.19.a illustrates the effect of the *DV* supply flow rate on the variation with time of the normalized concentration at the breathing level of the exposed person.

Logarithmic scale was used for the figure's axis for clarity of illustration. Three stages can be defined with respect to time for the different *DV* supply flow rates (Fig 5.19).

Table 5.5 summarizes the periods of the three stages for each *DV* flow rate.

Table 5.5: Periods of the three stages of the variation of inhaled concentration with time for different *DV* supply flow rates.

	DV supply flow rate (L/s)		
	50 L/s	75 L/s	100 L/s
First stage time interval	[0s; 10s]	[0s; 7.5s]	[0s; 4s]
Second stage time interval	[10s; 200s]	[7.5s; 100s]	[4s; 50s]
Third stage time interval	[200s; 2600s]	[100s; 1000s]	[50s; 300s]

The first stage is dominated by the propagation and decay of the exhaled jet (Fig. 19a) and is very fast lasting for few seconds (Table 5.5). In the second stage, particles are redistributed by the ventilation system for several minutes. A final stage is the removal stage by deposition and upward transport by the *DV* system and has the largest period (Fig. 5.19.a). The observation of different exposure stages is in agreement with the findings of Li et al [28]. The period of these three stages varied with the *DV* flow rate. The larger the flow rate is, the lower are the durations of the three stages (Fig. 5.19.a and Table 5.5). Furthermore, the effect of the *DV* flow rate on the duration of a stage is highest for the third stage and lowest for the first stage (Table 5.5).

For the different flow rates, a concentration peak (penetration peak) is observed during the first stage due to the jet propagation. The higher the *DV* flow rate is, the lower is the penetration peak because a larger number of particles is convected upward by the *DV* system (Fig. 5.19.a). This observation is in agreement with the findings of Licina et al. [130]. A second inhaled concentration peak (redistribution peak) at *DV* supply flow rate below 75 L/s appears during the second stage since the stratification

height is close to the breathing level which results in accumulating particles in the breathing zone (Fig. 5.19.a). As the *DV* flow rate increases from 50 to 75 L/s, the second peak is reduced and completely disappears for a flow rate of 100 L/s while the influence of the *DV* flow rate is less significant on the first peak which is dominated by the horizontal propagation of the exhaled jet (Fig. 5.19.a).

The penetration peak (first stage peak) is two to three orders of magnitude larger than the redistribution peak (second stage peak). However, the duration of the first stage is much smaller than the second stage (Table 5.5).

Fig. 5.19.b represents the effect of the *DV* supply flow rate on the variation with time of the infection index. The rate of increase of the infection index is relatively high during the first stage and is reduced progressively with time to reach nearly zero at the end of the third stage. The profiles of variation with time of the normalized concentration and infection index are consistent with the work of Xiaoping et al [28]. Within the set of studied conditions, the higher the *DV* flow rate is, the lower is the rate of increase of the infection index during the different stages. The inhaled dose during each stage for the different flow rates was calculated and results were summarized in Table 5.6.

Table 5.6: Inhaled dose during the different stages for different *DV* supply flow rates.

	DV supply flow rate (L/s)		
	50 L/s	75 L/s	100 L/s
First stage inhaled dose (kg)	15.79e-6	8.78e-6	3.98e-6
Second stage inhaled dose (kg)	3.89e-6	1.29e-6	0.19e-6
Third stage inhaled dose (kg)	4.42e-6	2.45e-6	0.05e-6

For the different flow rates, the first stage represented the highest inhaled dose. As the *DV* flow rate increases, the infection index is reduced for the three stages but the

rate of reduction is highest for stage 3 and lowest for stage 1 due to the decay of the exhalation jet with time (Table 5.6). Therefore, stage 1 presents the highest probability of cross-contamination between occupants. For a *DV* flow rate of 50 L/s, stages 2 and 3 represented a significant percentage of the total exposure. The *DV* system with a flow rate of 100 L/s reduced significantly the inhaled dose during stages 2 and 3 decreasing the total inhaled dose by 83% compared to a flow rate of 50 L/s. The *DV* flow rate of 100 L/s was adopted for the rest of the study.

5.1.1.5.2. Cough Velocity Effect

IPE was studied for different cough velocities (6, 11, and 22 m/s) for a *DV* flow rate of 100 L/s, 1 μm particles in diameter, and 1m separating distance between occupants. Figures 5.20.a and 5.20.b illustrate respectively the effect of the cough velocity on the variation with time of the normalized concentration at the breathing level of the exposed person and the infection index.

As the cough velocity increases, the exhaled mass flow rate is incremented proportionally (for the same mouth opening) and the proportion of particles penetrating the thermal plumes of the infected occupant increases, therefore the IPE is increased (Fig. 5.20). Hence, the higher the cough velocity is, the faster and stronger is the attained concentration peak (Fig. 5.20.a), and the higher is the infection index (Fig. 5.20.b). The coughing velocity largely affected the exposure during the first stage which explain the recommendation of covering the mouth during coughing to obstruct the exhaled jet reducing its velocity and thus reducing the IPE.

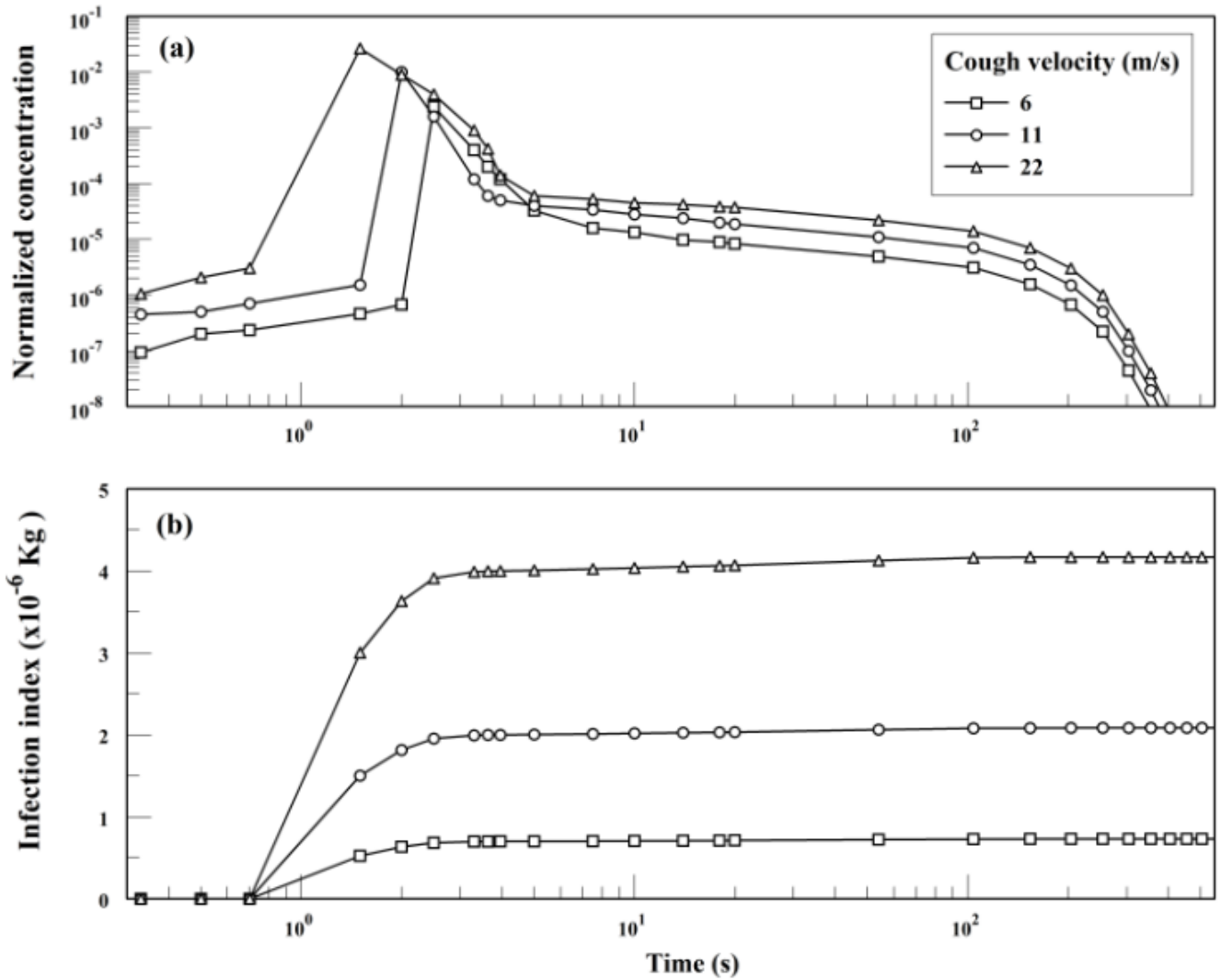


Fig. 5.20: Effect of the cough velocity on the tranient of: a) the normalized concentration at the breathing level of the exposed person; b) the infection index.

5.1.1.5.3. Particle Diameter Effect

IPE was studied for different particles diameters of 1, 20, 30, and 50 μm for a DV flow rate of 100 L/s, a cough velocity of 22 m/s and 1m separating distance between occupants. Figures 5.21.a and 5.21.b illustrate respectively the effect of the particle diameter on the variation with time of the normalized concentration at the breathing level of the exposed person and the infection index.

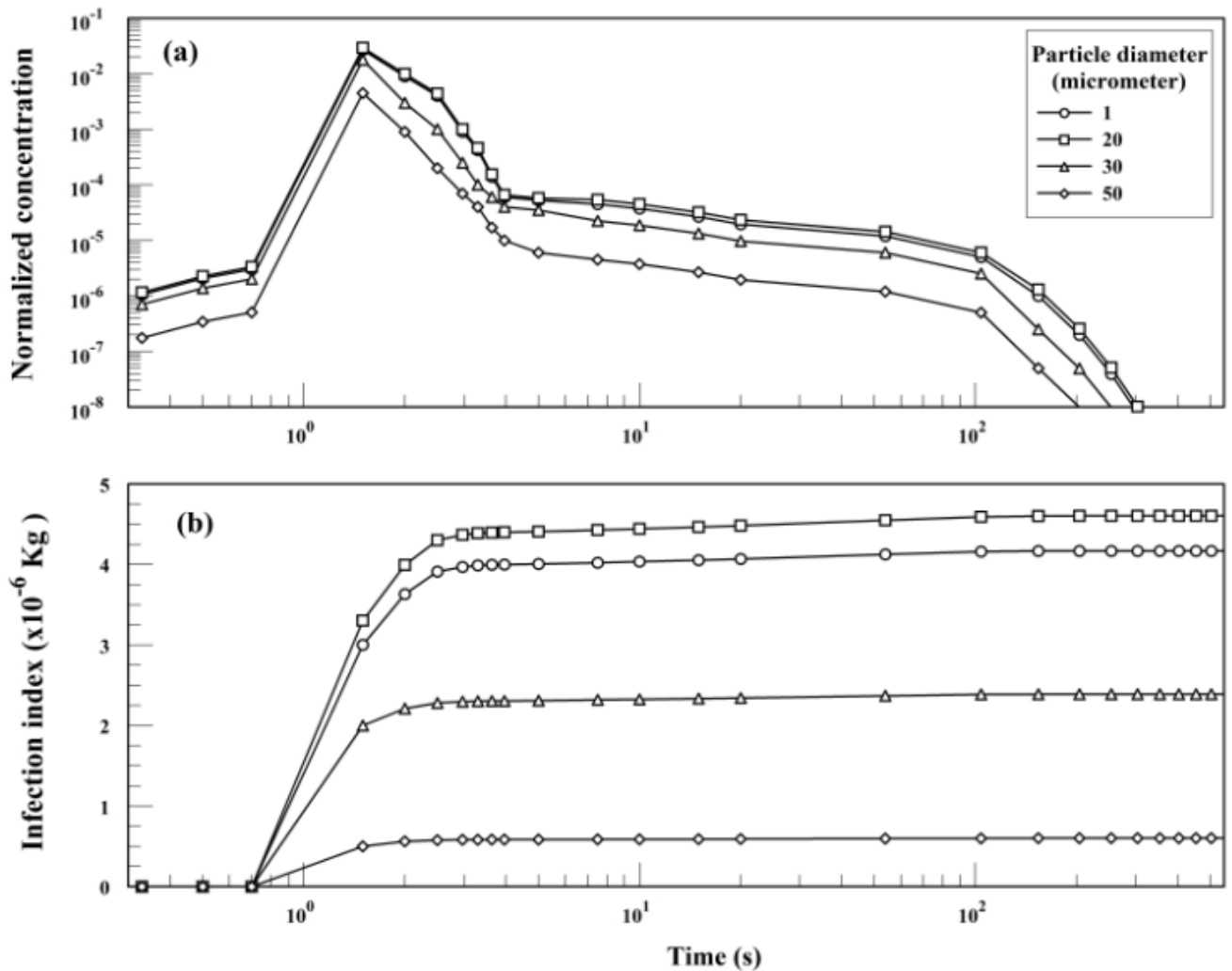


Fig. 5.21: Effect of the particle diameter on the variation with time of: a) the normalized concentration at the breathing level of the exposed person; b) the infection index.

With the increase of particle diameter, the gravitational settling effect opposing the upward transport of particles within the microclimate zones is strengthened leading to particle accumulation within the occupied zone. On the other hand, particle deposition by gravitation increases acting as a sink of particles. These two counter effects of increased particle diameter results in non-monotone variation of the concentration with particle diameter. This explains the fact that the IPE is higher when particle diameter is increased from 1 to 20 μm due to the opposition of particle removal

by the upward *DV*. For larger particle diameters, the deposition by gravitation becomes dominant playing a major role in decreasing IPE (Fig. 5.21).

5.1.1.5.4. Separating Distance Effect

IPE was studied for different distances between the occupants at 0.5, 1, 2, and 3m for a *DV* flow rate of 100 L/s, 1 μm particles in diameter, and cough velocity of 22 m/s. Figures 5.22.a and 5.22.b illustrate respectively the effect of the distance between occupants on the variation with time of the normalized concentration at the breathing level of the exposed person and the infection index.

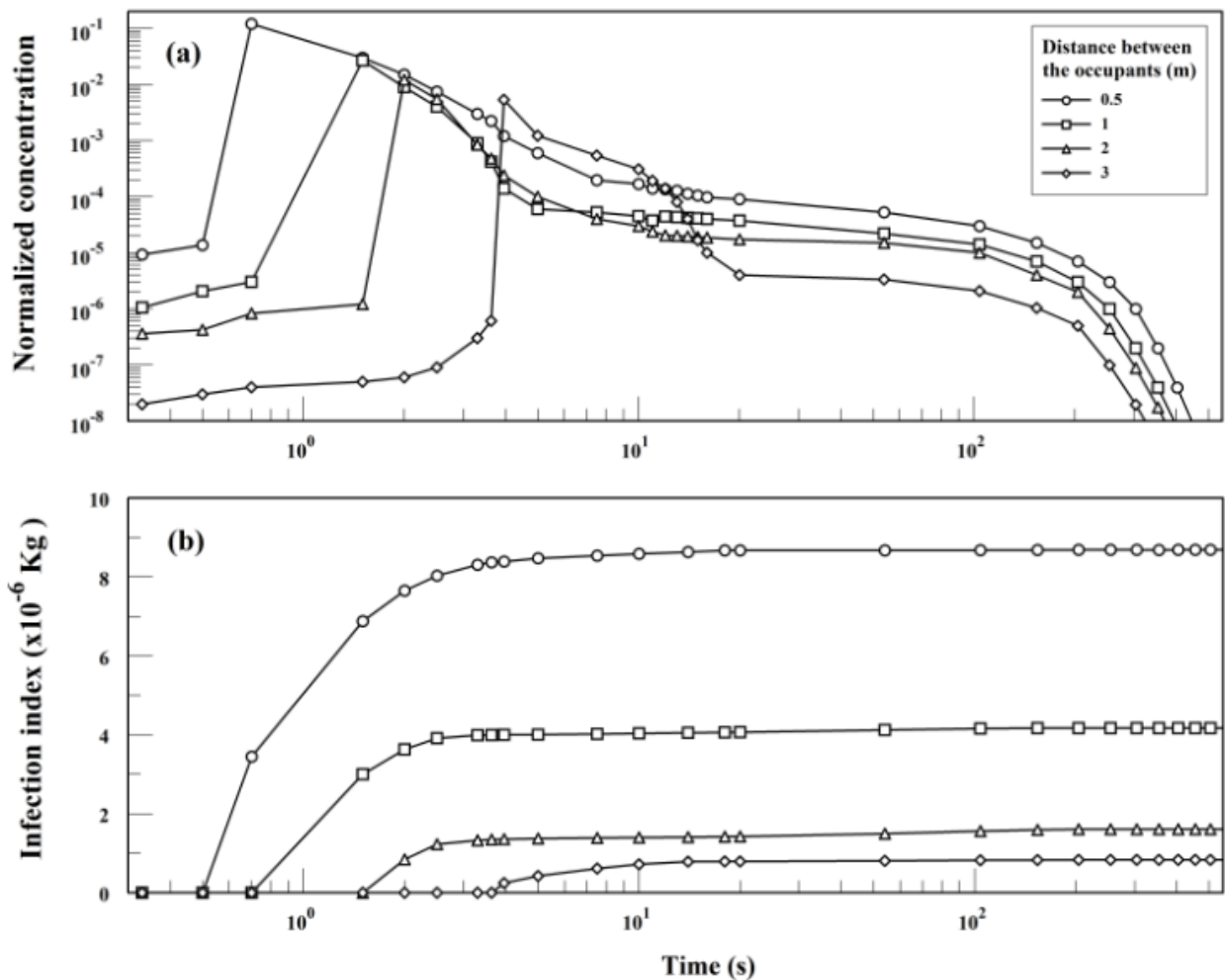


Fig. 5.22: Effect of the distance between occupants on the variation with time of: a) the normalized concentration at the breathing level of the exposed person; b) the infection index.

As the distance between occupants increases, the microclimate zone 2 relating the occupants is larger. Therefore, the IPE is reduced as the exhaled jet decay is higher reducing contaminant transmission to the exposed person with a larger time delay. These findings are consistent with the ones of Licina et al. [130]. The effect of the distance on the IPE is reduced in stages 2 and 3 compared with stage 1 due to the decay of the exhaled jet. Figure 5.23 represents the variation of the total inhaled dose with distance between the occupants showing that as the separating distance is reduced the rate of increase of the total inhaled dose is incremented and becomes significantly high below 1 m. The IPE is largely reduced for a separating distance of 3 m which justify the common recommendation of keeping a large distance between occupants for reduced exposure.

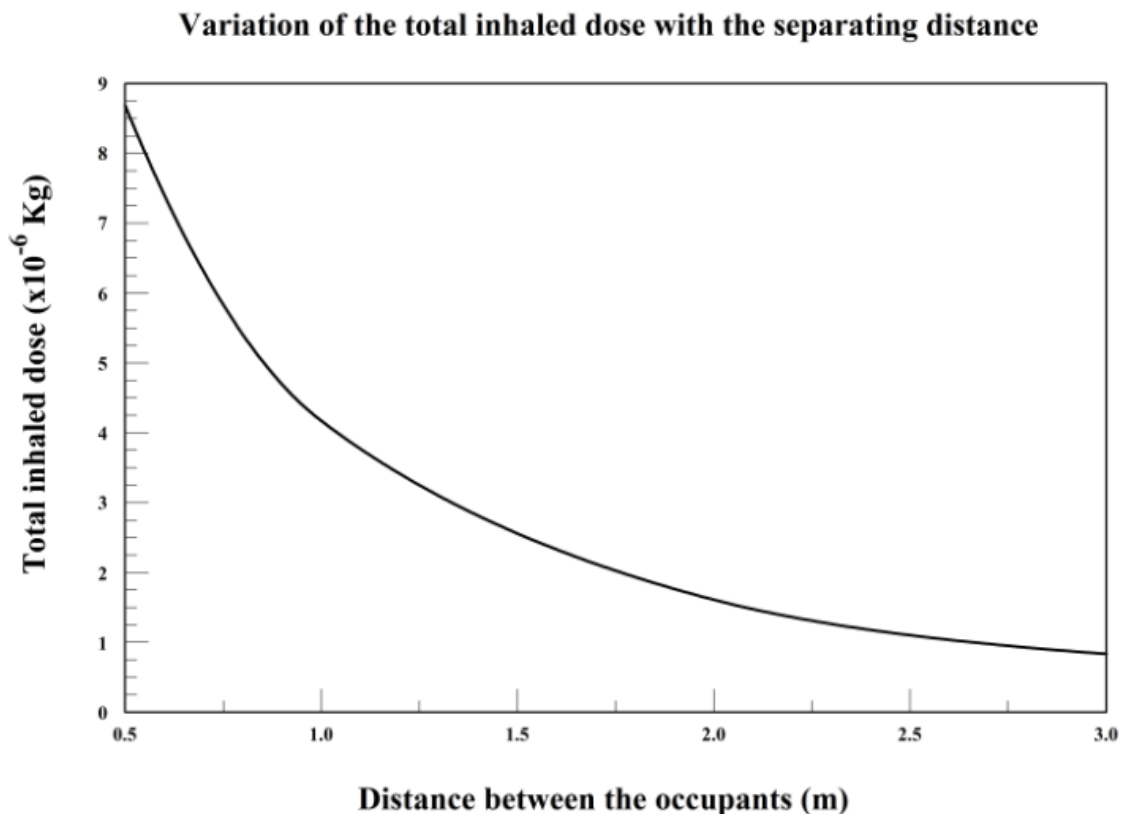


Fig. 5.23: Variation with distance between the occupants of the total inhaled dose.

5.1.1.5.5. Steady versus Transient Modeling

The physical effect of different parameters (*DV* flow rate, coughing velocity, particle diameter, and distance between the occupants) on particle behavior computed from the transient model is consistent with the conclusions made from the steady-model. Therefore, steady modeling is helpful in understanding the physics affecting particle spread resulting from HMRA. In order to compare the ability of steady and transient modeling in predicting the IPE, the inhaled dose during the first stage (which is dominated by the jet propagation) was calculated for both models. The inhaled dose computed by transient modeling was calculated using the concentration profile obtained from the transient simulation. On the other hand, the inhaled dose obtained by steady modeling was computed using the steady-state concentration. Figure 5.24 illustrates the comparison of the inhaled dose predicted by transient and steady modeling for variable *DV* flow rate, cough velocity, and distance between the occupants. Steady modeling significantly over-predicts the IPE (Fig. 5.24). For instance, if the threshold inhaled dose is set to 10^{-5} kg, for a cough velocity of 22 m/s during 1s, 1 μm particles in diameter, and a separating distance of 1 m transient modeling predicts a minimum required *DV* flow rate of 75 L/s while steady modeling predicts that even an oversized flow rate of 200 L/s is not enough (Fig. 5.24.a). Furthermore, for a *DV* flow rate of 100 L/s, 1 μm particles in diameter, and a separating distance of 1 m transient modeling predicts that the whole coughing velocity range is acceptable while steady modeling lead to the conclusion that the maximum possible coughing velocity is 10.25 m/s (Fig. 5.24.b). Finally, for a *DV* flow rate of 100 L/s and a cough velocity of 22 m/s during 1s, and 1 μm particles in diameter, the minimum required distance between the occupants is nearly 0.5 m by transient modeling while it is 2.15 m by steady modeling (Fig. 5.24.c).

Therefore, steady modeling should not be used to predict the inhaled dose since it leads to largely over-predicted values.

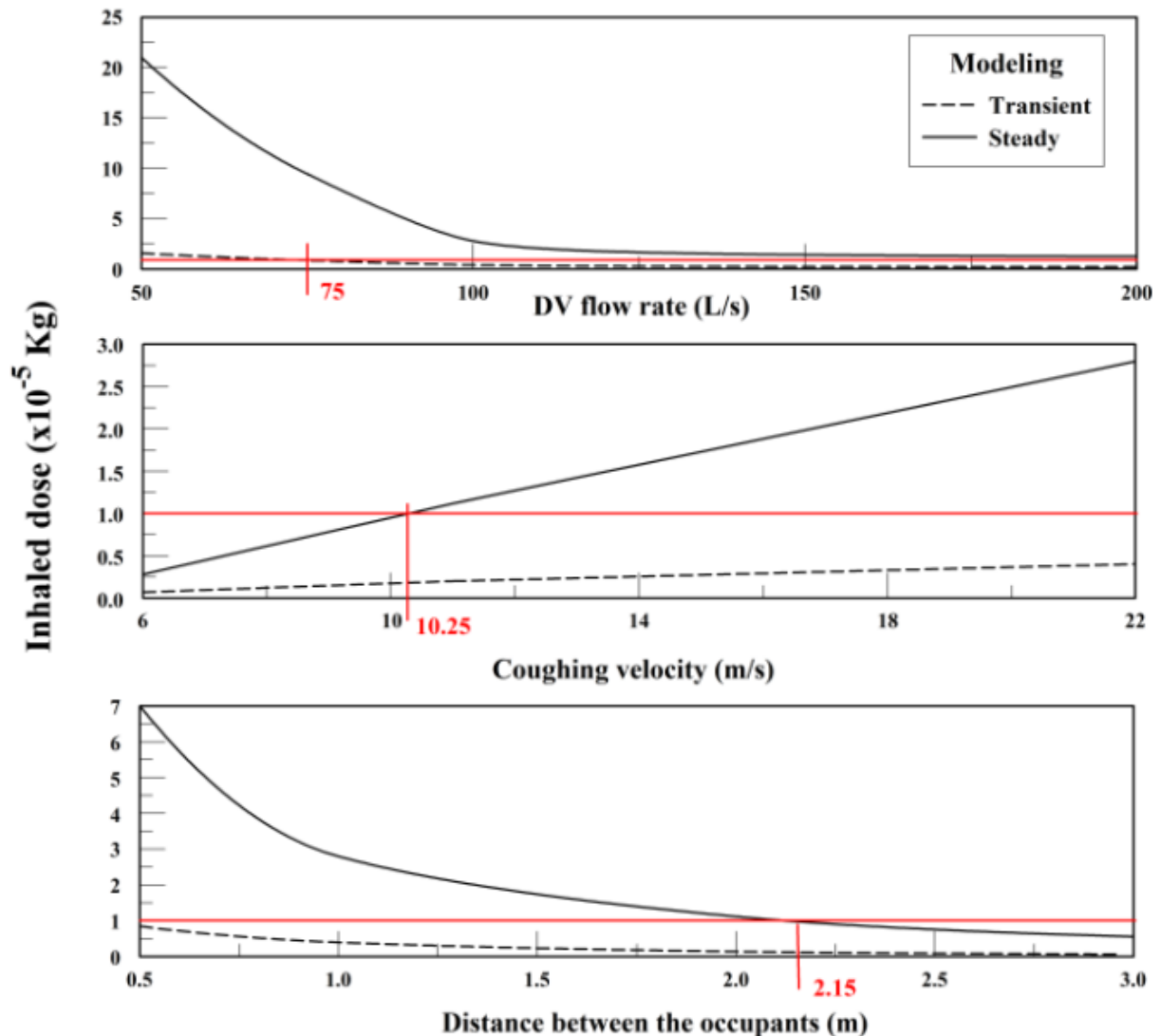


Fig. 5.24: Comparison of the inhaled dose predicted by transient and steady modeling for the parameters: a) DV flow rate; b) cough velocity; c) distance between the occupants.

5.1.2. Effect of Assisting DV with CF

5.1.2.1. DV+CF CFD Model Experimental Validation

In order to validate the CFD model, particularly its ability to capture the fans effect on particle transport, two configurations were tested experimentally for particle

concentration distribution in the *DV* conditioned space at *DV* supply flow rate of 100 L/s and temperature of 22 °C. The first was when fans were OFF and the second configuration when fans were ON with a chair fan flow rate of 7 L/s. The particle size of generated particles in both experiments was 0.5 μm. Normalized concentrations obtained at different locations and at different heights were compared with the ones obtained from the CFD model for point by point comparison.

Figures 5.25 and 5.26 show the predicted and experimentally derived normalized concentration variation with height for the fan OFF and ON configurations respectively within a 90% confidence interval along (a) the centerline of the infected plume; (b) the centerline of the exposed plume; and (c) the centerline between the occupants within the surrounding air. It is to be noted that all the points are with error bars but because the error bar length is relatively small for low concentration values the error bars do not appear for these points. Better agreement was obtained for concentrations within the plumes than for the surrounding air but the relative errors calculated were within the engineering accuracy. In general, good agreement between the predicted and experimentally obtained values of normalized concentration with a relative error below 10% was obtained at the different measurement locations. This shows the ability of the CFD model in predicting accurately the particles transport for the different configurations studied. The CFD model can then be used to assess the efficiency of using chair fans for the occupants.

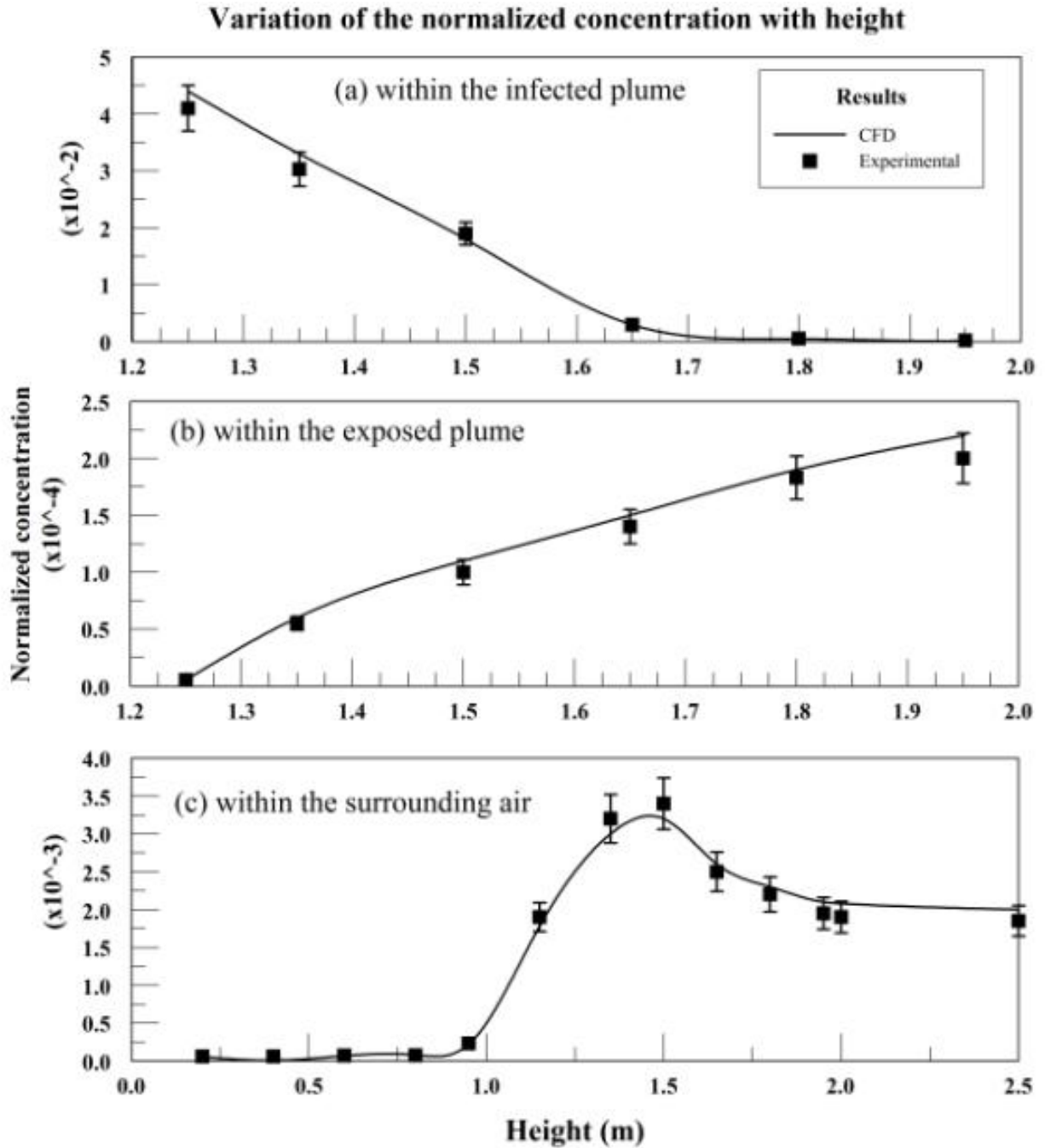


Fig. 5.25: Variation of the normalized concentration with respect to the concentration of generation with height for the fans-off configuration within a 90% confidence interval at a) the centerline of the infected plume; b) the centerline of the exposed plume; c) the centerline between the occupants within the surrounding air.

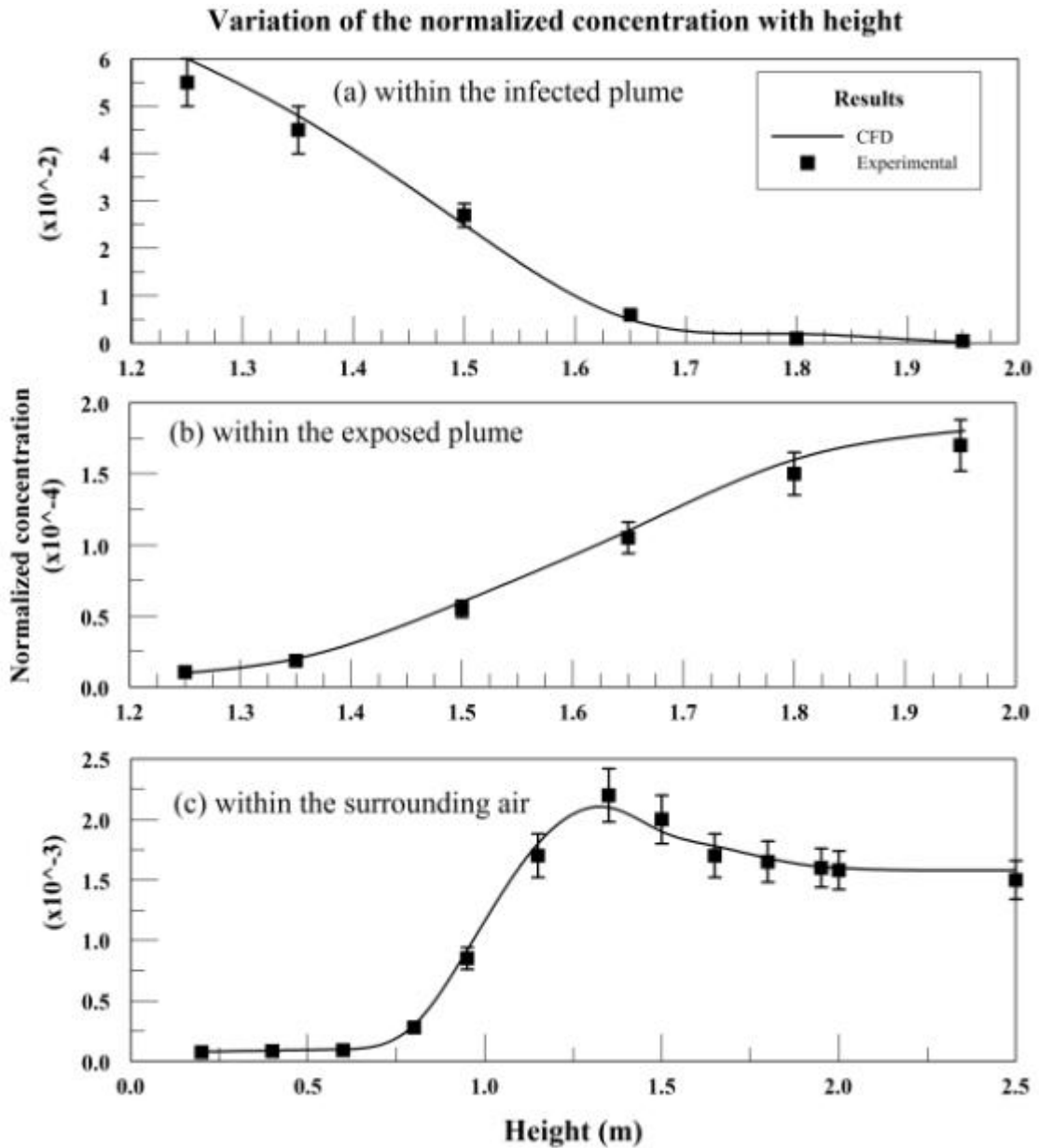


Fig. 5.26: Variation of the normalized concentration with respect to the concentration of generation with height for the fans-on configuration within a 90% confidence interval at a) the centerline of the infected plume; b) the centerline of the exposed plume; c) the centerline between the occupants within the surrounding air.

5.1.2.2. *DV+CF* Case Study

To understand the performance of the chair fans, the supply flow rate was fixed at 80 L/s and the behavior of different particle diameters (0.5 μm , 1 μm , 2.5 μm , 10 μm)

and their deposition on the different surfaces were investigated for different CF flow rates. The obtained results are summarized in (Table 5.7).

Table 5.7: Effect of particle diameter and fan flow rate on particle deposition

Simulated case [Q_s (L/s); q_f (L/s)]	Diameter (μm)	IF ($\times 10^{-4}$)	% of surface deposition				
			Floor	Ceiling	Walls	Exposed person	Infected person
(80; 0)	0.5	0.572	0.019	0.95	1.5	0.016	1.16
	1	0.599	0.023	0.79	1.6	0.019	1.18
	2.5	0.953	0.031	0.39	2.1	0.035	1.51
	10	7.012	10.89	0.07	4.9	0.41	2.13
(80; 5)	0.5	0.243	0.014	1.13	0.88	0.0055	1.01
	1	0.261	0.015	0.99	1.11	0.0065	1.04
	2.5	0.509	0.022	0.69	1.63	0.01	1.39
	10	4.987	4.95	0.04	2.5	0.12	1.99
(80; 7.5)	0.5	0.235	0.009	1.21	0.75	0.0035	0.95
	1	0.249	0.012	1.14	0.98	0.005	0.99
	2.5	0.451	0.015	0.85	1.51	0.007	1.25
	10	1.362	3.51	0.11	2.25	0.091	1.83
(80; 10)	0.5	0.475	0.032	0.24	1.14	0.032	1.21
	1	0.487	0.041	0.21	1.29	0.0435	1.25
	2.5	0.803	0.072	0.11	1.78	0.055	1.79
	10	1.71	10.91	0	4.5	0.44	2.56

The behavior of sub-micrometer particles (represented by the size of 0.5 μm) was found to be very close to the 1 μm size. The coarse mode (particle of diameter larger than 2 μm) is represented by the sizes of 2.5 and 10 μm . The gravitational effect begins to appear slightly for 2.5 μm and become significant for 10 μm particles. As the particle diameter increases ceiling deposition is decreased while deposition on the other surfaces and the IF increases (Table 5.7) since the removal effectiveness of the DV system decreases increasing particle concentration within the space.

The effect of the fans on the velocity field and the concentration field of particles at 1 μm diameter were examined. Figure 5.27 shows the effect of the chair fans

on the flow field contours (colored by the algebraic value of the vertical component of the velocity) in the chair fans symmetry plane while Figure 5.28 illustrates the associated normalized particle concentration at the occupants' plane.

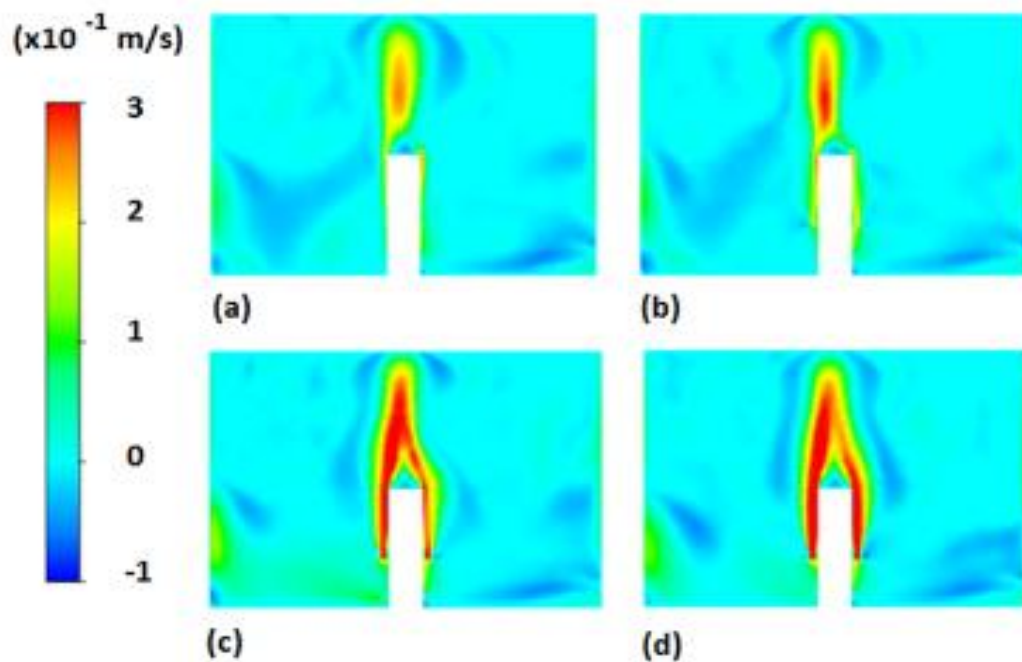


Fig. 5.27: Effect of the chair fans on the vertical component of the velocity field within the *CF* symmetry plane for a supply flow rate of 80 L/s of a fan flow rate of: (a) zero L/s; (b) 5.0 L/s; (c) 7.5 L/s; (d) 10.0 L/s.

It is clear that as the flow rate of the chair fans increases, the strength of the plume flows increases (Fig. 5.27) and the sucked clean air reaches higher levels within the exposed plume (see Fig. 5.28). Hence the chair fans at the front of the infected person enhance the upward transport of contaminant within the infected plume and reduce particle diffusion from the plume to the surrounding by decreasing their interaction.

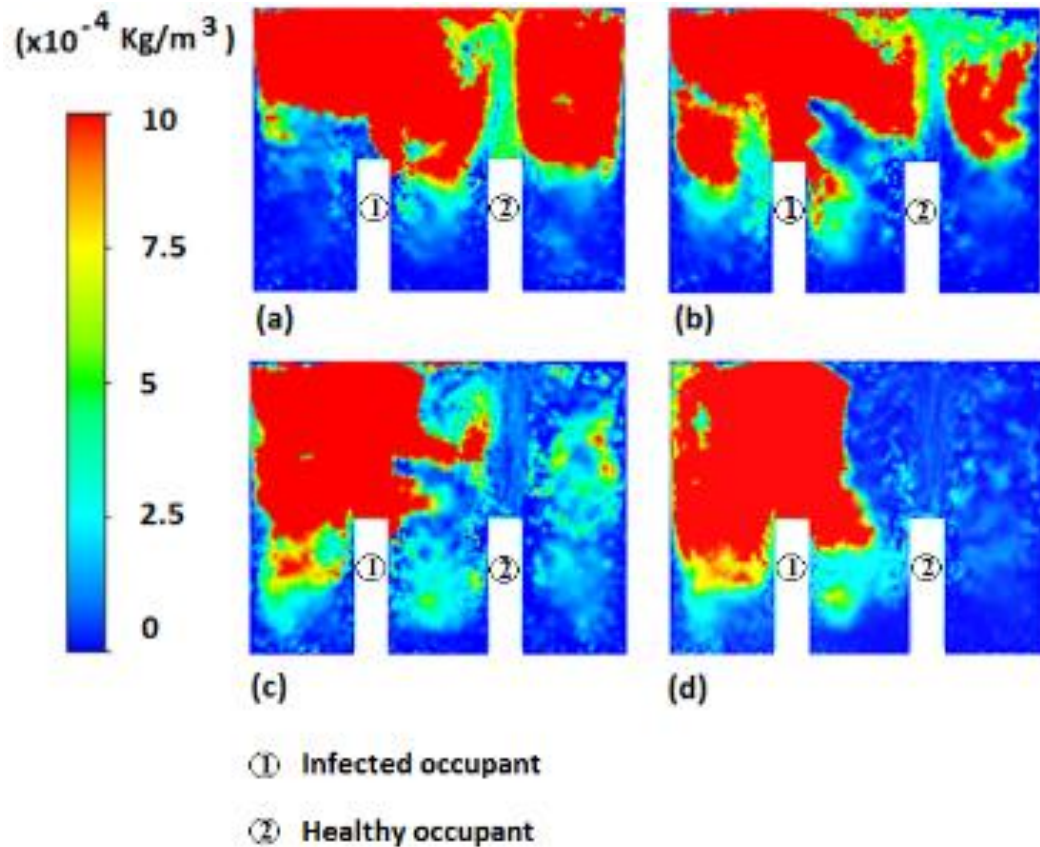


Fig. 5.28: Normalized concentration of $1 \mu\text{m}$ particles at the occupants' plane for a supply flow rate of 80 L/s for a flow rate per chair fan for (a) zero L/s ; (b) 5.0 L/s ; (c) 7.5 L/s ; (d) 10.0 L/s .

Furthermore, the protective effectiveness of the exposed plume is increased as the fans' jets provide a certain barrier to particle diffusion from the surrounding to the exposed plume and blow relatively clean air to the breathing level of the occupant. On the other hand, the downward motion in the air surrounding the plumes increases (see Fig. 5.27). Therefore, the positive effect of the chair fans increasing the strength of the rising plumes and blowing relatively clean air to the breathing level is opposed by the increase of contaminant transport downward towards the occupied zone due to increased recirculation in the upper zone. This is physically due to a decrease in the stratification height, which is defined as the elevation at which the vertical velocity

component in the surrounding air (the air zone outside the thermal plumes and *CF* jets) is equal to zero.

Figure 5.29 represents the variation of the averaged normalized concentration of 1 μm particles within the surrounding air for different flow rates of the chair fans. The stratification height corresponds to the separation between the clean and contaminated zones. Literature studies have indicated that at this height and for particles size in the range of 1 μm there is a jump in the vertical particle concentration profile [46] due to particle accumulation at the stratification height since above it the flow is downward whereas below it the flow is upward.

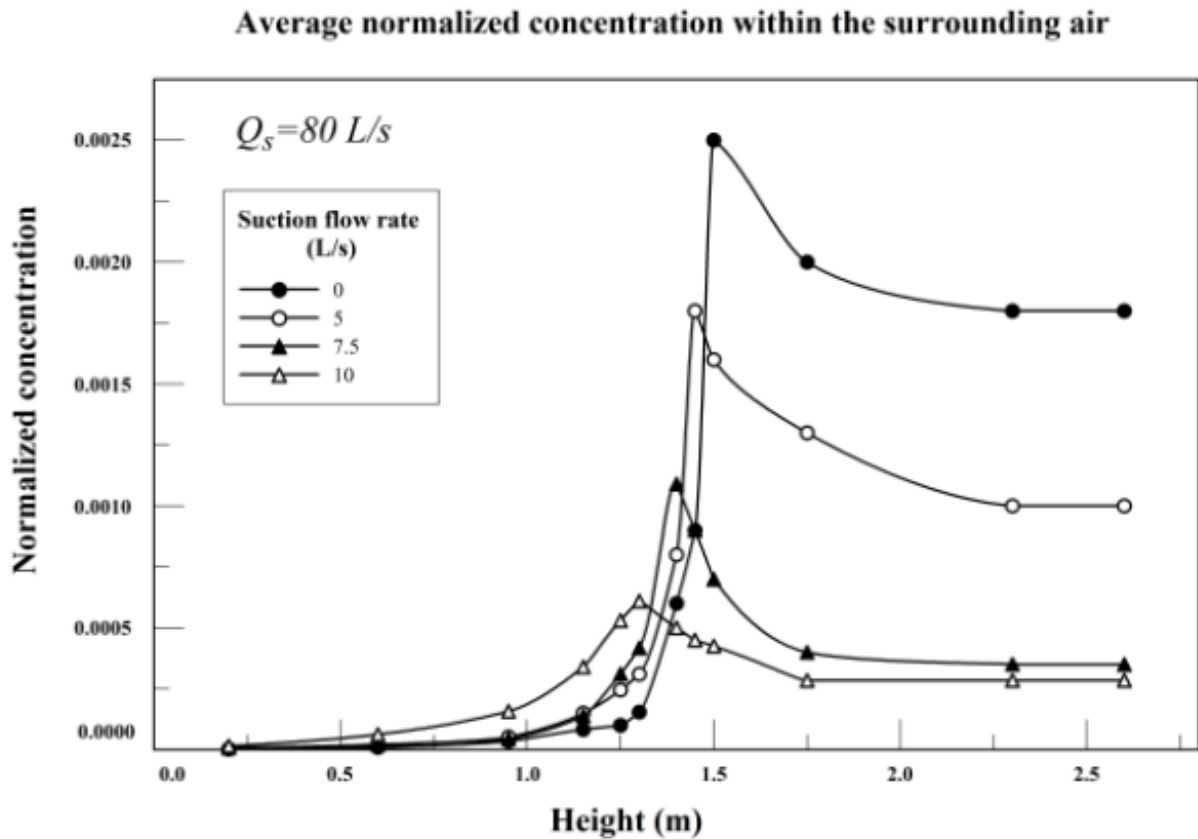


Fig. 5.29: Effect of the chair fans flow rate on the variation with height (*z* direction) of the average normalized concentration of 1 μm particles within the surrounding air for a supply flow rate of 80 L/s.

It is clear that as the *CF* flow rate increases, the stratification effect decreases dampening the variation of concentration within the surrounding air (Fig. 5.29). For instance the stratification level decreases from 1.4m for the standalone *DV* system to 1.3m for a *CF* flow rate of 7.5 L/s. In order to assess the performance of the chair fans the intake fraction at the breathing level of the exposed person should also be examined.

The two opposing effects of upward stronger plume flow created by the presence of the chair fans and downward contaminant flow due to increased recirculation in the upper zone lead to the existence of an optimal *CF* flow rate where the positive effect created by the chair fans is dominant and insures that contaminated air remains above the occupants away from the breathing level. Figure 5.30 shows the variation of the intake fraction of the exposed occupant as a function of the flow rate per chair fan for different supply flow rates.

For a fixed supply flow rate, as the *CF* flow rate increased from 0 to approximately 7 L/s, the normalized concentration at the breathing level of the exposed person decreased. Hence for this range of flow rates, the positive effect induced by the presence of chair fans is dominant leading to a reduction of particle deposition on the floor and exposed person and increase of particle deposition on the ceiling (Table 5.7). Figure 5.29 also shows that for *CF* flow rates below 7.5 L/s, the surrounding normalized concentration at the breathing level did not significantly increase as the stratification level remained above the breathing level by approximately 0.2 m. For higher *CF* flow rate of 10 L/s, the stratification height is degraded down to the breathing level increasing the risk of cross-contamination. Hence, for higher *CF* flow rates the negative downward motion effect overwhelms leading to an increase of the intake fraction at the breathing level and particle deposition on the exposed person and floor (Table 5.7).

The lower the supply *DV* flow rate, the more effective is the presence of the chair fans since the removal of contamination efficiency of the standalone *DV* system is higher with larger supply flow rates (Fig. 5.30) and the chair fans provide clean air to the breathing zone of the occupant which is more contaminated with smaller flow rates.

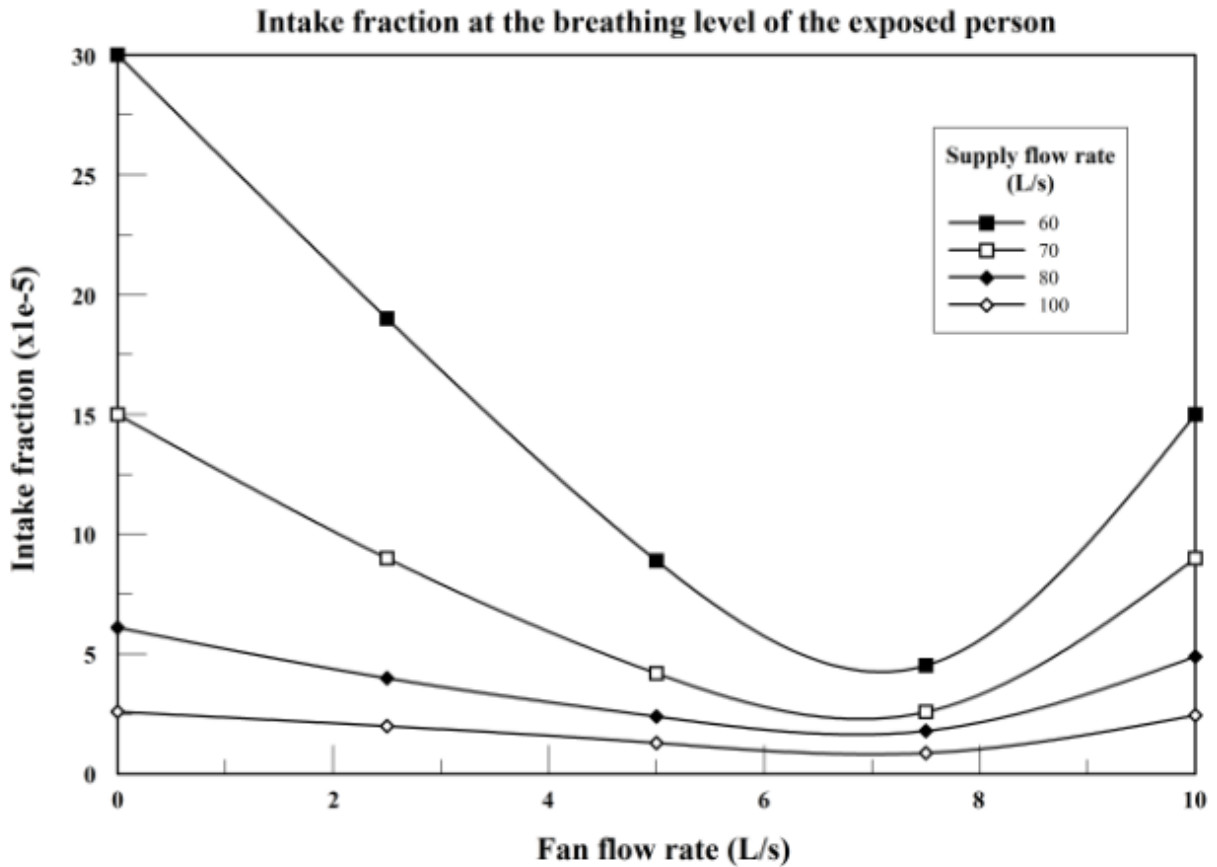


Fig. 5.30: Effect of the chair fans flow rate on the intake fraction of particles of 1 μm in diameter of the exposed occupant for different supply flow rates.

The same analysis was conducted for particle generation at 10 μm representing the coarse particles' mode within the inhalable range. Figure 5.31 shows the normalized concentration of 10 μm particles at the occupants' plane for a supply flow rate of 80 L/s for different flow rates per chair fan.

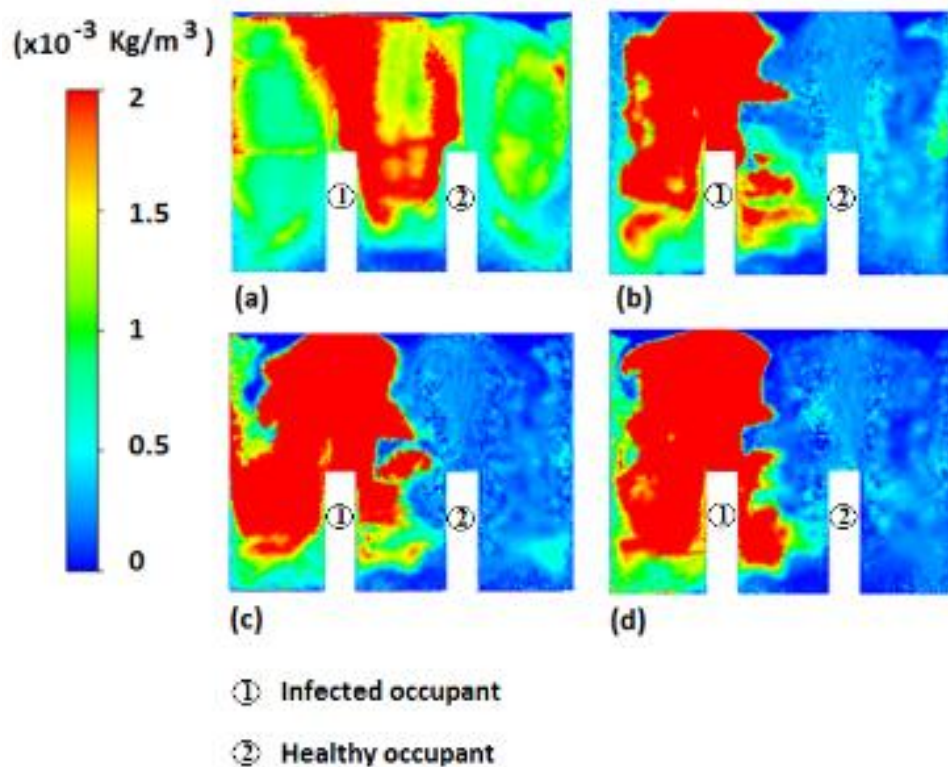


Fig. 5.31: Normalized concentration of 10 μm particles at the occupants' plane for a supply flow rate of 80 L/s for a fan flow rate per chair of (a) zero L/s; (b) 5.0 L/s; (c) 7.5 L/s; (d) 10.0 L/s.

Figure 5.32 illustrates the effect of the chair fans flow rate on the intake fraction of the exposed occupant for different supply flow rates. The presented results (Figs. 5.31-5.32) show that for particles of 10 μm in diameter, similar observations can be made concerning the presence of an optimal CF flow rate with some variations due to settling effect. For instance, the pattern of variation of the intake fraction with the CF flow rate presents some differences as observed in Fig. 5.32. Due to the gravitational effect that is more dominant for particles of 10 μm in diameter, CF flow rates below 5 L/s do not decrease significantly the intake fraction at the breathing level of the exposed person. Above a CF flow rate of 5 L/s per fan the settling effect is overwhelmed which higher the rate of decrease of the intake fraction. The higher the DV supply flow rate, the lower is the intake fraction decreasing the efficiency and the need for the chair fans

since the increased upward velocity flow resulting from the *DV* ventilation helps in overcoming the gravitational effect. It was found that the optimal *CF* flow rate for 10 μm (approximately 8 L/s) is slightly higher than the one for 1 μm (7 L/s) due to the increased particle settling effect. Thus, the fan should be designed such that the positive effect created by strengthening of the plumes overwhelms the counter-effect created due to increased downward motion of particles. In conclusion, for the geometry and conditions of this study, a *CF* flow rate of 7.5 L/s can be recommended to insure a small intake fraction for the critical inhalable range.

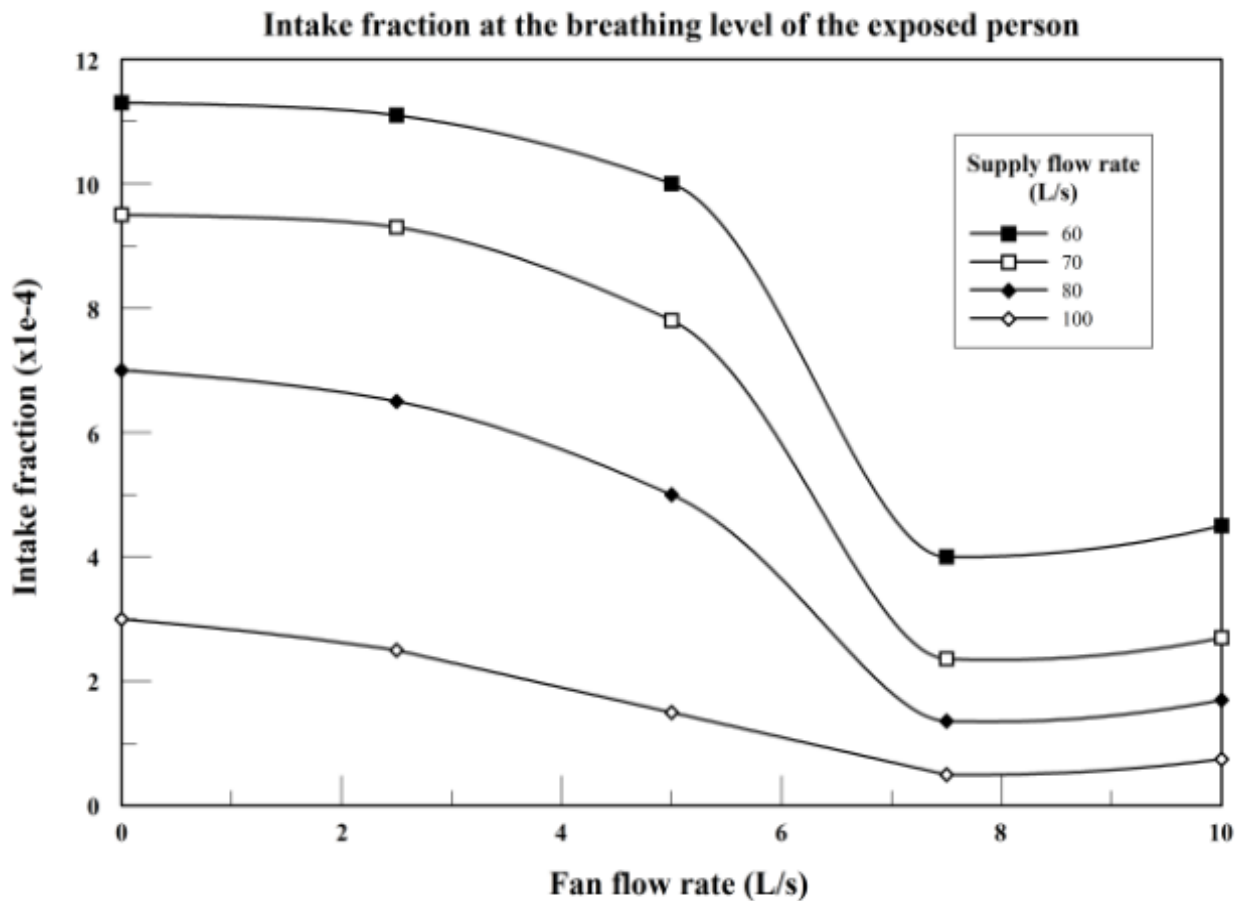


Fig. 5.32: Effect of the chair fans flow rate on the intake fraction of particles of 10 μm in diameter of the exposed occupant for different supply flow rates.

5.1.2.3. Energy Savings of the Optimal *DV+CF* Design

Table 5.8 illustrates the comparison of the performance in terms of IAQ of different HVAC configurations:(1) the case of supply flow rate of 70 L/s without chair fans (case a); (2) the case of supply flow rate of 70 L/s with fans blowing air at the optimal flow rate of 7.5 L/s (case b); and (3) the case of standalone *DV* system with a supply flow rate of 100 L/s (case c).

Table 5.8: Comparison of the performance of different HVAC configurations in terms of IAQ

IAQ Performance			
HVAC configuration	IAQ parameters	Intake fraction at the breathing level of the exposed person for 1 μm particles	Intake fraction at the breathing level of the exposed person for 10 μm particles
	(a) Standalone <i>DV</i> , $Q_s=70$ L/s		15×10^{-5}
(b) <i>DV+CF</i> , $Q_s=70$ L/s, $q_f=7.5$ L/s		2.4×10^{-5}	2.5×10^{-4}
(c) Standalone <i>DV</i> , $Q_s=100$ L/s		2.5×10^{-5}	3×10^{-4}

The presence of the fan blowing air at a flow rate of 7.5 L/s, with a supply flow rate of 70 L/s allowed to reach the same level of breathable IAQ of a standalone *DV* system supplying 100 L/s as shown in Table 5.8. In order to make sure that for this operation of the *DV+CF* system the thermal comfort is satisfied the temperature variation in the *CF* symmetry plane for the three HVAC configurations described above is illustrated in Fig. 5.33.

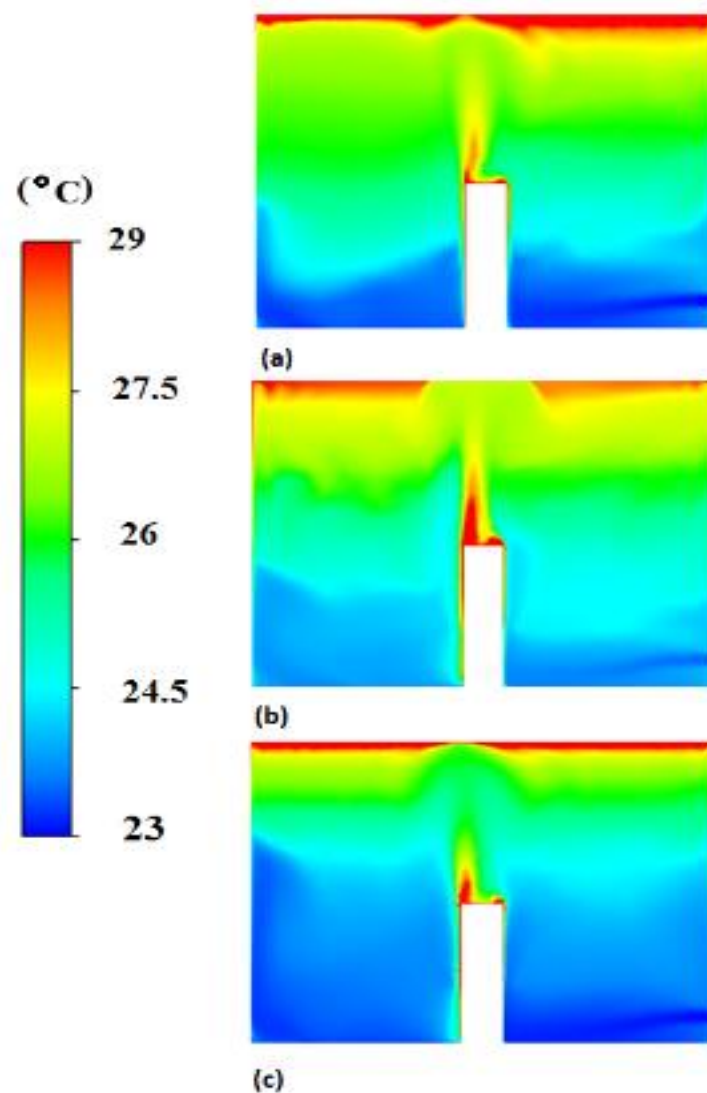


Fig 5.33: Fan effect on the thermal field within the CF symmetry plane showing (a) standalone DV , $Q_s = 70$ L/s; (b) $DV+CF$, $Q_s = 70$ L/s and $q_f = 7.5$ L/s; (c) standalone DV , $Q_s = 100$ L/s.

For the first case the temperature gradient in the occupied zone is greater than $2^\circ\text{C}/\text{m}$ while it is lower for cases (b) and (c). It is clear that the CF fans create a microclimate of relatively cold air around the occupant that allows maintaining an acceptable variation of the temperature in the occupied zone satisfying the ASHRAE standard 55 for thermal comfort. Furthermore the predicted mean vote (PMV) (which scales between -3 for very cold and +3 for very warm) and predicted Percentage of

People Dissatisfied (PPD) of the three ventilation configurations were computed using an online calculator [110] in order to compare their thermal performance. The online calculator requires as inputs the metabolic energy production (which can be between 58 and 232 W/m²), the rate of mechanical work (which is normally set to 0), the ambient air temperature (which can be between 10-30), the mean radiant temperature (which is often close to ambient air temperature), the relative air velocity (which can be between 0.1 to 1 m/s), the relative humidity of the air, and the basic clothing insulation (where 1 clo = 0.155 W/m²K) .

It was assumed that the indoor relative humidity is equal to 50 % and the sedentary occupants (metabolic energy production of 58.15 W/m²) are wearing medium clothing ($I_{cl} = 1$ clo) and that the mean radiant temperature equals the ambient air temperature. From the CFD simulations, the air velocity and temperature around the occupants were obtained by averaging air velocity and temperature of different points of the microclimate air around the occupants which is taken as 2 cm from the cylinder surface since for larger distances the temperature becomes nearly equal to the surrounding temperature. Once all the required inputs were specified, the online calculator [110] was used to obtain the PMV and PPD as outputs in order to assess the occupant thermal comfort in the different cases of fans ON and OFF as summarized in Table 5.9. Note that the vertical air flow around the person in presence of fans is still lower than 0.3 m/s (see Fig. 5.27) which makes the use of PPD and PMV models acceptable. Table 5.8 and 5.9 compare the performance of the three cases and shows that configurations (b) in which *DV* supply flow rate at 70 L/s with fans ON provides nearly equal performance in terms of IAQ and thermal comfort to the case (c) of *DV* supply flow rate at 100 L/s with fans OFF. Hence the *DV+CF* with a supply flow rate of

70 L/s and *CF* flow rate of 7.5 L/s presents an equivalent performance of the standalone *DV* system with a supply flow rate of 100 L/s resulting in a 30% reduction of the supply flow rate and thus leading to a significant decrease in the energy costs. Furthermore, on the economic side the implementation of *CF* to the *DV* system is very practical since the only extra cost is the one of chair fans as no ductwork and installation are needed with negligible maintenance cost.

Table 5.9: Comparison of the performance of different HVAC configurations in terms of thermal comfort

Thermal Comfort Performance				
HVAC configuration \ Thermal comfort parameters	Air temperature around the occupant (°C)	Air velocity around the occupant (m/s)	PMV [-3 to +3]	PPD (%)
(a) Standalone DV, $Q_s=70$ L/s	24.5	0.1	0.31	7
(b) DV+CF, $Q_s=70$ L/s, $q_f=7.5$ L/s	24	0.2	0	5
(c) Standalone DV, $Q_s=100$ L/s	23.5	0.15	-0.07	5.1

5.2. CPV System Performance

5.2.1. CPV+DF/CF CFD Model Experimental Validation

Figure 5.34 illustrates the comparison between the predicted results by CFD model and experiments of the intake fraction for variable desk fan flow rate and two different source locations S1 and S2 (Fig. 4.4.b). It is observed that for a fixed desk fan flow rate, as the source location gets closer to the thermal manikin higher is the intake fraction and thus the risk of infection. On the other hand, for a fixed separating distance,

an optimal desk fan flow rate of nearly 10 L/s is required to minimize the probability of contamination. Good agreement of the order of 10% with a maximum error of 15% was obtained between the CFD model and experimental results validating the ability of the CFD model in assessing the effect of the desk fan flow rate on particle behavior.

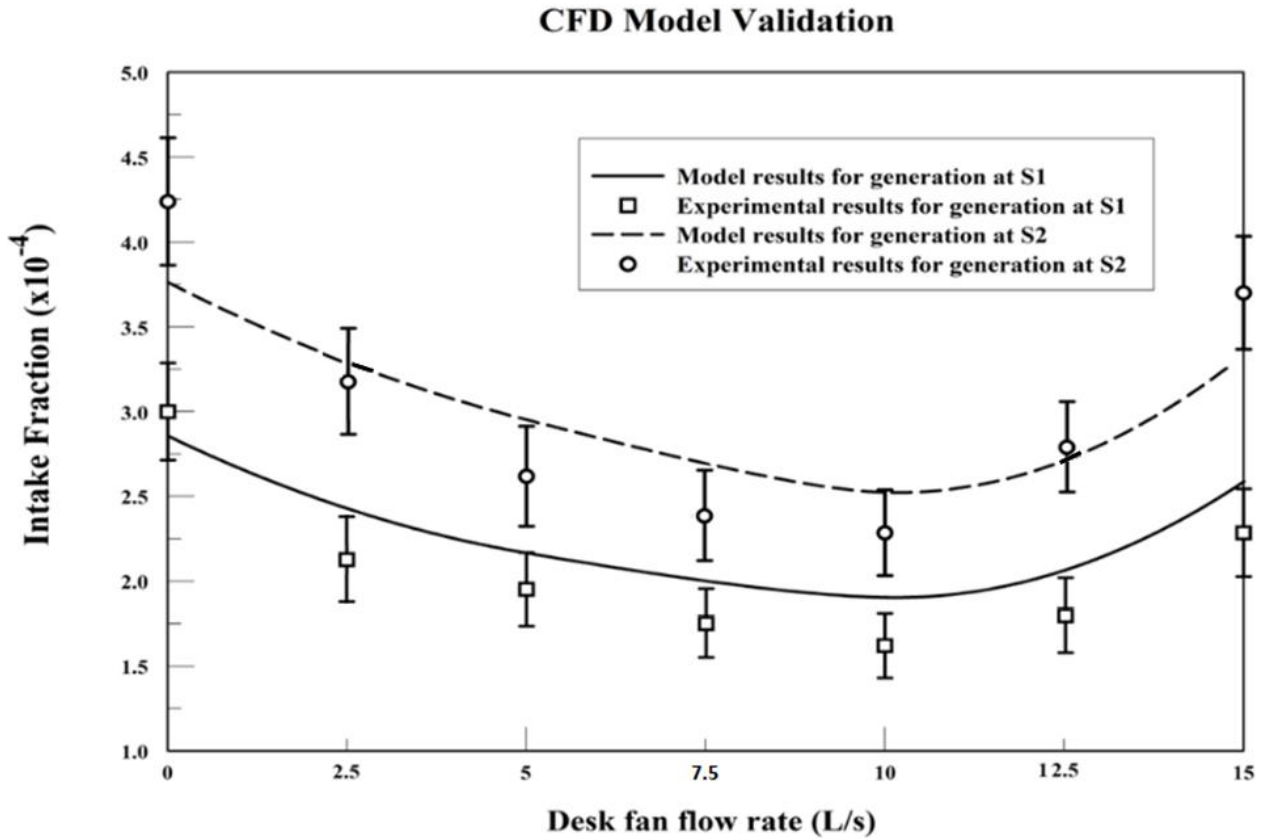


Fig. 5.34: Validation of the ability of the CFD model in predicting the effect of the desk fan flow rate on particle behavior.

CPV system assisted by DF/CF performance in terms of thermal comfort and ventilation effectiveness was found to be affected by the fan flow rate with an optimum of 10 L/s per occupant [22,43]. Experiments were conducted to determine the fan flow rate effect on the reduction of particle transport towards the breathing zone of the occupant.

The experimental and CFD predicted results of the intake fraction for both *DF* and *CF* for variable fan flow rates varying from 0 to 15 L/s were compared as illustrated in Fig. 5.35. It was found that for both *DF* and *CF* the operation reduced the possibility of cross-contamination with an optimal flow rate of 10 L/s for minimal *IF*.

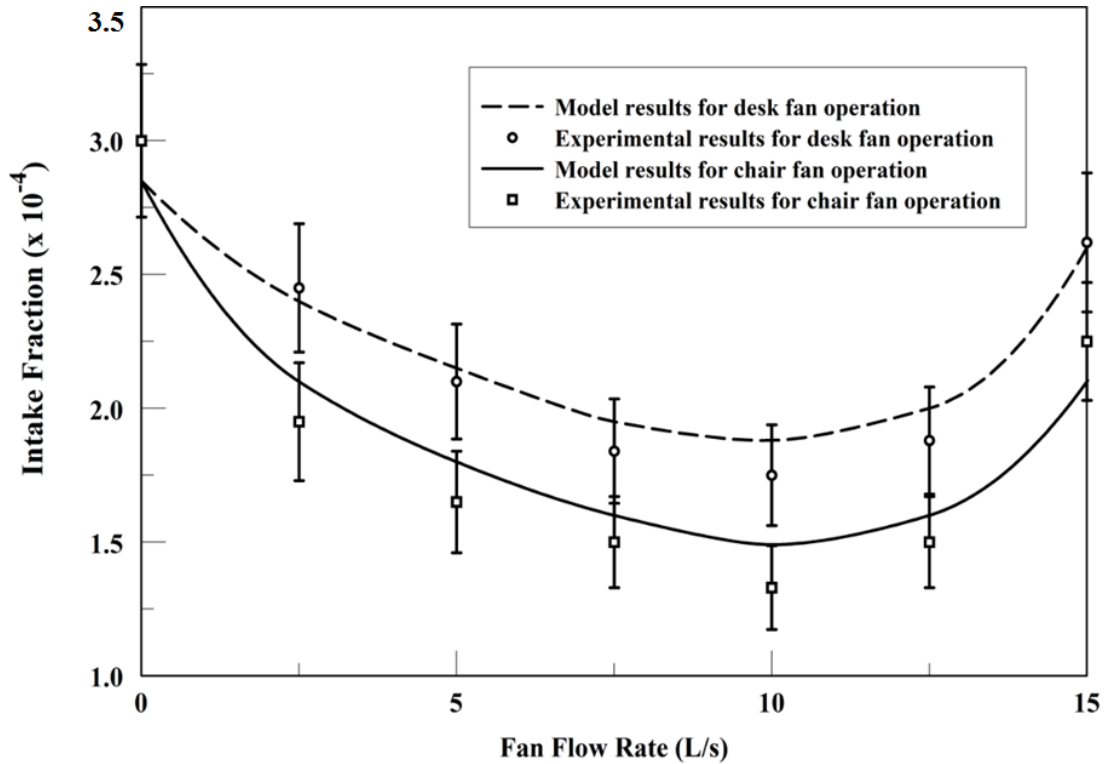


Fig. 5.35: Validation of the ability of the CFD model in assessing the effect of desk and chair fans on particle behavior.

The presence of this optimum was physically explained by the competition of two opposing effects as the fan flow rate increased. In fact, with the increase of the fan flow rate, the downward *CPV* jet momentum was strengthened thus it reached more effectively the breathing level but at the same time air mixing created by the fan operation tended to increase the *IF*. When the flow rate increased from 0 to 10 L/s, the positive effect of the fan operation was dominant leading to a decrease in the *IF*.

Nevertheless, for larger flow rates the negative effect was overwhelming leading to an increase of the *IF*. The same trend of *IF* variation with the flow rate was observed for *DF* and *CF* but *CF* performance was better than *DF* for the different flow rates investigated. This was attributed to the fact that the *CF* operation allowed reaching lower *IF* compared to the ones obtained for *DF* due to better localization of the flow around the occupant. For instance, when the fan flow rate increased from 0 to 10 L/s, the operation of *DF* and *CF* resulted in a reduction of the particle *IF* by 34.04% and 47.70% respectively. Therefore, experimentally *CF* showed a higher potential in enhancing the standalone *CPV* performance than *DF*. The agreement between CFD and experimental results was of the order of 10% with 15% as maximum error. The conducted experiments validated the ability of the CFD model in capturing the effect of the *CF* versus *DF* on particle behavior.

5.2.2. Effect of Assisting CPV with DF

5.2.2.1. CPV+DF Case Study

The purpose of the parametric study is to assess the performance of the different configurations studied and to come up with recommendations for the optimal use of fans in conjunction with the *CPV* system to decrease direct and indirect cross-contamination at minimal energy consumption. The comparison between mixing and personalized ventilation was performed under equal flow rate and comparable thermal comfort. The only design parameter varied in mixing ventilation was the distance between the occupants whereas for the personalized single nozzle system assisted by desk fans, the fan flow rate constituted an additional varied parameter.

The performance of MV was investigated for three different distances ($d_1 = 4.0$ m; $d_2 = 3.0$ m; $d_3 = 2.0$ m) between the occupants and four particle diameters ($0.5 \mu\text{m}$; $1 \mu\text{m}$; $2.5 \mu\text{m}$; $10 \mu\text{m}$) covering the inhalable range. Figure 5.36 shows the velocity, temperature, and concentration fields of $1 \mu\text{m}$ particles for MV for a distance of 3.0 m between the occupants.

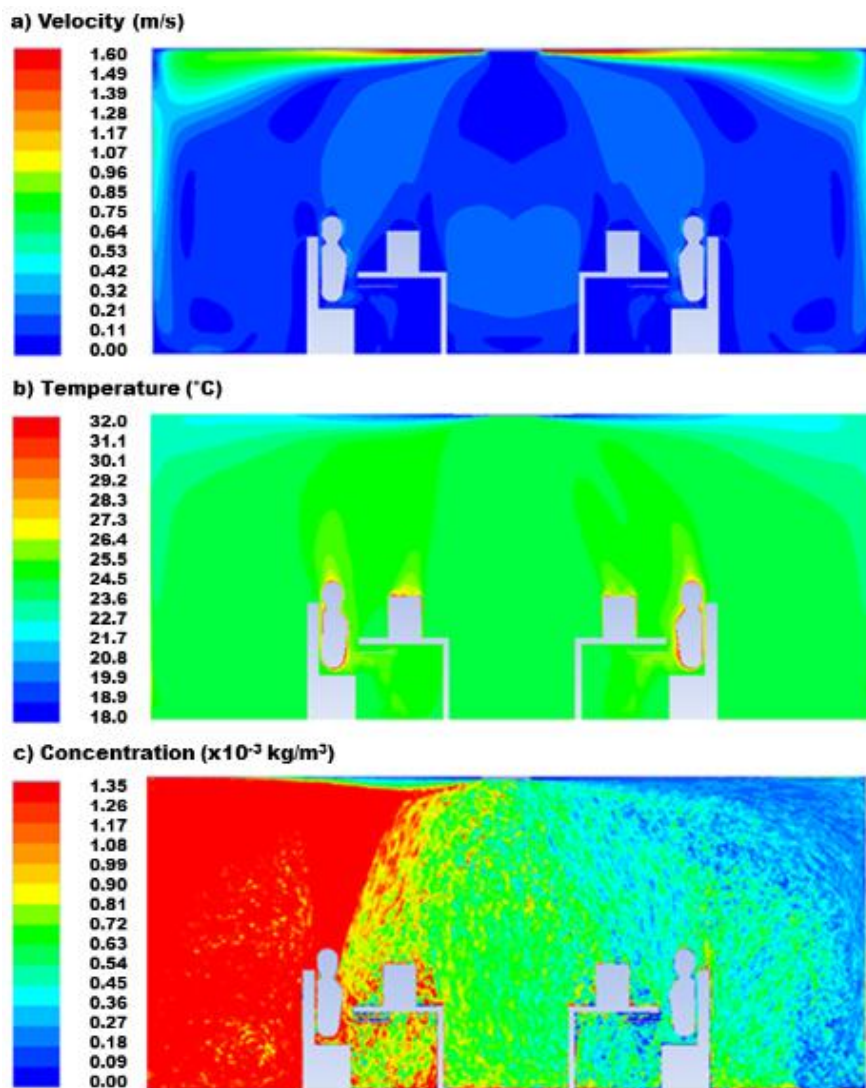


Fig. 5.36: Representation of the: a) velocity, b) temperature, and concentration fields of $1 \mu\text{m}$ particles in the two-station office space at the symmetry plane for mixing ventilation at d_2 .

Figure 5.37 represents the variation of deposited fraction (DFr) and intake fraction (IF) with the separating distance for the different diameters. The ability of MV in preventing contamination through its two paths was largely degraded with the reduction of the distance between the workstations for the different particle diameters investigated challenging efficient use of space.

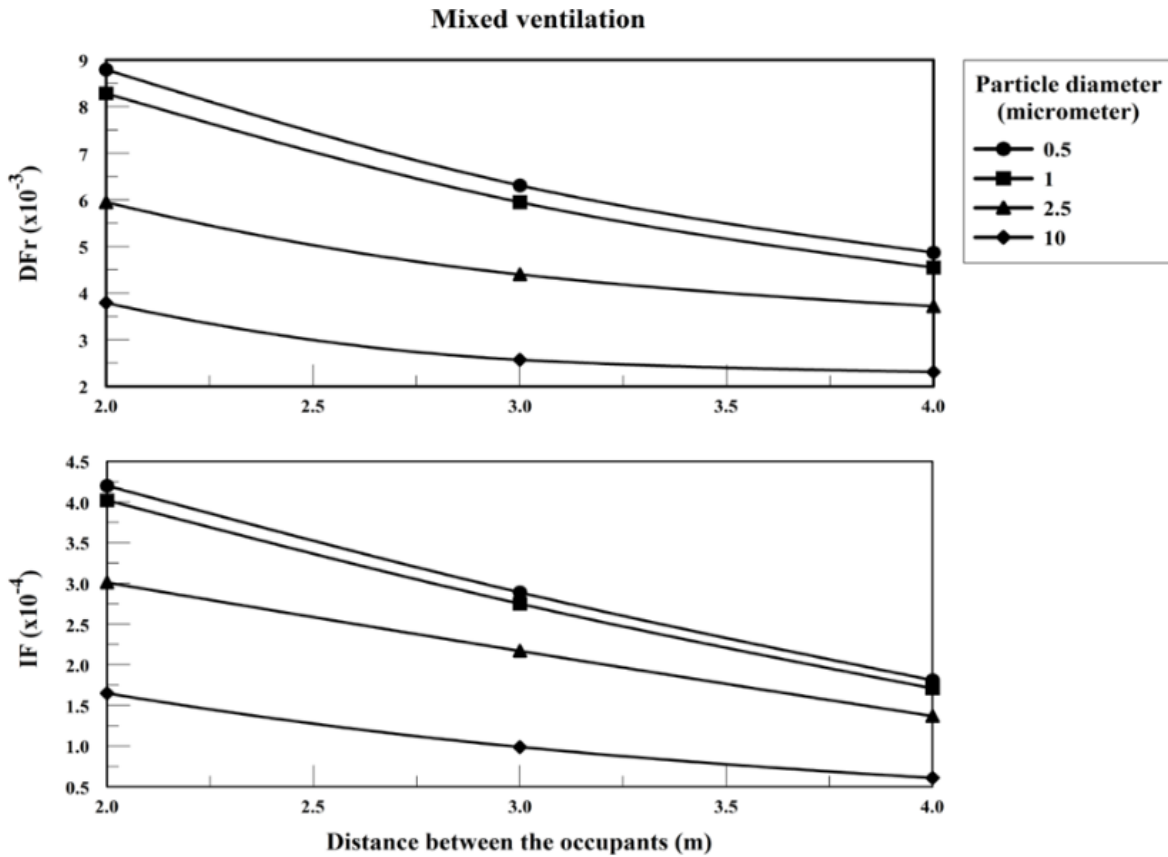


Fig. 5.37: Effect of the distance between the occupants on: a) the deposited fraction (DFr); and b) the intake fraction (IF) for different particle diameters in case of mixing ventilation.

It is clear from Fig. 5.37 that for the same diameter, the IF and DFr increased significantly when the distance between stations decreased. For instance, when the distance was decreased from 4.0 m to 2.0 m, both the DFr and IF were increased by 81.98% and 135.09% respectively, for 1 μm particles. The degradation of performance with distance was higher for fine particles (diameter below 1 μm) which were easily

carried by the flow. Increasing particle diameter resulted in significant gravitational effect that increased floor deposition and the floor acted as a sink of particles decreasing the *DFr* and the *IF* (Fig. 5.37). Table 5.10 summarizes the effect of gravitational settling on particle deposition. The settling effect started to appear for 2.5 μm particles and became considerable for 10 μm particles (Table 5.10). For example, the *DFr* and *IF* were reduced by 56.88 % and 60.71 %, respectively, when the diameter was increased from 0.5 μm to 10 μm for a separating distance of 2.0 m.

Table 5.10: Effect of particle diameter on particle deposition

Distance Particle diameter	d1=4.0 m		d2=3.0 m		d3=2.0 m	
	% of floor deposition	<i>DFr</i> (%)	% of floor deposition	<i>DFr</i> (%)	% of floor deposition	<i>DFr</i> (%)
0.5 μm	2.52	0.487	2.41	0.631	2.19	0.879
1 μm	3.12	0.455	2.85	0.595	2.44	0.828
2.5 μm	9.97	0.372	8.65	0.440	6.61	0.595
10 μm	32.29	0.231	30.51	0.257	26.64	0.379

A more efficient design of the space requires new ventilation techniques allowing smaller distance between occupants while maintaining acceptable IAQ. A similar analysis was conducted to investigate the performance of *CPV* assisted by desk fans with variable flow rate.

Figure 5.38 shows the velocity, temperature, and concentration of 1 μm particles fields for the *CPV* ventilation for a distance of 3.0 m between the occupants. It is obvious that the *CPV* system provided breathable air of higher local quality to the occupant explaining the lower concentration of particles within the space and higher protection of the exposed occupant (Fig. 3.38.c) compared to *MV* (Fig. 36.c).

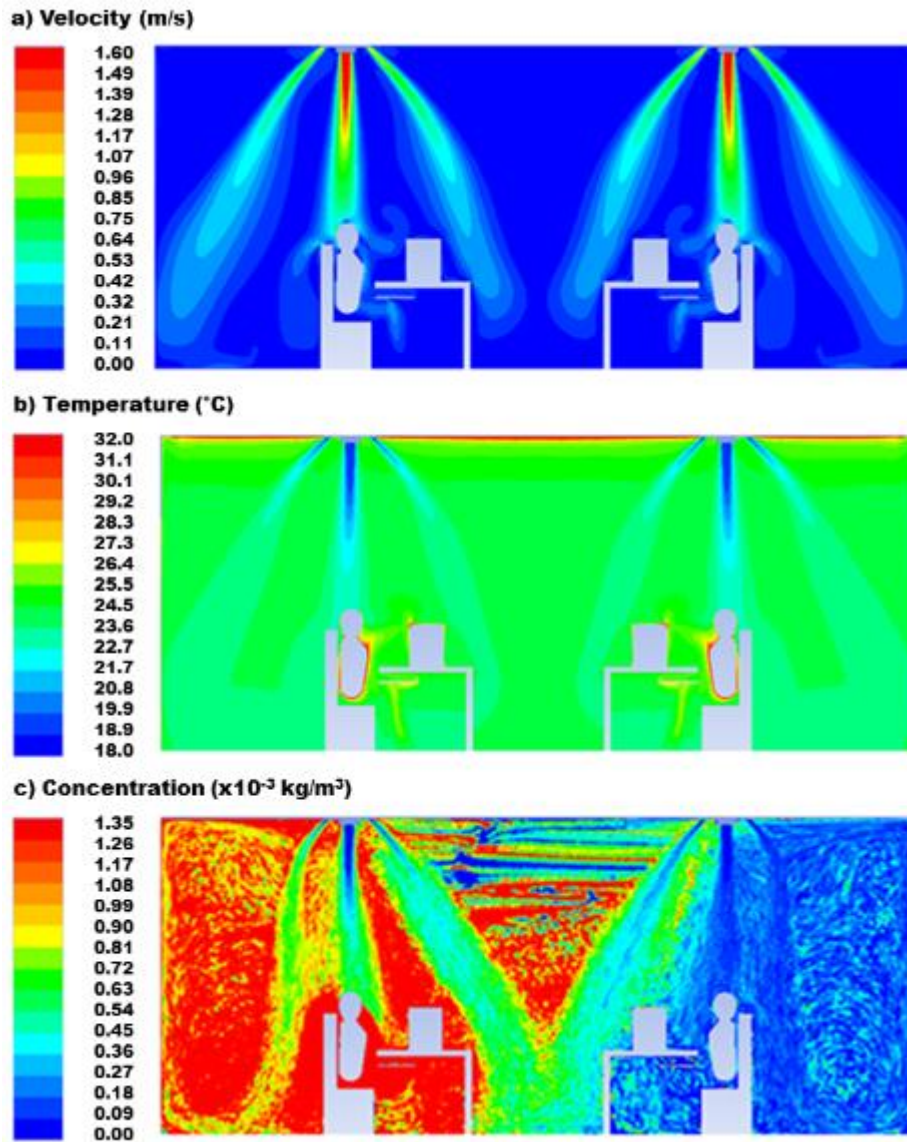


Fig. 5.38: Representation of the: a) velocity, b) temperature, and concentration fields of $1 \mu\text{m}$ particles in the two-station office space at the symmetry plane for *CPV* ventilation at $d2$.

Deposited and intake fractions were calculated for the different configurations and results are summarized in Table 5.11. As the distance between the workstations decreased, a higher number of particles reached the exposed station leading to increase of *DFr* and *IF* (Table 5.11).

Table 5.11: Effect of the HVAC configuration on a) particle deposition at the proximity of the exposed person (*DRF*) and b) intake fraction (*IF*) for different diameters.

HVAC configuration		Particle diameter							
		0.5 μm		1 μm		2.5 μm		10 μm	
		<i>DRF</i> ($\times 10^{-3}$)	<i>IF</i> ($\times 10^{-4}$)	<i>DRF</i> ($\times 10^{-3}$)	<i>IF</i> ($\times 10^{-4}$)	<i>DRF</i> ($\times 10^{-3}$)	<i>IF</i> ($\times 10^{-4}$)	<i>DRF</i> ($\times 10^{-3}$)	<i>IF</i> ($\times 10^{-4}$)
<i>MV</i>	d1=4.0 m	4.87	1.81	4.55	1.71	3.72	1.37	2.31	0.61
	d2=3.0 m	6.31	2.89	5.95	2.75	4.40	2.17	2.57	0.99
	d3=2.0 m	8.79	4.20	8.28	4.02	5.95	3.01	3.79	1.65
<i>CPV</i>	d1=4.0 m	4.21	1.36	4.05	1.33	3.01	1.09	1.89	0.51
	d2=3.0 m	4.72	1.71	4.52	1.66	3.48	1.37	2.18	0.69
	d3=2.0 m	5.71	2.30	5.41	2.23	3.99	1.71	2.65	0.97
<i>CPV+DF</i> ($Q_f=5$ L/s)	d1=4.0 m	3.25	0.79	3.18	0.77	2.53	0.65	1.71	0.36
	d2=3.0 m	3.48	0.99	3.52	0.95	2.81	0.75	1.94	0.42
	d3=2.0 m	3.97	1.32	3.89	1.27	3.13	1.05	2.21	0.65
<i>CPV+DF</i> ($Q_f=10$ L/s)	d1=4.0 m	2.73	0.51	2.68	0.49	2.32	0.43	1.61	0.22
	d2=3.0 m	2.95	0.63	2.89	0.61	2.5	0.51	1.74	0.25
	d3=2.0 m	3.32	0.95	3.21	0.91	2.75	0.81	1.89	0.45
<i>CPV+DF</i> ($Q_f=15$ L/s)	d1=4.0 m	3.88	0.91	3.83	0.89	2.99	0.75	1.75	0.38
	d2=3.0 m	4.41	1.29	4.33	1.25	3.27	0.99	2.01	0.55
	d3=2.0 m	4.99	1.69	4.87	1.62	3.60	1.34	2.32	0.79

Figures 5.39 and 5.40 show the variation of *DRF* and *IF* with distance for the different ventilation systems studied at 1.0 μm and 10 μm particles representing the fine and coarse modes respectively. The increase of *DRF* and *IF* with the reduction of distance between the occupants was also observed for the *PV* systems but at a lower rate compared to *MV* (Figs. 5.39 and 5.40).

The rate of increase of *DRF* and *IF* for the different cases studied were quantified by calculating the increments in *IF* and *DRF* (ΔIF and ΔDRF) when distance between the occupants was reduced from 4.0 m to 2.0 m and summarized in Table 5.12.

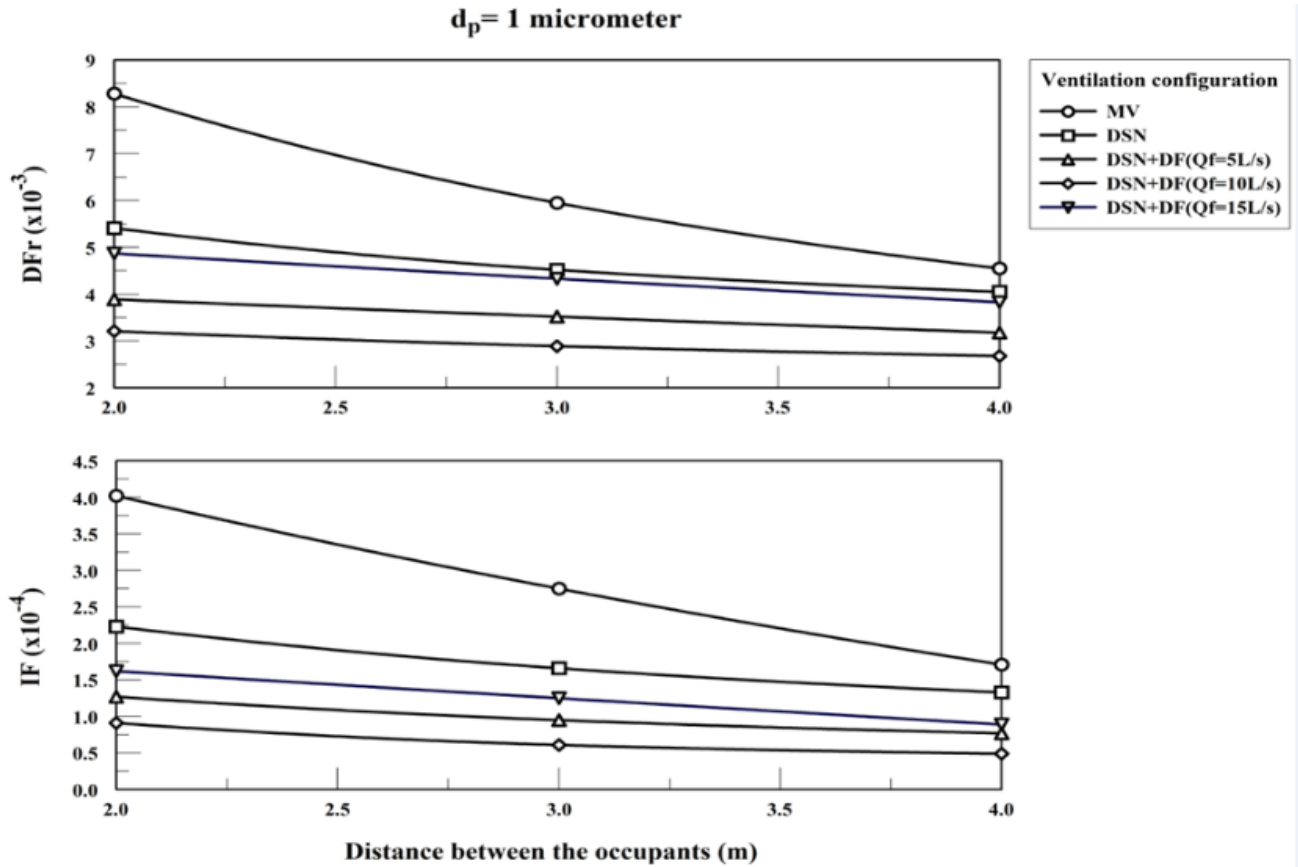


Fig. 5.39: Effect of the ventilation configuration on the variation with distance of: a) DFr ; b) IF for $1 \mu\text{m}$ particles.

Table 5.12: Effect of the HVAC configuration on a) the increments in DFr (ΔDFr) and b) the increments in IF (ΔIF) for different diameters when the distance between the occupants is reduced from 4.0 to 2.0 m.

HVAC configuration	Particle diameter							
	0.5 μm		1 μm		2.5 μm		10 μm	
	ΔDFr ($\times 10^{-3}$)	ΔIF ($\times 10^{-4}$)	ΔDFr ($\times 10^{-3}$)	ΔIF ($\times 10^{-4}$)	ΔDFr ($\times 10^{-3}$)	ΔIF ($\times 10^{-4}$)	ΔDFr ($\times 10^{-3}$)	ΔIF ($\times 10^{-4}$)
<i>MV</i>	3.92	2.39	3.73	2.31	2.23	1.64	1.48	1.04
<i>CPV</i>	1.5	0.94	1.36	0.9	0.98	0.62	0.76	0.46
<i>CPV+DF</i> ($Q_f=5$ L/s)	0.72	0.53	0.71	0.5	0.6	0.4	0.5	0.29
<i>CPV+DF</i> ($Q_f=10$ L/s)	0.59	0.44	0.53	0.42	0.43	0.38	0.28	0.23
<i>CPV+DF</i> ($Q_f=15$ L/s)	1.11	0.78	1.04	0.73	0.61	0.59	0.57	0.41

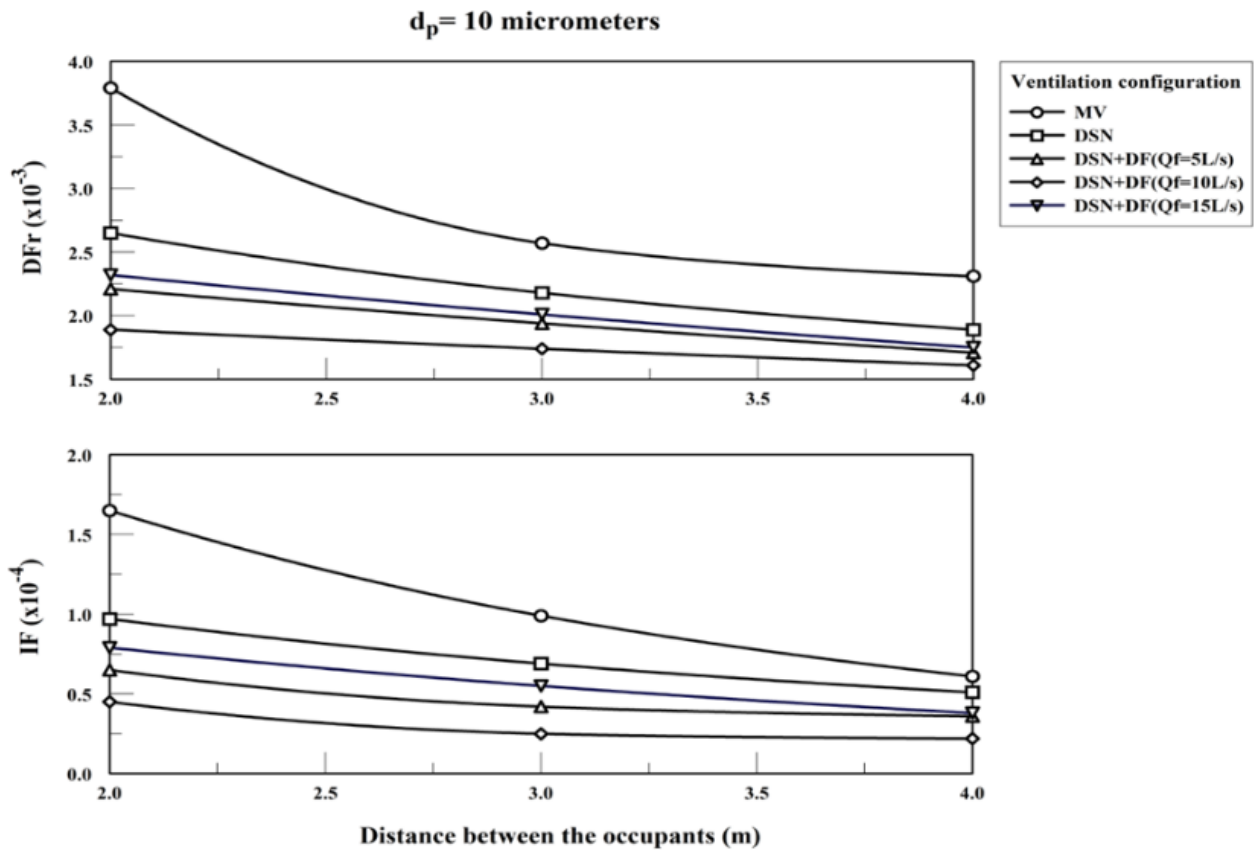


Fig. 5.40: Effect of the ventilation configuration on the variation with distance of: a) DFr ; b) IF for 10 μm particles.

It was observed that ΔIF and ΔDFr decreased by changing the ventilation system from MV to CPV and then decreased further by the introduction of desk fans (Table 5.12, Fig 5.39, and Fig. 5.40). When distance between the occupants was reduced from 4.0 m to 2.0 m, the increases in DFr and IF for 0.5 μm particles were reduced by 84.95%, and 81.59% respectively when replacing the MV by $CPV+DF$ at 10 L/s. The smaller the distance between the occupants was, the larger was the effectiveness of the $CPV+DF$ system compared to MV in reducing cross-contamination. At fixed distance, the increase in particle diameter increased the efficiency of the downward PV system. This is expected since PV aided by the gravitational settling boosts the downward transport of generated particles reducing their diffusion between

the workstations and increasing floor deposition. The floor in this case acted as a sink of particles thus decreasing considerably the *IF* and *DFr* compared to the fine particle mode (Table 5.11).

Figure 5.41 shows the variation of the deposited fraction and intake fraction respectively with fan flow rate for a particle diameter of 1 μm for different distances between the occupants. It is clear that up to a flow rate of 10 L/s per fan, the presence of a desk fan decreased both the deposited and intake fractions for the different distances and particle diameters investigated (Table 5.11, Fig. 5.41).

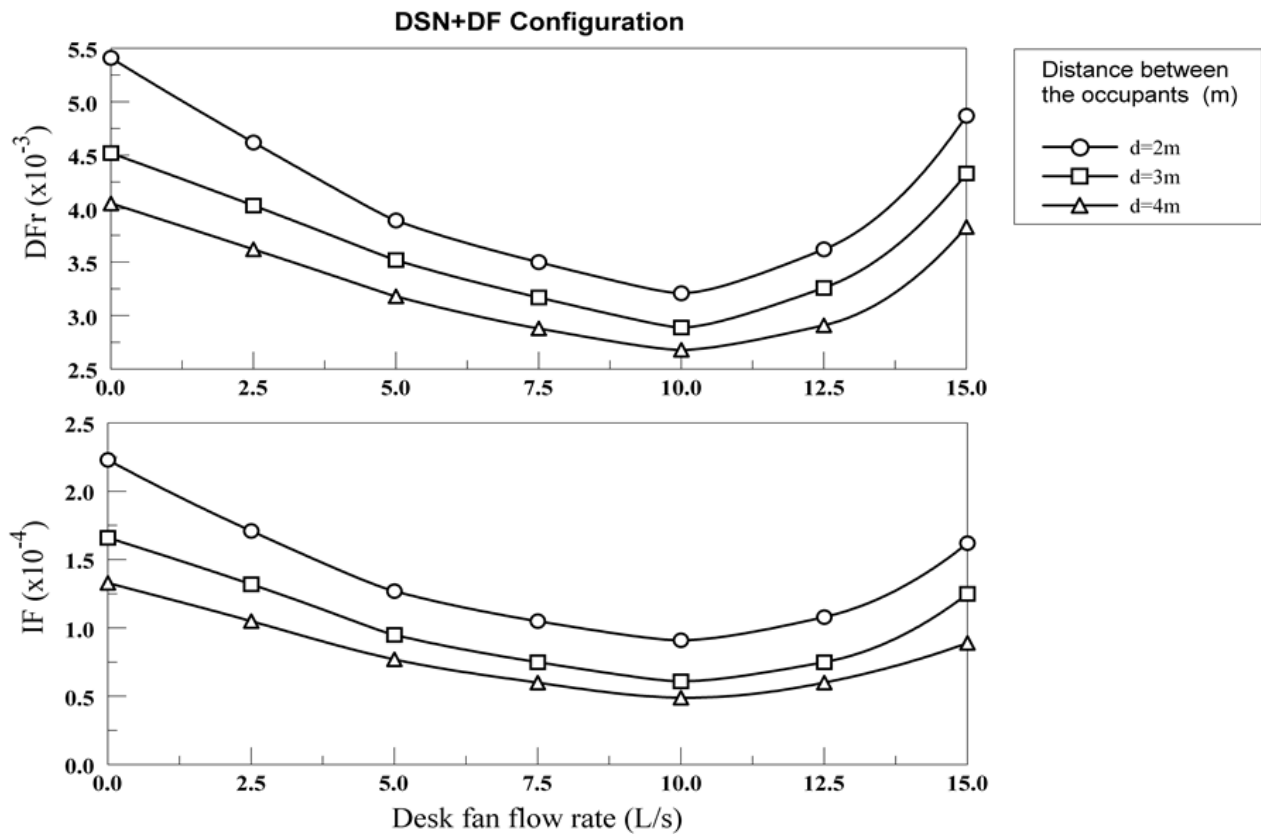


Fig. 5.41: Variation of a) the deposited fraction; and b) the intake fraction with the fan flow rate for different distances between the occupants in the case of *CPV+DF* configuration for 1 μm particle.

In fact, increasing the fan flow rate decreased the number of particles deposited at the human body and chair surfaces while the number of particles deposited on the desk and computer increased. This resulted in the presence of an optimal fan flow rate of 10 L/s for which the DFr was minimized (Fig.5.41).

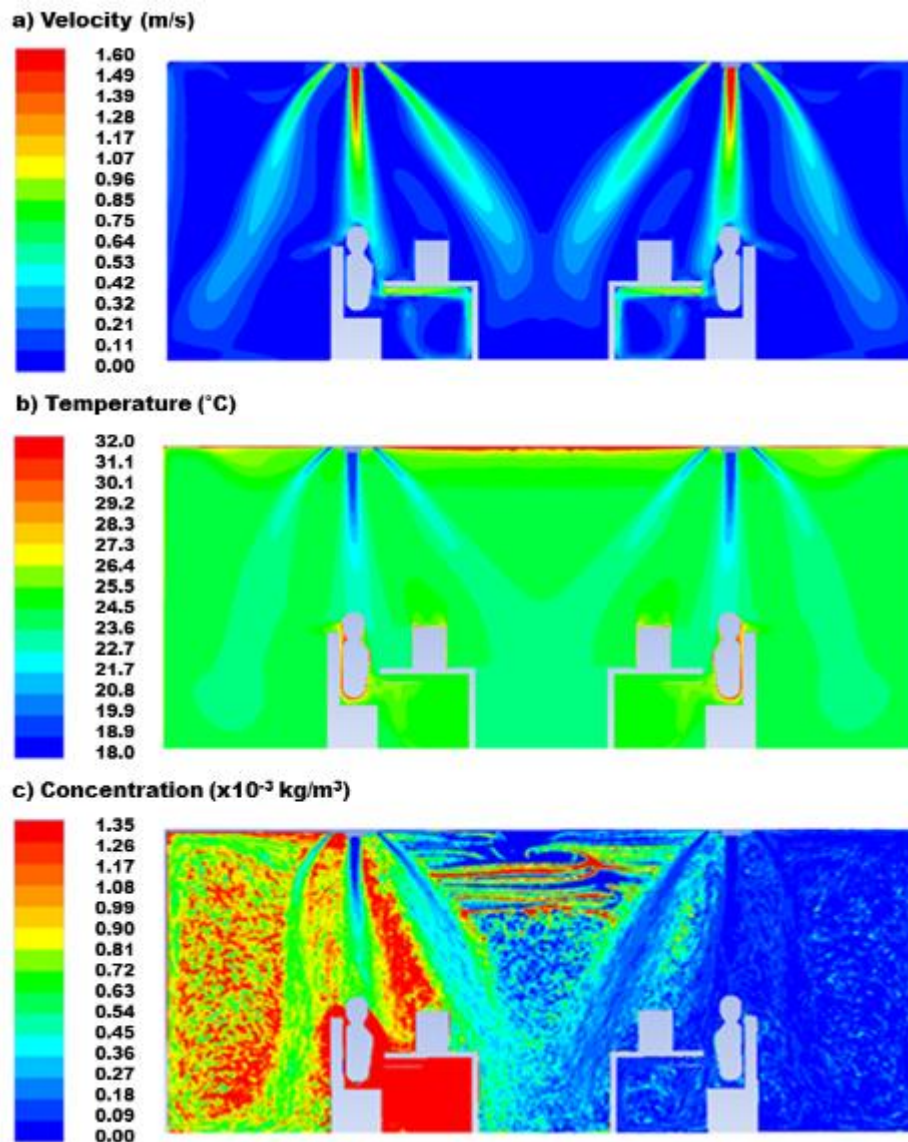


Fig. 5.42: Representation of the: a) velocity, b) temperature, and concentration fields of 1 μm particles in the two-station office space at the symmetry plane for the optimal $CPV+DF$ (10L/s) at d_2 .

Figure 5.42 shows the velocity, temperature, and concentration of $1\ \mu\text{m}$ particles fields for the *CPV+DF* at 10L/s for a distance of 3.0 m between the occupants. The presence of the desk fans led to significant enhancement of the performance of the system. The *DF* reduced the transport of particles between the two stations by facilitating the delivery of clean air to the breathing level providing more protection to the exposed person (Fig. 5.42.c).

The effectiveness of the *CPV* system was due to the combination of the ceiling nozzle delivering fresh air to the breathing level and the peripheral diffuser (*D*) creating a canopy acting as a barrier to the diffusion of particles between the two-stations. However, the particles that were able to penetrate the canopy were trapped in the zone between the angled diffuser and nozzle jet flows.

Figure 5.43 shows the concentration of $10\ \mu\text{m}$ particles at the symmetry plane of the exposed station for different desk fan flow rates. As the fan flow rate increased the momentum of the *PV* jet reaching the breathing level increased which provided higher protection to the occupant (Figs. 5.42.a, 5.43). However, air mixing in the zone between the nozzle jet and the canopy increased with increased fan flow rate leading to an increase in particle concentration at the breathing level of the exposed occupant (Fig. 5.43). These two opposing effects explain the existence of an optimal fan flow rate of nearly 10 L/s for which the *IF* is minimized (Table 5.11, Fig 5.43).

Therefore, the proper selection of the fan flow rate (10 L/s) and the introduction of *DF* to the *CPV* system were shown to be effective in reducing direct and indirect-contamination with efficient use of the space. The value of the optimal fan flow rate (10 L/s) for the different studied configurations was found to be independent of the distance between the occupants and particle diameter (Table 5.11, Fig. 5.40).

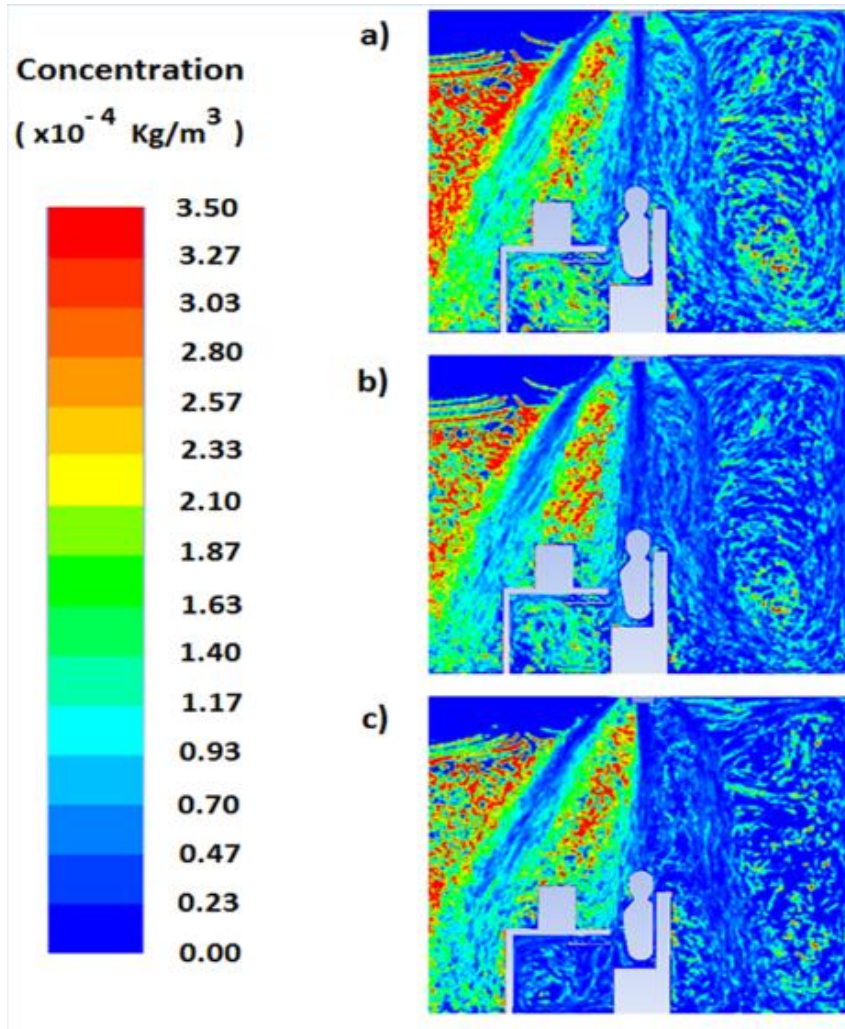


Fig. 5.43: Effect of the desk fan flow rate: a) 5L/s, b) 10L/s, and c) 15 L/s on the intake fraction of 10 μ m particles for the *CPV+DF* ventilation at *d2*.

5.2.2.2. Energy Savings of the Optimal *CPV+DF* Design

The optimized system presents many advantages compared to conventional *MV* which explain the high potential it presents for energy savings. In fact, the *CPV* system assisted by desk fans localizes the flow around the occupant forming a canopy allowing having higher macroclimate temperature while insuring acceptable thermal comfort and ventilation effectiveness. Makhoul et al [22] found that this flow localization induced considerable energy savings of 13.25 % by the optimized *CPV* system compared to *MV*

for equivalent thermal comfort and IAQ in terms of CO₂ in a space with occupancy density of 12 m²/occupant. When the occupancy density is improved to 8 m²/occupant, more energy savings are achieved due to reduced office space area for delivering same function leading to less heat gain through space external walls.

Furthermore, as observed in this study, the *CPV* jet and diffusers' canopy obstruct disease transmission between the workstations reducing significantly the probability of cross-infection and offering a potential for increased energy savings by reducing the space dimensions and thus the energy consumption [41,42].

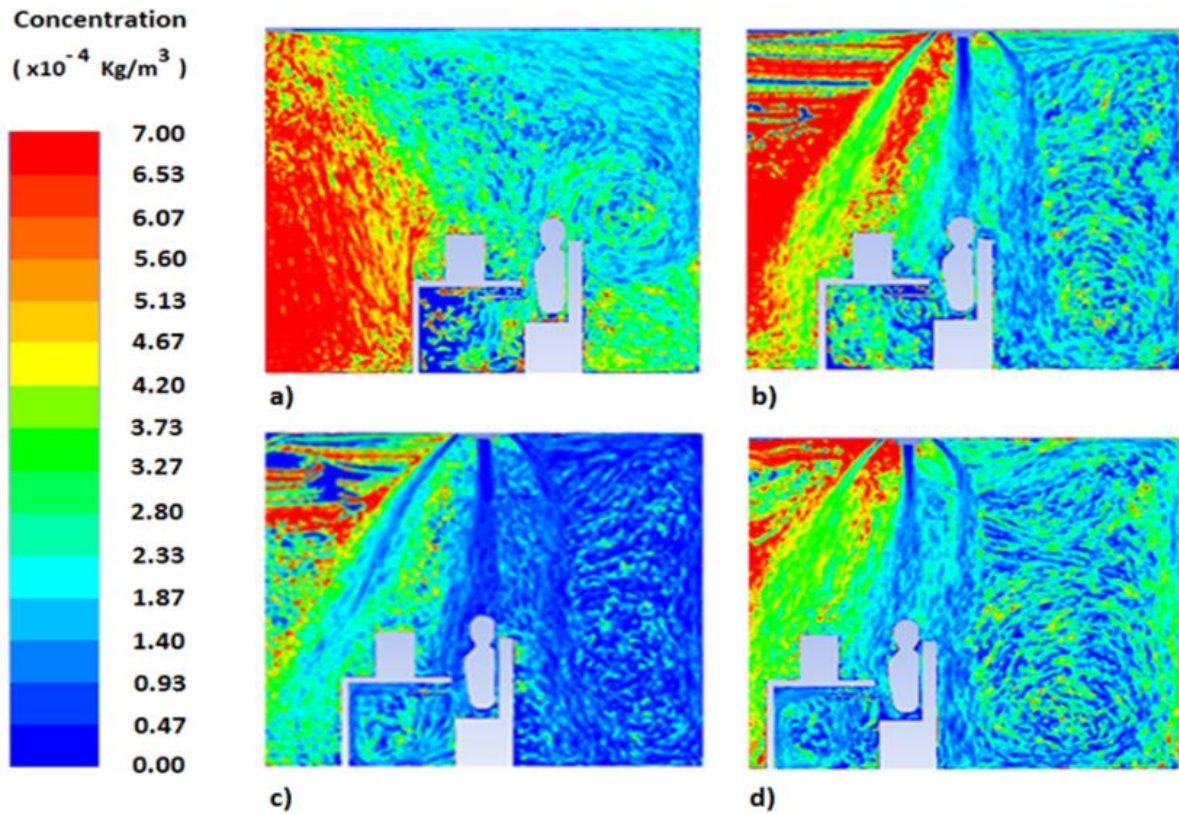


Fig. 5.44: Concentration field of 1µm particle in the exposed person station at the symmetry plane for: a) *MV* at $d1$; b) *CPV* at $d2$; c) *CPV+DF* (10 L/s) at $d2$; d) *CPV+DF* (10 L/s) at $d3$.

In fact, the optimal design of the ventilation system allowed reducing both direct and indirect contamination with efficient use of space as demonstrated in Fig. 5.44 where the concentration fields of 1 μ m particle in the exposed person station are shown at the symmetry plane for: a) *MV* at *d1*; b) *CPV* at *d2*; c) *CPV+DF* (10L/s) at *d2*; d) *CPV+DF* (10L/s) at *d3*.

The performance of *CPV+DF* (10 L/s) for the smallest distance studied between the occupants (2.0 m) was better than the performance of *MV* for the longest distance investigated (4.0 m) at different particle diameters (Table 5.11).

Even though the distance between occupants was decreased from 4.0 m to 2.0 m by changing the ventilation system, we were able to enhance the IAQ and reduce the risk of cross-contamination between occupants by decreasing significantly the *DFr* and *IF* (Fig. 5.43, Table 5.11). For example, the *IF* for 1 μ m particles was reduced from 1.71×10^{-4} to 0.91×10^{-4} despite the decrease of the separating distance by a factor of 2. The percentage of reductions of the *DFr* and *IF* when changing the configuration from *MV* at *d1* = 4.0 m to *CPV+DF* (10 L/s) at *d3*= 2.0 m were computed and summarized in Table 5.13. Reductions up to 31.83% and 47.51% were reached, respectively for *DFr* and *IF*, for the finest particle diameter of 0.5 μ m.

Table 5.13: % of reductions of the *DFr* and *IF* when changing the configuration from *MV* at *d1* to *CPV+DF* (10 L/s) at *d3* for different particle diameters.

Particle diameter	0.5 μ m	1 μ m	2.5 μ m	10 μ m
% decrease in <i>DFr</i>	31.83%	29.45%	26.08%	18.18%
% decrease in <i>IF</i>	47.51%	46.78%	40.88%	26.23%

Therefore, an occupancy density of 12 m²/occupant is needed for the *MV* system to maintain acceptable IAQ as its performance is degraded with reduced

distance between the occupants (Fig. 5.37, Table 5.12). On the other hand, for the optimized *CPV* system assisted by desk fans with a flow rate of 10 L/s, the occupancy density improved from 12 to 8 m²/occupant without augmenting the risk of cross-contamination compared to *MV* allowing to use the space more efficiently leading to higher energy savings [41,42].

5.2.3. *CPV System Assisted by CF versus DF*

5.2.3.1. *CPV+DF/CF Case Study*

A two-station office of dimensions 4.8 m × 3.4 m × 3.4 m corresponding to occupancy density of 8 m²/occupant was considered. Fresh air was supplied through the *CPV* jet at 8.5 L/s per occupant with 400 ppm of CO₂ according to the ASHRAE standard [131], while 35 L/s of recirculated air per diffuser were delivered. The optimal fan flow rate of 10 L/s was selected for the fans' operation. Two seated multi-segment manikin generated each nearly 70 W of sensible heat (characterizing sedentary activity [132]) simulating the occupants and their computers released 93 W [132]. For ventilation effectiveness assessment, a CO₂ flow rate of 0.62 L/min was generated within the space representing typical two-station office CO₂ load [133]. In order to study cross-contamination between occupants one of the occupants generates contaminated particles simulating an infected person while the other occupant is healthy representing an exposed occupant. Horizontal mouth generation at a flow rate of 8.4 L/min simulating sedentary respiratory activity and contaminated particle rate of 5e⁻⁵ kg/s [28] was considered. The investigation of chair motion effect on thermal comfort, ventilation effectiveness and cross contamination was conducted for two shift distances of 10 and 20 cm compared to the position of the occupant directly beneath the *CPV* jet.

5.2.3.1.1. IAQ Assessment

The effect of the shift distance and the ventilation system on the ventilation effectiveness, *IF* and *DRF* for different particles diameters covering the inhalable range from the fine to the coarse mode (0.5 μm ; 1 μm ; 2.5 μm ; 10 μm) were studied and the results were summarized in Table 5.14.

Table 5.14: Effect of the shift distance and the ventilation system on the ventilation effectiveness, intake fraction (*IF*) and the particle deposition at the proximity of the exposed person (*DRF*) for different particle diameters.

Shift Distance	Ventilation Configuration	Ventilation Effectiveness	<i>IF</i> ($\times 10^{-4}$)				<i>DRF</i> ($\times 10^{-3}$)			
			0.5 μm	1 μm	2.5 μm	10 μm	0.5 μm	1 μm	2.5 μm	10 μm
<i>sd1=0 cm</i>	<i>CPV</i>	9.51%	2.81	2.53	1.91	1.22	6.37	5.81	4.64	2.94
	<i>CPV+DF</i>	21.1%	1.29	1.15	0.86	0.49	3.96	3.61	3.03	2.12
	<i>CPV+CF</i>	23.1%	1.1	0.90	0.69	0.42	3.46	3.19	2.61	1.87
<i>sd2=10 cm</i>	<i>CPV</i>	12.8%	1.95	1.81	1.43	0.95	5.73	5.25	3.98	2.33
	<i>CPV+DF</i>	23.9%	0.88	0.83	0.59	0.31	3.72	3.44	2.75	1.91
	<i>CPV+CF</i>	25.2%	0.75	0.69	0.51	0.25	3.04	2.85	2.29	1.54
<i>sd3=20 cm</i>	<i>CPV</i>	6.1%	3.50	3.19	2.40	1.47	10.25	9.55	7.73	5.07
	<i>CPV+DF</i>	10.4%	1.94	1.77	1.32	0.72	7.51	7.11	5.85	4.07
	<i>CPV+CF</i>	19.5%	1.29	1.07	0.82	0.48	4.78	4.37	3.49	2.34

a) Ventilation Effectiveness

Figure 5.45.(a-c) shows the velocity field at the symmetry plane of the two-station office space for shift distances $sd1=0\text{ cm}$ (occupant at the left) and $sd3=20\text{ cm}$ (occupant at the right) for: (a) Standalone *CPV*; (b) *CPV+DF*; and (c) *CPV+CF*.

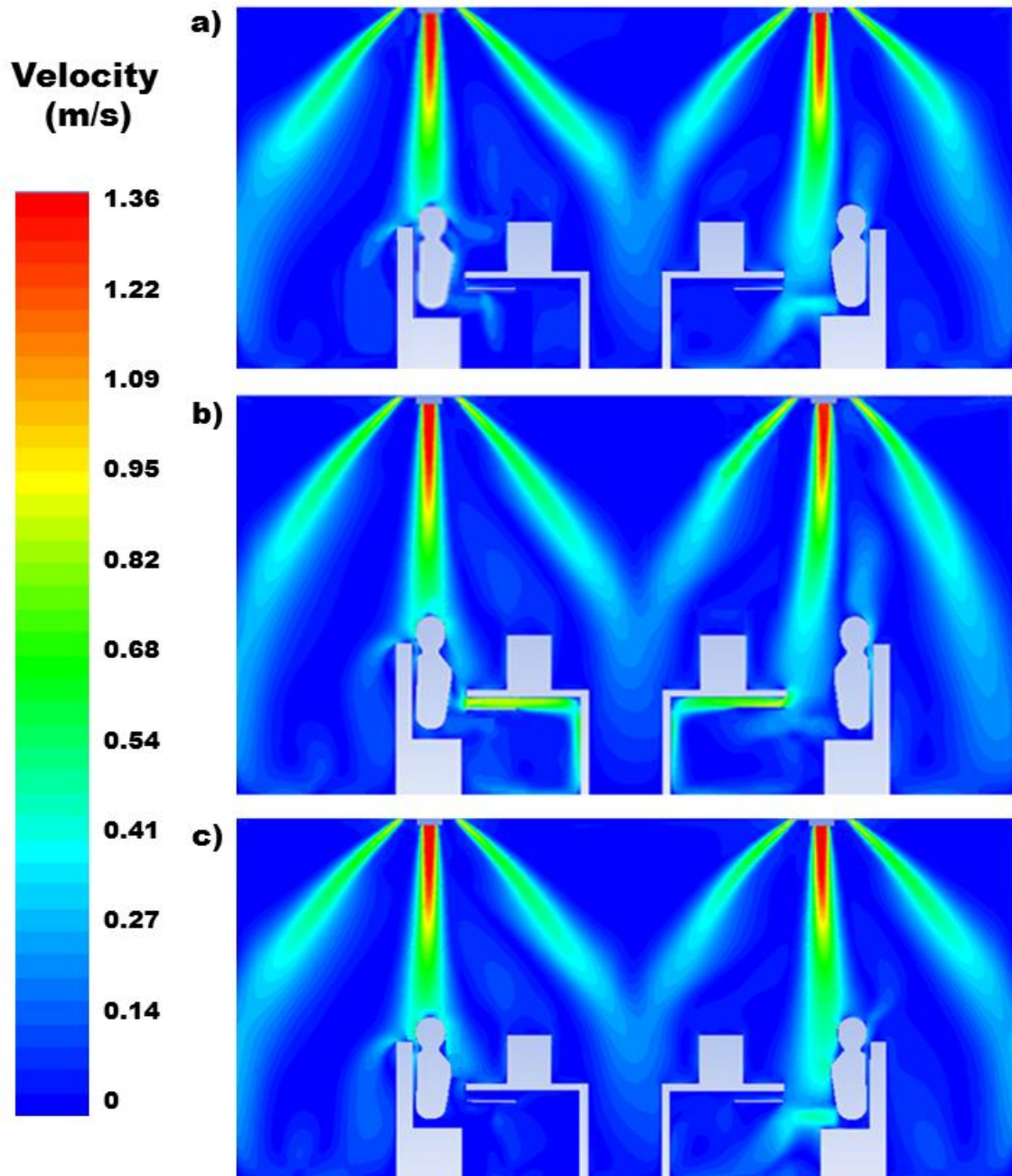


Fig. 5.45: Illustration of the velocity field at the symmetry plane of the two-station office space for shift distances $sd1=0\text{ cm}$ (occupant at the left) and $sd3=20\text{ cm}$ (occupant at the right) for: a) Standalone *CPV*; b) *CPV+DF*; c) *CPV+CF*.

For a zero chair shift, the downward *CPV* jet was opposed by the rising thermal plumes since it was directly above the occupant head (Fig. 5.45.(a-c)). The operation of *DF* and *CF* lead to suppression of the convective plumes, permitting to the *CPV* jet to reach the breathing level more effectively (Fig. 5.45.(b-c)) and thus improving the standalone *CPV* performance in terms of ventilation effectiveness (Table 5.14). For example, when changing the ventilation configuration from standalone *CPV* to *CPV+DF* to *CPV+CF*, the ventilation effectiveness was increased from 9.51% to 21.1% to 23.1% (see Table 5.14).

Figure 5.46.(a-c) illustrates the velocity field at the symmetry plane of the two-station office space for *CPV+DF* for the healthy occupant shift of: a) $sd1=0$ cm; b) $sd2=10$ cm; c) $sd3=20$ cm. For small shift distance of 10 cm, the *CPV* jet was less opposed by the rising thermal plumes since the jet was not directly above the convective plumes emanating from the occupant head (Fig. 5.46.(a-b)). This allowed the clean *CPV* jet to reach more effectively the breathing zone of the healthy occupant which explains the increase in the ventilation effectiveness at 10 cm shift compared to the case of no shift (Table 5.14). For moderate shift, the operation of both *DF* and *CF* was positive in terms of ventilation effectiveness with a better performance of the *CF* compared to *DF* (Table 5.14). For example, when the shift distance increased from 0 to 10 cm, the ventilation effectiveness increased from 21.1% to 23.9% for *CPV+DF* while it increased from 23.1% to 25.2% for *CPV+CF* (see Table 5.14).

For a shift distance of 20 cm, the fresh air *CPV* jet was away from the breathing level and became less localized around the occupant (Fig. 5.45.(a-c)-5.46.(a-c)) which explains the decrease in the ventilation effectiveness (Table 5.14).

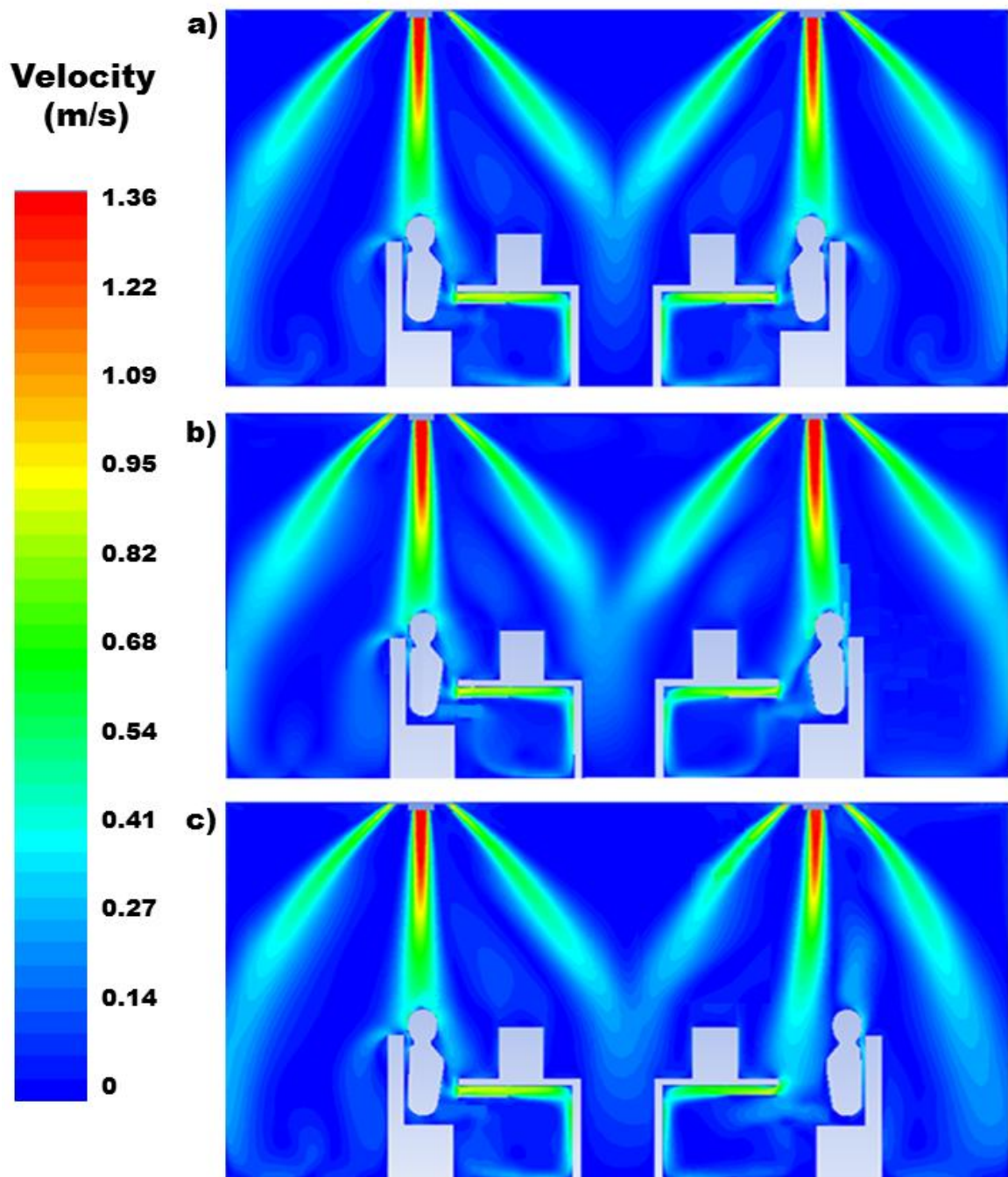


Fig. 5.46: Illustration of the velocity field at the symmetry plane of the two-station office space for *CPV+DF* for the healthy occupant shift of: a) $sd1=0$ cm; b) $sd2=10$ cm; c) $sd3=20$ cm.

Figure 5.47 compares the CO_2 fields at the symmetry plane of the two-station office space for shift distances $sd1=0$ cm (occupant at the left) and $sd3=20$ cm (occupant at the right) for: a) *CPV+DF*; b) *CPV+CF*.

**CO₂ mole
fraction in ppm**

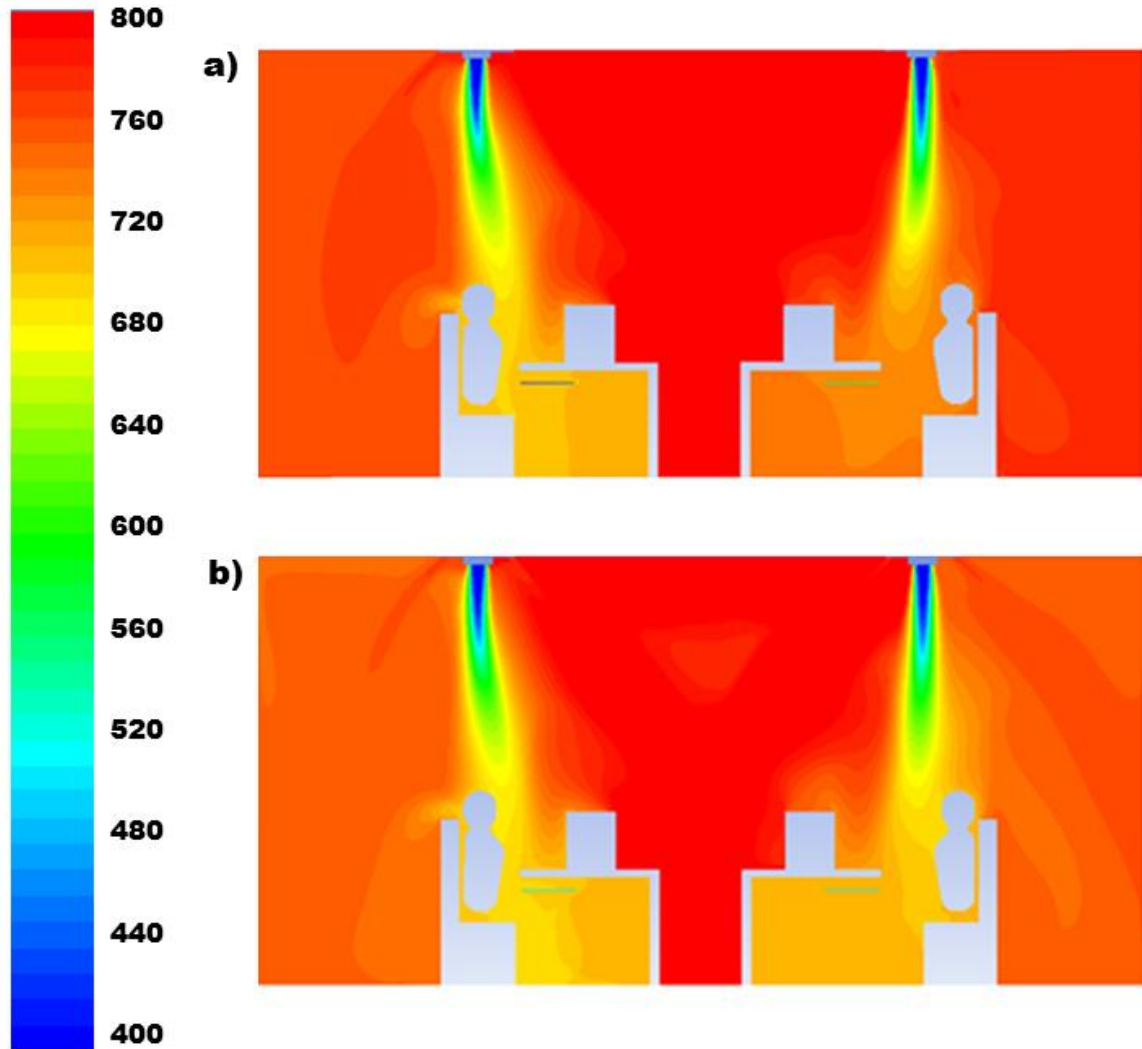


Fig. 5.47: Illustration of the CO₂ field at the symmetry plane of the two-station office space for shift distances $sd1=0\text{ cm}$ (occupant at the left) and $sd3=20\text{ cm}$ (occupant at the right) for: a) $CPV+DF$; b) $CPV+CF$.

The presence of both DF and CF enhanced the ventilation effectiveness of the system allowing the CPV jet to reach more effectively the breathing level of the occupant directly beneath the CPV jet (the occupant at the left) with slightly better performance for the case of CF compared to DF (Fig. 5.47, Table 5.14). On the other

hand, for the occupant with a shift distance of 20 cm (the occupant at the right), the standalone *CPV* and *CPV* assisted by *DF* the ventilation effectiveness of the system was largely degraded (Table 5.14) as the fresh jet was no longer directed towards the breathing zone (Fig. 5.47.a) while the operation of *CF* was largely more effective (see Fig. 5.47.b).

b) Cross-Contamination

The trend of variation with shift distance of *CPV* system effectiveness in terms of reducing direct and indirect cross-contamination was identical to the one of ventilation effectiveness since the same physics were involved. Direct and indirect cross-contaminations were reduced significantly with the increase of particle diameter (see Table 5.14) for the different shift distances. In fact, as the particle diameter increased the gravitational effect was strengthened constituting a particle sink by floor deposition. Figure 5.48 compares 1 μm particle concentration fields at the symmetry plane of the two-station office space for shift distances $sd1=0$ cm (occupant at the left) and $sd3=20$ cm (occupant at the right) for: (a) *CPV+DF* and (b) *CPV+CF*. The *CF* attached to the occupant chair moves with it helping in re-localizing of the fresh flow around it and reaching the breathing level more effectively reducing the negative effect of the chair shift (see Table 5.14, Fig. 5.46.(b-c), and Fig. 5.48.(a-b)). This was not the case when *CPV* was assisted by *DF* for which the system performance was largely degraded with the occupant position shift (see Fig. 5.48.a).

**Normalized
Concentration
($\times 10^{-4}$)**

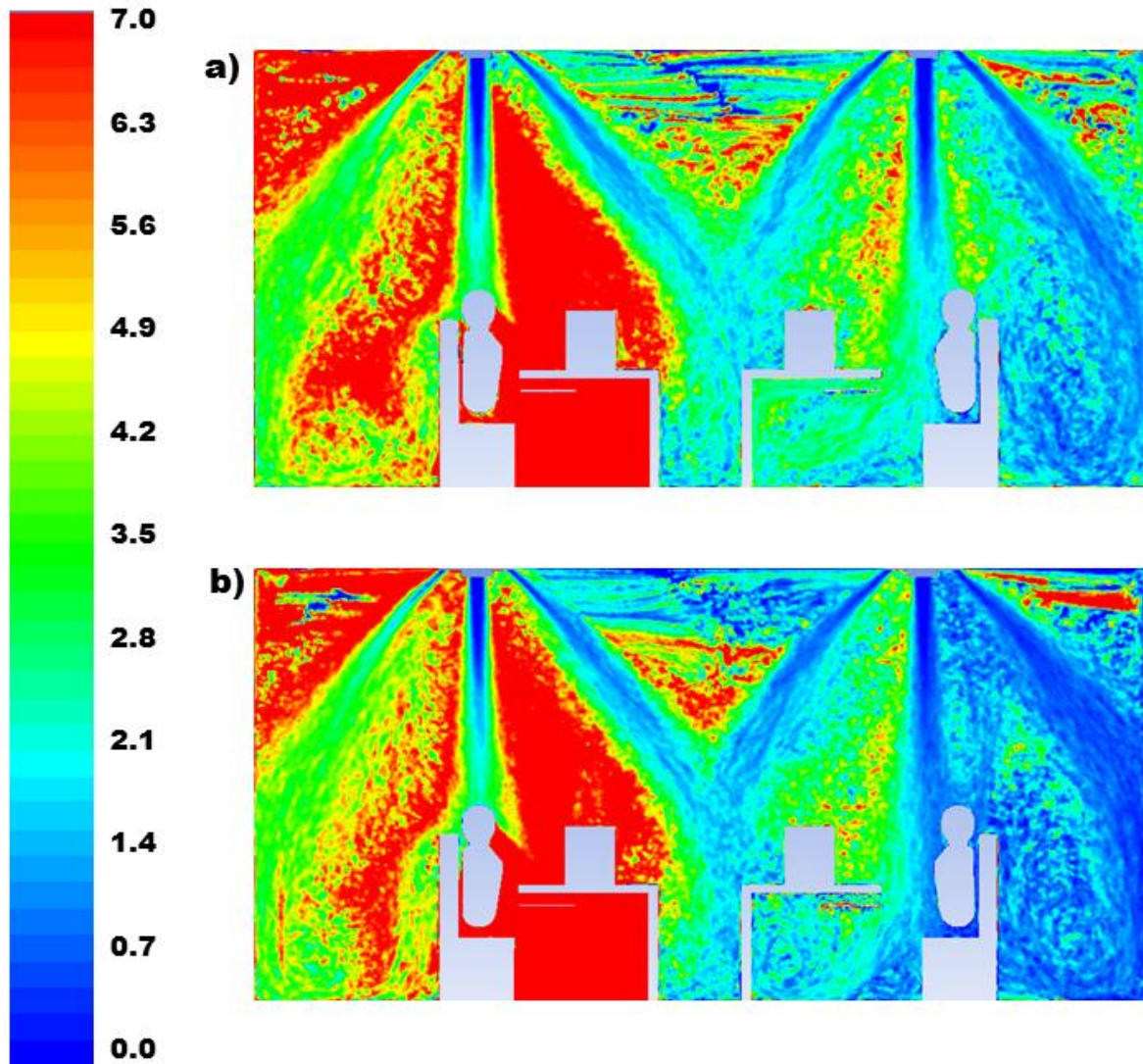


Fig. 5.48: Illustration of $1\mu\text{m}$ particle concentration field at the symmetry plane of the two-station office space for shift distances $sd1=0\text{ cm}$ (occupant at the left) and $sd3=20\text{ cm}$ (occupant at the right) for: a) $CPV+DF$; b) $CPV+CF$.

The performance degradation was quite different when the CPV jet was assisted by CF compared to DF as summarized in Table 5.15 which represented the effect of assisting CPV with DF and CF on the increase in DFr (ΔDFr) and IF (ΔIF) for different particle diameters when the shift distance was increased from 0 to 20 cm. For

instance, when the shift distance varied from 0 to 20 cm the IF for 0.5 μm particles was increased by 50.39% when DF were used while it was increased only by 17.27% when CF assisted the CPV jet. The performance degradation with shift distance was reduced with the increase of particle diameter due to the settling effect (Table 5.15).

Table 5.15: Effect of assisting ceiling personalized ventilation (CPV) with desk fans (DF) and chair fans (CF) on a) the increase in DFr (ΔDFr) and b) the increase in IF (ΔIF) for different diameters when the shift distance is increased from 0 to 20 cm.

Ventilation configuration	Particle diameter							
	0.5 μm		1 μm		2.5 μm		10 μm	
	ΔDFr ($\times 10^{-3}$)	ΔIF ($\times 10^{-4}$)	ΔDFr ($\times 10^{-3}$)	ΔIF ($\times 10^{-4}$)	ΔDFr ($\times 10^{-3}$)	ΔIF ($\times 10^{-4}$)	ΔDFr ($\times 10^{-3}$)	ΔIF ($\times 10^{-4}$)
CPV	3.88	0.69	3.74	0.66	3.09	0.49	2.13	0.25
CPV+DF	3.55	0.65	3.50	0.62	2.82	0.46	1.95	0.23
CPV+CF	1.32	0.19	1.18	0.17	0.88	0.13	0.47	0.06

5.2.3.1.2. Thermal Comfort Assessment

In order to quantitatively assess the thermal comfort for the different configurations studied, the CFD model was coupled with the bio-heat model and the segmental and overall comfort and sensation were determined and summarized in Figs. 5.49 and 5.50, respectively.

When the occupant was directly beneath the CPV jet ($sdl = 0$ cm), the operation of both DF and CF largely improved the standalone CPV performance in terms of thermal comfort, constituting a reference case to compare with the case of occupant shift (see Figs. 5.49 and 5.50). However, the enhancement potential was higher for CF compared to DF due to the symmetrical distribution of the four chair fans around the occupant.

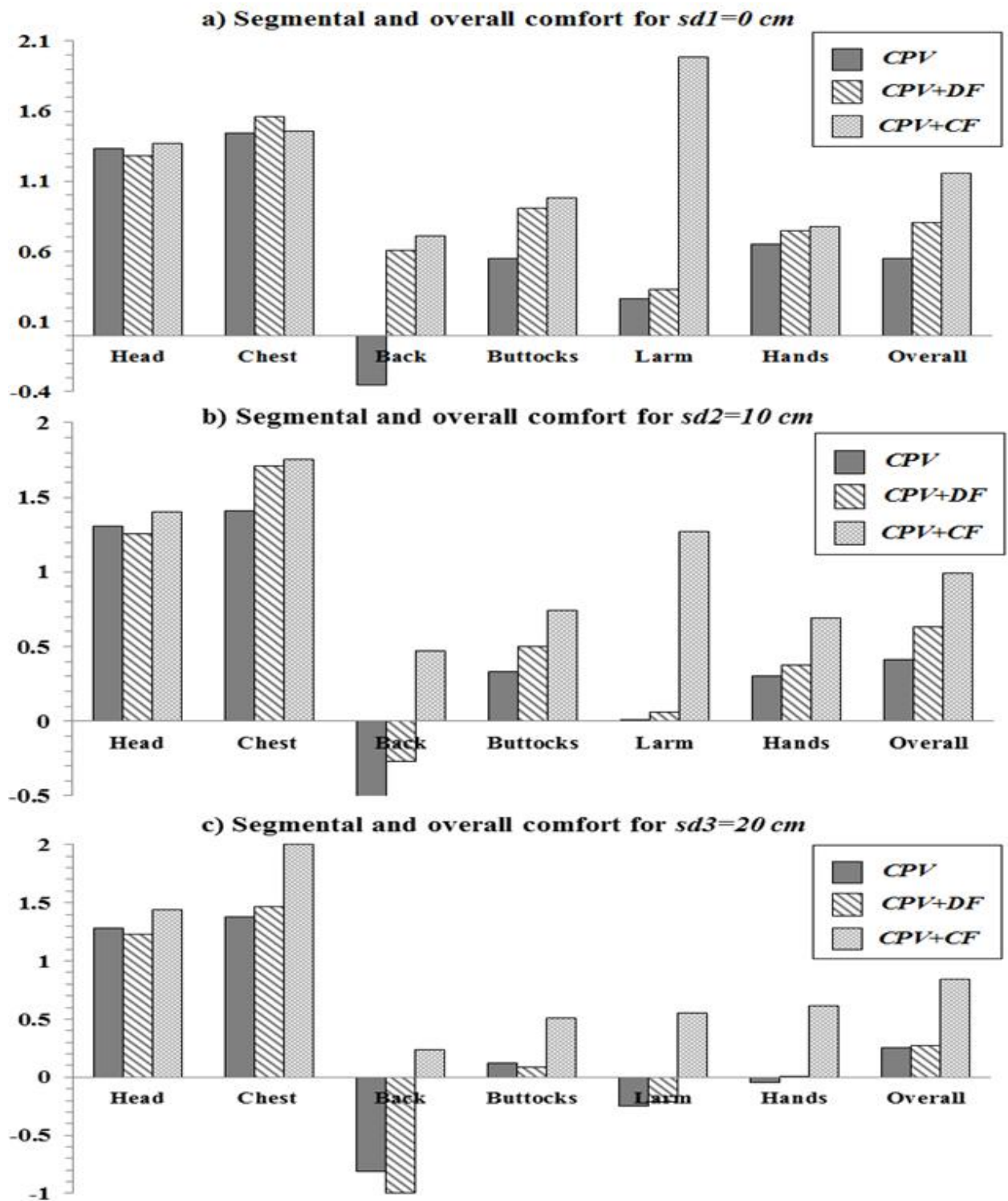


Fig. 5.49: Segmental and overall comfort for the different configurations studied.

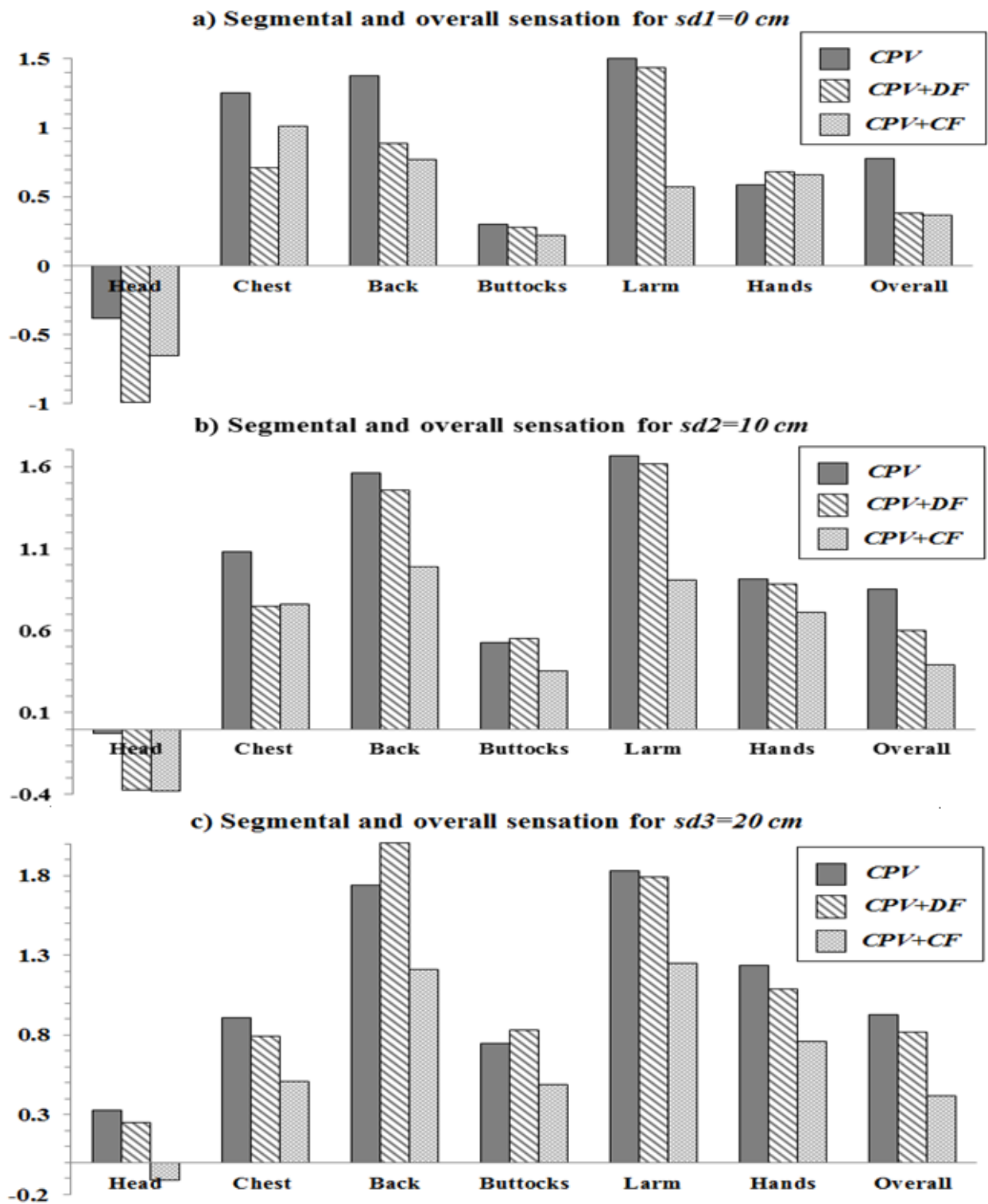


Fig. 5.50: Segmental and overall sensation for the different configurations studied.

For instance, when changing the ventilation configuration from standalone *CPV* to *CPV+DF* to *CPV+CF* the overall comfort was increased from 0.55 to 0.81 to 1.16 (see Fig. 5.49). For a moderate shift of $sd2 = 10$ cm, the chair motion lead to a change in the comfort state of the occupant since the head is no more directly beneath the *CPV* jet (see Fig. 5.46.b). Therefore, the cool sensation of the head is lower (see Fig. 5.50) and the *CPV* jet reaches more effectively the body parts close to it as the chest and abdomen however it does not effectively reach parts far from it as the back and buttocks increasing the comfort asymmetry which reduces the overall comfort compared to the case of no shift by 25.45% for the standalone *CPV*, 22.22% for *CPV+DF* and 14.65% for *CPV+CF* (see Fig. 5.49). The performance of the *CPV* system assisted by *CF* in terms of thermal comfort was the less affected by the moderate chair shift by re-localizing the flow around the occupant (see Figs. 5.49 and 5.50).

Figure 5.51 compares the temperature fields at the symmetry plane of the two-station office space for shift distances $sd1 = 0$ cm (occupant at the left) and $sd3 = 20$ cm (occupant at the right) for: (a) *CPV+DF* and (b) *CPV+CF*. When the shift distance increased from $sd1 = 0$ cm to $sd3 = 20$ cm, the comfort asymmetry effect was strengthened decreasing the overall comfort significantly for the standalone *CPV* system from 0.55 to 0.25 and *CPV* system assisted by *DF* from 0.81 to 0.27 (see Fig. 5.49). For *CPV* system assisted by *CF*, the four chair fans symmetrically distributed around the occupant helped in reducing the negative effect of this dissymmetry and thus limiting the reduction of the overall thermal comfort from 1.16 to 0.84 while this was not the case of the desk fans which were far from the occupant (Fig. 5.51.(a-b)).

Temperature
(°C)

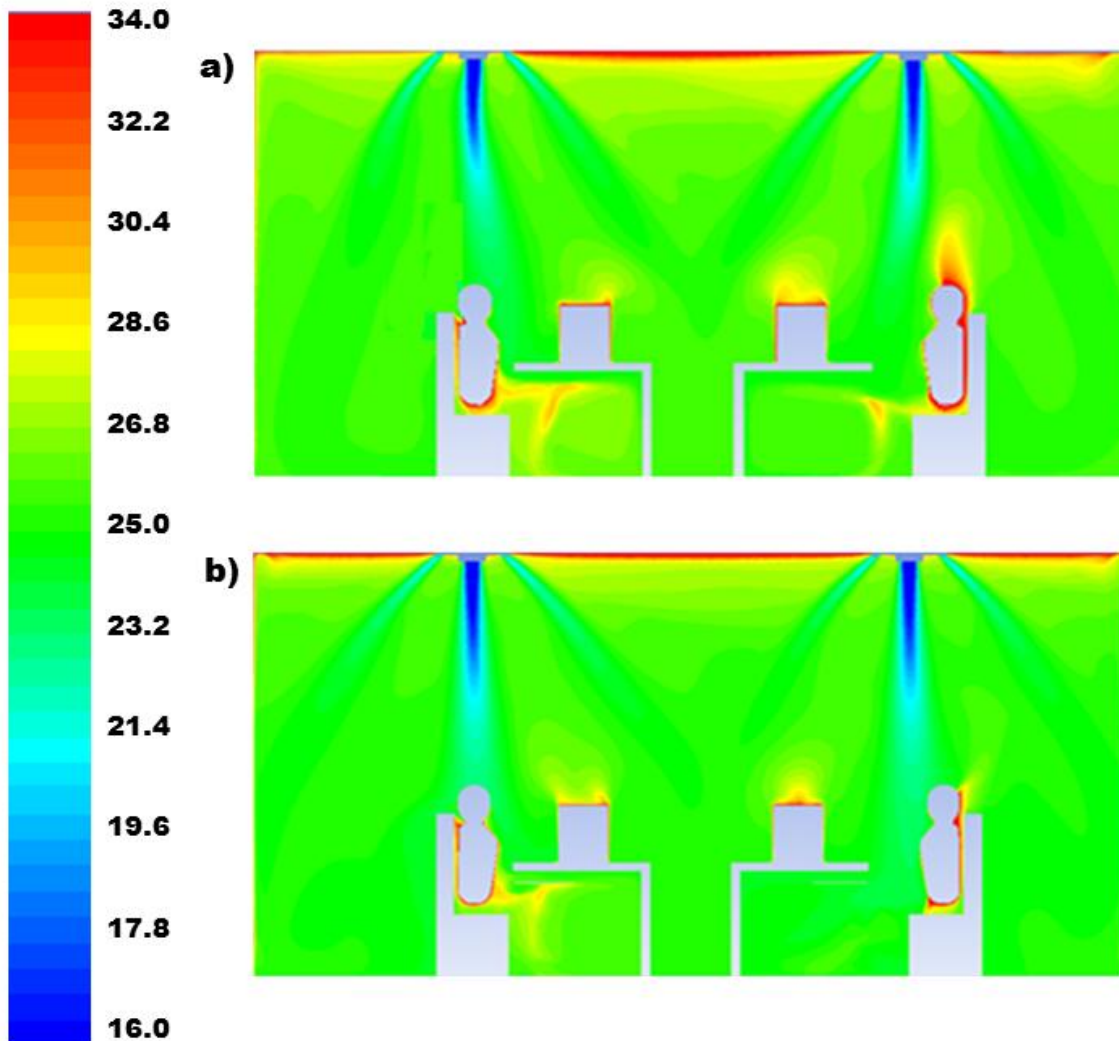


Fig. 5.51: Illustration of the temperature field at the symmetry plane of the two-station office space for shift distances $sd1=0\text{ cm}$ (occupant at the left) and $sd3=20\text{ cm}$ (occupant at the right) for: a) $CPV+DF$; b) $CPV+CF$.

For the lower arm, hands, back, and buttocks the shift increases largely the warm sensation which explains the decrease in segmental comfort (see Fig. 5.50). For these body parts which are not effectively reached by the CPV jet when a shift of 20 cm occurred, the system performance is significantly degraded when assisted by DF which failed to accomplish their function in suppressing the human thermal plumes as they are

far from the occupant (see Figs. 5.46.c, 5.51.a). On the other hand, the operation of *CF* reduced the comfort asymmetry created by the occupant position shift leading to acceptable comfort for the critical body parts (see Figs. 5.45.c, 5.51.b).

5.2.3.2. Energy Savings of the Optimal *CPV+CF* Design ...

In the process of quantifying the reduction in energy consumption induced by replacing *DF* with *CF*, an energy analysis was conducted. Comparison was conducted under equivalent thermal comfort and IAQ when the occupant was directly beneath the *CPV* jet for which case the operation of *DF* was effective. When assisted by *DF*, the *CPV* flow rate was increased until reaching equivalent performance of *CPV* assisted by *CF*.

The following details were used for the energy consumption calculation. The desk/chair fans nominal power (10 W×2) and the *CPV* fans nominal power (15 W×2) were added to the electrical cost of the chiller characterized by a typical COP of 3.5. The fresh air should be dehumidified and then sensibly heated to the required conditions.

Table 5.16 summarizes performance comparison of *DF* and *CF* for a *CPV* flow rate of 8.5 L/s. As the *CF* performance is much better with respect to thermal comfort, ventilation effectiveness and cross-contamination the *CPV* jet flow rate should be higher when assisted by *DF* to attain comparable performance. It was found that a *CPV* flow rate of 11 L/s assisted by *DF* gives nearly equivalent performance to the case of *CPV* flow rate of 8.5 L/s assisted by *CF* (Table 5.16).

Table 5.16: Comparison of the performance of *DF* and *CF* when the occupant is beneath the *CPV* jet.

Ventilation configuration	Ventilation effectiveness (ϵ_v)	Intake fraction for $1 \mu\text{m}$ ($\times 10^{-4}$)	Deposited fraction for $1 \mu\text{m}$ ($\times 10^{-3}$)	Overall thermal comfort
<i>CPV</i> (8.5 L/s) + <i>CF</i> (10 L/s)	23.1	0.90	3.19	1.16
<i>CPV</i> (8.5 L/s) + <i>DF</i> (10 L/s)	21.1	1.15	3.61	0.81
<i>CPV</i> (11 L/s) + <i>DF</i> (10 L/s)	22.9	0.905	3.21	1.13

Therefore, the use of *CF* reduced the *CPV* flow rate by 22.72% resulting in energy savings of 14.87% for the case where the occupant was beneath the jet and allowed maintaining good performance of the system when chair shift occurred while with *DF* the system performance was largely degraded. In this case, even if the *CPV* flow rate was increased it was not possible to reach the same performance of *CF* since the jet was not redirected towards the occupant due to the distance constraint.

CHAPTER 6

CONCLUSION

The compromise between high IAQ and occupant comfort in indoor spaces and reduced energy consumption constitute a real challenge in the design of ventilation systems. Localized ventilation presents a high potential in the removal of particle contaminants reducing infectious disease, while also providing thermal comfort and good indoor air quality (IAQ) at minimal energy cost. This thesis dissertation essentially aims towards enhancing the performance of horizontal and vertical localized ventilation in terms of reduced cross-contamination between occupants and energy consumption using innovative engineering strategies.

6.1. Development of a Simplified *DV* Model

A simplified model predicting active particle behavior in spaces ventilated by DV systems was developed. The developed model incorporated particles' deposition on walls of different orientations, and the gravitational settling affecting the particles' distribution within the space. Given that indoor heat sources are of different heat loads, the expansion of rising plumes at different critical heights was considered in the new multi-plume model. The model ability in predicting particle concentrations, intake fractions and deposition rates for different particle diameters was validated using data from literature revealing that the current simplified model is capable of capturing the physics of the problem with significant reduction of the computational time cost. The validated model was used to study cross-infection between occupants in typical internal offices. The investigation of different supply conditions was performed to come up with

recommendations on the required design of the DV system to satisfy both thermal comfort and IAQ criteria for the inhalable range particularly for particle of diameter lower than 10 μm presenting high probability of infecting the exposed person if inhaled.

The model results showed that as the particle diameter increases from the sub-micrometer mode the effect of the gravitational settling increases lowering the stratification in concentration created by the DV system and thus increasing the particle concentration at the breathing level of the exposed person. For a flow rate of 60 L/s, this effect remains until reaching a particle diameter above 10 μm where deposition on the floor opposing the DV principle acts as a removal factor. For the critical inhalable range of interest, gravitational settling accumulates particles in the occupied zone as the diameter increases leading to higher probability of cross-infection. In general, a stratification height significantly above the breathing level ensures good IAQ for the critical inhalable range.

The developed model presents a computationally low cost design tool that can be easily used in offices conditioned by DV system to ensure relatively safe intake fractions for the inhalable range and satisfy the thermal comfort criteria.

6.2. Cross-Contamination from HMRA in DV Spaces

The model results showed that as the velocity of the exhaled jet increases, the proportion of particles penetrating the rising thermal plumes increases. This penetration creates a concentration peak at the breathing level of the exposed person leading to a higher possibility of cross-contamination. Therefore, HMRA reduce the effectiveness of the DV system since particles are not completely transported by the rising convective plumes to be effectively evacuated from the space. It was shown that the standalone DV

system is not able of preventing accumulation at the breathing level of particles exhaled by high momentum jets even for over-designed flow rates. Equipping the *DV* system with personalized ventilation delivering fresh air to the breathing zone of the exposed occupant or with chair fans blowing air upward increasing the strenght of the plumes is expected to reduce significantly disease transmission. The gravitational effect can play significantly a positive role in reducing disease transmission for nuclei diameter above 50 μm . Altering the size of exhaled particles using a proper medical treatment can be beneficial to reduce disease transmission by enhancing particle deposition. In addition, the reduced distance between occupants significantly augments the risk of cross-infection. Distances lower than 1 m between occupants lead to dangerous microclimate zones since the risk of cross-contamination increases largely.

Three stages can be defined with respect to time for the variation of the IPE: a first stage dominated by the propagation and decay of the exhaled jet, a particles' redistribution stage, and a particles' removal stage. Within the set of studied conditions, the larger is the flow rate, the lower are the durations of the three stages and the effect of the *DV* flow rate on particle behavior is the highest for the third stage and the lowest for the first stage due to the decay of the exhaled jet with time. A concentration peak is always observed during the first stage due to the jet propagation, and for *DV* supply flow rate below 75 L/s there is a second inhaled concentration peak during the second stage. The first stage peak is two to three orders of magnitude larger than the second stage peak. However, the duration of the first stage is much smaller than the second stage. The inhaled dose during the first stage is the highest and is largely affected by the cough velocity, the particle diameter and the distance between the occupants.

A comparison between steady and transient modeling of the IPE results showed that steady modeling is helpful in understanding the physics affecting particle spread resulting from HMRA but should not be used to predict the inhaled dose since it leads to largely over-predicted values.

This study investigated the effect of several parameters (DV flow rate, coughing velocity, particle diameter, and distance between the occupants) on exhaled particle distribution and cross contamination between occupants. However, many other factors affect respiratory droplets spread and are worthy of future studies as the evaporation of exhaled droplets, enhanced particles' spread by velocity fluctuation, injection profile during coughing, and velocity decay along radial direction.

6.3. DV+CF Performance

Assisting DV by CF was shown to considerably enhance its performance if proper operating conditions of the CF were used. The positive effect of the CF increasing the strength of the rising plumes and blowing relatively clean air to the breathing level was opposed by the increase of contaminant transport downward towards the occupied zone due to increased recirculation in the upper zone. These two opposing effects led to the existence of an optimal CF flow rate where the positive effect created by the chair fans was dominant and insured that contaminated air remains above the occupants away from the breathing level. Therefore when designing a CF-DV system one must be aware of the existence of an optimum CF flow rate beyond which exposure actually increases due to recirculation.

It was found that the fan should be designed such that the positive effect created by strengthening of the plumes dominates the counter-effect resulting from the

increased downward motion of particles. The fans efficiency was investigated for different particle diameters covering the critical inhalable range. Similar observations can be made concerning the presence of an optimal *CF* flow rate with some variations due to settling effect. It was found that the optimal *CF* flow rate for 10 μm (approximately 8 L/s) was slightly higher than the one for 1 μm particles (7 L/s) due to the gravitational effect. The higher the *DV* supply flow rate, the lower is the intake fraction decreasing the efficiency and the need for the chair fans since the increased upward velocity flow resulting from the *DV* ventilation helps in the upward transport of particles. With appropriate selection of the *CF* flow rate, it was possible to realize a 30% reduction in *DV* energy use for a given level of thermal comfort and IAQ covering the inhalable particle range.

However, other transient breathing activities as coughing and sneezing which involve high momentum particle generation can alter the particle behavior. In fact, part of the exhaled jet might penetrate the thermal plume which can lead to an increase of the risk of cross-contamination. The presence of the chair fans in this case is promising since it increases the strength of the rising plumes which is expected to reduce the percentage of particles penetrating the rising plume to the surrounding air. These are worthy of further studies.

6.4. *CPV+DF* Performance

The ability of *MV* in preventing contamination through its two paths is largely degraded with the reduction of the distance between the workstations. As the distance between the workstations decreases, a higher number of particles reach the exposed station leading to the increase of deposited and intake fractions (*DFr* and *IF*). This

increase is common for the mixing and personalized ventilations but with a variable rate. The rate of increase of *IF* and *DFr* with distance was reduced when changing the ventilation system from *MV* to *CPV* and by the introduction of desk fans. The shorter the distance between the occupants the higher is the effectiveness of the *CPV+DF* system compared to *MV* in reducing cross-contamination through its different paths. For the different scenarios studied, gravitational effect played a positive role favoring floor deposition acting as a sink of particles decreasing the *IF* and *DFr*. With proper selection of the fan flow rate (10 L/s), the introduction of *DF* to the *CPV* system reduced significantly direct and indirect-contamination while allowing efficient use of the space. Reductions of the *DFr* and *IF* up to 31.82% and 47.51% respectively were reached despite the reduction of distance between occupants by 50% from 4.0 m to 2.0 m through using the optimized design compared to the reference *MV* case. Therefore, by implementing the optimized ceiling *PV* system assisted by desk fans with a flow rate of 10 L/s to the multi-station office space the occupancy density can be improved from the standard value of 12 m² to 8 m² per occupant while maintaining good IAQ allowing to reach 21.3 % of energy savings.

The current work does not consider other transient breathing activities as coughing and sneezing which involve high momentum particle generation that can alter the particle behavior. In fact, a larger part of the exhaled air might penetrate the *PV* jet which can lead to an increase of the risk of cross-contamination. The presence of the desk fans in this case is promising since it increases the strength of the *PV* momentum reaching the breathing level which is expected to reduce particle spread within the space. These are worthy of further studies.

6.5. Effect of Assisting *CPV* with *CF* versus *DF*

When the occupant is directly beneath the *CPV* jet, the operation of both *DF* and *CF* largely improved the standalone *CPV* performance in terms of thermal comfort, ventilation effectiveness and cross-infection between occupants. As the shift distance increased the comfort asymmetry effect was strengthened decreasing the overall comfort significantly for the standalone *CPV* system and *CPV* system assisted by *DF* but not for *CPV* system assisted by *CF* for which the four chair fans symmetrically distributed re-localize the *CPV* flow around the occupant helping in the reduction of the dissymmetry effect.

For moderate shift of 10 cm, the *CPV* jet was less opposed by the rising thermal plumes reaching more effectively the breathing zone of the occupant enhancing the IAQ. For larger shift distance of 20 cm, flow localization was weakened resulting in a decrease in the ventilation effectiveness and an increase in direct and indirect cross-infection between occupants. The performance degradation with shift distance was reduced largely with the operation of *CF* compared to *DF* by redirecting the *CPV* flow towards the occupant due to *CF* suction jets. Direct and indirect cross-contamination was reduced significantly with the increase of particle diameter for the different shift distances. In fact, as the particle diameter increases the gravitational effect is strengthened constituting a particle sink by floor deposition.

In summary, as the shift distance increased the effectiveness of *CF* compared to *DF* increased in terms of thermal comfort ventilation effectiveness and cross-infection between occupants. The limitation of using *DF* is that the occupant should be located very close to the desk so that the *DFs* are able to suck the human thermal plumes

effectively. *CF* allowed overcoming the distance reliance constraint since they move with the occupants.

The use of *CF* allowed the reduction of *CPV* flow rate by 22.72% resulting in energy savings of 14.87% for the case where the occupant was beneath the jet and allowed maintaining good performance of the system when chair shift occurred while with *DF* the system performance was largely degraded.

REFERENCES

- [1] Bruce N, Perez-Padilla R, Albalak R. Indoor air pollution in developing countries: a major environmental and public health challenge. *Bulletin of the World Health Organization* 2000; 78(9): 1078-1092.
- [2] Spengler JD, Sexton K. Indoor air pollution: a public health perspective. *Science* 1983; 221(4605): 9-17.
- [3] Sundell J. On the history of indoor air quality and health. *Indoor air* 2004; 14(s7): 51-58.
- [4] Guo H, Lee SC, Chan LY, Li WM. Risk assessment of exposure to volatile organic compounds in different indoor environments. *Environmental Research* 2004; 94(1): 57-66.
- [5] Viegi G, Simoni M, Scognamiglio A, Baldacci S, Pistelli F, Carrozzi L, Annesi-Maesano I. Indoor air pollution and airway disease [State of the Art]. *The International Journal of Tuberculosis and Lung Disease* 2004; 8(12): 1401-1415.
- [6] Klepeis NE, Nelson WC, Ott WR, Robinson JP, Tsang AM, Switzer P, Behar JV, Hern SC, Engelmann WH. The National Human Activity Pattern Survey (NHAPS): a resource for assessing exposure to environmental pollutants. *Journal of exposure analysis and environmental epidemiology* 2001; 11(3): 231-252.
- [7] Brook D, Franklin B, Cascio W, Hong Y, Howard G, Lipsett M, Luepker R, Mittleman M, Samet J, Smith C, Tager I. Air pollution and cardiovascular disease A statement for healthcare professionals from the expert panel on population and prevention science of the American Heart Association. *Circulation* 2004; 109: 2655-2671.

- [8] Ministry of Environment & Forests, Govt. of India Parivesh Bhavan, East Arjun Nagar Delhi – 110 032, Study on ambient air quality, respiratory symptoms and lung function of children in Delhi. Central Pollution Control Board. Environmental Health Series: Ehs/2/2008.
- [9] Englert N. Fine particles and human health—a review of epidemiological studies. *Toxicology letters* 2004; 149: 235-242.
- [10] Nazaroff WW. Indoor particle dynamics. *Indoor air* 2004; 14(s7): 175-183.
- [11] Melikov AK. Personalized ventilation. *Indoor Air* 2004; 14(s7): 157-167.
- [12] Nguyen TA, Aiello M. Energy intelligent buildings based on user activity: A survey. *Energy and buildings* 2013; 56: 244-257.
- [13] Lo LJ, Novoselac A. Localized air-conditioning with occupancy control in an open office. *Energy and Buildings* 2010; 42(7): 1120-1128.
- [14] Olli S. Ventilation Strategies for Good Indoor Air Quality and Energy Efficiency. *International Journal of Ventilation* 2008; 6(4): 297-306.
- [15] Makhoul A, Ghali K, Ghaddar N. The energy saving potential and the associated thermal comfort of displacement ventilation systems assisted by personalized ventilation. *Indoor Built Environment* 2013; 22: 508–519.
- [16] Brohus H, Knudsen HN, Nielsen PV, Clausen G, Fanger PO. Perceived air quality in a displacement ventilated room. *Indoor Air. Proceedings of the 7th Int. Conf. on Indoor Air Quality and Climate, Nagoya, Japan 1996*; 1: 811–816.
- [17] Lin Z, Chow TT, Fong KF, Wang Q, Li Y. Comparison of performances of displacement and mixing ventilations. Part I: thermal comfort. *International Journal of Refrigeration* 2005; 28: 276–287.

- [18] Behne M. Indoor Air Quality in Rooms with Cooled Ceilings: Mixing Ventilation or rather Displacement Ventilation? *Energy and Buildings* 1999; 30(2): 155-166.
- [19] Yuan X, Chen Q, Glicksman L. A Critical Review of Displacement Ventilation. *ASHRAE Transactions* 2001; 4101(RP-949): 78-90.
- [20] Yang B: Thermal comfort and indoor air quality evaluation of a ceiling mounted personalized ventilation system integrated with an ambient mixing ventilation system. PhD thesis. National University of Singapore; 2009.
- [21] Makhoul A, Ghali K, Ghaddar N. Low-mixing coaxial nozzle for effective personalized ventilation. *Indoor and Built Environment* 2013; 22(3): 508-519.
- [22] Makoul A, Ghali K, Ghaddar N. Desk fans for the control of the convection flow around occupants using ceiling mounted personalized ventilation. *Building and Environment* 2013; 59: 336-348.
- [23] Mundt E. Contaminant distribution in displacement ventilation-Influence of disturbances. *Building and Environment* 1994; 29: 311-317.
- [24] Kanaan M, Ghaddar N, Ghali K. Simplified Model of Contaminant dispersion in rooms conditioned by chilled-ceiling displacement ventilation system. *HVAC&R Research* 2010; 16: 765-783.
- [25] Miller FJ, Gardner DE, Graham JA, Lee RE, Wilson WE, Bachmann JD. Size considerations for establishing a standard for inhalable particles. *Journal of the Air Pollution Control Association* 1979; 29: 610-615.
- [26] Lai ACK, Cheng YC. Study of expiratory droplet dispersion and transport using a new Eulerian modeling approach. *Atmospheric Environment* 2007; 41: 7473–7484.

- [27] Gao N, Niu J, Morawska L. Distribution of respiratory droplets in enclosed environments under different air distribution methods. *Building Simulation* 2008; 1: 326–335.
- [28] Xiaoping L, Jianlei N, Naiping G. Spatial distribution of human respiratory droplet residuals and exposure risk for the co-occupant under different ventilation methods. *HVAC&R Research* 2011; 17(4): 432-445.
- [29] Li Y, Nielsen PV. Commemorating 20 years of Indoor Air CFD and ventilation research. *Indoor Air* 2011; 21: 442–453
- [30] Acred A, Hunt GR. A simplified mathematical approach for modelling stack ventilation in multi-compartment buildings. *Building and Environment* 2014; 71: 121-130.
- [31] Zhao B, Chen C, Tan ZC. Modeling of ultrafine particle dispersion in indoor environments with an improved drift flux model. *Journal of Aerosol Science* 2009; 40: 29-43.
- [32] Lai ACK, Nazaroff WW. Modeling indoor particle deposition from turbulent flow onto smooth surfaces. *Journal of Aerosol Science* 2000; 31: 463-476.
- [33] Fanger PO, Lauridsen J, Bluysen P, Clausen G. Air pollution sources in offices and assembly halls, Quantified by the olf unit. Laboratory of heating and air conditioning, Technical university of Denmark, DK-2800 Lyngby. *Energy and Buildings* 1988; 12, 7-19.
- [34] Pantelic J. Exposure generated by cough released droplets in the indoor environment- A comparison among four ventilation systems. Doctoral dissertation 2010.

- [35] Gao P, Niu JL. Modeling particle dispersion and deposition in indoor environments. *Atmospheric Environment* 2007; 41: 3862-3876.
- [36] Watanabe S, Shimomura T, Miyazaki H. Thermal evaluation of a chair with fans as an individually controlled system. *Building and Environment* 2009; 44:1392–1398.
- [37] Chen Q, James M, Jitendra G, Byron J, Sagnik M, Stephane P, John S. Infectious Disease Transmission in Airliner Cabins. Report No. RITE-ACER-CoE-2012-01.
- [38] Weber DJ, Rutala WA, Miller MB, Huslage K, Sickbert-Bennett E. Role of hospital surfaces in the transmission of emerging health care-associated pathogens: norovirus, *Clostridium difficile*, and *Acinetobacter* species. *American journal of infection control* 2010; 38(5): S25-S33.
- [39] Vasickova P, Pavlik I, Verani M, Carducci A. Issues concerning survival of viruses on surfaces. *Food and Environmental Virology* 2010; 2(1): 24-34.
- [40] Rusin P, Maxwell S, Gerba C. Comparative surface-to-hand and fingertip-to-mouth transfer efficiency of gram-positive bacteria, gram-negative bacteria, and phage. *Journal of Applied Microbiology* 2002; 93(4): 585-592.
- [41] IPD Occupiers. Efficiency Standards for Office Space, A report to Office of Government Commerce, [http:// ns.kinnarps.tm/Countries/UK/PS%20minisite/Agreement/Efficiency Standards _ for _Office _Space.pdf](http://ns.kinnarps.tm/Countries/UK/PS%20minisite/Agreement/Efficiency Standards _ for _Office _Space.pdf) 2007.
- [42] Bedford M, Harris R, King A, Hawkeswood A. Occupier density study. British council for offices (BCO); 2013.
- [43] El-Fil B, Ghali K, Ghaddar N. Optimizing performance of ceiling mounted personalized ventilation system assisted by chair fans: assessment of thermal

- comfort and indoor air quality. Master thesis. American University of Beirut; 2015.
- [44] Bourhan T, Molhim M, Al-Rousan M. Dynamic model of an HVAC system for control analysis. *Energy* 2005; 30 (10): 1729-1745.
- [45] Zaheer-Uddin M. Energy start-stop and fluid flow regulated control of multi-zone HVAC systems. *Energy* 1993; 18(3): 289-302.
- [46] Bjørn E, Nielsen PV. Dispersal of exhaled air and personal exposure in displacement ventilated rooms. *Indoor Air* 2002; 12: 147–164.
- [47] Mundt E. Convection flows in rooms with temperature gradients –Theory and measurements. *Proceedings of Roomvent Third International Conference on Air Distribution in Rooms* 1992.
- [48] Etheridge DW, Sandberg M. *Building Ventilation: Theory and Measurement*. Chichester Wiley 1996.
- [49] Mundt E. Displacement ventilation systems-Convection flows and temperature gradients. *Building and Environment* 1995; 30: 129-133.
- [50] Brohus H, Nielsen PV. Personal exposure in displacement ventilated rooms. *Indoor Air* 1996; 6:157-167.
- [51] Nielsen PV, Olmedo I, Ruiz de Adana M, Grzelecki P, Jensen RL. Airborne cross-infection risk between two people standing in surroundings with a vertical temperature gradient. *HVAC&R Research* 2012; 18:552-561.
- [52] Kaczmarczyk J, Melikov AK, Bolashikov Z, Nikolaev L, and Fanger PO. Human response to five designs of personalized ventilation. *International Journal of heating, Ventilation and Refrigeration Research* 2006; 12(2): 367-384.

- [53] Cermak R and Melikov AK. Air quality and thermal comfort in an office with underfloor, mixing and displacement ventilation. *International Journal of Ventilation* 2006; 5(3):5.
- [54] Cermak R, Melikov AK, Forejt L, Kovar O. Performance of personalized ventilation in conjunction with mixing and displacement ventilation. *International Journal of Heating, Ventilation and Refrigeration Research* 2006; 12(2): 295-311.
- [55] Cermak R, Melikov AK. Protection of occupants from exhaled infectious agents and floor material emissions in rooms with personalized and under floor ventilation. *HVAC&R Research* 2007; 13(1):23-38.
- [56] Halvoňová B, Melikov AK. Displacement ventilation in conjunction with personalized ventilation. In: *Proceedings of the 11th International conference on Indoor Air Quality and Climate. Indoor Air 2008, 17-22 August 2008, Copenhagen, Paper ID: 411.*
- [57] Yang B, Sekhar C, Melikov AK. Ceiling mounted personalized ventilation system in hot and humid climate - An energy analysis. *Energy and Buildings* 2010; 42: 2304-2308.
- [58] Melikov AK. Human body micro-environment: the benefits of controlling airflow interaction. *Build Environ* 2015; doi:10.1016/j.buildenv.2015.04.010.
- [59] Khalifa HE, Janos MI, Dannenhoffer JF. Experimental investigation of reduced mixing personal ventilation jets. *Building Environ* 2009; 44:1551-8.
- [60] Russo JS, Dang TQ, and Khalifa HE. Computational analysis of reduced-mixing personal ventilation jets. *Building and Environment* 2009; 44: 1559-1567.

- [61] Bolashikov ZD, Melikov AK, Krenek. Control of the Free Convective Flow around the Human Body for Enhanced Inhaled Air Quality: Application to a Seat-Incorporated Personalized Ventilation Unit. HVAC&R Research 2010; 16(2): 161-188.
- [62] Bolashikov ZD, Melikov AK, Krenek M, Improved Performance of Personalized Ventilation by Control of the Convection Flow around Occupant Body. ASHRAE Transactions 2009; 115(2), Paper ID: LO-09-038.
- [63] Makhoul A, Ghali K, Ghaddar N. Thermal comfort and energy performance of a low-mixing ceiling-mounted personalized ventilator system. Building and Environment 2013; 60: 126-136.
- [64] Makhoul A, Ghali K, Ghaddar N. Investigation of Particle Transport in Offices Equipped with Ceiling-Mounted Personalized Ventilators. Building and Environment 2013; 63: 97-107.
- [65] Morawska L, Johnson GR, Ristovski ZD, Hargreaves , Mengersen K, Corbett S, Chao CYH, Li Y, and Katoshevski D. Size distribution and sites of origin of droplets expelled from the human respiratory tract during expiratory activities. Journal of Aerosol Science 2009; 40(3): 256-269.
- [66] Sandle T. People in Cleanrooms: Understanding and Monitoring the Personnel Factor| IVT. Hand, 10, 100-000.
- [67] Nicas M, Nazaroff WW, Hubbard A. Toward understanding the risk of secondary airborne infection: emission of respirable pathogens. Journal of occupational and environmental hygiene 2005; 2(3): 143-154.
- [68] Morawska L. Droplet fate in indoor environments, or can we prevent the spread of infection? Indoor air 2006; 16(5): 335-347.

- [69] Melikov A, Kaczmarczyk J. Measurement and prediction of indoor air quality using a breathing thermal manikin. *Indoor air* 2007; 17(1): 50-59.
- [70] Xu C, Nielsen PV, Gong G, Jensen RL, Liu L. Influence of air stability and metabolic rate on exhaled flow. *Indoor air* 2014; doi: 10.1111/ina.12135.
- [71] Gao N, Niu J. Transient CFD simulation of the respiration process and inter-person exposure assessment. *Building and Environment* 2006; 41(9): 1214-1222.
- [72] Melikov AK. Improving comfort and health by personalized ventilation. *Proceedings of Roomvent, Coimbra, Portugal* 2004.
- [73] Mui KW, Wong LT, Wu CL, Alvin CK, Lai b. Numerical modeling of exhaled droplet nuclei dispersion and mixing in indoor environment. *Journal of Hazardous Materials* 2009; 167: 736–744.
- [74] Chen Z, Zhao B. Some questions on dispersion of human exhaled droplets in ventilation room: answers from numerical investigation. *Indoor Air* 2010; 20:95–111.
- [75] Dockery DW, Pope III CA. Acute respiratory effects of particulate air pollution. *Annual Review of Public Health* 1994; 15:107-32.
- [76] Bolashikov ZD, Melikov A. Methods for air cleaning and protection of building occupants from airborne pathogens. *Building and Environment* 2009; 44(7):1378-1385.
- [77] Ayoub M, Ghaddar N, Ghali K. Simplified thermal model of spaces cooled with combined chilled ceiling and displacement ventilation system. *HVAC&R Research* 2006; 12(4):1005–30.

- [78] Mundt E. The performance of displacement ventilation systems experimental and theoretical studies. PhD dissertation. KTH, Stockholm, Bygghvetenskapliga Vetenskapliga Institutionen; 1996.
- [79] Grzelecki P. The examination of comfort and cross infection in a displacement ventilated room. Master Thesis on Indoor Environmental Engineering. Aalborg University, The Faculty of Engineering and Science; 2010.
- [80] Goodfellow HD. Industrial ventilation design guidebook. San Diego: Academic Press; 2001.
- [81] Rouse H, Yih CS, Humphreys W. Gravitational convection from a boundary source. *Tellus* 1952; 4: 201–210.
- [82] Morton BR, Taylor G, Turner JS. Turbulent gravitational convection from maintained and instantaneous sources. *Proc. Royal Soc.* 1956; 234: 1-23.
- [83] Middleton JH. The asymptotic behavior of a starting plume. *Journal of Fluid Mechanics* 1975; 72: 753–771.
- [84] Jaluria Y. Natural Convection, Heat and Mass Transfer, Free boundary flows. Chapter 4, New York: Pergamon Press; 1980.
- [85] Makhoul A, Ghali K, Ghaddar N. A simplified combined displacement and personalized ventilation model. *HVAC&R Research* 2012; 18: 737-749.
- [86] Zhao B, Zhang Z, Li X, and Huang D. Comparison of diffusion characteristics of aerosol particles in different ventilated rooms by numerical method. *ASHRAE Transactions* 2004; 110(1): 88-95.
- [87] Zhao B, Zhang Y, Li X, Yang X, Huang D. Comparison of indoor aerosol particle concentration and deposition in different ventilated rooms by numerical method. *Building and Environment* 2004; 39(1): 1-8.

- [88] Zhao B, Wu J. Modeling particle deposition from fully developed turbulent flow in ventilation duct. *Atmospheric Environment* 2006; 40: 457–466
- [89] Zhao B, Wu J. Particle deposition in indoor environments: Analysis of influencing factors. *Journal of Hazardous Materials* 2007; 147: 439–448.
- [90] Chen C, Lin CH, Jiang Z, Chen Q. Simplified models for exhaled airflow from a cough with the mouth covered. *Indoor air* 2014; 24(6): 580-591.
- [91] Craven BA, Settles GS. A computational and experimental investigation of the human thermal plume. *Journal of Fluids Engineering* 2006; 128(6): 1251-1258.
- [92] Sparrow EM, Gregg JL. Laminar free convection heat transfer from the outer surface of a vertical circular cylinder. *Trans. ASME* 1956; 78(8): 1823-1829.
- [93] Gebhart B, Jaluria Y, Mahajan R, Sammakia B. Buoyancy-induced flows and transport. Hemisphere Publishing Corporation 1988.
- [94] Bergman TL, Lavine AS, Incropera FP, Dewitt DP. Introduction to heat transfer, Sixth edition.
- [95] Vedhanayagam M, Altenkirch RA, Eichhorn R. A transformation of the boundary layer equations for free convection past a vertical flat plate with arbitrary blowing and wall temperature variations. *International Journal of Heat and Mass Transfer* 1980; 23(9): 1286-1288.
- [96] Zhu S, Kato S, Yang JH. Study on transport characteristics of saliva droplets produced by coughing in a calm indoor environment. *Building and Environment* 2006; 41(12): 1691-702.
- [97] Chen C, Liu W, Li F, Lin CH, Liu J, Pei J, Chen Q. A hybrid model for investigating transient particle transport in enclosed environments. *Building and Environment* 2013; 62: 45-54.

- [98] Kanaan M, Ghaddar N, Ghali K. Quality of inhaled air in displacement ventilation systems assisted by personalized ventilation. *HVAC and R Research* 2012; 18 (3): 500-514.
- [99] Patankar SV. *Numerical Heat Transfer and Fluid Flow*, series in computational methods in mechanics and thermal sciences. Hemisphere Publishing Corporation 1980.
- [100] Zhang Z, Chen Q. Comparison of the Eulerian and Lagrangian methods for predicting particle transport in enclosed spaces. *Atmospheric Environment* 2007; 41: 5236–5248.
- [101] Chen FZ, Yu S, Lai A. Modeling particle distribution and deposition in indoor environments with a new drift–flux model. *Atmospheric Environment* 2006; 40: 357-367.
- [102] ANSYS Software: ANSYS Inc. <http://www.ansys.com/>
- [103] Zhang Z, Chen Q. Experimental measurements and numerical simulations of particle transport and distribution in ventilated rooms. *Atmospheric Environment* 2006; 40(18): 3396–3408.
- [104] Li A, Ahmadi G. Dispersion and deposition of spherical particles from point sources in a turbulent channel flow. *Aerosol Science and Technology* 1992; 16: 209–226.
- [105] Wang M, Lin CH, Chen Q. Advanced turbulence models for predicting particle transport in enclosed environments. *Building and Environment* 2012; 47: 40-49.
- [106] Rim D, Novoselac A. Transport of particulate and gaseous pollutants in the vicinity of a human body. *Building and Environment* 2009; 44: 1840-1849.

- [107] Pantelic J, Sze-To GN, Tham KW, Chao CYH, Khoo YCM. Personalized ventilation as a control measure for airborne transmissible disease spread. *Journal of the Royal Society Interface* 2009; 6: S715-726.
- [108] He Q, Niu J, Gao N, Zhu T, Wu J. CFD study of exhaled droplet transmission between occupants under different ventilation strategies in a typical office room. *Building and Environment* 2011; 46(2): 397-408.
- [109] Hinds WC. *Aerosol Technology: Properties, Behavior, and Measurement of Airborne Particles*. Wiley, New York; 1982.
- [110] JAVA applet for ISO 7730, Calculation of Predicted mean Vote (PMV), and Predicted Percentage Dissatisfied (PPD), PMV 2008 ver 1.0, Ingvar Holmer, http://www.eat.lth.se/fileadmin/eat/Termisk_miljoe/PMV-PPD.html.
- [111] Salloum M, Ghaddar N, Ghali K. A new transient bioheat model of the human body and its integration to clothing models. *Int J Thermal Sci* 2007; 46: 371-84.
- [112] Ghaddar N, Ghali K, Chehaitly S. Assessing thermal comfort of active people in transitional spaces in presence of air movement. *Energy and Buildings* 2011; 43 (10): 2832-2842.
- [113] Zhang H, Arens E, Huizenga C, Han T. Thermal sensation and comfort models for non-uniform and transient environments: Part I: Local sensation of individual body parts. *Building and Environment* 2010; 45 (2): 380-8.
- [114] Zhang H, Arens E, Huizenga C, Han T. Thermal sensation and comfort models for non-uniform and transient environments: Part II: local comfort of individual body parts. *Building and Environment* 2010; 45 (2): 389-98.

- [115] Zhang H, Arens E, Huizenga C, Han T. Thermal sensation and comfort models for non-uniform and transient environments: Part III: whole-body sensation and comfort. *Building and Environment* 2010; 45 (2): 399-410.
- [116] Cropper P, Yang T, Cook M, Fiala D, Yousef R. Simulating the effect of complex indoor environmental conditions on human thermal comfort. *Building Simulation*, Scotland, 2009.
- [117] Halvonova B, Melikov A. Performance of “ductless” personalized ventilation in conjunction with displacement ventilation: Impact of intake height. *Building and Environment* 2010; 45 (4): 996-1005.
- [118] Dygert RK, Dang TQ. Mitigation of cross-contamination in an aircraft cabin via localized exhaust. *Building and Environment* 2010; 45(9): 2015-2026.
- [119] Melikov AK, Kaczmarczyk J. Indoor air quality assessment by a breathing thermal manikin. *Indoor Air* 2007; 17(1): 50-59.
- [120] ANSI/ASHRAE Standard 90.1: Energy Standard for Buildings Except Low-Rise Residential Buildings. Atlanta, American Society of Heating, Air-Conditioning and Refrigeration Engineers, Inc.; 2013.
- [121] Lai ACK, Kang W, Chen FZ. Experimental and numerical study on particle distribution in a two-zone chamber. *Atmospheric Environment* 2008; 42(8): 1717-1726.
- [122] Zhao B, Li X, Zhang Z. Numerical Study of Particle Deposition in Two Differently Ventilated Rooms. *Indoor Built Environ* 2004; 13: 443–451
- [123] Zhao B, Li X, Yan Q. A simplified system for indoor airflow simulation. *Building and Environment* 2003; 38: 543–552.

- [124] Guha A. Transport and deposition of particles in turbulent and laminar flow. *Annual Review of Fluid Mechanics* 2008; 40: 311–341.
- [125] Mangili A, Gendreau MA. Transmission of infectious diseases during commercial air travel. *Lancet* 2005; 365: 989–996.
- [126] BS EN ISO 7730. Moderate thermal environments – Determination of the PMV and PPD indices and specification of the conditions for thermal comfort. British Standards Institute, London; 1995.
- [127] Price HVAC. Engineering Guide Displacement Ventilation. <http://www.pricehvac.com/Catalog/Section J>.
- [128] Sun W, Jie J. Transport of droplets expelled by coughing in ventilated rooms. *Indoor and Built Environment* 2007; 16(6): 493-504.
- [129] Gupta JK, Lin CH, Chen Q. Flow dynamics and characterization of a cough. *Indoor Air* 2009; 19: 517-25.
- [130] Licina D, Melikov A, Pantelic J, Sekhar C, Tham KW. Human convection flow in spaces with and without ventilation: Personal exposure to floor released particles and cough released droplets. *Indoor Air* 2015; DOI: 10.1111/ina.12177.
- [131] ANSI/ASHRAE. Standard 62.1-2013, Ventilation for Acceptable Indoor Air Quality. Atlanta: American Society of Heating, Air- Conditioning and Refrigeration Engineers, Inc; 2013.
- [132] ASHRAE Handbook-Fundamentals. Atlanta: American Society of Heating Air-conditioning and Refrigeration Engineers, Inc; 2009.
- [133] Dougan D, Damiano L. CO₂-Based demand control ventilation. *ASHRAE Journal* 2004; 47: 52-54.